Proteomic and molecular analysis in colorectal cancer: validation of the biomarkers desmin, SET and CK8

A thesis submitted for the degree of Doctor of Philosophy, February 2010

Georgia Arentz, Bachelor of Biomedical Science (Honours)

School of Molecular and Biomedical Sciences, Discipline of Physiology,
The University of Adelaide

Table of Contents

Declaration

This work contains no material that has been accepted for the award of any other degree or diploma in any university or other tertiary institution to Georgia Arentz except where due reference has been made in the text. To the best of my knowledge and belief this work contains no material previously published or written by another person, except where due reference has been made in the text. I give consent to this copy of my thesis, when deposited in the University Library, being made available for loan and photocopying, subject to the provisions of the Copyright Act 1968. I also give permission for the digital version of my thesis to be made available on the web, via the University's digital research repository, the Library catalogue, the Australasian Digital Theses Program (ADTP) and also through web search engines, unless permission has been granted by the University to restrict access for a period of time.

Georgia Arentz

Acknowledgements

I would sincerely like to thank my supervisors Jenny Hardingham and Tim Chataway for their constant support and guidance over the last 5 years of my honours and PhD projects. I especially need to thank Jenny for her ability to pass on skills and her unwavering commitment. Her willingness to help and her understanding throughout my time at The Queen Elizabeth Hospital and beyond has been touching. Tim I need to thank for his openness, kindness and advice (science related and not). I especially need to thank Tim for all of the hours I spent in his office, wasting his time whilst I acquired vast amounts of technical knowledge, whilst he acquired…… a headache? Thank you both for your patience.

I was lucky enough to work with a number of people over the past few years who made me look forward to going to work and who made great contributions to my life. Amy, Amanda, Meeying and Yin Ying (my spiritual advisor) thank you. Thanks to everyone at Adelaide Microscopy for letting me consume the Leica LMD system for eight months. A big thanks also to everyone at Adelaide Proteomics Centre, in particular Peter Hoffmann for letting me use the facilities and Mark Condina for somehow making proteomics fun. I would also like to thank the QEH Research Foundation and the University of Adelaide for providing my honours and PhD scholarships respectively.

Lastly, thank you to all of my family and friends for their love and support, especially my parents Amy and Peter. It is also imperative that I thank Sascha for his help, plus his unconditional caring and patience with me through the horror that has been writing up.

Abbreviations

%:	percentage
x g:	x gravity
°C:	degrees Celsius
μg:	microgram
μl:	microliter
μM:	micromolar
1°:	primary
1-DE:	one-dimensional electrophoresis
2°:	secondary
2-DE:	two-dimensional electrophoresis
2D:	two-dimensional
aa:	amino acid
ACN:	acetonitrile
bp:	base pair
BSA:	bovine serum albumin
BVA:	biological variation module
CHAPS:	3-[(3-cholamidopropyl)dimethylammonio]-1-propanesulphonate
CID:	collision-induced dissociation
cM:	centimetre
Cy:	Cyanine
Da:	Dalton
DIGE:	direct in gel analysis
DNA:	deoxyribonucleic acid
dNTP:	deoxynucleoside triphosphate
DTT:	dithiothreitol
EDTA:	ethylenediaminetetraacetic acid
ESI:	electro spray ionisation
EtOH:	ethanol
FA:	formic acid
Fig:	figure
GE:	General Electric
H_2O:	water
HCCA:	α-cyano-4-hydroxycinnamic acid

HPLC:	high performance liquid chromatography
IEF:	isoelectric focusing
IF:	immunofluorescence
IPG:	immobilised pH gradient
KCl:	potassium chloride
kDa:	kilodalton
LC:	liquid chromatography
LMD:	laser microdissection
M:	molar
mA:	milliampere
MALDI:	matrix assisted laser desorption ionisation
ml:	millilitre
mm:	millimetre
mM:	millimolar
mRNA:	messenger RNA
MS:	mass spectrometry
MS/MS:	tandem mass spectrometry
m/z:	mass-to-charge
n:	number of replicates
NaCl:	sodium chloride
NaPO4:	sodium phosphate
NCBI:	National Centre for Biotechnology Information
ng:	nanogram
nl:	nanolitre
p:	pico
PAGE:	polyacrylamide gel electrophoresis
PBS:	phosphate buffered saline
PCR:	polymerase chain reaction
pH:	hydrogen ion concentration
pI:	isoelectric point
ppm:	parts per million
PS:	phosphoserine
RNA:	ribonucleic acid
RO:	reverse osmosis
rpm:	revolutions per minute
RT:	reverse transcription

RT-PCR:	reverse transcription polymerase chain reaction
SDS:	sodium dodecyl sulphate
TBE:	Tris/boric acid/EDTA buffer
TBST:	Tris-buffered saline Tween-20
TFA:	trifluoroacetic acid
TOF:	time of flight
Tris:	Tris (hydroxymethyl) aminomethane
U:	units
V:	volts
v/v:	volume per volume
w/v:	weight per volume
w/w:	weight per weight

Abstract

There is potential for significant improvements to be made in the diagnosis, staging, treatment and monitoring of colorectal cancer (CRC). The elucidation of proteins and pathways involved in CRC would aid in the development of biomarkers for detection, identify patients at risk of relapse and potentially give rise to new molecular targets of treatment. Laser microdissection (LMD) was used with minimal labelling two-dimensional gel electrophoresis (2D DIGE) and mass spectrometry to identify proteins significantly increased in eight early stage paired tumour-normal tissues. Seventeen individual proteins were identified as upregulated by >2 fold (P<0.05). The role of the proteins cytokeratin 8 (CK8) and SET in CRC were chosen for further analysis. A third protein, desmin, was chosen from a pilot study performed using LMD and saturation labelling 2D DIGE for further analysis.

The protein desmin was identified as significantly upregulated in a pilot study that aimed to identify proteins with altered expression in the cancerous epithelium and surrounding microenvironment. Using immunofluorescence (IF), desmin expression levels in the tissue stroma of late stage tumours compared to early stage tumours was significantly increased, P<0.0001. The desmin expressing cells were identified to be pericytes, formed around mature vasculature as a result of angiogenic stimulation. From this work desmin appears to have potential use as a histopathology marker for the identification of late stage patients and may help identify patients who would not benefit from the current anti-angiogenic therapies due to the presence of mature tumour microvasculature.

Three isoforms of CK8 were found to be upregulated in the DIGE study, with each isoform containing the phosphoserine (PS) residues 23, 431 and 73. Western blotting showed significantly increased phosphorylation levels at these sites in tumour compared to normal tissues. The MAP kinase ERK is known to phosphorylate the 73 and 431 residues and 50% of CRC patients have mutations in the EGFR/Ras/Raf/MEK/ERK signalling pathway (KRAS or BRAF mutations) resulting in constitutive ERK activation. Inhibition of EGFR activation in Caco2 cells showed a significant decrease (P<0.0001) in PS73 and PS431 levels by 59% and 65% respectively, indicating that patients with KRAS or BRAF mutations may have significantly increased PS73 and PS431 levels. Previously it has been shown that high levels of CK8 phosphorylation may help to protect cells against caspase degradation and evasion of apoptosis. This is the first report of the differential expression of phospho-CK8 isoforms in CRC.

SET is a known inhibitor of the tumour suppressor PP2A, a component of the GSK3 β complex that targets β catenin for degradation in the Wnt signalling pathway. Ninety percent of CRC patients have Wnt signalling pathway mutations resulting in constitutive pathway activation. The effect of knocking down SET via siRNA on β catenin levels was analysed in SW480 with constitutive Wnt signalling and

HEK293 with low levels of Wnt signalling. No changes in β catenin levels were observed in the SW480 cells, however a 24.5% reduction was detected in the HEK293 cells. The role of SET in other cancer associated pathways was analysed in the SET knock down cells using the RT^2 Profiler PCR Array 'Human Cancer Pathway Finder' plates with the expression of genes involved in apoptosis, angiogenesis and adhesion found to be altered.

1 Literature Review

1.1 Introduction

In 2005, 13,076 people were diagnosed with colorectal cancer (CRC) in Australia. Currently 1 in 23 people will develop CRC before the age of 75, making CRC the second most prevalent cancer in Australia (AIHW, Cancer in Australia: an overview, 2008). Early detection and correct staging results in significantly higher survival rates, but as yet there are no definitive non-invasive detection methods for the disease. Currently the diagnosis of CRC relies on the analysis of sample biopsies obtained by invasive procedures such as a colonoscopy. The development of a non-invasive assay for CRC would greatly aid in the screening and diagnosis of the disease. Patients diagnosed with CRC undergo tumour resection surgery, and those with lymph node metastasis also receive adjuvant therapy. Up to 30% of early stage patients who undergo presumably curative tumour resection surgery (who do not receive adjuvant therapy) relapse within five years. It is thought that disseminated tumour cells (that dislodge from the primary tumour during surgery, entering the lymphatic or peripheral circulation), can be the cause of such relapse. The improvement of assays able to predict patients at risk of disease relapse due to disseminated tumour cells would greatly aid in the treatment decision-making strategy for CRC.

The treatment of advanced CRC with current cytotoxic therapies has reached a plateau.[1] The detailing of the molecular pathways involved in the development of CRC such as cell cycle progression, apoptosis and angiogenesis has provided new molecular targets for treatment of patients with metastatic disease. Currently monoclonal antibody treatment designed to inhibit epidermal growth factor receptor (EGFR) activation is being used in a clinical trial setting, and has been found to significantly enhance the efficacy of standard treatment in some patients. The further elucidation of proteins and pathways altered in CRC could give rise to more treatment targets.

The main aim of this PhD was to identify protein biomarkers significantly upregulated in tumour tissue compared to matched normal mucosal tissue from patients with CRC. The secondary aim was to assess the use of such proteins as biomarkers for diagnosis, staging, detection of disseminated tumour cells, and as potential therapeutic targets.

1.1.1 Colorectal cancer development

CRC develops from the aberrant growth and reproduction of the epithelial cells lining the colon or rectum. The colon and rectum form the large intestine, and make up the last five to six feet of the digestive system, with the colon comprising the upper five feet, and the rectum comprising the last six inches of the large bowel (Fig. 1). The primary function of the colon and rectum is to prepare and pass waste products from food undigested in the stomach and small intestine and to absorb water and some vitamins and minerals. Hence epithelial cells lining the large intestine come into direct contact with all the food that remains undigested and enters the colonic luminal space.

(http://www.nlm.nih.gov/medlineplus/ency/imagepages/19220.htm)

Fig 1. The large intestine. The large intestine is comprised of the colon and rectum. Here water is absorbed from undigested food. Waste material is passed from the ileocecal valve of the ileum or small intestine, into the ascending colon at the cecum. The undigested waste is passed from the ascending colon through to the transverse, descending, and sigmoid segments, and finally into the rectum where the waste is expelled.

1.1.2 Anatomy of the bowel wall

The bowel wall is comprised of four distinct layers; the mucosa, submucosa, muscularis propria and subserosa (Fig. 2). The mucosa lines the inside of the intestine and has finger like fimbria that function to absorb water from food waste. The mucosa itself is comprised of three layers; the surface epithelium where epithelial cells form crypts, the lamina propria or basement membrane which is comprised of connective tissue, blood vessels and lymphatic vessels, and the muscularis mucosa that forms an outer layer of thin smooth muscle. A fifth layer, the serosa, forms a single cell layer on the outside of the colon. Cancer initiates in the mucosal lining that interfaces with the luminal space inside the colon, and penetrates through the bowel wall, invading normal tissue as it grows and develops. An example of a section of normal tissue compared to cancerous colon tissue is given in Fig. 3. The staging of CRC is based on the extent of tumour growth through the bowel wall, and on the extent to which the tumour cells have metastasised to local and distant sites.

NOTE:
This figure is included on page 4
of the print copy of the thesis held in
the University of Adelaide Library.

(http://oreilly.com/medical/colon/news/crc.0101.gif)

Fig 2. A cross-section of the colon. A schematic diagram of the colon wall cross-sectioned and displaying the various tissue layers.

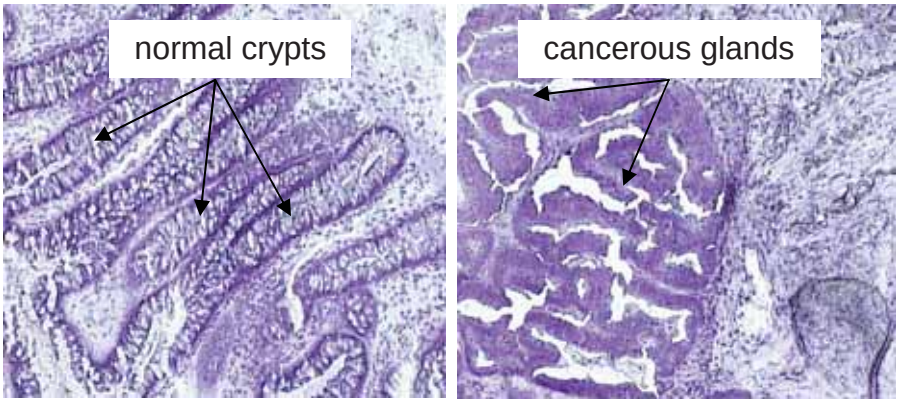

Fig 3. Normal and cancerous colon crypt morphology. Hematoxylin stained sections of normal (left) and cancerous (right) colonic tissue, 20 x magnification. In the section of normal tissue the epithelial cells form elongated crypts approximately 50 cells deep. In the cancerous tissue, the aberrant growth of the epithelial cells destroys the structure and morphology of the crypts.

1.1.3 Staging

The tumour node metastasis (TNM) staging is a standardised system used to describe the extent of the primary tumour growth into the wall of the intestine, the spread of metastatic cells to regional lymph nodes, and the metastasis of the primary tumour to other organs of the body (American Cancer Society http://www.cancer.org/) (Table 1, Fig. 4). Within the 'tumour' component of TNM staging there are five categories. 'Tis' is the earliest cancer stage and involves only the mucosa, a 'T1' cancer exhibits growth through the muscularis mucosa into the submucosa, a 'T2' exhibits growth through the submucosa into the muscularis propria, a 'T3' exhibits growth into the subserosa but not into neighbouring organs or tissues, and a 'T4' exhibits growth through the wall of the colon or rectum into neighbouring organs or tissues. Fig. 2 shows a cross section of the colon detailing the tissue layers. There are three 'node' TNM categories, 'NO' defines no lymph node involvement found, 'N1' defines metastatic cells found in one to three regional lymph nodes, and 'N2' defines metastatic cells found in four or more regional lymph nodes. There are only two TNM categories detailing metastasis, 'M0' is negative for metastatic spread to other organs, and 'M1' is positive for metastatic spread to other organs. Once the TNM categories of a patient have been assessed the information is compiled and the patient is classified as having stage I, II, III or IV CRC. A stage I cancer is defined as having grown through the muscularis mucosa into the submucosa or into the muscularis propria with no metastasis to lymph nodes or distant

sites. A stage II cancer has grown to or through the outer wall of the colon or rectum with no metastasis to lymph nodes or distant sites. A stage III cancer has grown through the muscularis mucosa or further and has lymph node metastasis. A stage IV cancer has spread to distant organs, commonly the liver or the lungs.

Table 1. TNM staging of CRC

T0	No primary tumour identified.
Tis	The carcinoma is in situ, limited to the mucosa.
T1	Involvement of submucosa, but no penetration through muscularis propria.
T2	Invasion into, but not penetration through, muscularis propria.
T3	Penetration through muscularis propria into subserosa, but not into peritoneal cavity or other organs.
T4	Invasion of other organs.
N0	No nodal metastasis.
N1	1–3 regional lymph nodes involved.
N2	4 or more regional lymph nodes involved.
M0	No distant metastases.
M1	Distant metastases.

(American Cancer Society http://www.cancer.org/)

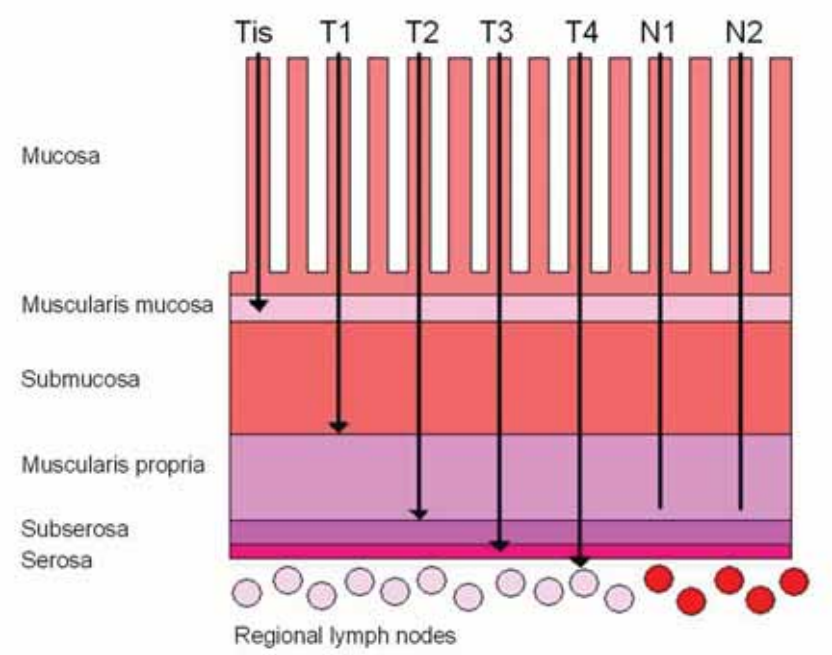

(American Cancer Society http://www.cancer.org/)

Fig 4. The TNM staging system for CRC. A diagram describing the staging of tumours based on their growth through the bowel wall and lymph node involvement.

1.2 The Genetic Basis of CRC

CRC can be hereditary, familial or sporadic. Hereditary CRC denotes a distinct and defined genetic basis. Familial CRC displays an increased predisposition to cancer, but it is still unknown whether there is a hereditary basis, such as the inactivation of vital tumour suppressor genes in the germline, or whether the predisposition is random. Studies performed on monozygotic twins suggest up to 35% of CRC may be attributed to genetic susceptibility.[2] Sporadic CRC is defined as 'being of average risk' within the population, or not of increased risk.[3] It is estimated that 70% to 80% of all CRC is sporadic, 20% to 30% is familial and 3% to 4% is due to hereditary conditions.[3] The study of hereditary and familial CRC has given great insight into the genetic development and progression of the disease.

1.2.1 Familial Adenomatous Polyposis (FAP)

FAP is an autosomal dominant disease that is responsible for approximately 1% of all CRC.[3 4] The disease is characterised by the onset and progression of hundreds to thousands of small adenomatous polyps that normally develop between the ages of twenty to thirty. A total proctocolectomy with ileoanal anastomosis (removal of the colon and rectum, with the connection of the terminal ileum of the small bowel to the anal canal) must be performed, as without it CRC will develop.[3] Mutation in the adenomatous polyposis gene (APC) is responsible for FAP[5,6 7] causing an activation mutation in the Wnt signalling pathway. Mutations of this pathway are the only known genetic alterations present in early premalignant lesions of the gastrointestinal tract.[8]

1.2.2 Hereditary nonpolyposis colorectal cancer (HNPCC) or Lynch Syndrome

HNPCC or Lynch Syndrome is an autosomal dominant disease that represents 3% to 4% of all CRC.[3,4] The risk of CRC for HNPCC patients is 80%, with relatively early onset of the cancer. Extra-colonic tumours are also common and can originate in the endometrium, ovary, stomach, bile duct, kidney, bladder, ureter or skin. HNPCC is caused by germline mutations in the mismatch repair (MMR) genes. Commonly genes mutated include MLH1, MSH2, and MSH6, which account for around 60% to 80% of the detectable germline mutations.[9-11] Somatic genetic alterations in the wild-type allele of the colonic and extracolonic tumours lead to DNA replication errors in repeat sequences.[9,12,13] This results in length changes of microsatellite sequences that can occur throughout the genome, resulting in microsatellite instability (MSI). Markers of MSI include BAT26, BAT25, D5S346, D2S123 and D17S250 as recommended by the American National Cancer Institute. Tumours are considered MSI high when positive for two or more markers, MSI low when positive for one marker, or MSI stable when no loci are found to be unstable. There are no unique histopathological features of MSI high tumours.

1.2.3 MUTYH associated adenomatous polyposis (MAP)

The MUTYH gene is a base excision repair gene (8-hydroxyguanine repair gene) found on human chromosome 1q33–34. Germline mutations in this gene have been found in association with colorectal adenomatous polyps.[14] Approximately 15% of patients with adenomatous polyps have no mutation in the APC gene, but biallelic mutations in MUTYH.[15] Inheritance of the disorder is autosomal recessive. Mutations in the MUTYH gene resulting in MAP are normally missense or nonsense, and the mutations Y165C and G382D account for greater than 80% of the known mutations. The risk of CRC in biallelic carriers of the MUTYH mutation is 100%, whereas there appears to be no increased risk for monoallelic carriers.[15,16]

1.2.4 Peutz-Jeghers syndrome

Peutz-Jeghers syndrome is a hamartomatous polyposis syndrome with an autosomal dominant mode of inheritance. A few medium sized to large hamartomatous polyps occur in the small bowel, stomach or colon of those affected in early childhood. The gene causing the disease is a serine/threonine kinase II (STKII) also known as LKB1.[17] Tumours associated with Peutz-Jeghers syndrome have a 19 bp loss of heterozygosity or somatic mutations in LKB1. LKB1 has known roles in cell proliferation and growth[18-22], cellular polarity[23] and metabolism.[24,25]

1.2.5 Juvenile polyposis

Familial juvenile polyposis (FJP) is an autosomal dominant syndrome, characterised by ten or more polyps in the gastrointestinal tract that appear in childhood to adolescence. However, juvenile polyposis can be sporadic. It is associated with an increased risk of CRC.[26] In tumours associated with juvenile polyposis, germline mutations have been found in the bone morphogenic protein receptor 1 (BMPR1A), SMAD4 and ENG[27,28], implicating the important role of the TGF β pathway.

1.2.6 Hyperplastic-serrated polyposis syndrome

Hyperplastic polyps were originally considered non-neoplastic, but a subset—classified as serrated polyps—are considered to present an increased predisposition to CRC. These polyps have a varying degree of adenomatous components. The mode of inheritance is unclear, but is probably heterogeneous.[29]

1.2.7 Sporadic CRC

Approximately 80% of all sporadic CRC contain somatic mutations in the adenomatous polyposis gene (APC), indicating the majority of CRC follow the adenoma-carcinoma sequence of tumorigenesis.[30] Around 15% of sporadic CRC are MSI high[31] and are thought to be caused by the hypermethylation of the MMR gene MLH1.[32,33] This is in contrast to HNPCC tumorigenesis, which is a result of MMR inactivation, not promoter hypermethylation. The gene BRAF is also commonly mutated at V600E in MSI high sporadic CRC, but not HNPCC patients.[34] Up to 1% of sporadic CRC contain biallelic germline MUTYH mutations.[35,36]

A study by Liechtenstein *et al* (2000)[2] assessed the environmental and heritable factors that contributed to a number of cancers, including colorectal. The study analysed data from over 44,000 pairs of twins, one of whom had developed cancer, listed in Swedish, Danish and Finnish twin registries. Based on the knowledge that monozygotic twins are genetically identical and dizygotic twins share approximately 50 percent of their segregated genes, they estimated the magnitude of the shared and non-shared contributions of genetic and environmental factors to the development of cancer. Using statistical modelling it was estimated that the contribution of non-shared environmental factors for CRC was 60%, suggesting environmental factors play a large role in the development of sporadic CRC. The heritable component of susceptibility to cancer contributed 35%.

1.3 Diet and lifestyle

Comparison of the incidence of CRC between developed and developing nations, and amongst migrant populations in Western countries, suggests environment and lifestyle may play an important role in CRC.[37] It is believed that dietary factors such as increased consumption of red meat, fat and refined carbohydrates may increase the risk of CRC, where as increased consumption of fibre from fruits and vegetables, calcium and β carotene may decrease the risk.[38,39] A positive correlation between low energy expenditure or physical activity and increased body size has also been shown.[40]

1.4 Wnt signalling

Intestinal epithelial adult stem cells are responsible for the normal cellular turnover and tissue repair in the colon and rectum. These cells reside in the bottom of the crypts in the large intestine, and as their progeny differentiate and amplify they migrate towards the middle of the crypts until they reach terminal differentiation and are shed into the lumen. Genetic defects in colon stem cells can lead to adenoma formation, and later carcinoma formation. The Wnt signalling pathway plays an important role in the

regulation of colon stem cell function and has been shown to play an important role in stem cell renewal.[41]

Wnt signalling induces two main intra-cellular signal transduction cascades; the canonical Wnt/β catenin dependent pathway and the β catenin independent pathway. Signalling in the β catenin independent pathway can transduce to the JNK (c-Jun N-terminal kinase) pathway known as the Planar Cell Polarity pathway, or to the Ca^{2+}-releasing pathway. Wnt proteins are secreted glycoproteins with at least nineteen known family members expressed in humans. They bind to the N-terminal extra-cellular cysteine-rich domain of the Frizzled receptors (Fz), of which there are ten Fz family members in humans. Fz receptors have seven transmembrane spanning domains with high topological similarity to G-protein coupled receptors. The co-receptors low-density-lipoprotein-related protein 5/6 (LRP5/6) are needed to moderate signalling between Wnt proteins and Fz receptors in the canonical Wnt pathway.[42] Upon binding of Wnt to the Fz and LRP5/6 receptor complex, the signal is transduced to the phosphoprotein Dishevelled (Dsh/Dvl) in the cytoplasm. Here the Wnt signal can transduce down either the canonical Wnt signalling pathway, the Planar Cell Polarity pathway or to the Ca^{2+}-releasing pathway. More than 90% of all CRC have an activating mutation in the canonical Wnt signalling pathway.

1.4.1 Canonical Wnt signalling

Canonical Wnt signalling controls the accumulation and translocation of β catenin from the cytoplasm into the nucleus. In the absence of Wnt signalling β catenin is degraded by β catenin degradation complex, comprised of Axin, adenomatosis polyposis coli (APC), protein phosphatase 2A (PP2A), glycogen synthase kinase 3 β (GSK3 β) and casein kinase 1 β (CK1 β).[43] CK1 β phosphorylates β catenin at serine 45, priming β catenin for GSK3 β phosphorylation at sites threonine 41, serine 37 and serine 33 respectively.[44] This targets β catenin for binding to the F-box protein β TrCP and subsequent ubiquitination and degradation by the proteosome (Fig. 5).[44] GSK3 β is active in resting cells and inactive during cell stimulation and response, generally leading to the dephosphorylation of its substrates. Activity of GSK3 β is regulated by Dsh, but the exact mechanism of this regulation is unknown. In stimulated cells, a complex is formed containing Axin, GSK3 β, Dsh and Frat1 protein. Upon Wnt binding to the Fz and LRP5/6 receptor complex, Dsh is recruited to the membrane and is phosphorylated. It is thought this may cause a conformational change, allowing Frat 1 to mediate the dissociation of GSK3 β from Axin. GSK3 β is now unable to phosphorylate β catenin, allowing it to accumulate in the cytoplasm and translocate to the nucleus (Fig. 6). The presence of PP2A in the GSK3 β complex has been shown to result in decreased β catenin levels, due to the inhibition of Wnt signalling. [46] The catalytic unit of PP2A binds directly to Axin[45] and the regulatory subunit binds the N-terminus of APC.[46]

Within the degradation complex, APC and Axin form a scaffold that allows GSK3 β to specifically phosphorylate β catenin. GSK3 β also phosphorylates APC and Axin. The phosphorylation of Axin by GSK3 β is important for its stability. In the presence of Wnt signal, the degradation complex is dissociated and Axin is dephosphorylated. Axin then translocates to the membrane where it binds to a conserved sequence in the cytoplasmic tail of LRP5/6.[47] [48] A decrease in the cytoplasmic levels of Axin have been observed [49] upon dephosphorylation.

Once the activity of GSK3 β is inhibited β catenin stabilises, accumulates in the cytoplasm, and translocates to the nucleus. In the nucleus β catenin acts as a transcriptional co-activator. β catenin does not directly bind to DNA, but has a C-terminal transactivation domain[50] and acts as an essential cofactor for the TCF/LEF transcription factors. The TCF/LEF family is comprised of four proteins; TCF1, LEF1, TCF3 and TCF4, all of which contain a high-mobility group box (HMG) that binds DNA in a sequence specific manner.[51] Other target genes of Wnt signalling involved in CRC include c-myc, cyclin D1, cyclooxygenase 2 (COX2), PPAR-delta and matrix metalloproteinase 7 (MMP7) or matrilysin. In the absence of β catenin binding, the transcription of TCF/LEF target genes is inhibited by the binding of the transcriptional repressor proteins Grg or groucho to TCF1, LEF1, TCF3 and TCF4.[52] [53] Once bound, the Grg proteins recruit histone deacetylases to condense chromatin.

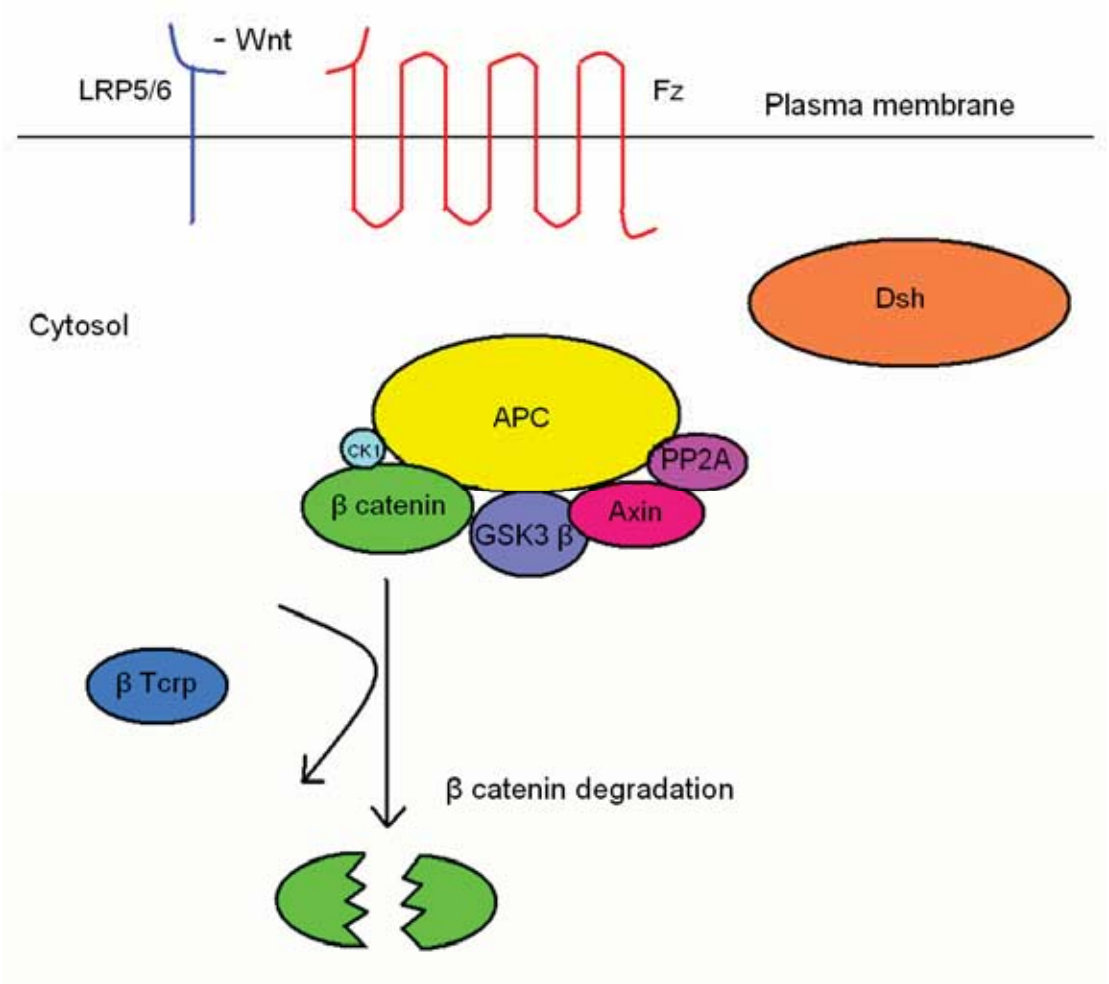

Fig 5. The Wnt signalling pathway in the absence of Wnt signal. When no extracellular Wnt ligand is present, a β catenin degradation complex is formed comprised of APC GSK3 β, Axin and PP2A. CK1 phosphorylates βcatenin, priming the protein for phosphorylation by GSK3 β. This targets β catenin for binding to the F-box protein β Trcp, resulting in ubiquitination and degradation by the proteosome.

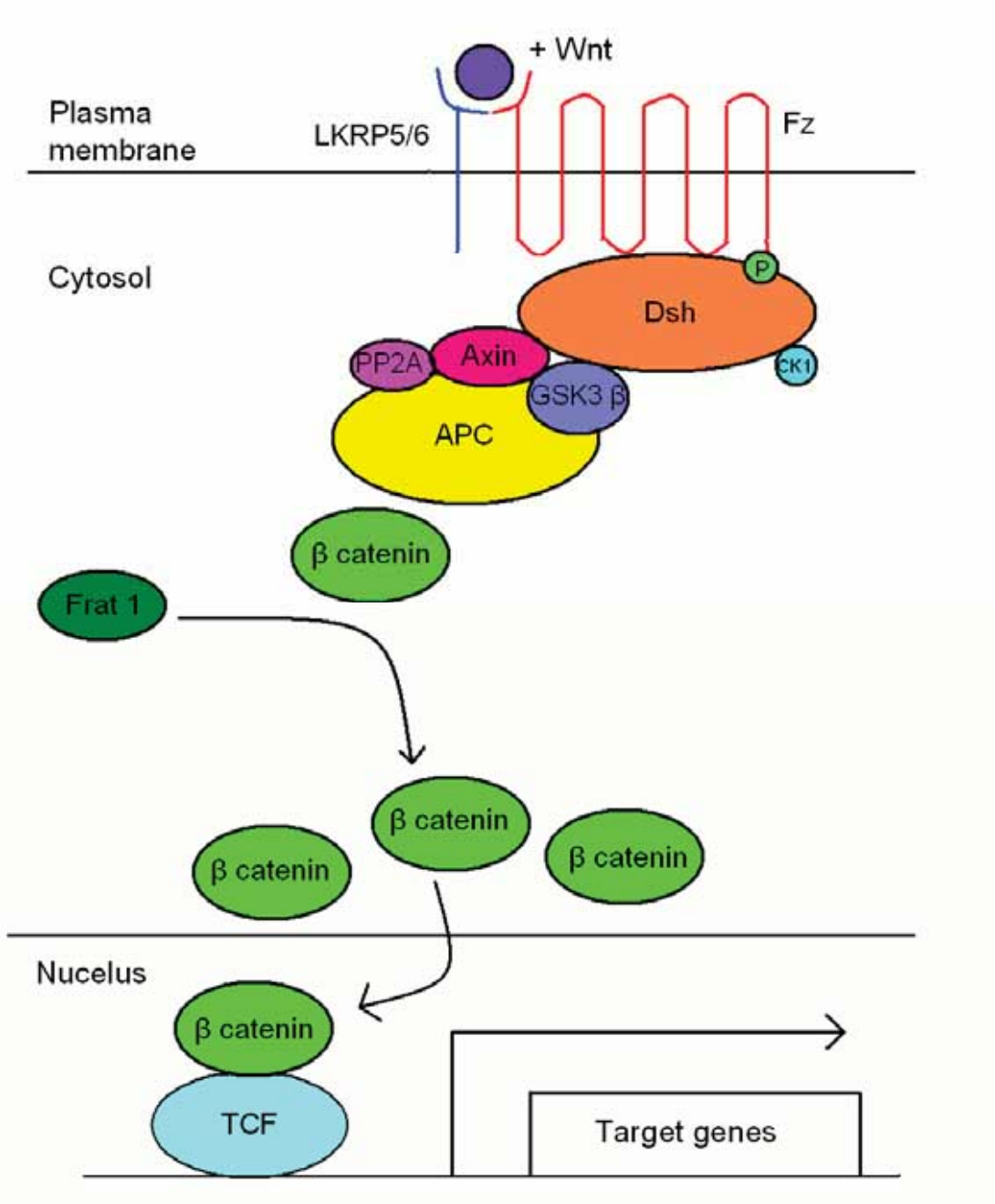

Fig 6. Activated Wnt signalling. Extracellular Wnt binds to a receptor complex formed by Fz and LRP5/6. Binding of Wnt leads to the recruitment of Dsh to the membrane where it is phosphorylated causing a conformational change that allows Frat 1 to mediate the dissociation of GSK3 β from Axin. GSK3 β is no longer able to phosphorylate β catenin, resulting in the accumulation and translocation of β catenin to the nucleus where it acts as a transcriptional co-activator.

1.4.2 APC Mutations in CRC

APC is mutated in approximately 85% of CRC cases, with over 300 disease-causing mutations reported in the gene.[54] Most APC mutations are insertions, deletions and nonsense mutations resulting in frameshifts and premature stop codons in the gene transcript. This leads to truncated APC proteins with a broad range of molecular masses smaller than the predicted 310 kDa of the wild-type protein. Wild-type APC contains three 15 amino acid repeats and seven 20 amino acid repeats that bind with β catenin. Truncation of the protein eliminates too many of the 20 amino acid binding sites used by β catenin, allowing β catenin to escape phosphorylation by the degradation complex. The APC gene has an open reading frame of 8,538 nucleotides, containing 15 exons, with exon 15 being the largest coding region of 6.5 kb. The germline mutations appear throughout all the exons, in particular exon 15. The most common APC mutation is a deletion of AAAAG in codon 1309 that appears in 10% of FAP patients.[54]

Commonly in CRC, germline mutations of APC lead to truncation of the protein product and to the initiation of the 'adenoma-carcinoma' sequence.[30,55] Further mutations in genes such as KRAS and p53 are needed for the transformation of adenomas to carcinomas with invasive growth and metastatic properties.

1.4.3 β catenin mutations in CRC

Mutations in the gene encoding β catenin, CTNNB1 are present in approximately 10% of the cancers that do not contain an APC mutation. Mutations in APC and CTNNB1 appear to be mutually exclusive. However, β catenin mutations in small adenomas are less likely to develop into large adenomas and invasive carcinomas, suggesting β catenin and APC mutations do not result in exactly the same cellular pathology.[56] CTNNB1 mutations commonly occur in the area of exon 3, resulting in the inability of GSK3 β to properly phosphorylate and target β catenin for degradation.[57]

1.5 CRC statistics and therapy

1.5.1 Australian statistics

The National Cancer Statistic Clearinghouse at the Australian Institute of Health and Welfare (AIHW) (http://www.aihw.gov.au/cancer/data/index.cfm) compiles data on CRC in Australia. The last set of information published was in December 2005 in which CRC was found to be the most common cancer in Australia (excluding basal cell carcinoma), and is the second most common cause of cancer related deaths. Interestingly, the incidence rate of CRC was found to have increased 43% from 1983 to 2001.

This large increase was put down to an ageing population, as the incidence of sporadic CRC increases significantly in people over the age of 75. The incidence rates in men and women over the age of 75 are one in 17 and one in 26 respectively, and CRC in people under the age of 65 is rare.[58] However, when these statistics were age standardised an increase of 15% from 1983 to 2001 was still found. It is thought better detection and public awareness accounts for the majority of this increase.

The age standardised mortality rate from CRC has decreased 32% from 1983 to 2002 (32.0 deaths per 100,000 population in 1983 to 21.7 deaths per 100,000 in 2002). The relative five-year survival rates are in concordance with the mortality rates, as they have improved from 50% in 1982–1986 to 58% in 1992–1997 for men, and from 52% in 1982–1986 to 59% in 1992–1997 for women.[59] Such improvements can be explained by better surgical outcomes, better and earlier detection, and by better therapy targeted at treating metastatic cells in later stage patients following primary tumour resection surgery.

1.5.2 Treatment

CRC is a potentially curable disease depending on the stage at which the tumour is detected. The survival and relapse rates are greatly improved for patients who receive treatment while the cancer is still contained within the bowel wall and has not yet metastasised. A South Australian study performed on data collected from 1980 to 1995 found that the relative five year survival rates of patients with stage I disease was 88%, stage II was 70%, stage III was 43%, and stage IV was 7%.[60] Hence, 57% to 93% of patients with late stage disease relapsed and died within five years of their treatment, and up to 30% of early stage patients who underwent presumably curative tumour resection surgery also relapsed and died within five years of their treatment.

1.5.3 Surgery relapse rates

The majority of CRC patients that undergo potentially curative tumour resection surgery have stage II or III disease, and following surgery only stage III patients are offered adjuvant chemotherapy due to lymph node metastases. Surgery for stage II patients is presumed curative. It is controversial as to whether stage II patients should be offered adjuvant chemotherapy following surgery. Such therapy has not been shown to produce a significantly different five year survival rate in stage II patients.[61]

The high relapse rate of stage II and III patients is a result of a number of factors. As stage III patients present with later stage disease, their chances of the surgery being curative are decreased. During diagnosis, if an inadequate number of lymph nodes are sampled, metastases may be missed and stage

III patients may be misdiagnosed as stage II patients.[62] These patients would undergo surgery, but not be given adjuvant chemotherapy. A study by Liefers *et al*. (1998)[63] used reverse transcription (RT) PCR to detect carcinoembryonic antigen (CEA) mRNA in lymph nodes removed from 26 stage II CRC patients who had undergone curative tumour resection surgery. Lymph node metastases were detected in fourteen of the patients, only 50% of whom were alive after five years (seven patients died due to tumour recurrence), in comparison to 91% of patients who had been detected as negative for lymph node metastasis. Another explanation for the high relapse rate is that residual disease may be left from the tumour resection[64] or that viable tumour cells may dislodge from the tumour during removal. These cells may remain in the colon, in the peritoneal cavity or may enter the bloodstream.[65] Such cells are termed disseminated or circulating tumour cells.

1.6 Disseminated tumour cells

A number of studies have linked the presence of disseminated tumour cells at the time of surgery to recurrent local or metastatic disease[65] [66]. Work done previously in the laboratory used the immunobead technique[67] [65] with a panel of five CRC markers to detect occult disseminated tumour cells in the peripheral venous blood and intra-peritoneal saline lavage fluid of stage II and III patients post tumour resection. The study found 41 of 125 (32.8%) early stage patients were positive for disseminated tumour cells. This data was able to predict 80% of the patients who relapsed within five years post-surgery. Guller *et al*. (2002)[68] used real-time reverse transcription PCR to detect CEA and CK20 transcripts in the peritoneal lavage fluid, peripheral and mesenteric venous blood of 39 patients undergoing curative resection. Disseminated cells were detected in eleven of the patients, and after twelve months, nine of these patients had recurrence. In comparison, only two of the 28 patients who were negative for disseminated cells had recurrent disease. Seven patients were detected as being positive for tumour cells in their peritoneal lavage fluid, and after 31 months, five of these patients (71%) had relapsed. A study by Schott *et al*. (1998)[66] used monoclonal antibodies directed against four tumour associated antigens to detect disseminated cells in the peritoneal lavage fluid of CRC patients undergoing tumour resection surgery. Thirty-five of 105 patients (33%) were found to have disseminated cells in their peritoneal lavage, and after four years, 28% of these patients were alive compared to 60% of patients who were negative for disseminated cells *(*P=0.0079).

These studies illustrate that stage II patients undergoing tumour resection surgery may benefit from adjuvant chemotherapy if found to be positive for disseminated tumour cells. Currently this laboratory uses immunomagnetic beads to extract epithelial cells from pre- and post-operative lavage fluid and peripheral blood samples taken from patients who have undergone tumour resection surgery. The immunomagnetic beads are coated with an antibody against the epithelial specific cell surface protein

EpCAM (also known as tumour-associated calcium signal transducer 1, TACSTD1), a cell adhesion molecule expressed on the surface of both cancerous and normal epithelial cells.[69] During the process of surgery a mixture of normal and cancerous colorectal epithelial cells are shed from the site of excision and may enter the patient's peripheral blood. In order to differentiate between normal and cancerous epithelial cells captured by the immunobeads real-time RT-PCR with a panel of CRC markers is performed on the RNA extracted from the captured cells. The detection of such cells depends on the sensitivity and specificity of tumour markers. In the study by Lloyd *et al*. (2006)[65], the markers carcinoembryonic antigen, laminin γ 2, ephrin B4, matrilysin, and cytokeratin 20 were used. While the markers were able to predict 80% of the patients who relapsed, 23% of patients who did not relapse and 22.8% of negative control patients with benign disease were detected as marker positive. This suggests more specific biomarkers for the immunobead RT-PCR need to be found. Accordingly, a specific aim of this PhD was to improve the marker panel for the immunobead RT-PCR technique by comparing the profile of enriched epithelial cells from matched paired tumour normal tissue samples.

1.7 Current CRC Biomarkers

Currently the only marker for CRC used in a clinical setting is carcinoembryonic antigen (CEA). The American Society of Clinical Oncology (ASCO) publishes guidelines on the use of markers for CRC screening, diagnosis, staging, surveillance, and the monitoring of treatment (http://www.cancer.org/docroot/CRI/content/). The most recent guidelines were released in 2006[62] and were based on data published since 1999. In these guidelines, CEA was not recommended in the screening of CRC. The sensitivity level of CEA for early stage patients is poor, as CEA is abnormally up regulated in only 4% of stage A and 26% of stage B patients.[70] CEA levels are also commonly increased in various benign diseases and cancers other then CRC, and may not be elevated at all in CRC patients regardless of stage [71,72] . It is estimated that as many as 60% of all CRC would be missed if CEA testing were to be used alone.[71,72] However, the ASCO ascertained pre-operative testing may be useful in staging and surgical treatment and that elevated levels above 5 mg/ml in blood may correlate with poorer prognosis. Therefore CEA should not be used to determine if a patient should receive adjuvant chemotherapy. CEA may also be useful in the post-operative monitoring of metastatic disease in stage II and III patients, who may benefit from regular testing for a minimum of three years.

Other markers assessed by the ASCO were CA 19–9, DNA ploidy or flow cytometric analysis, p53, ras, microsatellite instability/hMSH2 or hMLH1 and 18q loss of heterozygosity/deletion. Data was found to be insufficient to recommend the use of any of the markers in screening, diagnosis, staging, surveillance or the monitoring of treatment in CRC.

1.7.1 Biomarker discovery work performed previously in the laboratory

Previously in this laboratory, a microarray study had been performed with the aim of identifying tumour-specific markers for the detection of disseminated tumour cells in patient peripheral venous blood and intra-peritoneal saline lavage fluid samples collected after tumour resection surgery.[73] In order to identify genes with the greatest level of differential expression between matched pairs of colon tumour and normal tissues, an 8 K human cDNA microarray was probed with samples from four patients. The cDNA microarray analysis found the gene DPEP1 to be upregulated in two of the four tumour samples. Relative real-time RT-PCR was carried out on 68 matched paired tissue samples in order to verify the upregulation of DPEP1 in CRC. Eighty-two percent (56/68) of tumours had an expression ratio of ≥2 compared to matched normal tissue. The mean expression of DPEP1 mRNA between colon tumour and normal mucosa was significantly different, $P=3.3 \times 10^{-}$.[15] There was no statistical difference in mean expression of DPEP1 mRNA in colon tumour samples between the stages of disease (P=0.65). DPEP1 was used as a marker in the immunobead RT-PCR technique to identify disseminated tumour cells in intra-operative lavage and venous blood samples from 38 CRC cases. Fifteen samples (39%) were found to be positive for DPEP1 expression, suggesting the presence of disseminated tumour cells. However, four control patients with inflammatory bowel disease were also positive for DPEP1 expression, indicating DPEP1 is not a highly specific marker for CRC. Following this microarray study, it was decided the proteomic profiling CRC tissue may lead to the discovery of a different subset of potential markers, as the expression of a gene at the mRNA level and protein levels usually correlate.

In a separate study in this laboratory, RT-PCR was performed on colorectal lymph node tissues from 44 CRC patients, and on fourteen controls with benign bowel disease.[74] The expression of the markers CEA, cytokeratin 20 (CK20), and guanylyl cyclase C (GCC) were analysed. The study was performed to assess the markers ability to detect lymph node metastasis. Lymph node metastasis are the main determining factor when selecting patients for adjuvant therapy, and whilst adjuvant therapy has been shown to increase the survival times of late stage patients, it has not been shown to increase the survival of early stage I and II patients. Hence, accurate staging of patients is of great importance when deciding their treatment course. Commonly, lymph node metastases are diagnosed by histological staining and examination of tissue sections with hematoxylin and eosin stains. One or more sections are examined, but not usually the whole lymph node, hence micrometastatic foci may be missed. The markers CEA, CK20 and GCC were identified by RT-PCR in 97.9%, 91.5% and 95.7% respectively of lymph nodes containing metastasised cells by routine histopathology. The markers also detected tumour cells in 43.9% of the lymph nodes that were deemed negative by routine histopathology. Only 6.1% of lymph nodes from the benign bowel disease control samples were positive for one or more of the markers. The detection of marker expression in the lymph nodes of CRC patients who were deemed negative by routine histopathology may be due to the presence of tumour cells or normal epithelial cells

that had been shed into the lymphatic circulation. It is known that normal epithelial cells are shed from the colon and rectum during surgery when the bowel wall is excised.[67] All of the markers discussed above are expressed under normal conditions by epithelial cells and may explain why a number of nodes were found to be marker positive by RT-PCR, yet tumour cell metastasis negative by routine histopathology. Therefore the identification of lymph nodes positive for metastasis by RT-PCR would be greatly improved by the inclusion of markers with increased specificity for carcinoma cells compared to normal epithelial cells.

1.7.2 The Effects of Inflammatory Bowel Disease and Benign Tumours on CRC Biomarker Discovery

In previous biomarker discovery projects, such as the ones discussed above, a perpetual issue has been the detection of potential markers in control patients with inflammatory bowel disease (IBD) and benign tumours or polyps. In the study by Lloyd *et al*. (2006) 70 patients with nonmalignant surgical colorectal disorders were used as negative controls, including patients with IBD, diverticulitis and polyps. Marker positive samples were found in 12 of 70 (17.2%) patients having surgical resection for nonmalignant colorectal disorders. At least one of the markers (Cytokeratin 20, CEA, carcinoembryonic antigen, Ephrin type-B receptor 4, laminin-5 g2 chain, matrilysin) were found to be positive in at least one patient sample in either the pre- or post-resection lavage fluid or the post-resection peripheral blood. This displays the difficulty in identifying markers with high levels of specificity. One aim of this biomarker discovery work was to identify markers with higher levels of tumour specificity.

1.8 Current detection methods for CRC

Common symptoms of CRC include prolonged changes in bowel habits (such as diarrhoea or constipation), rectal bleeding or blood in the stool, cramping or abdominal pain, and weakness and fatigue. Symptoms do not normally manifest until the cancer is progressed. Such symptoms may also be associated with a number of other diseases and conditions such as infection, haemorrhoids, diverticulosis or colitis. Currently a physical examination and a number of tests may be used to aid diagnosis. A complete blood count can be used to check for anaemia, as prolonged tumour bleeding in a CRC patient can result in a significant loss of red blood cells. A faecal occult blood test (FOBT) is used to look for small amounts of blood in faeces. If the FOBT comes back positive, a colonoscopy is required to determine the source and cause of bleeding as it may occur from the colon, rectum or digestive tract and may be caused by cancer, polyps, ulcers, haemorrhoids, diverticulosis or colitis.

A number of screening methods can be used to look for colorectal polyps or cancer. Computed tomography (CT) scans may be used to look for abnormal growths in the colon and rectum, and to check for cancer spread to other organs. A CT guided needle biopsy may also be used to sample an abnormal growth, which can then be analysed by a pathologist. Magnetic resonance imaging (MRI) scans may be used to analyse the extent of rectal cancers and to check for secondary cancers in the abdomen and liver. Alternatively a sigmoidoscopy can be used to visualise the entire rectum and abnormal growths may be biopsied, but only about half of the colon can be visualised due to the length of the sigmoidoscope tube. A colonoscopy is able to visualise the entire length of the colon and rectum and to sample any polyps and abnormal growths. Biopsied specimens are then analysed by a pathologist for diagnosis. Currently, biopsies are the only definitive method of diagnosing CRC.

Despite the conclusive nature of diagnosing CRC by biopsy, the procedures are not entirely favourable as they are invasive, can cause discomfort and possible associated complications. Following sigmoidoscope or colonoscopy prolonged bleeding may occur, and in rare cases the sigmoidoscope or colonoscope may perforate the bowel wall resulting in reparative surgery. Hence more definitive non-invasive detection methods for CRC are required.

1.9 Better therapy

1.9.1 Current therapy

From the mid-seventies up until the nineties, patients with metastatic CRC received treatment with 5 fluorouracil (5 FU) alone. The overall response rate to the treatment was approximately 10% with a median survival of ten months.[75] The main mode of action of 5 FU in the treatment of CRC is as a thymidylate synthase inhibitor thus blocking the synthesis of pyrimidine to thymidine, a nucleotide required for DNA replication. 5 FU treatments may be administered by a bolus or by infusion to block DNA synthesis therefore inducing cell cycle arrest and apoptosis. Over the last ten years 5 FU has been used in combination with leucovorin (LV), or in combinations of 5 FU/LV with irinotecan, or 5 FU/LV with oxaliplatin.[76] The use of LV, also known as folinic acid, with 5 FU improved response rates by 23%.[77] In CRC treatment, LV is used to enhance the efficacy of 5 FU by inhibiting thymidylate synthase and the addition of irinotecan or oxaliplatin to treatment regimes has seen the overall survival rate of patients nearly double. Irinotecan can also be used in conjunction with 5 FU/LV as a chemotherapy agent as irinotecan is activated by hydrolysis to SN-38, which acts as an inhibitor of topoisomerase 1, leading to the prevention of DNA replication and transcription. Oxaplatin may also be used with 5 FU/LV, however the exact mode of action of oxaplatin is unclear, but it is thought to also inhibit the replication of DNA. It has been shown that the most important factor in the efficacy and outcome of such cytotoxic

chemotherapy is that all active treatments are given, regardless of the sequence or combination in which they are given.[1] This indicates the treatment of advanced CRC with current cytotoxic therapies has reached a plateau.

1.9.2 Targeted therapies

The detailing of the molecular pathways involved in the development of CRC, such as cell cycle progression, apoptosis, angiogenesis and invasion has provided new molecular targets for treatment of patients with metastatic disease. Currently treatments designed around the inhibition of vascular endothelial growth factor (VEGF) and epidermal growth factor receptor (EGFR) are being used in clinical trials here in this institution.

The inhibition of VEGF is based on the dependence tumours have on angiogenesis.[78] New blood vessels are formed in the tumour and are regulated by the secretion of pro-angiogenic factors such as VEGF, platelet derived growth factor, and angiopoietin-1, by the cancerous epithelia and surrounding stromal cells. This promotes the activation of endothelial cells within the cancerous tissue. VEGF is a heparin-binding glycoprotein, critical in the regulation of neoangiogenesis, and is an endothelial cell mitogen. VEGF receptors contain an extracellular ligand-binding domain, a transmembrane domain and an intracellular tyrosine kinase-binding domain. The tyrosine kinase domain of the receptor is activated upon VEGF binding, resulting in the activation of signal transduction pathways such as raf/MEK/ERK, PI3K/AKT, and mTOR.

Bevacizumab is a humanised monoclonal antibody against VEGF that when combined with infusional regimes of 5 FU/LV with either irinotecan or oxaliplatin, has had modest effects in terms of survival rates (reviewed in [79]). Other anti-angiogenic treatments involve the use of tyrosine kinase inhibitors such as Sunitinib and Vatalanib, but unfortunately both treatments have failed to show significantly increased disease free survival in metastatic CRC (reviewed in [79]).

EGFR is from the ErbB family of transmembrane receptor tyrosine kinases. EGFR inhibition is being targeted in treatment as receptor activation results in the initiation of signal transduction pathways that promote the differentiation and survival of epithelial cells. Hence, increased EGFR signalling is advantageous to carcinoma cells. Like the VEGF receptor, EGFR has an extracellular ligand-binding domain, a transmembrane domain and an intracellular tyrosine kinase-binding domain. EGF, TGF α, epiregulin and amphiregulin are endogenous ligands of EGFR. Upon ligand binding and tyrosine kinase domain activation, the Ras/raf/MEK/ERK1/2 and PI3K/PTEN/Akt pathways are activated. The upregulation of EGFR has been found in 60% to 70% of CRC.[80] [81] [82] Currently EGFR activation is

inhibited by either blocking the ligand-binding site of the receptor, or by blocking the activation of the tyrosine kinase domain.

Treatment with the chimeric IgGI monoclonal antibody against the ligand binding site of EGFR, Certuximab, has been shown to significantly improve the response rate and progression free survival by a month when used in the first line of treatment with 5 FU/LV and irinotecan (reviewed in [79]). In second line treatment, patients who were treated with irinotecan plus Cetuximab had a progression free survival 63% longer than patients who received irinotecan alone.[83] Gefitinib, a tyrosine kinase inhibitor of EGFR, has not been shown to enhance efficacy of treatment in first or second line settings.[84]

It is important to note that the mutation status of proteins downstream of a molecular target is highly relevant to the efficacy of treatment. Mutations in KRAS and BRAF are present in approximately 36% and 12% of CRC patients respectively, and appear to be mutually exclusive. These mutations cause the constitutive activation of the Ras/raf/MEK/ERK1/2 pathway, downstream of ligand binding and EGFR tyrosine kinase domain activation. Hence inhibition of EGFR activation with Cetuximab or Gefitinib will have no benefit to KRAS or BRAF mutation positive patients. Similarly patients positive for PTEN mutations are also unlikely to benefit from Cetuximab or Gefitinib treatment as PTEN mutations cause constitutive activation of the PI3K/PTEN/Akt pathway, downstream of ligand binding and EGFR tyrosine kinase domain activation. Therefore, mutation status screening of patients prior to the administration of targeted therapies may see the efficacy levels rise.

1.10 Detection of differentially expressed proteins in CRC

There is potential for significant improvements to be made in the diagnosis, staging, treatment and monitoring of CRC. The elucidation of upregulated proteins and pathways in CRC that lead to enhanced disease pathogenesis would aid in the development of biomarkers for the detection of disease, the prediction of patients at risk of relapse, and potentially give rise to new molecular targets of treatment. The technique of two-dimensional difference gel electrophoresis (2D DIGE) coupled with mass spectrometry allows for the detection and identification of differentially expressed proteins across a cohort of tumour-normal samples.

1.10.1 2D DIGE

Two-dimensional electrophoresis (2DE) involves the separation of proteins based on their isoelectric points (pI) and molecular weight (MW) providing a protein spot 'map' that can be visualised with the fluorescent labelling of protein samples prior to electrophoresis, or post-electrophoresis with protein stains such as Coomassie blue, sypro ruby or silver stain. The separation of proteins is influenced not

only by pI and MW, but also by protein solubility and abundance. Two thousand to five thousand protein spots can be resolved by 2DE with the detection of less than 1 ng of protein in a single spot.[85] Separation and analysis of complex lysates by 2DE confers a number of advantages to other proteomics methods, such as liquid chromatography tandem mass spectrometry (LC-MS/MS) alone. Separation by 2DE allows for the visualisation and quantification of intact proteins (as opposed to peptides) and visualisation of protein isoforms with post-translational modifications (PTMs). Mass spectrometry is required to identify proteins of interest excised from 2DE gels, and ideally 2DE and LC-MS/MS are used in conjunction with each other.

Challenges involved with 2DE include the detection of low abundance proteins and highly hydrophobic proteins, such as membrane proteins, which are difficult to solubilise. In complex lysates from eukaryotic cells as many as 10,000 different proteins may be present, with abundant housekeeping proteins in copy number of up to 10^6 per cell in comparison to lowly abundant signalling molecules that may be present in copy number of less than 100 per cell.[85] However, the detection of low abundance proteins can be improved by the enrichment of samples and by the quality of analysis methods used. The enrichment of cancerous and matched normal cells from tissue by laser microdissection reduces cell type heterogeneity within a sample, thus greatly improving the detection of biologically relevant proteins. The detection of low abundance proteins can also be improved by increasing the sensitivity of protein detection/visualisation, and by increasing the quality of the quantification method used. Another common problem encountered by traditional 2DE is technical gel to gel variation that has made 2D gels notoriously difficult to replicate[86] and difficult to confidently detect and quantify differences in protein expression. This has meant that traditionally multiple gel replicates have been needed to be produced per sample. The sensitivity of detection, quantification and the ability to confidently detect real changes in protein expression levels have since been improved with the technology of two-dimensional difference gel electrophoresis (2D DIGE).

2D DIGE was pioneered by Unlu *et al*. (1997)[87] who used minimal CyDyes to label protein preparations prior to electrophoresis, thus allowing multiplexing of samples within a single gel. Three spectrally distinct fluorophores are available (Cy2, Cy3, Cy5) containing N-hydroxysuccinimidyl esters that form an amide with lysine epsilon amine groups on proteins by a nucleophilic substitution reaction (GE Healthcare, Sweden). The protein to dye labelling ratio is low at only 1% to 2%, so that each visualised protein is likely to have one dye molecule attached. All three dyes are of a very similar molecular weight and are positively charged to match the charge on lysine groups, meaning there is only a very small to no shift in protein isoelectric points. Due to the three CyDyes available, the DIGE technique can be used to effectively compare and quantify the protein expression profiles of matched pairs of colon tumour-normal mucosa within a patient and across a patient cohort without multiple technical replica gels. The

Cy3 and Cy5 dyes (Amersham Biosciences) are used to separately label the normal and tumour protein extracts, and the Cy2 dye is used to label an internal standard, generated by pooling equal amounts of each of the tumour and normal samples within the tested cohort. Equal amounts of the differentially labelled matched tumour and normal samples are separated within a single gel, along with the labelled internal standard. This alleviates the problem of spot matching within tumour-normal pairs. The gels are then scanned at three different emission frequencies corresponding to the fluorescence of each of the dyes and these scans are analysed using the DeCyder software (GE Healthcare). Abundance changes over a linear dynamic range of four to five orders of magnitude are obtainable with the CyDyes. Using the pooled internal standard, the differential in-gel analysis (DIA) module of the DeCyder software performs pair-wise comparisons of each tumour and normal sample to the internal standard, generating protein spot abundance ratios. The biological variation analysis (BVA) module then simultaneously matches all of the spot maps across the patient cohort and uses the 'tumour: internal standard' and 'normal: internal standard' ratios to calculate the average abundance change and significance value (Student's paired T-test) of each tumour-normal protein pairs across all of the patients.

A significant advantage of DIGE is its ability to detect significant abundance changes of proteins based on their variance from the mean due to the presence of the internal standard. If the internal standard is not used and abundance changes are detected—based on a direct comparison of tumour-normal pairs—the identification of a significant abundance change would be limited to the designated confidence level, e.g. 95th percentile, based on the variation between samples. This means the greater the difference between tumour-normal samples, the higher the abundance change must be to meet the confidence level. When the internal standard is used, the identification of significant abundance changes is based on the variance of the mean change within the cohort. This allows biologically relevant changes in protein abundance between tumour-normal samples to be detected at a higher confidence level. A study by Friedman *et al*. (2004)[88] analysed whole colon tumour-normal tissue from six patients using 2D DIGE and found 83 spot features to be significantly changed in abundance across the cohort, of which 40 would not have been identified as significant changes if the internal standard had not been present.

1.10.2 2D DIGE and CRC

To date, a number of studies have used minimal labelling 2D DIGE to examine whole biopsies of colorectal tumour and normal tissue. Friedman *et al.* (2004)[88] analysed extracts from whole pieces of matched paired tissue from six CRC patients of different stages and a number of proteins were found to be significantly differentially expressed across the patients, both upregulated and downregulated. The proteins leukocyte elastase inhibitor, macrophage capping protein, α-1-antitrypsin, α-tubulin,

tropomyosin-α-1, tropomyosin-α-4 chain, an actin fragment, annexin 5, annexin 3, P13693 translationally controlled tumour protein and calgranulin B were found to be upregulated by >2 fold across the six patients, *P*<0.05. However, no validation experiments were carried out in this study. Alfonso *et al*. (2005)[89] compared seven matched tumour-normal pairs and found 53 proteins to be significantly differentially expressed, with 41 of the 53 proteins successfully identified by mass spectrometry, of which 32 were individual proteins (the remaining nine were isoforms). The identified proteins functioned in the regulation of transcription, cellular reorganisation and cytoskeleton, cell communication and signalling, and protein synthesis and folding. MTA1 protein, SSX5 protein, dynein heavy chain, CPS1 (cytochrome P450), cytokeratin 10, cytokeratin 8, vimentin, and annexin IV were found to be significantly upregulated >2 fold across the seven patients. The upregulation of MTA1, cytokeratin 8 and vimentin were confirmed by western blotting. Another study used tissue from seven patients to analyse basic proteins in the pH range 7–10.[90] Thirty-four spot features were found to be significantly altered in expression, with eleven distinct proteins significantly upregulated >2 fold. These proteins were identified as enolase 1, fructose-bisphosphate aldolase A, GAPDH, malate dehydrogenase, TAGLN protein transgelin, phosphoenolpyruvate carboxykinase, carbonic anhydrase II, UGDH, UDP-glucose pyrophosphorylase 2, aconitate hydratase and aconitase. The functions of these proteins include glucuronate metabolism, glycolysis, glucogenesis, the TCA cycle and cytoskeleton remodelling.

Kim *et al*. (2009)[91] analysed matched tumour-normal pairs from six CRC patients using 2D DIGE with the isoelectric focusing step carried out using narrow range pH strips of 5.5 to 6.7. Fifty-one proteins were detected as increased >2 significantly, 34 of which were upregulated. Twenty-four of these upregulated proteins were successfully identified, of which adenosylhomocysteinase (AHCY), nucleoside diphosphate kinase A (Nm23-H1), calgranulin A (S100A8), and calgranulin B (S100A9) were verified by western blotting and semi-quantitative RT-PCR. The S100A8 and S100A9 were chosen for further analysis given their previous identification in patient plasma, and it was found by immunohistochemistry that the proteins were distributed in tumour-infiltrating cells and that the plasma levels of the proteins were elevated in CRC.

All of the studies discussed analysed whole pieces of tumour and normal tissue. This makes the discovery of truly differently expressed proteins more difficult. Whole pieces of colon tumour contain heterogeneous populations of cells, meaning the percentage of epithelial cells in the tumour and normal tissue from the same patient is generally not even, skewing DIGE results. To my knowledge, no studies to date have been published using laser microdissection in conjunction with minimal labelling 2D DIGE to analyse matched pairs of tumour-normal tissues from CRC patients. This is most likely due to the time consuming nature of laser microdissection (LMD).

1.10.3 Laser microdissection

It is known that CRC tissue contains a heterogeneous cell population and may be comprised of not only epithelial and stromal cells, but blood vessels, bacterial, necrotic cells, lymph, muscle and inflammatory cells.[92] Laser microdissection (LMD) can be used to collect designated areas of cells from tissue sections mounted on slides, allowing the enrichment of specific cell types. Using LMD, areas of cancerous and normal mucosal crypts may be collected, allowing for the proteomic or genomic profiling of more homogeneous populations of epithelial colon tumour or normal cells. Lawrie *et al*. (2001)[93] demonstrated that laser microdissection of tumour-normal tissue samples can successfully be used in conjunction with 2DE. In the study, protein extracts from LMD tissue and whole tissue from the same samples were compared by 2DE and a number of proteins were identified by MALDI-TOF mass spectrometry. Importantly, they found neither the morphology of cell areas captured by LMD nor the ability to collect mass spectra from protein spots excised from the LMD gels, was altered. A number of proteins not expressed by epithelial cells were detected on the whole tissue gels and the LMD of samples resulted in the enrichment of epithelial specific intracellular proteins, such as CK8 and CK18.

Sugiyama *et al*. (2005)[94] used gene expression arrays to compare RNA expression profiles of endometrial cancer tissue versus LMD endometrial cancer cells. Genes encoding immune system proteins were found to be more strongly expressed in the non-LMD tissue profiles compared to the LMD tissue profiles, probably due to the presence of infiltrating lymphocytes in the whole samples. Sixty-eight other genes were also found to be more strongly expressed in the whole samples of which 40 genes were found to be increased in the LMD tissue profiles in comparison to the whole, including nine genes encoding transcription factors with functions in malignant transformation. This suggests non-target cells within whole tissue can dilute target cell populations, and may hinder the discovery of biologically relevant proteins. For this reason it was concluded LMD was a vital step in the preparation of samples for biomarker discovery.

1.11 Aims

1.11.1 Biomarker discovery

The first aim of the project is to enrich populations of colonic epithelial cells from matched paired tumour-normal tissue biopsies from early stage CRC patients by LMD. Proteins significantly upregulated across the tumour samples compared to the matched normal samples will then be detected by 2D DIGE and identified by LC MS/MS.

1.11.2 Biomarker verification

Following the discovery of potential biomarkers, the project aims to validate the differential expression of proteins between paired tumour-normal samples across a large cohort of early and late stage CRC patients. This will be done to assess the use of such proteins as biomarkers for diagnosis, staging and detection of disseminated tumour cells. Differential expression of the potential markers will be validated at both the mRNA level by relative real-time RT-PCR, and at the protein level by western blot analysis. The cellular localisation, tissue distribution and abundance of proteins will also be assessed by immunofluorescence.

The project also aims to analyse the function of the biomarkers that showed potential as therapeutic targets. This will be done by siRNA knock down studies in cell culture. The effect of target knock down on the expression of genes involved in cancer pathogenesis will be assessed.

1.12 Hypotheses

- The 2D DIGE technique is capable of detecting the differential expression of proteins between matched pairs and across a cohort of cancerous and normal colonic mucosal tissue.
- The enrichment of epithelial cell populations by LMD prior to biomarker discovery will increase the specificity of the biomarkers identified and the sensitivity of the 2D DIGE technique.
- Proteins differentially expressed between colon tumour-normal epithelial cells can be used as biomarkers of CRC. Such markers will have use in the diagnosis and staging of CRC, or in the detection of disseminated tumour cells following tumour resection surgery.
- Markers differentially expressed between the tumour-normal tissues of a large percentage of CRC patients will be useful in a clinical setting.

- Some cancer biomarkers play important roles in cancer development. Silencing the gene expression of such biomarkers in CRC cells may alter the regenerative and migratory and invasive capacity of tumour cells.

1.12.1 Expected outcomes

The proposed LMD 2D DIGE study will compare the proteomic profiles of early staged matched paired tumour and normal tissue samples, identifying a number of differentially expressed proteins. A small number of proteins found to be increased in expression from the DIGE study will be chosen for further analysis. In order to determine the potential of the chosen proteins as biomarkers, their level of expression will be verified in a larger cohort of matched paired tumour-normal tissues. The usefulness of the chosen proteins as biomarkers of staging, therapy efficacy and risk of disease relapse, and the involvement of the proteins in CRC pathogenesis will be analysed.

2 Materials and Methods

2.1 Materials

Laser microdissection

Polyethylene terephthalate (PET) slides (Leica Microsystems, Wetzlar, Germany)

Tissue-Tek OCT (optimum temperature cutting compound) (Ted Pella, Redding, CA)

2D DIGE

Minimal labelling DIGE CyeDyes (GE Healthcare, Buckinghamshire, UK)

Ampholytes pH 3–7 (GE Healthcare)

Mass spectrometry

Trypsin Gold (Promega, Madison, WI, USA)

Immunofluorescence

Histogrip-coated glass slides

PAP pen

Image-iT FX signal enhancer (Invitrogen, Carlsbad, CA, USA)

ProLong Gold anti-fade reagent (Invitrogen)

1° antibodies:	Desmin: mouse monoclonal, used at 1:100 (ab6322, Abcam, Cambridge, MA, USA)
	Vimentin: rabbit monoclonal, used at 1:100 (ab16700, Abcam)
	von Willebrand factor: rabbit polyclonal, used at 1:400 (ab6994, Abcam)
2° antibodies:	Alexa 488: used at 1:500 (Invitrogen)
	Alexa 568: used at 1:500 (Invitrogen)
	Cy5: used at 1:250 (GE Healthcare)

DAPI (Sigma, St Louis, MO, USA)

RNA extraction

Tri Reagent (Sigma)

qRT-PCR

Superscript III (Invitrogen)

Taq Polymerase (Invitrogen)

RNase Out (Invitrogen)

Oligonucleotide primers

Validated primers for the genes CK8 (QuantiTect QT01847741) and SET (PPH20624E) were purchased from Qiagen (Valencia, CA, USA) and SA Biosciences (Frederick, MD, USA) respectively. These primers had been experimentally validated to amplify a single amplicon of the correct size with uniform PCR efficiency.

DNA oligos were synthesised by GeneWorks Pty Ltd (Thebarton, SA) and were obtained at the standard PCR grade.

PSMB6 forward 5' ACT GGG AAA GCG CAG

PSMB6 reverse 5' CCC AGT GGT TGT TCT

PMM1 forward 5' CAG ACC ATC CAG AAC

PMM1 reverse 5' GGA ACT CGA TGA AGG

Protein enzymes and markers

Halt Protease Inhibitor Cocktail (Pierce, Rockford, IL, USA)

Halt Phosphatase Inhibitor Cocktail (Pierce)

Calf Intestine Alkaline Phosphatase (Calbiochem, Gibbstown, NJ, USA)

Precision Plus Dual Colour Protein Standards (Biorad, Hercules, CA, USA), sizes in kDa: 10, 15, 20, 25, 37, 50, 75, 100, 150, 250

Western blotting

1° antibodies: CK8: mouse monoclonal, used at 1:500 (ab9023, Abcam)

CK8 PS23: rabbit monoclonal, used at 1:5000 (EP1629Y, Novus Biologicals, Littleton, CO)

CK8 PS73: rabbit monoclonal, used at 1:1000 (ab32579, Abcam)

CK8 PS431: rabbit polyclonal, used at 1:1000 (ab59434, Abcam)

β actin: mouse monoclonal, used at 1:500 (sc47778, Santa Cruz, CA, USA)

β actin: rabbit polyclonal, used at 1:1000 (ab8227, Abcam)

SET: rabbit polyclonal, used at 1:200 (sc25564, Santa Cruz)

β catenin: rabbit monoclonal, used at 1/ 5000 (ab32572, Abcam)

2° antibodies: ECL Plex Cy3 and Cy5 CyDyes (GE Healthcare) 0.5 μg/μl in 50% glycerol, used at 1:1000

siRNA

Validated SET Stealth RNAi™ siRNA duplexes were purchased from Invitrogen

ACGUUCGAGUCAAACGCAGAAUAAA

UUUAUUCUGCGUUUGACUCGAACGU

Stealth RNAi™ siRNA negative control LO GC duplexes were purchased from Invitrogen (12935–200) to match the GC content of the SET siRNA duplexes

Cy3 labelled siRNA transfection control (Invitrogen)

siPORT NeoFX Transfection Agent (Applied Biosystems, Scoresby, Victoria, Australia)

RT² Profiler PCR Arrays

RT² First Strand Kit (SA Biosciences)

RT² Profiler PCR Arrays (SA Biosciences)

Kits

Diff Quik Stain

ReadyPrep 2D Protein Cleanup Kit (Biorad)

EZQ protein quantitation kit (Molecular Probes)

Phos Trap Titanium Dioxide (TiO_2) Kit (Perkin Elmer, Waltham, Massachusetts, USA)

SV Total RNA Isolation System (Promega)

2.2 Solutions

Protein extraction buffer

5 M Urea, 2 M Thiourea, 2% CHAPS, 2% SB 3–10, 40 mM Tris, 0.2% ampholytes

DIGE labelling buffer

7 M Urea, 2 M Thiourea, 4% CHAPS, 30 mM Tris pH 8.0

IEF rehydration buffer

7 M urea, 2 M thiourea, 4% CHAPS, 30 mM Tris, 1% Pharmalytes 3–7, 65 mM DTT

Agarose

1% agarose in 1 x running buffer

Running buffer

25 mM tris, 192 mM glycine, 0.1% SDS, pH 8.3

Equilibration buffer

6 M Urea, 75 mM Tris-HCl pH 8.8, 23.9.5 (v/v) Glycerol, 2% (w/v) SDS

Equilibration solution 1 (1% DTT)

1% DTT in equilibration buffer

Equilibration solution 2 (4% idoacetamide)

4% idoacetamide in equilibration buffer plus 0.002% (w/v) bromophenol blue solution.

Fixative

20% methanol, 7% acetic acid

Coomassie blue

1% coomassie blue in fixative solution.

Silver stain solutions (250 ml each)

- Fixative solution: 25 ml acetic, 100 ml methanol, 125 ml deionised water
- Sensitisation solution: 75 ml methanol, 10 ml 5% sodium thiosulphate, 17g sodium acetate, 165 ml deionised water

- Silver stain: 0.625 g silver nitrate, 250 ml deionised water
- Develop solution: 6.25 g sodium carbonate, 10 μl formaldehyde, 250 ml deionised water

MS wash buffer

25 mM ammonium bicarbonate/50% ACN solution.

Trypsin Gold solution

20 μg/ml Trypsin Gold (Promega) in 25 mM ammonium bicarbonate/10% ACN

HPLC buffer A

98% water/2 % ACN/0.1% FA filtered solution

HPLC buffer B

20% water/80% ACN/ 0.1% FA filtered solution

PBS

145 mM NaCl, 7.5 mM Na_2HPO_4, 2.5 mM NaH_2PO_4

Trypsin antigen retrieval solution

0.05% trypsin, 0.00125% calcium chloride, 20 mM Tris pH 7.8

Sample buffer

2% SDS, 10% glycerol, 62.5 mM TrisHCl, 6 M urea, 1 x Halt Protease Inhibitor Cocktail (Pierce), 65 mM DTT, 150 U Benzonase (Sigma), pH 6.8

Transfer buffer

25 mM Tris base pH 8.8, 192 mM Glycine, 20% Methanol, 0.05% SDS

PBST

0.1% Tween-20 in PBS

Blocking buffer

5% skim milk in PBST

DEPC treated water

1 ml diethyl pyrocarbonate (DEPC) in 1 L HPW, stood for 24 hours at 37°C and autoclaved

10 x MOPs buffer, pH 7

4.18 g MOPs free acid, 0.14 g sodium acetate, 200 μl 0.5 M EDTA, adjust to pH 7 with 6 M sodium hydroxide (DEPC treated) and made up to 100 ml with DEPC treated water

2x RNA loading buffer

500 μl formamide, 100 μl 10 x MOPs buffer, 167 μl 37% formaldehyde, 100 μl glycerol, a few grains of bromophenol blue, 3 μl 10mg/ml ethidium bromide, 130 μl DEPC water added to 1 ml

FACS buffer

1% foetal calf serum, 0.1% sodium azide in PBS

2.3 Methods

2.4 Specimen collection

Ethics approval for the collection of colorectal tissue samples from patients undergoing colorectal surgery was received from the Queen Elizabeth Hospital's institutional Ethics of Human Research Committee (protocol 1993/59). Informed consent was obtained from all patients involved. Areas of tumour and normal mucosa from the colon or rectum was obtained directly after the removal of the tissue from the patient, placed in 2 ml cryovials, immediately snap frozen and stored in liquid nitrogen.

2.5 Laser microdissection (LMD)

2.5.1 Tissue preparation for LMD

Prior to use, the cryostat was sterilised with 70% ethanol and chilled to -25°C. Scalpel blades, cryostat blades and polyethylene terephthalate (PET) slides (Leica Microsystems, Wetzlar, Germany) were equilibrated to the temperature of the cryostat. Frozen tissue pieces were attached to the cryostat chuck using a small amount of Tissue-Tek OCT (optimum temperature cutting compound) (Ted Pella, Redding, CA), and the chuck was secured into position in the cryostat. Tissue was cut into 30 μm thick sections and carefully placed on the PET slide. Serial sections were placed on plain glass slides for diff quick staining. Multiple sections from the same piece of tissue were placed on the same slide. Tissue sections were briefly thawed onto the PET slide and stored at -80°C until use in LMD.

2.5.2 LMD

Ten minutes prior to the microdissection of a sample, the PET slides were removed from -80°C storage and thawed at room temperature. The slide was loaded into the stage of a Leica AS LMD 6000 system (Leica Microsystems, Wetzlar, Germany). The cap of a 0.5 ml microfuge tube was filled with 40 μl of protein solubilisation buffer and the cap was loaded into the holder, situated directly underneath the area of tissue microdissection. The area of tissue to be cut was outlined using the computer mouse in the Leica AS LMD software (Leica Microsystems, Wetzlar, Germany). The speed, intensity and aperture of the laser were adjusted to achieve the optimum dissection of each sample. During the LMD of a tissue section, the serial section stained with Diff Quick was referred to in order to ensure epithelial cell areas were collected, and contaminating cell areas were avoided (such as stroma, muscularis mucosa and infiltrating lymphocytes). Following LMD samples were centrifuged at 13,400 x g for 30 seconds, and sonicated in a water bath on ice three times for 30 seconds. Protein was purified using the 2D Clean Up Kit (Biorad) and re-suspended in 10 μl of DIGE labelling buffer. An aliquot (0.5 μl) of each sample was diluted in 4.5 μl of deionised water and quantified using an EZQ assay (Invitrogen) as per manufacturer's recommendations. The process of LMD was repeated and each sample was pooled until a minimum of 75 μg of protein was obtained.

2.5.3 Diff Quick staining

Sections were briefly air-dried and immersed in fixative solution for ten seconds. Slides were then immersed in staining solution 1 for five seconds, washed in deionised water, immersed in staining solution 2 for five sections, and washed in deionised water. Tissue sections were air-dried and cover-slipped.

2.6 2D Difference gel electrophoresis (2D DIGE)

2.6.1 Cy Dye DIGE labelling

Protein samples were labelled as described in Chapter 6.3.3 of the 2D Electrophoresis Principals and Methods Handbook 80-6429-60AC (GE healthcare) (80). Briefly, each sample was diluted to 5 μg/μl with DIGE labelling buffer. Each of the three Cy dyes was reconstituted to a concentration of 400 μM with high quality anhydrous DMF. An internal standard was generated by pooling 25 μg of protein from each of the eight tumour and eight normal LMD tissue samples. To 400 μg of the internal standard, 3200 pmol of Cy2 dye was added and incubated on ice in the dark for 30 minutes. The labelling reaction was quenched by the addition of 8 μl of 10 mM lysine. Fifty μg of protein from six of the normal LMD tissue samples was separately labelled with 400 pmol of Cy3 dye, and 50 μg of protein from six of the

tumour LMD tissue samples was separately labelled with 400 pmol of Cy5 dye as previously described. The labelling reaction of each individual sample was quenched by the addition of 1 μl of 10 mM lysine. A dye swap was performed on the two remaining tumour and normal paired samples under the same parameters.

2.7 2 DE

2.7.1 1st dimensional IEF

Two-dimensional electrophoresis was carried out as described in the 2D Electrophoresis Principals and Methods Handbook 80-6429-60AC (GE healthcare) (80). Briefly, labelled matched pairs of tumour-normal protein were mixed with 50 μg of the labelled internal standard. IEF rehydration buffer was added to each sample to a final volume of 450 μl. Samples were coffin loaded into 24 cm pH 3–7 NL IPG strips and coated with Dry Strip Cover Fluid (GE Healthcare). Rehydration was carried out over night using the IPGphor system (GE Healthcare) at 50 V, 21°C, in the dark. IPG strips were removed from coffins, and the coffins were cleaned of any residual oil. Small pieces of filter paper (approximately 3 mm x 3 mm), moistened with deionised water, were placed over the coffin electrodes. IPG strips were placed back in the coffins and coated with Dry Strip Cover Fluid (GE Healthcare). Isoelectric focusing was performed for approximately 80,000 Vhrs using the focusing protocol detailed below.

2.7.2 Isoelectric focusing

Step and hold	500 V	30 minutes
Step and hold	1,000 V	30 minutes
Gradient	10,000 V	30 minutes
Step and hold	10,000 V	60,000 Vhrs
Gradient	1,000 V	30 minutes
Step and hold	1,000 V	Hold

2.8 2nd dimension SDS PAGE

Following IEF, each IPG strip was incubated in equilibration solution 1 for fifteen minutes, followed by incubation in equilibration solution 2 for fifteen minutes. IPG strips were sealed at the top of 8% to 15% gradient polyacrylamide gels, cast in non-fluorescing glass plates, using 1% agarose. SDS PAGE was performed at 350 V using an Ettan DALT 6 gel electrophoresis tank coupled to a cooling unit set at 10ºC.

2.8.1 Imaging and analysis

Gels were imaged using the Typhoon 9400 Variable Mode Imager (GE Healthcare) using green (532 nm), red (633 nm) and blue (488 nm) lasers at photo-multiplier tube values of 600 V, 595 V and 645 V respectively. Scans were performed at 200 μ. Each gel image was cropped to the same area of interest using Image Quant v5 software (GE Healthcare). Cropped images were loaded into the DeCyder Batch Processor Module and processed. Protein spots were analysed in the DeCyder Differential In gel Analysis and Biological Variation Analysis modules.

The average ratio of tumour-normal abundance of each protein spot across the eight gels was calculated using the DeCyder Biological Variation Analysis module, and a Student's paired T-test was performed in order to determine statistically significant differences in expression. Proteins with a tumour-normal abundance ratio of ≥ 2 fold, $P \leq 0.05$, were considered to be of interest. The individual matched paired tumour-normal abundance ratios for each of these protein spots, for each patient, were also collected from the DeCyder Differential In gel Analysis module.

2.8.2 Preparative gels

Preparative gels were run with tumour LMD protein in order to excise proteins spots of interest for identification by mass spectrometry. For each gel 150 μg of protein was labelled with 400 pmol of Cy dye, and two-dimensional electrophoresis was carried out as previously described. The Cy dye to protein ratio was reduced, as the gels were not intended for analysis purposes, and were imaged only for spot matching back to the analytical gels using the DeCyder software. Following imaging, the preparative gels were removed from the gel plates and stained by incubation with Coomassie blue for one hour with gentle agitation. Gels were destained by repeated incubations in fresh fixative until the gel background was completely clear. A mass spectrometry compatible silver stain was then performed. Protein spots of interest were matched from the analytical gels to the preparative gel, excised from the preparative gels with a sterile scalpel blade, and placed in 1.5 ml Eppendorf tubes (Eppendorf).

The minimal labelling CyDyes label proteins via N-hydroxysuccinimidyl esters that form an amide bond with the lysine epsilon amine groups on proteins by a nucleophilic substitution reaction. Because of the labelling chemistry and the dye: protein ratio used in the reaction, each protein is likely to have only one dye molecule attached. All three of the dyes are of a very similar molecular weight and are positively charged to match the charge on lysine groups; hence there is only a very small to no shift in the isoelectric point of each protein. This means the overall protein spot map of a sample labelled with the minimal CyDyes is easily comparable with the overall protein spot map of an unlabelled sample. Because of this matching the analytical gels back to the silver stained preparative gel is possible. All of

the proteins analysed and presented in this study were confidently and accurately matched to and cut from the preparative gel.

2.8.3 Silver staining (MS compatible)

Gels were incubated in sensitisation solution with gentle agitation for 30 minutes, followed by three seven-minute washes with deionised water. Gels were incubated with silver stain solution for 30 minutes, followed by two one-minute washes in deionised water. Gels were incubated in developer solution until the spots of interest were visualised. The developing reaction was stopped by the addition of fixative to the gels.

2.9 LC MS/MS

2.9.1 Trypsin digestion

Gel pieces were washed by the addition of 50 μl of MS wash buffer, tubes were vortexed, and incubated at room temperature for ten minutes. This was repeated five times. ACN (50 μl) was added to each gel piece and incubated at room temperature for five minutes or until the plugs had shrunk and become opaque. The ACN was removed and gel pieces were dried at 37°C for 30 minutes. Trypsin Gold solution (20 μl) was added to each gel piece and allowed to rehydrate at room temperature for 30 minutes. Samples were incubated at 37°C overnight.

2.9.2 HPLC linear ion trap MS

The digested peptides were analysed with a Thermo LTQ XL linear ion trap mass spectrometer, fitted with a nanospray source (Thermo Electron Corp, San Jose, CA). Five microliters of each sample was applied to a 300 μm i.d. x 5 mm C18 PepMap 100 precolumn and separated on a 75 μm x 150 mm C18 PepMap 100 column using a Dionex Ultimate 3000 HPLC (Dionex Corp, Sunnyvale, CA) with a 55 minute gradient from 2% acetonitrile to 45% acetonitrile containing 0.1% formic acid at a flowrate of 200 nl/minute followed by a step to 77% acetonitrile for nine minutes. The mass spectrometer was operated in positive ion mode with one full scan of mass/charge (m/z) 300–2000 followed by product ion scans of the three most intense ions with dynamic exclusion of 30 s and collision-induced dissociation energy of 35%.

The MS spectra were searched with Bioworks 3.3 (Thermo Electron Corp, San Jose, CA) using the Sequest algorithm against the IPI Human database v3.39 using Trypsin digestion as the protease, allowing for two missed cleavages, with homoserine and homoserine lactone as variable methionine

modifications and using the following filters: 1) the cross-correlation scores of matches were greater than 1.5, 2.0 and 2.5 for charge state 1, 2 and 3 peptide ions respectively, 2) peptide probability was greater than 0.001 and 3) each protein identified had at least two different peptides sequenced. The mass tolerance for peptide identification of precursor ions was 1 Da and 0.5 Da for product ions.

2.10 CK8 Phosphopeptide enrichment and MALDI TOF/TOF

2.10.1 CK8 sample preparation

The CRC cell line SW480 was purchased from the American Type Culture Collection (ATCC, Rockville, MD) and maintained in RPMI 1640 at 37°C, 5% CO_2, in T75 flasks. Cells were washed in PBS, pelleted and lysed with IEF rehydration buffer. Protein was quantified using the EZQ kit (Invitrogen) according to manufacturer's recommendations. Seven hundred and fifty micrograms of the SW480 protein was separated by 2DE using 24 cm pH 3–7 NL IPG strips and 8% to 15% polyacrylamide gels as previously described. Gels were stained with Coomassie blue and destained in fixative. The three CK8 isoforms of interest were individually excised from the gels and placed in separate 1.5 ml Eppendorf tubes.

2.10.2 Trypsin digestion

Gel pieces were completely destained by washing in 500 μl of 50 mM ammonium bicarbonate for five minutes, followed by 400 μl of 50 mM ammonium bicarbonate/30% ACN for fifteen minutes in a sonicating water bath. The 50 mM ammonium bicarbonate/30% CAN washes were repeated until the gel plugs were clear. Gel pieces were shrunk with 200 μl of ACN and incubated for fifteen minutes at room temperature. The ACN was removed and the gel pieces were dried in a vacuum centrifuge for ten minutes. Gel pieces were rehydrated with 10 μl of Trypsin Gold at 10 ng/μl in 5 mM ammonium bicarbonate and incubated at room temperature for 30 minutes. Ten microlitres of 5 mM ammonium bicarbonate/20% ACN was added to each sample to give a concentration of 10% ACN, and samples were incubated at 37°C overnight. To extract the peptides from the gel pieces, 20 μl of 1% formic acid was added to the samples and incubated in a sonicating water bath for fifteen minutes. Samples were briefly centrifuged, excess liquid was removed and placed into the final sample collection tube and 50 μl of 50% ACN/1% formic acid was added to each tube and incubated in a sonicating water bath for fifteen minutes. Samples were centrifuged and excess liquid was place into the final sample collection tube. One hundred microlitres of 100% ACN was added to each gel piece and was incubated in a sonicating water bath for fifteen minutes. Samples were centrifuged and excess liquid was place into the final sample collection tube. The peptide extracts were reduced to approximately 5 μl using vacuum centrifugation.

2.10.3 Phosphopeptide enrichment and MALDI TOF/TOF

Samples (3 μl) were subjected to the Phos Trap Titanium Dioxide (TiO_2) (Perkin Elmer) magnetic beads according to the manufacturer's recommendations to enrich for phosphorylated peptides. The eluted peptide solution (1.5 μl) was spotted onto a 600 μm AnchorChip (Bruker Daltonics, Bremen, Germany) target with 1 μl of 2,5-DHB (10 mg/ml) matrix in 50% ACN/0.1% TFA. MALDI TOF MS/MS was carried out as previously described.[95] Briefly, MALDI-TOF mass spectra were acquired using a Bruker ultraflex III MALDI TOF/TOF mass spectometer (Bruker Daltonics) operating in reflection mode under the control of the flexControl software (Version 3.0, Bruker Daltonics). External calibration was performed using peptide standards (Bruker Daltonics) that were analysed under the same conditions. Spectra were obtained randomly over the surface of the matrix spot at a laser intensity determined by the operator. A signal to noise ratio threshold of ten was used for peak selection. Peak masses and intensities of TOF and LIFT spectra were detected with flexAnalysis (Version 3.0, Bruker Daltonics). MS and MS/MS spectra were subjected to smoothing, background subtraction and peak detection using flexAnalysis and using the SNAP algorithm. The spectra and mass lists were exported to BioTools (Version 3.1, Bruker Daltonics GmbH). Here, the MS and corresponding MS/MS spectra were combined and submitted to the in-house Mascot database-searching engine (Matrix Science: http://www.matrixscience.com). Data was matched against the SwissProt 57.1 database (462,764 sequences). Search parameters allowed for a mass tolerance of MS: 100 ppm, MS/MS tolerance of 0.5 Da, taxonomy chosen was mammalian (64,438), the variable modifications of oxidisation of methionines and phosphorylation of S, T and Y, the fixed modification carbamidomethylation of cysteines, and two missed trypsin cleavages. Positive protein identifications were assigned on the basis of combined ion scores (calculated by the software) that exceeded the calculated deprecated protein identification threshold. In addition, an in silico digest of CK8 was performed using the sequence editor platform of BioTools to identify potential phosphopeptides.

Precursor ions suspected to be phosphorylated peptides were chosen for MS/MS analysis. Spectra ion annotation was performed using MOWSE and probability scores. For spectra that matched to precursor ions of potential phosphorylated peptides, annotation was performed using BioTools and the different phosphorylation positions were evaluated manually.

2.11 1DE and western blotting

2.11.1 Sample preparation and 1DE

For protein extraction, 30 μ cryo-sections were cut from matched pairs of tumour-normal tissue and pulverised in a mortar and pestle under liquid nitrogen. Prior to use the cryostat was sterilised with 70% ethanol and chilled to -25°C. Scalpel blades, cryostat blades and mortar and pestles were equilibrated to the temperature of the cryostat. Frozen tissue pieces were attached to the cryostat chuck using a small amount of Tissue-Tek OCT (optimum temperature cutting compound) (Ted Pella, Redding, CA). Pulverised tissue was placed in 200 μl of buffer sample buffer, purified using the 2D Clean Up Kit (GE Healthcare), resuspended in 100 μl of sample buffer, and quantified using the EZQ assay (Invitrogen). Bromophenol blue solution (0.002%) was added to each sample and 50 μg of each sample plus 10 μl of molecular weight markers (Biorad) was loaded onto 4%–20% polyacrylamide gels and cast using a Multiple Gel Caster Mini (GE Healthcare) according to manufacturer's recommendations. Electrophoresis was carried out using the MiniVE 1D vertical gel system (GE Healthcare) at 200 V until the bromophenol blue dye front reached the bottom of the gels.

2.11.2 Western blotting

Following 1DE, gels were incubated in 25 ml of freshly made transfer buffer for fifteen minutes with agitation. Low fluorescence PVDF membrane (GE Healthcare) cut to the size of each gel was washed in methanol and incubated in freshly made transfer buffer for fifteen minutes with agitation. Each gel was placed on top of a piece of membrane, ensuring no air bubbles were present, and was sandwiched with three pieces of filter paper, moistened in transfer buffer, either side . Protein transfer was carried out using a semi-dry apparatus (GE Healthcare) for one hour at 70 mA per gel.

Following transfer, the low fluorescence PVDF membranes were incubated in blocking buffer at room temperature for one hour with agitation, and washed three times for five minutes in PBST with 0.1% skim milk powder. Membranes were incubated in primary antibodies diluted in 0.1% skim milk powder PBST overnight at 4°C with agitation. Membranes were washed three times for ten minutes in PBST, and then incubated with the Cy3 and Cy5 secondary antibodies diluted 1:1000 in PBST for one hour at room temperature, in the dark, with agitation. Membranes were washed three times for ten minutes in PBST and dried in an oven at 37°C. Scanned images of each membrane were collected using the Typhoon 9400 Variable Mode Imager (GE Healthcare) using the red (633 nm) and blue (488 nm) lasers at 200 μ. Cy3 and Cy5 images were separated using FluorSep (GE Healthcare) and protein bands were quantified using Image Quant v5 software (GE Healthcare).

2.12 Immunofluorescence

2.12.1 Frozen tissue preparation

Prior to use, the cryostat was sterilised with 70% ethanol and chilled to -25°C. Scalpel blades and cryostat blades were equilibrated to the temperature of the cryostat. Frozen tissue pieces were attached to the cryostat chuck using a small amount of Tissue-Tek OCT and the chuck was secured into position in the cryostat. Tissue sections were cut 10 μ thick and placed on histogrip-coated glass slides at room temperature. Slides were immediately placed in ice-cold acetone for five minutes. Slides were washed three times for one minute in PBS. The tissue sections were circled with a PAP pen.

2.12.2 Paraffin embedded tissue preparation

Tissue sections were cut 7 μ thick and placed on histogrip-coated slides. Slides were washed twice in xylene, once in 50% xylene/50% ethanol, twice in 100% ethanol, once in 95% ethanol, once in 70% ethanol, and once in 50% ethanol. All washes were performed for three minutes. Slides were washed thoroughly under running water and were kept moist. The trypsin antigen retrieval solution was pre-heated to 37°C. Tissue sections on slides were circled with a pap pen and the trypsin solution was pipetted onto each tissue section. The slides were placed in a humidity box and incubated at 37ºC for fifteen minutes. Slides were then rinsed under running water for three minutes.

2.12.3 Staining procedure

Tissue sections were covered with Image-iT FX signal enhancer (Invitrogen), and incubated in a humidity box for 30 minutes at room temperature. Slides were washed three times for one minute in PBS, covered with 10% goat serum in PBS, and incubated in a humidity box for 30 minutes at room temperature. Tissue sections were incubated with 50 μl of the primary antibodies diluted in 10% goat serum in PBS at 4°C overnight. Slides were washed three times for one minute in PBS, and incubated in the secondary antibodies diluted in 10% goat serum in PBS at room temperature, in the dark, for 60 minutes. Slides were washed three times for one minute in deionised water and incubated in DAPI at 0.5 μg/ml (Sigma) for fifteen minutes in the dark. Slides were washed three times for one minute in deionised water and left to air dry. Tissue sections were cover-slipped with ProLong Gold Anti-fade reagent (Invitrogen) and sealed with clear nail polish.

2.13 Real-time RT-PCR

2.13.1 Sample preparation

For RNA extraction, 30 μ cryo-sections were cut from matched pairs of tumour-normal tissue and pulverised in a mortar and pestle under liquid nitrogen. Prior to use, the cryostat was sterilised with 70% ethanol and chilled to -25°C. Scalpel blades, cryostat blades, and mortar and pestles were equilibrated to the temperature of the cryostat. Frozen tissue pieces were attached to the cryostat chuck using a small amount of Tissue-Tek OCT (Ted Pella). Pulverised tissue was placed in 500 μl of Tri Reagent (Sigma) and RNA was extracted according to the manufacturer's protocol. RNA integrity was checked by denaturing gel electrophoresis. Samples that did not show distinct 28S and 18S bands were excluded from further analysis. RNA was quantified at 260 nm using the NanoDrop ND-1000 Spectrophotometer (NanoDrop Technologies, Wilmington, DE).

2.13.2 RNA check gel

Agarose gel tanks and combs were washed in decon and dried with ROAR wipes prior to use. To make a 50 ml gel, 0.5 g of agarose was added to 36.5 ml of DEPC water in a conical flask and dissolved by boiling in a microwave for 45 seconds on high. The agarose mixture was cooled by placing the bottom of the conical flaks under cold running water. In a fume hood 5 ml of 10x MOPs buffer and 8.5 ml of formaldehyde was added. Gels were poured into the assembled tanks under the fume hood and allowed to set for 20 minutes. RNA sample were thawed and stored on ice just prior to use. Two microliters of each RNA sample was added to 2μl 2x RNA loading buffer. The samples were heated at 68°C for 3 minutes then place on ice immediately. The tubes were spun down and the 4 μl samples were loaded into the agarose gel lanes. The gels were covered with 1x MOPs buffer run at 100 V until the bromophenol blue dye front reached 1 cm from the bottom of the gel. Gels were photographed under UV light and studied for distinct 28s and 18s bands.

2.13.3 Reverse Transcription

Total RNA (1 μg per sample) was reverse transcribed for 60 minutes at 50°C in a 20 μl reaction volume containing 5 x First Strand buffer, 200 U Superscript III reverse transcriptase (both from Invitrogen), 100 ng Random Primers (Promega), and 0.6 mM of each deoxynucleotide triphosphate (Promega, Sydney, Australia). The reverse transcription reaction was terminated with a five minute incubation at 70°C.

2.13.4 Real-time PCR

Relative real-time PCR was performed using the MJ Research DNA Engine Opticon 2 (Biorad, Hercules, CA). PCR was performed as previously described [96] . Briefly, the final PCR reaction volume was 20 μl, containing a 2 μl aliquot of cDNA in 10 x PCR buffer (Qiagen, Melbourne, Australia), 200 μM of each deoxynucleotide triphosphate (Promega), 40 ng of each primer, 0.33 U HotStar Taq polymerase (Qiagen), 0.3 μl (1/1000 dilution of stock) SYBR Green (Adelab Scientific, Adelaide, Australia). The PCR cycling parameters are given below. The RT negative control consisted of RNA and master mix without reverse transcriptase, while the PCR negative (no target) control consisted of PCR master mix alone. All samples were amplified in triplicate and the mean C(t) value was obtained.

2.13.4.1 Opticon 2 PCR protocol

1. Incubate 95°C, 00:15:00
2. Incubate 95°C, 00:00:15
3. Incubate *optimised melting temperature for primer*, 00:00:20
4. Incubate 72°C, 00:00:20
5. Plate Read
6. Incubate 80°C, 00:00:02
7. Plate Read
8. Go to line 2 45 more times
9. Melting curve from 75°C to 95°C, read every 1.0°C, hold 00:00:01

End

2.13.5 Expression ratio calculations

Tumour to normal expression ratios were calculated using the $2^{-\Delta C(t)}$ method of relative quantification (K.J. Livak, T.D. Schmittgen, 2001). This method relies on reverse transcribing the same total starting amount of RNA for each sample, and calculates the expression ratio of tumour-normal pairs by comparing their threshold cycle C(t) values. The $2^{-\Delta\Delta C(t)}$ method was then used to compare the expression of CK8 in the tumour samples compared to matched normal mucosa after normalisation to housekeeping genes. A Kruskal-Wallis test was performed on the tumour-normal fold change ratios obtained by each method.

2.14 siRNA transfection

The cell lines SW480 and HEK 293 were purchased from the American Type Culture Collection (ATCC, Rockville, MD) and maintained in RPMI 1640 at 37°C, 5% CO_2, in T75 flasks. For siRNA transfection, cells were grown to approximately 50% confluence. The lipid-based transfection reagent siPORT NeoFX (Applied Biosystems) was used for transfection as per the manufacturer's protocol. Briefly, in preparation for SET siRNA treatment, 1 μl of siPORT NeoFX transfection reagent was incubated with 100 μM SET siRNA in 50 μl of Opti-MEM medium per well for ten minutes at room temperature. As a siRNA negative control, 1 μl of siPORT NeoFX transfection reagent was incubated with 100 nM Stealth RNAi negative control LO GC siRNA in 50 μl of Opti-MEM medium per well for ten minutes at room temperature. For a positive transfection control, 1 μl of siPORT NeoFX transfection reagent was incubated with 20 nM Cy3 labelled negative siRNA (Invitrogen) in 50 μl of Opti-MEM medium per well for ten minutes at room temperature. Untreated cells were also plated as negative controls. Cells were plated at 1 x 10^5 cells per well in 24 well plates in quadruplicate per treatment. Each well was made up to a final volume of 0.5 ml with RPMI. Plated cells were incubated at 37°C in a 5% CO_2 humidified incubator.

2.15 RT^2 Profiler PCR Arrays

RNA samples were reverse transcribed using the RT^2 First Strand Kit (SA Biosciences) according to manufacturer's recommendations to a final volume of 20 μl. PCR was carried out using the RT^2 Profiler PCR Array plates (SA Biosciences) according to the manufacturer's protocol. Briefly, the cDNA from each sample was added to 960 μl of 2 x Super Array RT^2 PCR master mix (SA Biosciences) and 960 μl of UPW. Twenty μl of this mixture was pipetted into each of the 96 wells on the array plate, and the plates were briefly centrifuged. The PCR was carried out using the Opticon 3 (MJ research) with the cycling parameters of ten minutes at 95°C, followed by 40 cycles of fifteen seconds at 95°C, 30 seconds at 55°C, and a 30 second extension at 72°C. The RT and PCR array was repeated for each of the samples.

2.16 Flow cytometry

Caco2 cells were washed with FACS buffer and blocked with 10% heat-inactivated rabbit serum for 20 minutes at 4ºC. Cells were washed with FACS buffer and aliquoted out to 1 x 10^5 cells per tube. Differing amounts of the sc-120 antibody (0.0 μg, 0.5 μg, 1.0 μg, or 2.0 μg) was added to each tube and the cells were incubated for twenty minutes at 4ºC. Cells were washed with FACS buffer and goat anti-mouse FITC was added at 1:1000 and incubated for 20 minutes at 4ºC. Cells were washed with

FACS buffer and fixed with 4% paraformaldehyde in PBS for fifteen minutes at 4ºC. Cells were washed with FACS buffer, resuspended in filtered PBS and analysed.

3 Identification of CRC biomarkers

3.1 Introduction

In order to detect proteins with increased abundance in CRC, proteomic analysis of matched paired tumour-normal tissue samples was carried out. The purpose of this analysis was to identify proteins consistently increased in expression in carcinoma cells, as it was hypothesised such proteins had a use as biomarkers for CRC. Following the identification of proteins significantly increased in abundance, the potential of each candidate protein as a biomarker of CRC was assessed and three proteins were chosen for further analysis. In this assessment the pre-existing knowledge of the proteins and their involvement in cancer, the potential of the proteins to act as novel biomarkers of the disease (in aspects such as staging, the detection of disseminated tumour cells and targeted therapies), and the potential to shed new light on the involvement of the proteins in CRC pathogenesis was taken into account.

My honours thesis (submitted in 2005) describes the proteomic profiling of matched paired tumour-normal tissues from late stage CRC patients using LMD, scare labelling 2D DIGE and mass spectrometry. This work acted as a pilot study for my PhD project, but the results from this work could not be used in the results section of my PhD as they had already undergone assessment. However, the data from the pilot study is used in this PhD thesis to calculate the number of patient samples needed in the proteomic analysis to give the study adequate statistical significance and power. Although the pilot study was not carried out as part of this PhD, the statistical analysis of the data is included here as it was performed as part of this PhD. One protein from the pilot study was also chosen for further analysis in this PhD work and is discussed later.

3.1.1 Scarce labelling DIGE Pilot study

To my knowledge, there is currently no published literature using minimal labelling DIGE to analyse protein extracted from laser microdissected human colon tissue (there has however been a small number of studies combining laser microdissected colon tissue with saturation labelling DIGE). The feasibility of collecting enough protein from LMD samples for minimal labelling DIGE analysis (requiring 75 μg of protein from each sample) was therefore unknown. At this point in time the minimal labelling DIGE technique had started to become established in Australia, with one publication from an Australian laboratory in 2005.[97] However, the scarce labelling DIGE technique (requiring only 7.5 μg of protein from each sample) had yet to have been used in Australasia. It was decided that the collection of samples by LMD prior to proteomic analysis was of great importance to the study[98 99], despite the time consuming and labour intensive nature of the technique. However, a concern of the study was the ability to extract sufficient protein from tissue for DIGE analysis, from a sample cohort large enough to yield

statistically significant results. A pilot study using LMD with scarce labelling 2D DIGE was therefore carried out on four late stage CRC tumour-normal tissues.

The pilot study had three main aims. The first was to detect proteins differentially expressed between colon tumour and normal samples, while the second was to help determine the cohort number required to give an experimental power of >80% for a larger DIGE study. The third aim was to determine how much protein could be extracted from LMD colon tissue, and whether it was feasible to perform LMD with minimal labelling DIGE on a cohort of samples large enough to meet the experimental power criteria. If possible, samples would be preferentially labelled with minimal CyDyes over the scarce labelling CyDyes. Despite the fact minimal labelling requires ten times the amount of protein as scarce labelling, the minimal labelling approach offers some advantages over the scarce labelling method.

Minimal labelling uses three CyDyes, allowing paired tumour-normal samples to be run in a single gel with an internal standard, alleviating tumour-normal spot matching within patient samples. Scarce labelling only has two available CyDyes, meaning matched paired tumour-normal samples must be run on separate gels (for example, gel 1 contains the tumour sample plus the internal standard, and gel 2 would contain the normal sample plus the internal standard). This increases the time spent spot matching gels, as the matching of all protein spots across all gels must be checked. If paired tumour-normal gels do not electrophorese in the same manner, errors in spot matching within patient tumour-normal samples may be introduced.

Identifying proteins of interest by mass spectrometry is also more difficult when using saturation labelling as the saturation dyes label all available cysteine residues. Due to the addition of the charged dye molecules, the isoelectric point and molecular weight of proteins may be altered depending on the number of cysteine residues present, thus affecting the position to which protein spots will resolve on a 2D gel. As there is only 10 μg of total protein on each scarce labelling gel, proteins for mass spectrometry analysis must be excised from a preparative gel containing a larger amount of protein labelled with a large amount of dye for accurate spot matching. Depending on the type of mass spectrometer available for protein spot identification, typically 150 μg to 500 μg of labelled protein is run on a preparative gel and large amounts of scarce labelled protein can lead to a decrease in the solubility of samples, and a decrease in the quality of protein spot resolution. This makes spot matching of the post-stained preparative gel back to analytical gels extremely difficult. Additionally, producing preparative gels containing large amounts of dye can also substantially increase the cost of the technique. In contrast, CyDye labelled preparative gels do not need to be run for a minimal labelling experiment, as the minimal labelling dyes aim to only label 1 lysine residue per protein, and the overall

protein spot map generated by analytical gels are not altered, meaning any preparative gels can be run with unlabelled protein.

From the pilot study, it was concluded that laser microdissection of unfixed and unstained tissue sections gave sufficient protein yields to consider using minimal labelling DIGE (shown in Table 1). The pilot data was then used to determine the sample size required to give the study a statistical significance and an experimental power of greater than 0.80. To determine this, spot volume data from the pilot study was entered into the software program Emphron tools (www.emphron.com).

Patient	Protein Yield (µg)	Area Dissected (mm2)
1 Tumour	65.1	11.54
1 Normal	72.1	14.71
2 Tumour	58.8	22.37
2 Normal	79.1	20.78
3 Tumour	57.05	12.11
3 Normal	30.55	10.92
4 Tumour	62.65	17.09
4 Normal	56.71	10.15

Table 1. Total protein yield and area laser microdissected of the samples for scarce labelling 2D DIGE analysis. Tissue was laser microdissected using the Leica AS system. Thirty micron thick tissue sections were placed in PEN foil framed slides and remained unfixed and unstained during LMD. Results from G Arentz honours thesis, 2005.

3.1.2 Statistical analysis of pilot study data

There are two main sources of variation when comparing 2D gels in a control vs diseased experiment, biological and technical variation. Biological variation is the result of genetic and environmental factors. This is the variation that studies aim to detect, determining the differential expression of proteins of genuine interest. Technical variation occurs from differences in sample preparation and separation, and from gel staining, gel imaging and analysis. 2D gels are notoriously difficult to reproduce, resulting in high levels of technical variation and traditionally, multiple 2D gel replicates were needed for each sample in a single experiment to try and account for technical variation. The DIGE technology has alleviated this need through the use of multiple fluorescent dyes, paired control and diseased samples can be run within the same gel, along with an internal standard, present on every gel. This allows for variations arising from separation, staining, gel imaging and analysis to be realised and corrected. However, it is still important to assess the number of samples needed in order to analyse and detect real minimum expression differences between disease and control sample groups. Using the pilot study data, a power analysis was performed using the Emphron Tools website (www.emphron.com) to determine the number of patient samples needed to give the proposed minimal labelling DIGE study statistical significance. Given that samples would be enriched by the time-consuming process of LMD, it

was important to calculate the size of the cohort needed to make the study biologically relevant in order to balance this with the number of samples that could be realistically collected by LMD.

3.1.3 Emphron Tools

A power analysis was performed using the spot volume data taken from the pilot study using the website www.emphron.com. The spot volume data of 25 random protein spots from each tumour-normal sample taken from the pilot study were used in the power calculation software. The software used an estimate of the analytical and biological variability to calculate the standard error of differences between tumour-normal groups given an experimental design of eight patient samples and one analytical gel per sample. A significance or hypothesis test is used to calculate the probability of detecting a type I error, which is the probability of rejecting the null hypothesis when it is in fact true, or the probability of falsely detecting an effect. Results were subjected to a hypothesis test set to meet a significance value of <0.05, giving a 95% probability of accepting or rejecting the null hypothesis correctly. A result may appear to be statistically significant (the null hypothesis is rejected) but may in fact be false due to an inadequate sample size, meaning the tested cohort is not large enough to detect the falseness of rejecting the null hypothesis. This is known as a type I error. The power of a study is 1 minus the probability of a type II error (accepting the null hypothesis given a real difference exists) (http://www.stats.gla.ac.uk/).

The power of an experiment can be increased by reducing experimental variability (for example, using DIGE as opposed to traditional 2DE), increasing the sample size (the number of tumour-normal pairs) and increasing the effect size (the true difference between the means, in this case the tumour-normal expression ratio). The power of an experiment is inversely influenced by the significance level required. Hence the larger the cohort of samples analysed, the more confidently smaller changes in tumour-normal expression ratios could be deemed 'true' or 'biologically significant'. During the design of this work, it was determined the experimental power needed to be equal to or exceed 0.8. Given the pilot data entered and the design criteria, Emphron tools calculated an experimental power of 0.9 when looking for a minimal detectable difference in tumour-normal abundance fold change of >3, 0.05 (Fig. 1). The experimental power of detecting a fold tumour-normal expression ratio would be approximately 0.75. From these results it was decided extracting 75 μg of protein from eight paired tumour-normal samples by LMD for minimal DIGE labelling was a viable option. Hence, minimal labelling DIGE was used in preference to saturation labelling DIGE for the larger study.

Fig 1. Experimental power calculation. Using spot volume data from the pilot study, the power of a larger study was calculated using Emphron tools with an experimental design criteria of eight matched pair tumour-normal samples, one analytical gel per sample, aiming to detect a tumour to normal fold change of 3, P≤0.05. The calculated power of the experiment is plotted on the X-axis, and is dependent on the effect size plotted on the Y-axis. An increase in the effect size of 50% represents an increase in fold change of 1 (i.e. 50% represents a 1:1 tumour to normal ratio, 100% represents a 2:1 tumour to normal ratio and 150% represents a 3:1 tumour to normal ratio).

3.1.4 Results from the scarce labelling DIGE pilot study

The pilot study analysed matched paired tumour-normal tissue from four stage III tumours. Colonic crypts from the normal samples, neoplastic glands from the tumour samples and directly adjacent cancerous stroma were laser microdissected avoiding areas of muscularis mucosa and muscularis propria. Six 2D gel protein spots were detected that displayed an increase in abundance with an average of fold or greater (P≤0.05), across the four patients. Four of these proteins were identified as β tubulin, chaperonin HSP60, desmin and 14–3–3 β. A number of proteins were also detected as significantly increased in abundance 2 fold or greater within individual patient's tumour-normal samples. Four of these proteins were identified as 14–3–3 zeta, calpain (small subunit), tropomyosin 1 and actin α 1. The roles of HSP60[88], 14–3–3 β[100] and zeta[101], tropomyosin 1[88], and calpain[102] have previously been described in epithelial cancers, thus verifying the results of the study.

3.2 Materials and methods

3.2.1 Laser microdissection

Tumour and matched normal samples were obtained fresh from eight-stage II CRC patients undergoing tumour resection surgery. Areas of tumour tissue and normal mucosa were placed in vials and immediately snap frozen on dry ice. Tissues were prepared for LMD as described in Chapter 2. Epithelial cells from the colonic crypts of the normal tissues and from the neoplastic glands of the tumour tissues were enriched by LMD, avoiding areas of muscularis mucosa, lymphoid aggregates and propria. Following LMD samples were purified using the 2D Clean-Up kit (GE Healthcare), resuspended in 5–10 μl DIGE labelling buffer and quantified using the EZQ kit (Molecular Probes). Samples were laser microdissected, purified, pooled and quantified until a minimum of 75 μg of each sample was obtained.

3.2.2 DIGE labelling

Samples were diluted with DIGE labelling buffer to a concentration of 5 μg/μl, and the pH of each sample was checked and adjusted to pH 8.5. An internal standard was generated by pooling 25 μg/5 μl of each of the eight tumour and eight normal protein samples. As described in Chapter 2, 400 μg of the internal standard protein was labelled with 3200 pmol of Cy2 dye. Fifty μg of six of the normal samples was separately labelled with 400 pmol of Cy3 dye, and 50 μg of six of the tumour samples was separately labelled with 400 pmol of Cy5 dye. A dye swap was performed on the remaining two matched paired tumour-normal samples. Labelled matched pairs of tumour-normal protein were mixed with 50 μl of the labelled internal standard, and made up to a volume of 450 μl with rehydration buffer (Chapter 2).

3.2.3 Electrophoretic separation of proteins

Samples were rehydrated overnight into 24 cm pH 3–7 non-linear IPG strips (GE Healthcare) at 50 V, 20°C. Isoelectric focusing was carried out for approximately 80,000 Vhrs (see Chapter 2). Second dimension SDS PAGE was performed as described in Chapter 2 at 350 V on 8%–15% gradient polyacrylamide gels using an Ettan DALTsix Large Vertical electrophoresis system (GE Healthcare).

3.2.4 Gel imaging and analysis

Imaging of Cy2, Cy3 and Cy5 labelled protein spot maps was performed using a Typhoon 9400 Variable Mode Imager (GE Healthcare). The tumour-normal gel images were cropped with Image Quant v3 software (GE Healthcare) and loaded into the DeCyder™ v5 Batch Processor software. The DeCyder software carries out automated spot matching between gels during the analysis process. The matching of each individual protein spot analysed in this study was manually checked back to the corresponding protein spot on all eight analytical gels. Spot matches that were incorrectly made by DeCyder were broken, and correct matches were made. The software was then set to calculate the average abundance change ratio of proteins across the eight gels and the significance of the change using Student's paired T-test. The gels were analysed using the Biological Variation Analysis module of the DeCyder™ v5 software. The DeCyder software performs

3.2.5 Protein identification

A 2D preparative gel containing 150 μg of pooled unlabelled LMD tumour protein was electrophoresed as previously described. Protein spots were visualised with a MS compatible silver stain (Chapter 2), and protein spots of interest from the analytical gels were manually matched to the preparative gel. These protein spots were excised from the preparative gel and digested with trypsin for ion trap mass spectrometry (Chapter 2). The digested peptides were analysed with a Thermo LTQ XL linear ion trap mass spectrometer fitted with a nanospray source (Thermo Electron Corp, San Jose, CA). Five microliters of each sample was applied to a 300 μm i.d. x 5 mm C18 PepMap 100 precolumn and separated on a 75 μm x 150 mm C18 PepMap 100 column using a Dionex Ultimate 3000 HPLC (Dionex Corp, Sunnyvale, CA) with a 55 min gradient from 2% acetonitrile to 45% acetonitrile containing 0.1% formic acid at a flowrate of 200 nl/minute followed by a step to 77% acetonitrile for nine minutes. The mass spectrometer was operated in positive ion mode with one full scan of mass/charge (m/z) 300–2000 followed by product ion scans of the three most intense ions with dynamic exclusion of 30 s and collision induced dissociation energy of 35%.

The MS spectra were searched with Bioworks 3.3 (Thermo Electron Corp, San Jose, CA) using the Sequest algorithm against the IPI Human database v3.39 using Trypsin digestion as the protease, allowing for two missed cleavages, with homoserine and homoserine lactone as variable methionine modifications and using the following filters: 1) the cross-correlation scores of matches were greater than 1.5, 2.0 and 2.5 for charge state 1, 2 and 3 peptide ions respectively, 2) peptide probability was greater than 0.001 and 3) each protein identified had at least two different peptides sequenced. The mass tolerance for peptide identification of precursor ions was 1 Da and 0.5 Da for product ions.

3.3 Results

3.3.1 LMD

LMD was used to enrich and collect areas of epithelial cells from eight matched pairs of stage II tumour-normal tissues, from which protein was extracted. Examples of the laser microdissection of cancerous glands and normal colon crypts are shown in Fig. 2. The tissue sections placed on the LMD slides were relatively thick at 30 μ (approximately five to six cells thick) and large areas of crypts were microdissected one at a time (Fig. 2). Because of this the epithelial cell populations collected would not have been 100% pure, as some non-target cells (such as stromal cells or lymphocytes) within the thickness of the tissue may have also been captured. This was partially controlled by the analysis of tissue sections stained with Diff Quick that had been cut serially before and after each tissue section intended for LMD (see Chapter 2).

In order to obtain enough protein for each sample, multiple tissue sections were microdissected. The number of sections needed for any single sample depended on the size (diameter) of each section and the percentage of epithelial cells within each section. The number of sections used for each sample ranged from approximately 20–40 sections per tissue sample.

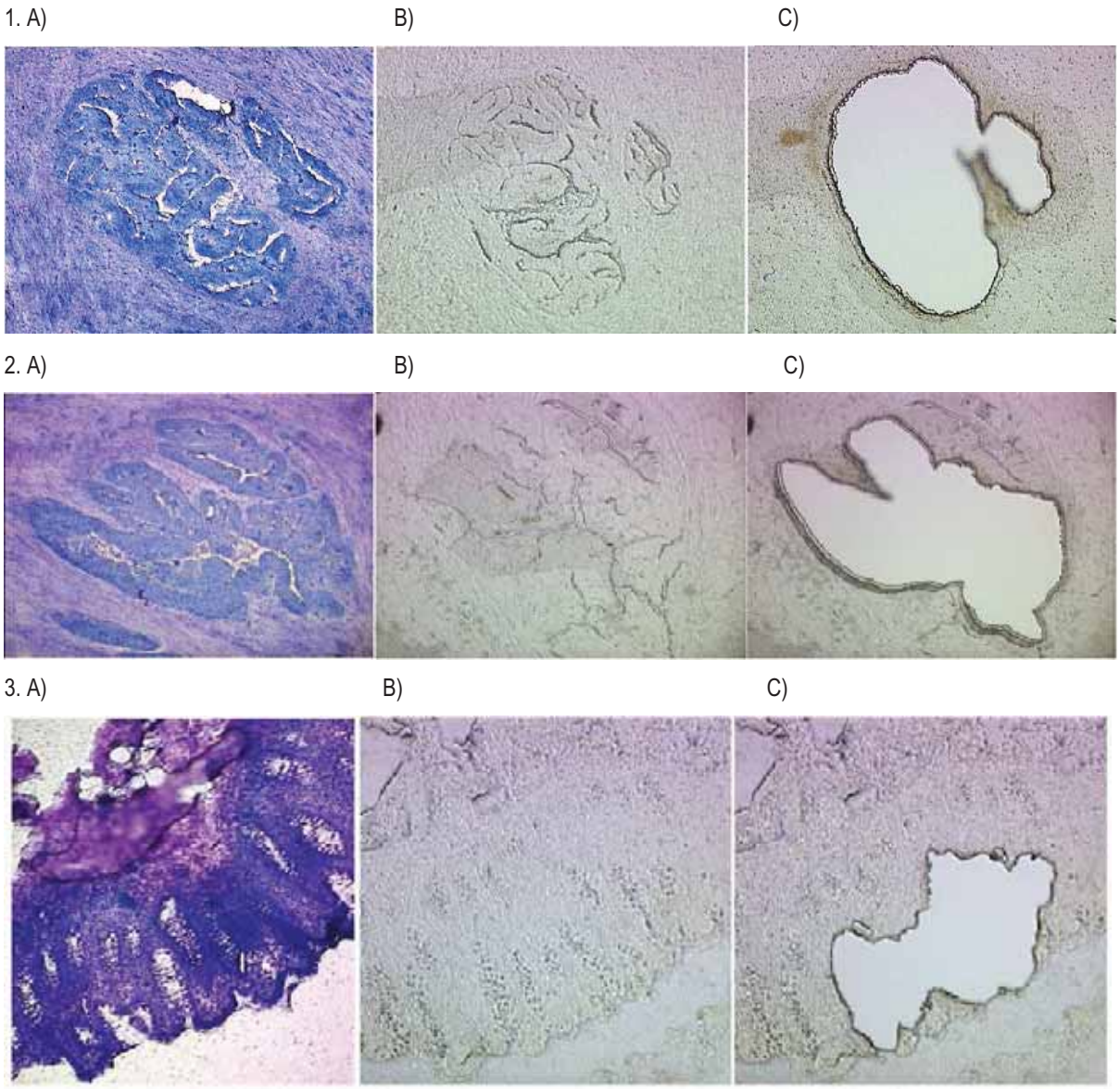

Fig 2. **Examples of LMD.** Laser microdissection of cancerous glands (1,2), and normal colon crypts (3). For LMD sections were cut 30 μ thick, placed on PEN foil framed membrane slides, stored at -80ºC, and thawed just prior to LMD. Serial sections were placed on plain glass sides, fixed, and stained with haematoxylin for reference during LMD. A) Fixed and haematoxylin stained section, B) unfixed and unstained section prior to LMD, and C) after LMD.

3.3.2 Tumour-Normal proteome changes detected by DIGE

Following isoelectric focusing and SDS PAGE, each of the eight DIGE gels was scanned to produce three independent spot maps corresponding to the Cy2, Cy3 and Cy labelled proteins run on each gel. A total of 24 spot maps were produced and were analysed using the DeCyder v5 software. Using the DeCyder software, in conjunction with manual spot matching, a total of 1,745 protein spots were matched across all eight gels. Student's paired T-test was performed on this data set, calculating the significance of the tumour-normal expression ratio of each protein spot across the eight gels. Following the statistical test, the data set was filtered by applying a significance threshold of $P \leq 0.05$, with an average ratio change in tumour-normal abundance of ≥ 2 fold and limited to spots matched on all gels. A summary of this analysis is presented in Table 1, which revealed nine protein spots to be significantly increased in abundance ≥3 fold, with 25 proteins significantly increased in abundance ≥2 fold over all, across the eight tumour-normal pairs. Fig. 3 shows a DeCyder gel image with the 25 significantly increased protein spots circled and numbered corresponding to the data presented in table 2.

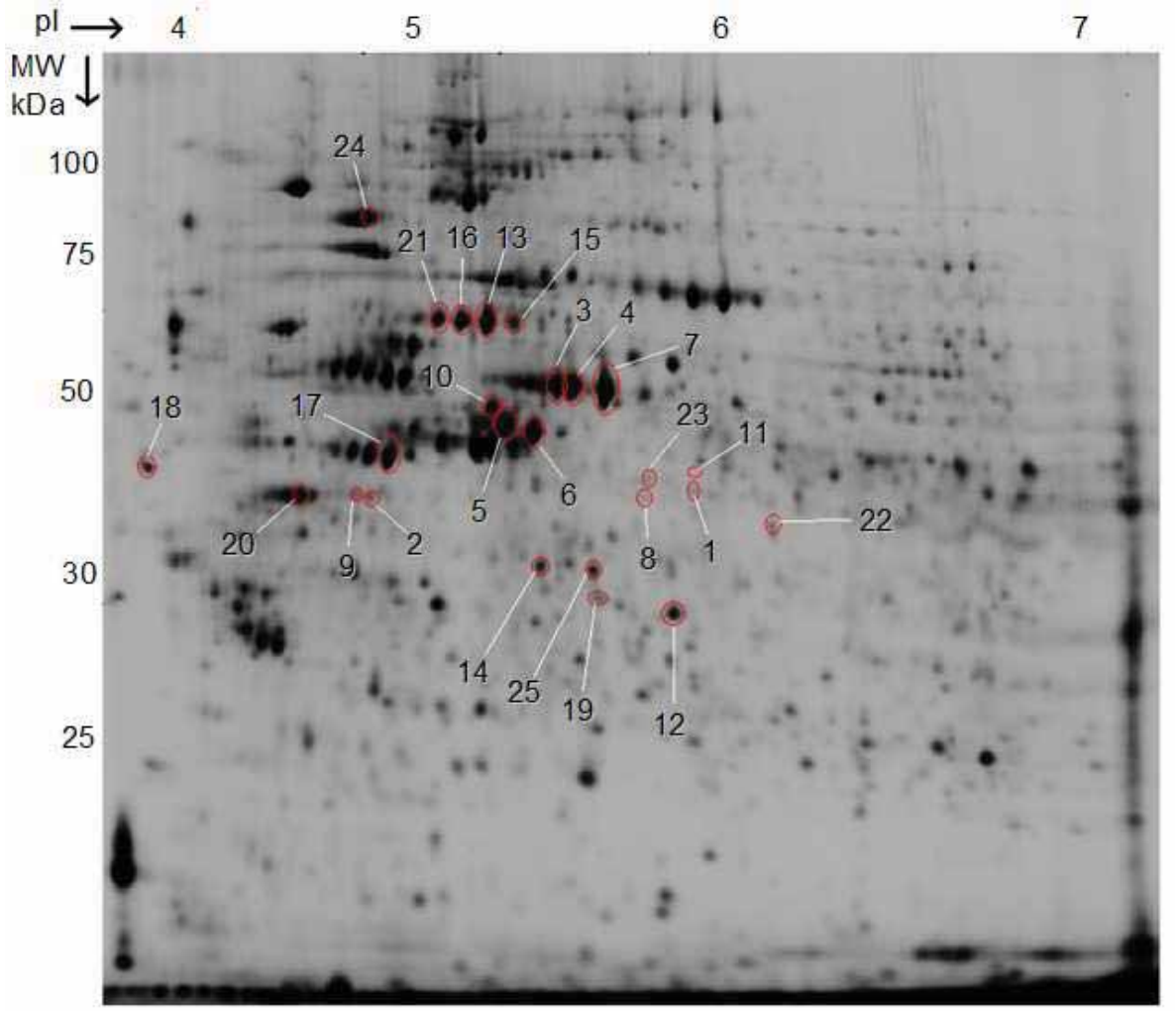

Fig 3. **Spot map of proteins significantly increased in the tumour compared to matched normal samples.** Scanned DeCyder gel image with proteins of interest identifiable by MS circled. Protein spots labelled 1–9 were found to be increased in abundance in the tumour compared to normal samples on average (n=8) ≥3 fold, P≤0.05. Protein spots labelled 10–25 were found to be were increased in abundance in the tumour compared to normal samples on average (n=8) ≥2 fold, P≤0.05.

Table 1. Quantitative 2D DIGE data of the proteins of interest.

				Tumour- normal abundance ratio for each patient							
Spot	Protein Identification	Ave. Ratio [a]	*P* [b]	1	2	3	4	5	6	7	8
1	Serpin B5	5.63	0.011	11.30	2.50	1.20	5.30	1.20	7.30	1.50	14.70
2	STRAP	4.65	0.024	1.00	3.40	4.40	1.20	2.00	21.50	2.10	1.60
3	Cytokeratin 8	4.55	0.00026	2.50	8.70	3.50	6.20	5.20	5.10	1.30	3.90
4	Cytokeratin 8	4.31	0.0052	1.30	7.50	4.30	7.50	3.40	7.70	0.80	2.00
5	Cytokeratin 18	4.20	0.013	1.20	10.50	4.40	2.00	4.60	8.50	1.60	0.80
6	Cytokeratin 18	4.00	0.037	0.70	9.60	4.20	3.00	4.60	7.70	1.70	0.48
7	Cytokeratin 8	3.97	0.0019	1.40	4.50	2.70	4.40	5.30	5.70	0.95	6.80
8	26S proeasome subunit 13	3.23	0.0019	2.30	2.20	1.40	1.00	1.90	3.80	1.50	11.70
9	hnRNP C1/C2	3.13	0.02	6.00	3.20	2.10	1.10	2.80	8.00	0.91	0.90
10	Actin	2.89	0.012	1.35	2.88	6.21	1.75	3.06	5.53	0.77	1.60
11	Macrophage Capping Protein	2.76	0.00094	2.65	1.82	3.66	4.08	4.14	3.06	1.35	1.29
12	Annexin IV	2.70	0.022	1.57	9.91	1.73	0.95	2.25	1.61	1.68	1.90
13	HSP60	2.58	0.00004	1.88	1.57	2.78	2.53	3.85	3.04	2.12	2.84
14	Inorganic Pyrophosphatase	2.50	0.0053	1.75	1.61	7.01	1.46	2.15	2.92	1.35	1.76
15	HSP60	2.42	4.40E-05	2.40	1.36	2.52	1.64	4.59	2.58	2.36	1.93
16	HSP60	2.40	0.0013	1.85	1.18	3.87	3.13	3.38	2.66	1.74	1.42
17	Cytokeratin 19	2.35	0.018	0.93	4.32	1.71	2.01	1.83	4.96	0.87	2.13
18	SET	2.32	0.021	1.18	1.10	3.33	2.73	3.73	4.35	0.87	1.25
19	Transaldolase	2.32	0.0064	1.17	6.08	2.54	1.70	1.80	1.73	2.24	1.27
20	Nucleophosmin	2.14	0.0073	1.19	1.56	2.84	3.11	3.24	2.96	1.14	1.08
21	HSP60	2.10	0.013	1.45	0.67	3.72	3.16	2.60	2.48	1.76	0.94
22	Transaldolase	2.02	0.025	1.74	1.62	1.30	5.93	1.32	0.99	1.50	1.73
23	Homology to dercidin precursor	2.02	0.015	1.88	2.36	2.77	1.35	2.69	1.81	-	1.25
24	HSP90	1.81	0.012	1.90	1.08	1.27	1.70	1.85	2.80	1.80	2.05
25	Inorganic Pyrophosphatase	1.95	0.0011	1.52	1.34	2.50	1.09	1.74	2.50	2.39	2.48

[a] Average tumour-normal abundance ratio
[b] Significance value, Student's paired T-test

3.3.3 Identification of proteins increased in abundance in colorectal cancer epithelial cells

The 25 protein spots outlined in Table 1 were selected for identification by MS. These protein spots were excised from a preparative gel containing unlabelled LMD tumour protein, digested with trypsin, and identified using HPLC MS/MS. Two or more unique peptides were sequenced for each protein. Table 2 gives the identification, SwissProt accession number, and calculated isoelectric point and molecular weight of the circled proteins. Graphical views displaying the differential expression of tumour-normal pairs for each protein increased in abundance by ≥3 fold and fold are given in Fig. 4 and Fig. 5 respectively. Table 2 displays the MS data, giving the Xcorr score, the number of peptides identified for each protein and the percentage of the full-length protein sequence covered by identified peptides.

Table 2. MS identification of the proteins exhibiting a significant change in abundance between tumour-normal matched pairs.

Spot	Protein Identification	Acc. No. [a]	Calc. pI [b]	Calc. MW (Da) [c]	App. pI [d]	App. MW (Da) [e]	Xcorr [f]	No. Peptides [g]	% Sequence Coverage [h]
1	Serpin B5	P36952	5.66	42112	5.8	40000	50.2	5	18.93
2	STRAP	Q9Y3F4	4.85	38415	4.8	39000	20.1	2	7.43
3	CK8	P05787	5.38	53672	5.4	52000	270.2	19	39.75
4	CK8	P05787	5.38	53672	5.5	52000	230.3	16	39.13
5	CK18	P05783	5.21	48029	5.2	48000	100.3	9	30.39
6	CK18	P05783	5.21	48029	5.3	48000	120.2	8	31.40
7	CK8	P05787	5.38	53672	5.6	52000	210.3	15	34.78
8	26S proteasome subunit 13	Q9UNM6	5.46	42891	5.7	40000	20.1	2	9.31
9	hnRNP C1/C2	P07910	4.8	33650	4.8	37000	30.1	2	8.82
10	Actin	P63261	5.2	41766	5.2	50000	60.2	5	18.40
11	Macrophage Capping protein	P40121	5.85	38494	5.9	41000	30.1	3	12.64
12	Annexin IV	P09525	5.75	35861	5.8	28000	160.2	11	48.28
13	HSP60	P10809	5.59	61017	5.3	59000	170.3	11	33.86
14	Inorganic pyrophosphatase	Q15181	5.47	32640	5.4	31000	50.2	4	21.45
15	HSP60	P10809	5.59	61017	5.4	59000	100.2	17	32.11
16	HSP60	P10809	5.59	61017	5.2	59000	160.3	13	35.95
17	CK19	P08727	4.9	44065	4.9	43000	180.3	14	53.50
18	SET	Q01105	4.07	33469	3.9	40000	30.2	3	13.45
19	Inorganic pyrophosphatase	Q15181	5.47	32640	5.6	29000	20.2	2	7.96
20	Nucleophosmin	P06748	4.49	32555	4.6	37000	60.2	4	18.03
21	HSP60	P10809	5.59	61017	5.1	59000	110.2	11	30.45
22	Transaldolase	P37837	6.38	37517	6.2	35000	140.2	4	12.46
23	Homology dercidin precursor	P81605	6.12	11278	5.8	40000	20.2	2	22.73
24	HSP90	P07900	4.79	84607	4.8	85000	40.2	4	6.01
25	Inorganic pyrophosphatase	Q15181	5.47	32640	5.6	31000	60.2	5	24.57

[a] SwissProt accession number
[b] Calculated isoelectric point
[c] Calculated molecular weight, Da
[d] Apparent isoelectric point
[e] Apparent molecular weight, Da
[f] Xcorr significance score
[g] Number of unique peptides sequenced
[h] % of the full-length amino acid sequence covered by identified peptides

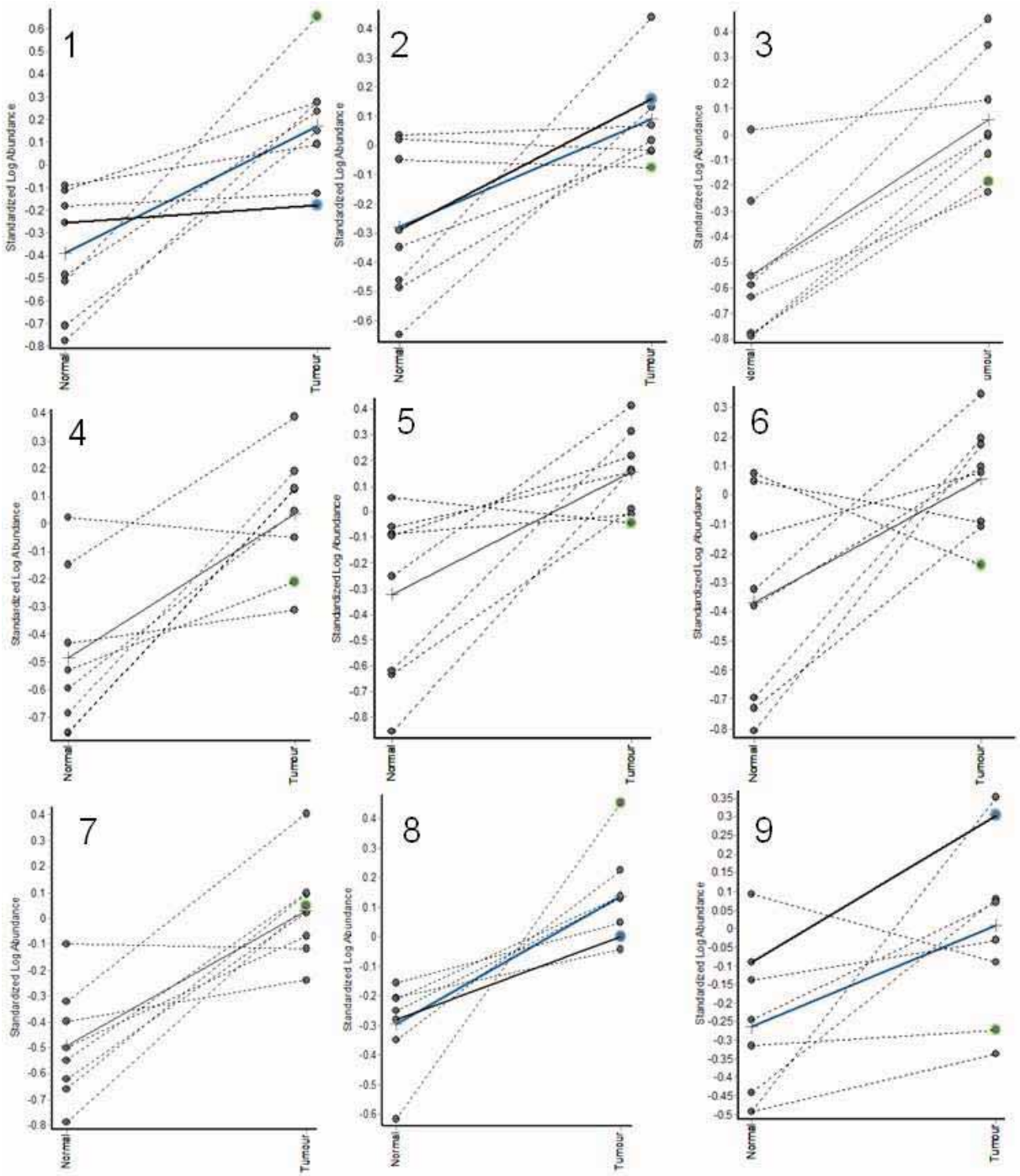

Fig 4. **Graphical view generated by DeCyder displaying the differential expression of the proteins (Table 3) with an average tumour-normal ratio of ≥3 fold.** The standardised log abundance of protein expression is displayed on the Y-axis, with the eight normal (left) and tumour (right) samples displayed on the X-axis. Each dashed line connects matched paired tumour-normal samples. The solid line represents the average increase in log abundance.

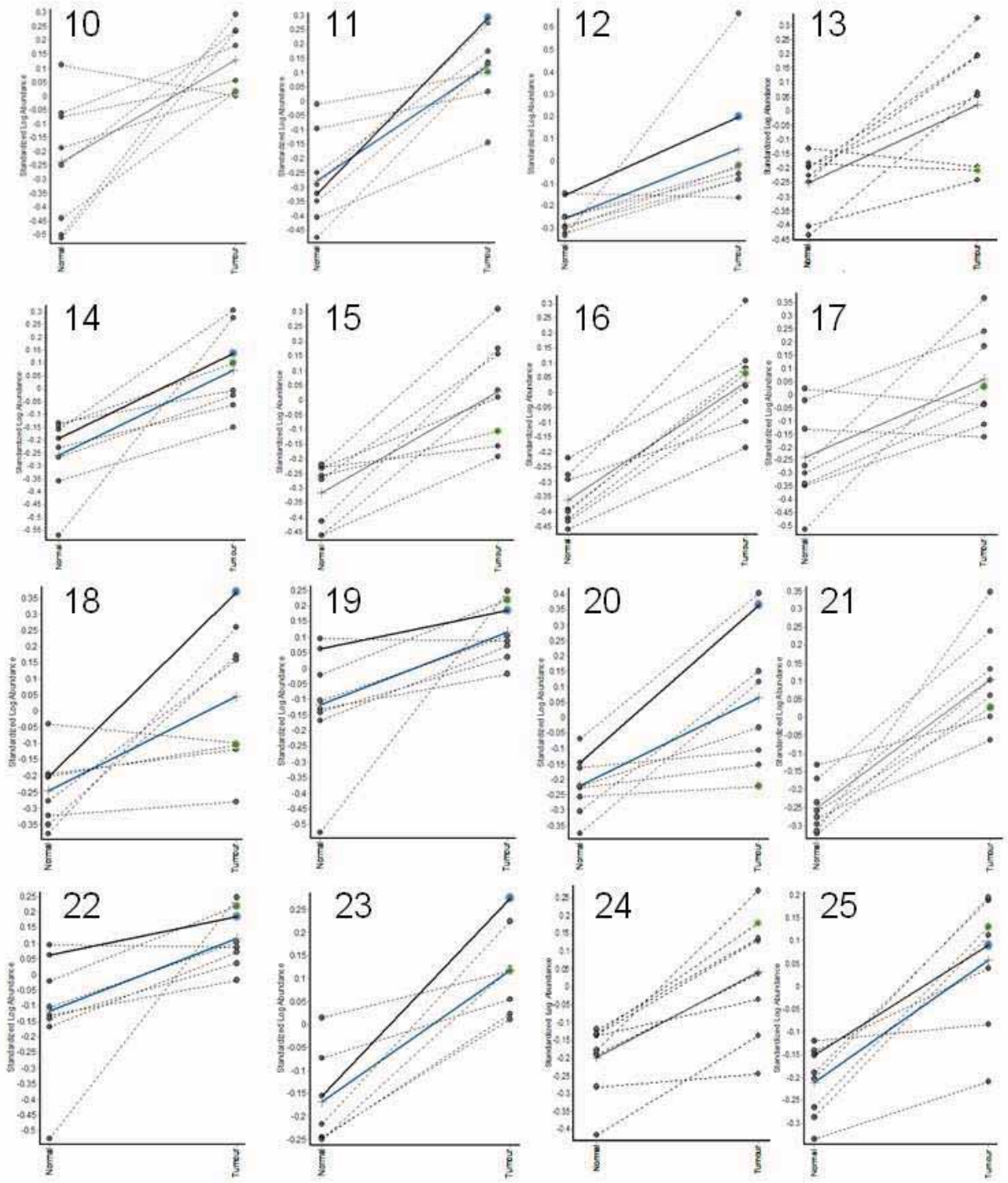

Fig 5. **Graphical view generated by DeCyder displaying the differential expression of the proteins (Table 3) with an average tumour-normal ratio between 2 and 3 fold.** The standardised log abundance of protein expression is displayed on the Y-axis, with the eight normal (left) and tumour (right) samples displayed on the X-axis. Each dashed line connects matched paired tumour-normal samples. The solid line represents the average increase in log abundance.

3.4 Discussion

In this study, the quantitative analysis of 1,754 resolved and detected protein spots across 24 gel images, from eight tumour-normal tissue pairs was performed. The overall aim of this study was to identify proteins that exhibited increased expression in LMD tumour samples compared to LMD normal mucosal samples. It was expected that mass spectrometry identification of the proteins that comprise these spots would lead to the elucidation of proteins and pathways altered in CRC, potentially aiding in the disease pathogenesis.

3.4.1 LMD

It was decided the collection of 75 μg of protein from eight tumour-normal matched paired tissue samples by LMD was viable. Given that a cohort size of eight also produced a good experimental value, this was the number of samples used in the minimal labelling study. Given that a relatively large amount of tissue was required to be collected by LMD, the collection of completely pure epithelial cell populations was not viable and the technique of LMD was intended to be used as a method of enrichment. For LMD tissue sections were cut at 30 μ, hence the tissue areas microdissected would have been approximately four to five cells thick, which would have introduced a small number of contaminating cells. The tissue areas microdissected were also relatively large (in comparison to other laser capture methods that involve the collection of single cells), which would have introduced more cellular contamination. Despite this, the predicted epithelial cell purity of the LMD samples was around 90%. Given that whole pieces of colon tissue contain large areas of muscularis mucosa, stromal elements, plus infiltrating lymphocytes in the case of tumour tissues, this is significant epithelial cell enrichment.

3.4.2 2D DIGE and LC MS/MS

All eight of the 2D gels show good reproducibility and protein spot focusing, with little to no streaking in the horizontal or vertical directions. The quality of the MS data obtained for each protein sample was high, with only one protein identified in each sample (excluding skin and hair keratins) when applying the parameters of at least two unique peptides sequenced per protein. Only one protein, identified as 'homology to dercidin precursor', did not correlate when comparing the calculated MW and pI to the apparent MW and pI as seen on the 2D gels. Ideally this protein sample needs to be reanalysed by LC MS/MS.

Overall 25 protein spots were identified as being significantly increased in abundance ≥2 fold in the tumour compared to matched normal samples, conferring to seventeen individual proteins. A number of proteins were also found to be significantly decreased in abundance in the tumour compared to normal samples,

however these proteins were not taken into consideration for analysis in this study. The proteins identified in this work have all been previously linked to cancer, as discussed in more detail below.

3.4.3 Proteins identified as significantly increased in abundance in tumour compared to normal >3 fold

Serpin B5 (or Maspin) was found to be increased in abundance in the tumour compared to normal samples 5.63 fold, P=0.011. Serpin B5 is a well documented tumour suppressor in breast cancer, known to block the growth, invasion and metastatic properties of mammary tumours[103] [104] [105], and is an apoptosis-inducing factor secreted by normal breast epithelial cells.[106] Homozygous loss of the gene is lethal, but the precise physiological role of the protein is unclear.[107] A study by Song *et al*. (2002)[108] compared the expression levels of serpin B5 in adenomas, adenocarcinomas and metastasis from human colon specimens. They found serpin B5 to be downregulated in the adenocarcinomas and metastases compared to the adenomas, signifying a downregulation of the tumour suppressor in the more advanced cancer stages. Other studies have found serpin B5 to be significantly upregulated in CRC.[109,110] Findeisin *et al*. (2008)[111] quantitated levels of serpin B5 in the peripheral venous blood of 63 CRC patients and 36 controls without malignant disease using relative real-time RT-PCR. Results indicate serpin B5 may be a marker for the detection of minimal residual disease in the peripheral blood of CRC patients.

The serine-threonine kinase receptor associated protein (STRAP) exhibited increased expression in the tumours 4.65 fold, P=0.024, in comparison to the normal samples. STRAP interacts with the serine/threonine kinase receptors TbR-I and TbR-II, which form heteromeric complexes upon ligand binding to mediate responses to TGF β signalling.[112] The TGF β signalling pathway is an important regulator of cell proliferation and differentiation, and acts as a tumour suppressor through growth inhibition, apoptosis induction, and the ability to inhibit genomic instability in non-transformed cells.[113] Through association with TGF β receptors, STRAP synergises with the inhibitory Smad protein, Smad7, resulting in negative regulation of TGFβ-induced transcription.[112] STRAP is ubiquitously expressed and localises in both cytoplasm and nucleus.[113] Stable expression of STRAP results in activation of the mitogen-activated protein kinase/extracellular signal-regulated pathway (MAPK/ERK), resulting in the downregulation of the cyclin-dependent kinase inhibitor p21 (Cip1), leading to retinoblastoma protein hyperphosphorylation. Gene expression knock down of STRAP has been shown to increase TGF β signalling, reducing ERK activity, increasing p21 (Cip1) expression, decreasing tumourigenicity.[113] Previously STRAP has been found to be upregulated in a large proportion of colorectal adenomas and carcinomas.[114] Therefore an observed increase in STRAP expression is consistent with a role in CRC tumourigenesis.

Three isoforms of Cytokeratin 18 (CK18) were found to be significantly increased in abundance in the tumour compared to normal samples. CK18 is an intermediate filament protein involved in cytoskeletal organisation[115] that interacts with cytokeratin 8 (CK8) to form insoluble 10 nm filaments that extend from the nucleus to the internal leaflet of the plasma membrane.[116] [117] Both CK18 and CK8 were found to be significantly upregulated in the tumour samples. Phosphorylation of CK18 at serine 52 plays a role in filament organisation in interphase cells[118], and phosphorylation of serine 34 is increased during mitosis.[119] Phosphorylation of CK18 may explain the observation of multiply detected isoforms. CK18 has been described as a potential marker of disseminated tumour cells detected in the bone marrow of patients with transitional cell carcinoma[120] and lung carcinoma.[121] Upon tumour cell apoptosis, CK18 is specifically cleaved by caspases and released into the blood by the dying tumour cells. It is thought the caspase cleaved form of CK18 has use as a serum marker of patient responsiveness to anticancer therapies.[122]

The protein 26S proteasome non-ATPase regulatory subunit 13 had the highest level of average tumour-normal upregulation at 3.23, P=0.0019 (Table 3). This fold change ratio was skewed however by one tumour-normal pair with a fold change of 11.17. The 26S proteasome non-ATPase regulatory subunit 13 protein is a component of the 26S proteasome, which consists of a 20S core particle capped by 19S regulatory complexes at each end.[123] The 19S regulatory complexes are composed of two main subcomplexes; a base containing six ATPases and two non-ATPase subunits, one of which is the identified regulatory subunit 13.[124] Degradation by the 26S proteasome requires ATP and the protein targeted for degradation to have been conjugated with a polyubiquitin chain.[125] It is thought that the 19S regulatory complex is responsible for the recognition of the polyubiquitinated target proteins and cleavage of the polyubuquitin chains[125], unfolding of the target proteins and their translocation into the catalytic chamber of the 20S core particle.[126] Eighty to 90% of cellular proteins are degraded by the 26S proteasome[127], and due to the roles it plays in cell cycle regulation, apoptosis, and angiogenesis, the 26S proteosome is an important regulator of carcinogenesis.[128] Currently the proteosome inhibitor bortezomib (Velcade, PS-341) is being used clinically as an anticancer therapy [128].

The heterogeneous nuclear ribonucleoproteins C1/C2 (hnRNP C1/C2) were found to be increased in abundance in the tumour samples 3.13 fold, P=0.02, in comparison to normal. hnRNP C1/C2 are nuclear pre-mRNA binding proteins, derived from alternative splicing events. hnRNP C1/C2 have been found to be significantly upregulated in human hepatocellular carcinoma samples.[129] Various heterogeneous nuclear ribonucleoproteins are thought to bind to telomeres and telomerase in order to gain access to telomeres to help regulate their length. hnRNP C1/C2 are known auxiliary proteins of human telomerase [130] and hence may aid carcinoma cells in gaining immortality.

3.4.4 Proteins identified as significantly increased in abundance in tumour compared to normal >2 fold

The macrophage capping protein (CapG), annexin IV, HSP60, inorganic pyrophosphatase, transaldolase, nucleophosmin and HSP90 were found to be increased in abundance in the tumour samples compared to normal greater than 2 fold, but less than 3 fold. CapG is a target gene of the transcriptional activator AP-1, which is implicated in the regulation of tumour cell proliferation and Ras-dependent morphological transformation, and is composed of members of the Jun and Fos proto-oncogene families.[131] CapG has been reported as increased in pancreatic, brain, and lung carcinomas, and in ocular melanoma, and is known to promote invasion of epithelial cells via the Ras-PI3K pathway and CDC42 or RhoA.[132]

Annexin IV is a calcium regulated phospholipid binding protein found almost exclusively in epithelial cells.[133] Duncan *et al*. (2008)[134] found Annexin IV to be upregulated in colorectal tumours compared to matched normal tissues by 2DE and MALDI-TOF MS, and found Annexin IV expression to increase significantly with tumour stage by microarray and immunohistochemistry (IHC). Zimmermann *et al*. (2004)[133] identified Annexin IV to be increased in abundance in renal clear cell carcinoma by 2DE, and found the subcellular localisation of Annexin IV by IHC was linked to a loss of cell-to-cell adhesion and increased tumour dissemination. Over expression of Annexin IV promoted cell migration in a model carcinoma system. Annexin IV has also been suggested as a marker of drug resistance to certain cancer therapies.[135]

HSP60 is upregulated during times of cellular stress[136] and has been identified as over-expressed in prostate cancer[137], breast cancer[138] and previously in CRC[88]. HSP60 expression has also been identified on the surface of lymphoblasts[139], pancreatic adenoma[140] and colon adenocarcinoma cells.[141] Capello *et al.* (2005)[142] studied HSP60 expression by IHC and western blotting in primary tumours and lymph node metastasis of the large bowel, and found a significant correlation between HSP60 expression and tumour grade, and between high levels of HSP60 expression and lymph node metastasis. There was no significant correlation between the degree of inflammation in the tumours and the level of immunopositivity for HSP60. HSP60 forms a complex with HSP10 in the mitochondria, and this complex is involved in the activation of the caspase cascade triggered during hypoxic-ischemic damage. The HSP60/HSP10 complex has been shown to help prevent the activation of apoptotic machinery.[143] [144] [145] Pro-caspase 3 complexes with HSP60 and HSP10 in the mitochondria of the Jurkat T-cell line, and the release of the complex into the cell cytoplasm may increase the speed of caspase activation.[145] Overexpression of HSP60 and HSP10 in an in vitro model of ischemia/reperfusion injury has been suggested as a protective mechanism for myocytes against apoptosis.

Inorganic pyrophosphatase has been previously reported as upregulated in CRC.[146]

Inorganic pyrophosphatase catalyses the hydrolysis of PPi to inorganic phosphate, which is involved in the biosynthesis of macromolecules, a wide range of metabolic activations and the direct hydrolysis of nucleoside triphosphates. The increased expression of inorganic pyrophosphatase in CRC may relate to increased energy requirement of rapidly growing tumour cells.[147] Inorganic pyrophosphatase has been patented as an early stage marker of CRC (IP (WO/2005/124353)).

Transaldolase is an enzyme involved in the non-oxidative part of the pentose phosphate pathway (PPP), which synthesises the majority of the cellular NADPH. NADPH dependent antioxidant defence enzymes, such as catalase and glutathione reductase, contribute to counteract effects of reactive oxygen species, which frequently give rise to DNA damage and mutation. It is thought that control of both the oxidative (via NADPH synthesis) and non-oxidative branch of the PPP (via ribose 5-P or NADPH levels) may be critical in cancer. Transaldolase has a large impact on the balance between the non-oxidative and oxidative branches of PPP, and ultimately the output of NADPH and ribose 5-P. High transaldolase activity has been shown to correspond with low catalase activity in Xeroderma Pigmentosun patients who have a high predisposition to developing skin cancer[148], and hence may promote DNA damage and mutation via the inhibition of catalase activity.[148]

Nucleophosmin is involved in the transport of pre-ribosomal particles and in ribosome biogenesis, response to stress stimuli (UV irradiation, hypoxia), and maintenance of genomic stability including control of cellular ploidy, participation in DNA-repair processes, and regulation DNA transcription through modulation of chromatin condensation and decondensation events. Nucleophosmin is also involved in regulating the activity and stability of p53 and ARF, and has been reported as over-expressed in various tumours including gastric, colon, ovarian and prostate carcinomas.[149]

HSP90 is a chaperone protein that interacts with a number of proteins involved in signalling pathways vital for cell proliferation, regulation of cell cycle progression and apoptosis (reviewed in [150]). Heat shock proteins can be generalised into two categories of protein 'folders' or protein 'holders'. HSP90 is a protein holder that binds to unfolded polypeptide sequences of its protein substrates, stabilising proteins with otherwise unstable tertiary structure. HSP90 then releases unstable proteins to 'folding' chaperones, such as HSP60, which self-associate to form folding complexes where substrate proteins undergo the required intramolecular interactions to attain their correct tertiary structure in an ATP dependent process. HSP90 is an important cell regulator given its ability to stabilise and maintain the active confirmation of receptor proteins, kinases and transcription factors involved in oncogenic transformation, such as Her 2, Raf 1, Akt, Cdk 4, Polo 1 kinase, cMET, mutant B raf, mutant p53, AR, ER, Brc-Abl, HIF 1 α, and hTERT (reviewed in [150]).

HSP90 inhibitors provided insight into the role of HSP90 in tumour progression, and are a promising therapeutic agent. It was discovered that the HSP90 inhibitor geldanamycin bound to HSP90 and altered the chaperonin function, thus driving the degradation of HSP90 substrate proteins by stimulating HSP90 mediated presentation to the ubiquitin proteasome machinery. The substrate proteins could not attain their correct active confirmation and were degraded by the proteasome.[151] HSP90 inhibitors appear to selectively target tumour cells, as they appear to accumulate where there is active HSP90. In tumour cells, HSP90 exists predominantly in an active state in complex with co-chaperones; conversely in normal cells, HSP90 is predominantly in a latent un-complexed state.

3.5 Proteins chosen for further analysis

Basic selection criteria were used in order to choose a small number of proteins for further analysis. Proteins were chosen for novelty when questions existed as to why their levels were increased in CRC, and how this may promote tumourigenesis. Expression levels of the chosen proteins in carcinoma cells and tumour tissues also needed to be relatively high to make the proteins useful biomarkers of single cancer cells.

3.5.1 Cytokeratin 8

Three isoforms of the protein cytokeratin 8 (CK8) were found to be significantly increased in abundance across the eight tumour samples ≥3 fold, $P<0.05$ (Table 3). In six of the eight tumours, all three CK8 isoforms had a matched paired tumour to normal expression ratio of >2 fold. CK8 was chosen to be of interest as the three isoforms were the most consistently found to be increased in abundance across the individual matched paired tumour-normal samples. Of particular interest was the increased level of the protein isoforms, what was causing the formation of the isoforms, and how this process may be relevant to CRC. CK8 is commonly only expressed by epithelial cells, making CK8 an attractive potential marker given its cell type specificity.

The three isoforms of CK8 appeared at approximately the same molecular weight with differing isoelectric points (pI), and so were predicted to be a result of post-translational modifications. Multiple phosphorylation sites for CK8 have been annotated, and the phosphorylation of intermediate filament proteins has been shown to regulate assembly, disassembly, and organisation in vitro and in vivo.[152] [153] [154] It has also been shown that CK8 is hyperphosphorylated during mitotic arrest, in times of stress, and during apoptosis[155] to such an extent that it appears at a slightly higher MW on a 1D gel in comparison to the basally phosphorylated form.[119] A small amount of hyperphosphorylated CK8 occurs during regular mitosis, with low steady state levels in resting cells.[155] The phosphorylation of CK8 was chosen for investigation, as it was hypothesised that levels of phosphorylated CK8 were significantly increased in colon carcinoma cells compared to matched normal mucosa. This was of interest as CK8 is known to be phosphorylated by the

MAP kinases JNK and p38 during cell stress and by ERK1 in response to EGFR.[119] [156] [157] [158] Increased via the EGFR pathway has been well documented in CRC, and can be a result of upregulation of activating ligands such as EGF and TGF α or by activating mutations in the EGFR pathway. Constitutive activation of the EGFR/Ras/Raf/MEK/ERK pathway occurs in almost 50% of CRC patients due to mutations in the KRAS and BRAF genes.[159] [160] [161] The increased levels of CK8 phosphorylation in tumour compared to matched normal tissues, and the relationship between CK8 phosphorylation and the EGFR/Ras/Raf/MEK/ERK pathway forms the basis of chapter 5.

3.5.2 Phosphatase 2A inhibitor protein, SET

The phosphatase 2A inhibitor protein, SET, was found to have an average increase in tumour to normal abundance 2.32 fold, P=0.021. Four of the eight samples showed a matched paired tumour to normal expression ratio of about 1, ranging from 0.9 to 1.25. However, the remaining four samples showed significantly higher matched paired tumour to normal expression ratios of 2.7, 3.3, 3.73 and 4.55. SET was chosen as a protein of interest given the role it plays in multiple signalling pathways involved in cell cycle progression and oncogenesis.

The role of SET in leukaemia and some cancer pathways has previously been described, but has not yet been detailed in CRC. A SET fusion protein, SET-CAN, is known to play a role in acute undifferentiated leukaemia.[162] It is thought SET is involved in G1/S transition via the regulation of cyclin E-CDK2 activity[163], and in G2/M transition via the regulation of cyclin B-CDK1 activity.[164] Al-Murrani *et al*. (1999)[165] have shown levels of the proto-oncogene c-Jun increased in HEK-293 cells transfected with SET, and that SET is an inhibitor of the tumour metastasis suppressor NM23-H1.[166] SET has also been shown to play a role in the Wnt signalling pathway. Ninety percent of all colorectal cancers have Wnt signalling pathway mutations. SET is an inhibitor of the tumour suppressor serine/threonine protein phosphatase 2A (PP2A).[167] [168] PP2A comprises part of the β catenin turnover complex, together with GSK3 β, APC and Axin. In normal cells, when no Wnt signalling is present, β catenin is phosphorylated by the turnover complex that targets the protein for degradation. Wnt signalling pathway mutations in CRC inhibit β catenin phosphorylation and the protein is no longer degraded. As a result β catenin accumulates in the cytoplasm before translocating to the nucleus where it binds to TCF transcription factors, activating the expression of downstream oncogenes. Mutations in the Wnt signalling pathway are known to be an early event and an initiating factor of the adenoma-carcinoma sequence.

Chapter 6 analyses the level of SET upregulation in matched tumour-normal pairs in a larger cohort of CRC patients by relative real-time RT-PCR, and the effect of reducing SET expression by siRNA on β catenin

levels and Wnt signalling in cell lines. The effect of SET expression on signalling pathways involved in transformation and tumourigenesis are also analysed using the RT^2 Profiler PCR Arrays (SA Biosciences).

3.5.3 Desmin

In the pilot study, tissue was laser microdissected with the aim of detecting proteins differentially expressed between tumour-normal epithelial cells, however some stromal elements closely associated with the epithelial glands were collected in order to determine changes in the stromal cells due to alterations in the tissue microenvironment. Desmin was identified as increased in abundance by an average of 2.25 fold, P=0.017, in four late stage tumours relative to matched normal mucosa using scarce labelling DIGE. Desmin is a smooth-muscle type intermediate filament protein, used as a muscle cell marker. Epithelial cells and differentiated stromal cells of the colon do not typically express the protein. Desmin was chosen for further analysis as part of this PhD work given the atypical expression of the protein in the colon tissue. It was hypothesised that alterations in the tumour microenvironment were causing the transdifferentiation of colonic cells to express desmin, or the recruitment of desmin expressing cells to the tumour area. This process was thought to be of interest as it may involve cancer processes such as epithelial-mesenchymal transition and angiogenesis. The characterisation of desmin expression in CRC by immunohistochemistry forms Chapter 4.

3.6 Repeat offenders—proteins commonly identified in 2DE MS studies

Recently, two papers have been published in the journal *Proteomics* detailing a list of proteins that are repeatedly identified in 2DE MS studies[169 170], irrespective of the studies' designs or objectives, species, tissues or organs sampled. This raised the question—is the list of commonly identified proteins due to artefacts and is the technology biasing results? The commonly identified proteins included glycolytic enzymes, heat shock proteins (HSPs), proteasomal subunits, heterogeneous nuclear ribonucleoproteins (hnRNPs), keratins and annexins, and were grouped into the functional classes of energy metabolism, cytoskeleton re-organisation, cellular growth or molecular chaperones by Wang *et al*. (2009).[169] A number of proteins detected in this study fall into the list of commonly identified proteins such as CK8, CK18, CK19, HSP60, hnRNP C1/C2, annexin IV and 26S proteasome non-ATPase regulatory subunit 13. Wang *et al*. (2009)[169] suggests that the repeat detection of such proteins in studies on inflammatory conditions, cancer, drug treatments, ageing, apoptosis, cellular stress conditions and signal transduction may be due to artefacts associated with the techniques of 2DE MS, or may be due to cellular stress responses. However, it is not surprising that diseased cells or cells exposed to the treatment conditions that Wang *et al*. (2009)[169] and Petrak *et al*. (2008)[170] describe undergo significant changes in structure, explaining the detection of proteins involved in cytoskeleton, the speed of cellular replication or death, the detection of proteins involved in

metabolism and growth, or signal transduction and the expression alterations and detection of chaperonins. The proteins detected in this study that overlap with proteins listed by Wang *et al*. (2009)[169] and Petrak *et al*. (2008)[170] have all been previously described in cancer, and the significance of the roles they play in the disease pathogenesis has been discussed as before. In particular, multiple isoforms of CK8/CK18 and HSP60 were both identified. Petrak *et al*. (2008)[170] point out that often the identification of keratins in DIGE MS studies is due to skin, hair and mucosal contamination. It is important to point out that CK8 and CK18 are epithelial specific keratins, not expressed in the skin, hair, or mucosal secretions. Wang *et al*. (2009)[169] suggest that the identification of proteins such as HSP60 is due to global cellular stress and inflammatory responses. However, the upregulation of HSP60 in CRC has been previously described and no significant correlation between the degree of inflammation in the tumours studied and the level of immunopositivity for HSP60 was found[142] suggesting the increase of HSP60 in the tumours was not due to an inflammatory response.

The common identification of certain proteins in 2D MS studies is most likely due to their relatively high abundance, the way in which they resolve by 2DE, and their ease of identification by MS. For example, the proteins listed are mainly cytosolic and hydrophilic, with in a molecular weight range of around 20 kDa to 100 kDa favouring 2DE, and trypsin digest into peptides easily ionisable by MS. This however does not mean they are not biologically significant to the disease or condition being studied. What it does mean is that innovative technical approaches need to be applied in the future, in order to identify novel proteins involved in disease pathogenesis or certain treatment conditions; ideally approaches that favour the identification of hydrophobic and low abundance proteins. It is also important to note that while the two studies discussed here found significant overlap in the proteins identified amongst the studies assessed, there also appeared to be a list of proteins specific to each study displaying the technical ability of 2D MS to discover experimentally relevant proteins.

4 Desmin

4.1 Introduction

4.1.1 Identification of desmin as a potential biomarker

The LMD scarce labelling DIGE pilot study identified desmin as over-expressed by an average of 2.25 fold, P=0.017, in four late stage tumours relative to matched normal mucosa. In this work, LMD was used to enrich colonic crypts and adjacent stroma in tight association with the colon epithelial glands, from the normal samples and neoplastic glands from the tumour samples (avoiding areas of muscularis mucosa). Areas of tumour where the cancerous growth had penetrated the muscularis propria were not used for LMD. This study aimed to examine proteins differentially expressed between tumour-normal epithelial cells, and in the stromal elements closely associated with the epithelial glands, in order to analyse alterations in the tissue microenvironment. Changes in a tumour microenvironment can influence the gene expression profiles of surrounding epithelial[171,172] and stromal cells.[173] Host factors and signalling between carcinoma and neighbouring cells play a role in invasion and metastasis[173-175], hence a change in the tumour microenvironment can lead to changes in the molecular cross-talk between epithelial and stromal cells, achieved by heterotypic cell-to-cell contacts or signalling molecules. Correct and controlled cross-talk between these cells is of significant importance, and is vital for organ development and function during embryogenesis.[176-178]

A scanned DeCyder 2D DIGE gel image from the pilot study with desmin marked is shown in Fig. 1. Three of the analysed tumours were stage III, and had individual tumour-normal abundance values of 2.8, 1.2 and 1.6. The fourth sample used was a primary tumour from a patient with liver metastasis and had a tumour-normal abundance value of 3.45. A standardised log abundance graph generated by DeCyder displaying the differential expression of desmin between normal and tumour samples is shown in Fig. 2. The protein spot pattern of the 2D DIGE gel image displayed in this chapter looks different to the protein spot pattern of the 2D DIGE gel image displayed in chapter 3. The difference in the overall spot patterns can be explained by the labelling chemistry of the different CyDyes used for each gel. In the pilot study the scarce labelling CyDyes were used, these dyes aim to label all available cystine residues. The dyes themselves add extra charge and mass to a protein, hence the isoelectric point and molecular weight of a protein may be altered by the addition of the dye, depending on the number of cystine residues available for labelling. The minimal labelling dyes used in the biomarker discovery phase of this project label lysine residues at a low ratio, only 1% to 2%, so that each visualised protein is likely to have one dye molecule attached. As all of the proteins within a sample are labelled uniformly, the overall spot pattern of the sample is not altered.

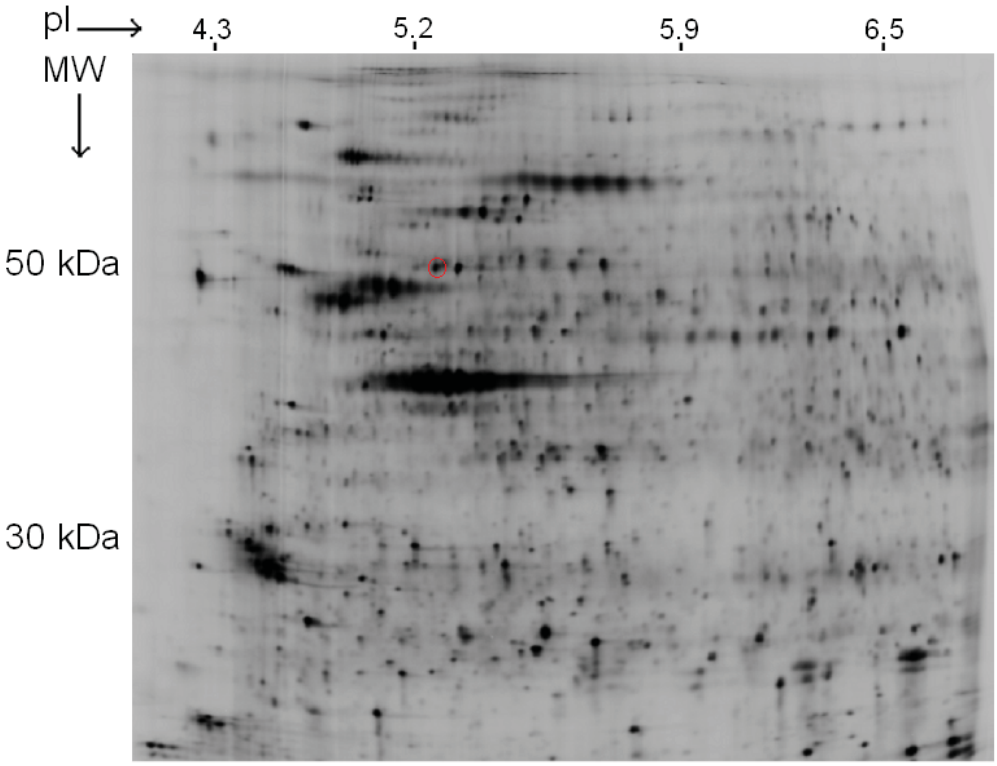

Fig 1. Saturation labelling DIGE gel image. The gel map shown is of a Cy5 labelled tumour sample with the protein identified as desmin is circled in red, displaying an apparent molecular weight (MW) of 53 kDa, and isoelectric point (pI) of 5.21.

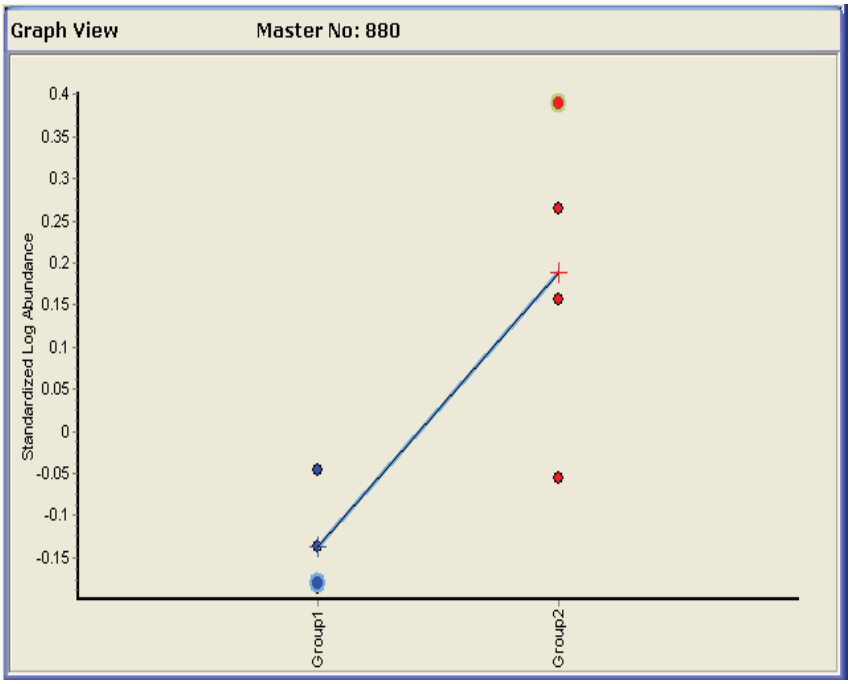

Fig 2. **Tumour-normal expression levels of desmin.** Graphical view generated by DeCyder, displaying the differential expression of desmin between normal and tumour samples. The standardised log abundance of desmin is displayed on the Y-axis, with the four normal (Group 1) and tumour (Group 2) samples displayed on the X-axis. The line represents the average increase in log abundance.

The identification of desmin from LMD-enriched colonic mucosal cells and closely associated stromal elements was unexpected as desmin is a smooth-muscle type intermediate filament protein, normally expressed by smooth-muscle cells. Epithelial cells do not express desmin and nor do stromal cells. Stromal desmin expression has only normally been observed in the uterus undergoing decidual cell differentiation.[179] Low levels of focal desmin expression amongst the stromal element has been seen in colorectal adenomas.[180] Low levels of sporadic desmin expression can sometimes be observed amongst the cells situated between the base of the crypts and the muscularis mucosa in normal tissue, most probably due to displaced muscularis mucosal cells.

Immunofluorescence (IF) was performed on tissue from stage I, II and III tumours in order to evaluate the origin of the desmin expression, and this showed desmin expression by cells closely associated with the neoplastic glands amongst the stromal element. The level of these desmin expressing cells within the tissue stroma also appeared to increase with tumour stage. Previously, such cells had been defined as myofibroblasts[181] or pericytes.[182] [183] It was also thought that the desmin expressing cells could be mural cells (vascular smooth-muscle cells and pericytes) or muscularis mucosae into which the tumour had invaded.

4.1.2 Desmin

The protein desmin is a 53 kDa intermediate filament protein expressed in cardiac, skeletal and smooth muscle cells. Desmin is encoded by a single gene on chromosome 2q35 [184], consisting of nine exons and eight introms within a 8.4 kb region encoding 476 amino acids. [185] The desmin gene is highly conserved amongst vertebrate species. The protein is comprised of a 308 amino acid central alpha helical rod domain which forms double-stranded coils, flanked by globular N- and C- terminal head and tail domains respectively. [186] The alpha helical rod domain contains a seven residue repeat pattern with a common sequence of hydrophobic and hrydrophilic amino acids. This structure allows desmin molecules to self assemble into 10 nm homopholymer or heretopolymer coiled coil dimmer filaments.

In skeletal muscle fibers the major filaments (intermediate filaments, microfilaments and microtubules [187]) primary function is to link and stabilize cell components such as myofibrils, mitochondria, the sacrotubular system and nuclei [188]. Sarcomeres are the contractile unit of the myofibrils in striated muscle and the cytoskeleton can be divided into extra-sarcomeric, intra-sarcomeric and subsarcolemmal segments. Desmin intermediate filaments form the extra-sarcomeric cytoskeleton.

In heart and skeletal muscle cells desmin filaments form a scaffold around the myofibrillar Z-discs, keeping the adjacent myofibrils in lateral alignment at the Z-disc periphery. [189] This binds the contractile

apparatus to the sarcolemma, nuclei and other organelles, giving the cells structural integrity and allowing for a continuous cytoskeletal network. Desmin intermediate filaments in striated muscle also aid in force transmission and cell signaling. In the heart desmin is a significant component of the Purkinhe fibres and is increased at the intercalated discs. [190] In smooth muscle the cytoskeletal region at the dense bodies and dense plaques contains high levels of desmin.

The role of desmin in development has been studied using demin knockout mice (Des-/-). Such knockout mice appear to develop normally and are fertile, only after birth do defects appear to develop in skeletal, smooth and cardiac muscles. [185,186,191] The most significant effects can be seen in weight-bearing muscles and in constant use muscles such as the diaphragm of the heart. Desmin knockout mice are weaker and fatigue more easily than their wild-type counterparts and desmin insufficiency leaves fibers more vulnerable to damage during muscle contraction. In the knockout mice the myofibers would degenerate and macrophages would invade the muscle tissue. The fibers would then regenerate, but would often be disorganized and aberrant. Interestingly, desmin ablation from the sarcomere did not interfere with the primary muscle formation or regeneration, but myofibrillogenesis in the regenerating fibers was often abortive, implicating desmin in the repair process. The knockout studies showed desmin to be vital in the structural integrity of skeletal muscle, but nor for myogeneis commitment or differentiation. The hearts of the knockout mice developed myopathy with impaired active force generation, suggesting desmin plays a role in the active force generation by cardiac muscle cells, perhaps by supporting the sarcomere alignment or force transmission. [192]

4.1.3 Hypotheses for the cell type expressing desmin

There is evidence to suggest vascular smooth-muscle cells and pericytes may be able to migrate into tissue stroma during cancer progression as a result of angiogenic stimulation.[193-195] [196,197] Smooth-muscle cells within a colonic tumour tissue microenvironment have also been shown to alter in phenotype, becoming more like eosinophilic spindle cells.[198] Fibroblastic stromal cells have altered expression profiles during wound healing in normal tissue and in cancerous tissue where they take on a more myofibroblast phenotype.[199] During the differentiation of proto-myofibroblasts to myofibroblasts the expression of smooth-muscle cell markers, such as desmin and smooth-muscle cell myosin, heavy chains can occur.[200] Hence, the presence of desmin expression may indicate the differentiation of myofibroblasts, as a result of a changing tumour microenvironment, may be due to pericytes or vascular smooth-muscle cells as a result of angiogenesis. .

4.1.4 Immunofluorescence experimental study design

Co-staining of desmin and vimentin, plus desmin with von Willebrand factor was performed to help determine the cell type expressing desmin. It is known that stromal fibroblast-like cells are vimentin positive and smooth-muscle cells are typically vimentin negative. Additionally, desmin and vimentin have been shown to be co-expressed only in some smooth-muscle cells of the aorta and during myogenic differentiation,[201,202] while pericytes are typically desmin positive and are a type of myofibroblast so may also be vimentin positive.[183] Co-staining of desmin and von Willebrand factor, an endothelial cell marker, was also performed to determine if the cells were mural. Endothelial cells form a monolayer on the inner surface of vasculature, pericytes become embedded within the endothelium of the basement membrane[203] and coat the vessel surface in a discontinuous layer at the endothelial cell junctions[204], whereas vascular smooth-muscle cells are separated from the vascular basement membrane by a layer of mesenchymal cells and extracellular matrix (intima). von Willebrand factor is a ubiquitous endothelial cell marker, localising to venules, capillaries and arterioles in both normal and inflamed tissue, and is also highly specific to endothelial cells as it is not expressed by pericytes, smooth-muscle cells, intima, macrophages, mononuclear infiltrates or fibroblast cells.[205] Hence, if co-localisation of desmin and vimentin is observed, but not von Willebrand factor, the cells may be differentiating myofibroblasts, but not specifically pericytes. If no co-localisation is seen to vimentin or von Willebrand factor, then the cells may be muscularis mucosal cells. If the IF desmin staining is seen in close association with von Willebrand factor, then the cells are likely to be pericytes as they tightly coat the blood vessel walls, whereas vascular smooth-muscle cells would appear to be more loosely associated with an endothelial cell layer.

Previously, CRC 2D DIGE studies on whole pieces of tissue determined desmin to be decreased in tumour compared to matched normal tissues.[88] This can be explained by the higher presence of muscularis mucosa in normal tissue samples resected from the bowel in comparison to tumour samples; pieces of whole tumour form have a higher percentage of epithelial cells compared to normal tissue due to uncontrolled carcinoma growth, hence a smaller percentage of other cell types. Muscularis mucosal cells also have very high levels of desmin, skewing the results of studies performed on whole pieces of tissue. For this reason, western blotting could not be used to quantify desmin expression levels between tumour-normal tissues. Prior to my study, the presence of desmin expressing cells amongst the stromal elements in colorectal adenomas had only been observed[180], but not properly described or quantified using immunofluorescence or immunohistochemistry in CRC.

4.1.5 Aims

To determine if desmin is increased in expression amongst the cells of the tumour and/or tumour stroma, in tight association with the malignant crypts in CRC between early and late stage tumours.

To identify the type of cell aberrantly expressing desmin.

4.1.6 Hypotheses

- The level of desmin expressing stromal cells is significantly increased in late stage tumours compared to early stage tumours, hence desmin has potential use as an immunohistochemical biomarker of tumour staging.
- The desmin expressing cells amongst the tumour stroma are pericyte cells that have accumulated around cancerous glands as a result of angiogenesis and prolonged angiogenic stimulation.

4.2 Materials and methods

4.2.1 Characterisation of the desmin antibody

Western blotting was performed to assess the integrity and specificity of the desmin antibody intended for use in IF. Western blotting was carried out as described in Chapter 2 with 50 μg of protein extracted from a whole tumour tissue sample (Chapter 2) using a mouse monoclonal desmin antibody (1:200 dilution, Abcam ab6322) (Chapter 2). Secondary detection was carried out using a fluorescent anti-mouse Cy3 antibody.

4.2.2 Immunofluorescence on frozen tissue

4.2.2.1 Desmin IF

IF for desmin was performed on fifteen stage I, eleven stage II and nine stage III matched pairs of tumour-normal tissues. Briefly, frozen tissue sections were cut 10 μm thick and placed on histogrip coated glass slides. Tissue was fixed in ice-cold acetone, washed in PBS, blocked using Image-iT FX signal enhancer (Invitrogen) followed by 10% goat serum in PBS. Sections were incubated at 4°C overnight with a desmin antibody (mouse monoclonal, Abcam, ab6322) at a 1:100 dilution. Sections were washed with PBS and incubated in anti-mouse Alexa 488 conjugate (Molecular Probes) at 1:500. Sections were washed with deionised water and stained with DAPI at 0.5 μg/ml (Sigma).

4.2.2.2 Desmin and Vimentin IF

IF for desmin and vimentin, co-localisation was performed on seventeen randomly chosen tumour tissues as previously described. Primary antibody incubations were performed simultaneously, with a mouse desmin antibody (Abcam, ab6322) at 1:100 and the rabbit vimentin antibody (Abcam, ab16700) at 1:100 dilutions. Following PBS washes the secondary antibody incubations were performed simultaneously, with an anti-mouse Alexa 488 conjugate (Molecular Probes) at 1:500 and an anti-rabbit Cy5 conjugate (GE Healthcare) at 1:250 dilutions. All sections were stained with DAPI at 0.5 μg/ml (Sigma).

4.2.3 IF of paraffin embedded tissue

IF for desmin and von Willebrand factor co-localisation was performed on an additional five stage III formalin fixed paraffin embedded (FFPE) tumour-normal tumour tissues. For this experiment FFPE tissue was used as the preservation of morphology in stained FFPE sections is better than that of frozen sections, making visualisation and interpretation of slides easier and more accurate. This was of great importance as the co-localisation between the desmin and von Willebrand factor staining needed to be critically assessed. Paraffin removal and antigen retrieval by trypsin digestion was performed as

described in chapter 2. IF was then performed as previously described. Primary antibody incubations were performed simultaneously, with a mouse desmin antibody **(**Abcam, ab6322) at 1:100 and rabbit von Willebrand factor antibody (Abcam, ab6994) at 1:400 dilutions. Following PBS washes, the secondary antibody incubations were performed simultaneously, with an anti-mouse Alexa 488 conjugate (Molecular Probes) at 1:500 and an anti-rabbit Alexa 568 conjugate (Molecular Probes) at 1:500 dilutions. All sections were stained with DAPI at 0.5 μg/ml (Sigma).

4.2.4 IF Analysis

The IF of desmin was evaluated by imaging the entire area of each section at a 10 x magnification in monochrome. Images were captured using 460–495 nm, 330–385 nm, 590 nm and 663 nm long pass filters to capture the Alexa 488, DAPI, Alexa 568, and Cy5 images respectively. Colour was added, and images overlayed. The level of desmin staining was quantified using the AnalySIS LS Research (Soft Imaging Systems Olympus) phase analysis tool, giving the area (μm^2) and % area of the total image positive for desmin staining. This process was repeated to quantify the level of DAPI staining. Prior to phase analysis, the pixel threshold of each image was adjusted to only include areas of positive fluorescence, excluding background. The final percentage area positive for desmin staining was then calculated against the total cell area, as determined by the quantified level of DAPI staining. This was done to account for any tissue 'dead space'. As desmin is a known smooth-muscle cell marker, areas of muscularis mucosa and vasculature were excluded from analysis. For each tumour the % area of desmin staining across the entire tissue section was averaged.

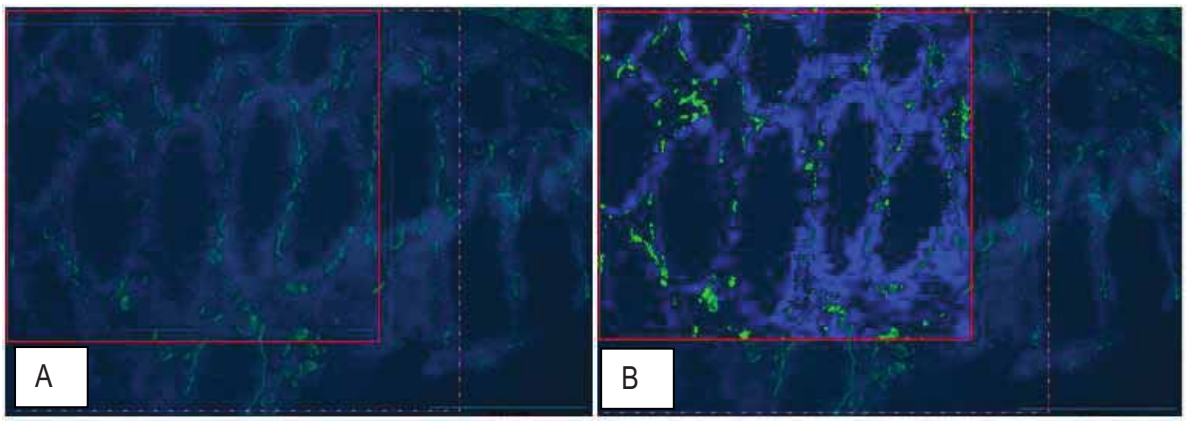

Fig 3. Quantification of desmin expression levels by IF. The phase analysis tool of the AnalySIS LS Research software program was used to highlight and quantify the area of each image positive for desmin staining (green) or DAPI staining (blue). Image A displays a section prior to quantification. The bright green and blue colours highlighted within the red box of image B display the areas of either desmin or DAPI fluorescence respectively, that were included in the analysis of this image.

4.3 Results

4.3.1 Characterisation of the desmin antibody

The integrity and specificity of the desmin antibody was checked by western blotting. A band at approximately 53 kDa was expected and a single band at a molecular weight of slightly below 50 kDa was observed (Fig. 4). Given a single band within 30% of the calculated molecular weight was observed, the desmin antibody was shown to be intact and binding specifically to desmin.

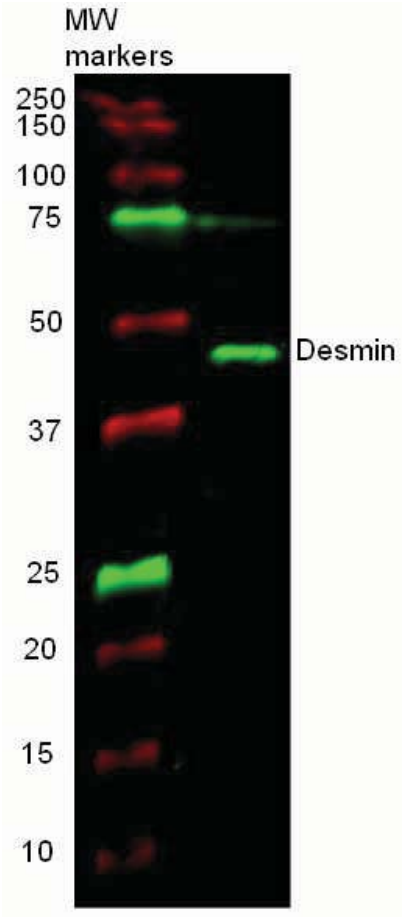

Fig 4. Confirmation of the specificity and integrity of the desmin antibody by western blotting. Fifty micrograms of whole tumour protein was separated by 1DE, immunoblotted with the desmin antibody ab6322 and detected using a fluorescent Cy3 secondary antibody. A single band slightly below 50 kDa, around the calculated MW of desmin, was observed. The molecular weight markers used on this blot are 'Dual Color' prestained SES-PAGE standards (Biorad). The standards appearing at the MW of 250 kDa, 150 kDa, 100 kDa, 50 kDa, 37 kDa, 20 kDa, 15 kDa and 10 kDa are prestained with Cy5, appearing red. The standards ar the MW of 75 kDa and 25 kDa are prestained with Cy3, appearing green.

4.3.2 Desmin IF

IF was performed in order to identify the source of the desmin expression, as epithelial cells are regarded as desmin negative, and it was highly unlikely that cells from the muscularis mucosae, muscularis propria or large vessel walls were captured during tissue collection by LMD in the scarce labelling DIGE study. Desmin was found to be expressed in the stromal cell area closely associated with the epithelial glands of the cancer tissue (Fig. 5). The desmin stained cells appeared to form short lines surrounding the crypts. Very low levels of stromal desmin staining were observed in the normal tissues and were generally sparse and discontinuous.

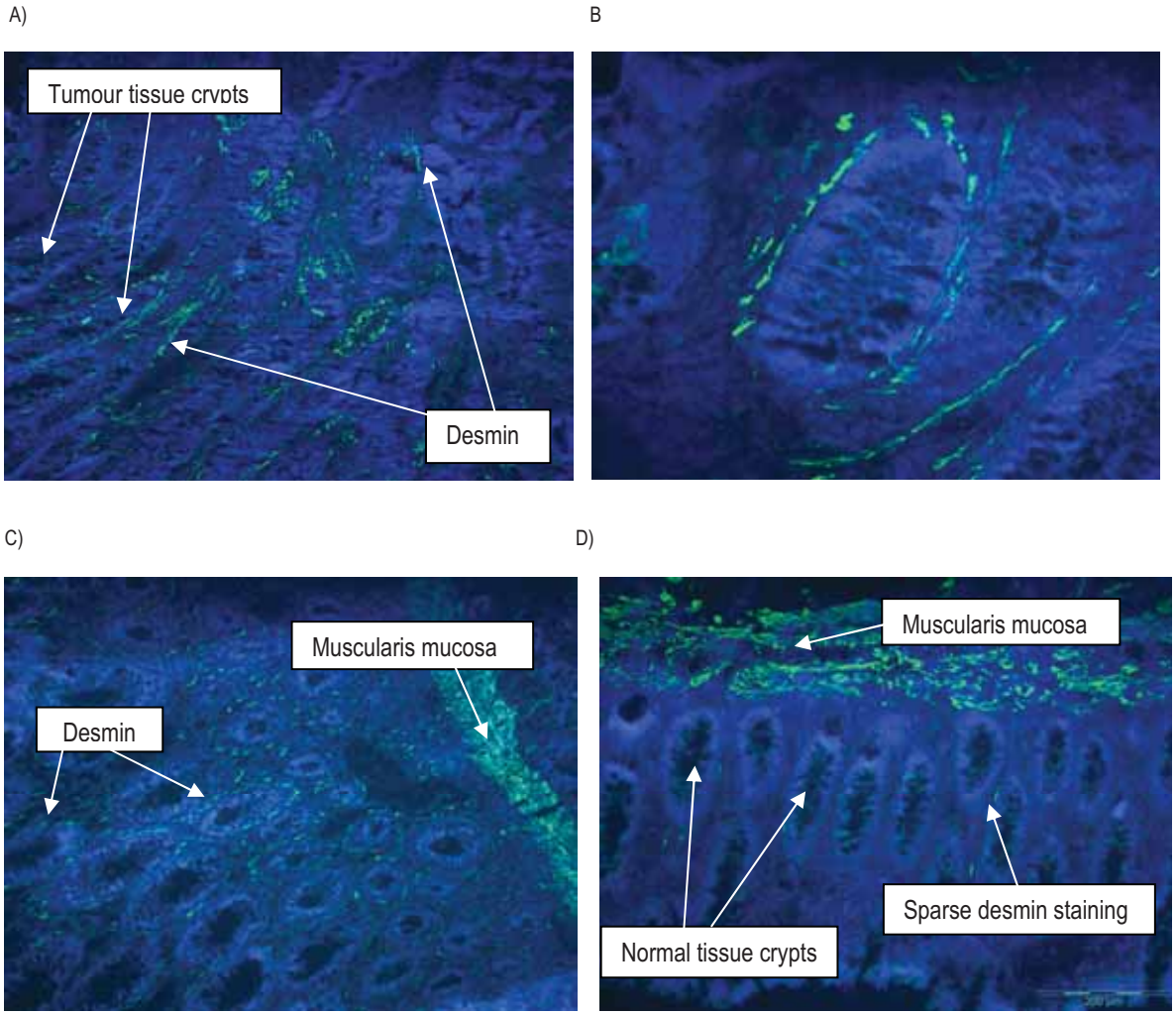

Fig 5. **Examples of desmin IF with Alexa 488 (green) and DAPI (blue) performed on colon tissues** (n=31)**.** Images A), C), D) were taken at 10 x magnification, and image B) was taken at 40 x magnification. A) and B) images were taken from the same section of a stage II tumour. Image C) was taken from a stage II tumour, and shows an area of muscularis mucosa across the top right hand corner. Image D) was taken from a normal tissue section, and shows muscularis mucosa across the top of the section.

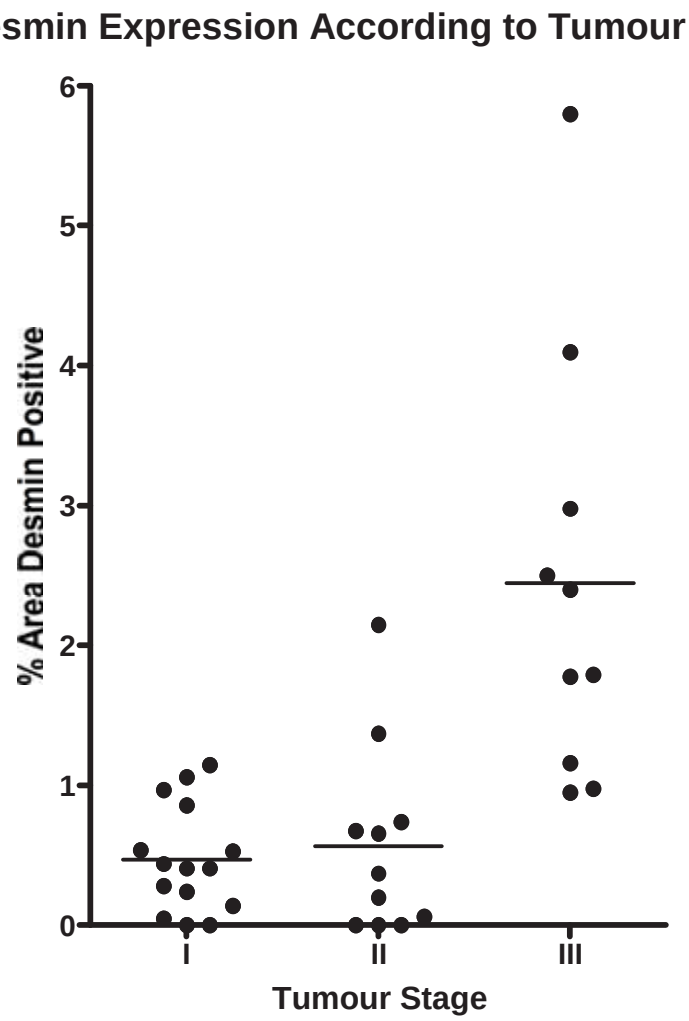

Fig 6. **Scatter plot displaying the % area of each tissue section positive for desmin staining within the stromal element according to tumour stage.** Areas of Muscularis mucosa and vasculature were excluded from analysis. Levels of staining significantly increase between early stage (stage I and II) and stage III tumours, * *P*<0.0001 (ANOVA).

The average percentage area of positive desmin staining (within the epithelial and stromal cell areas, excluding muscularis mucosa) for fifteen stage I, eleven stage II and nine stage III tumours was quantified, and results according to patient stage are shown in Fig. 6. The level of stromal cell desmin expression was significantly higher in stage III tumours when compared to both stage I and II tumours, *P*<0.0001. There was no significant difference in the level of stromal cells desmin expression between stage I and II tumours.

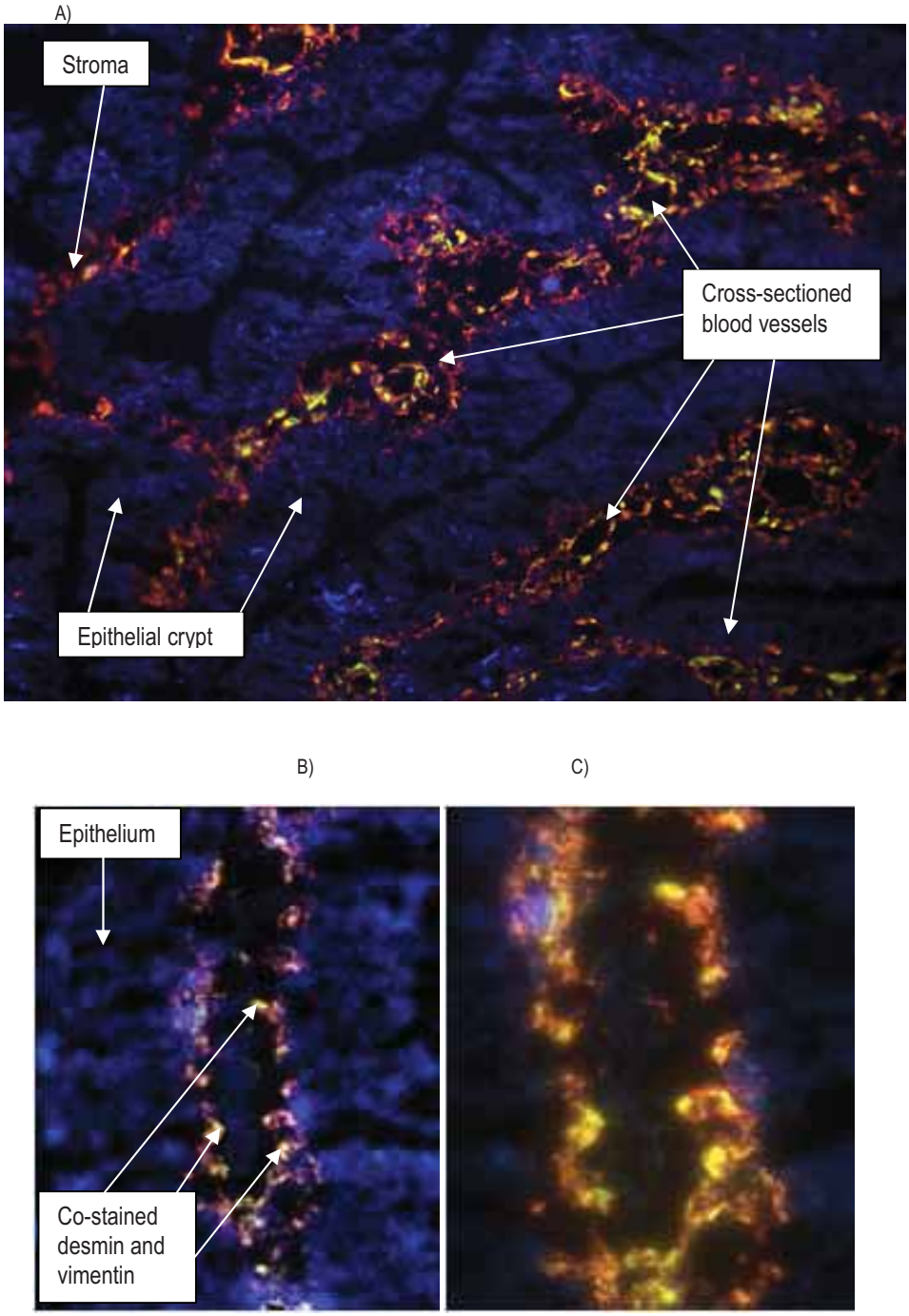

Fig 7. **Examples of desmin and vimentin co-localisation performed on tumour tissue using Alexa 488 (green) and Cy5 (red) respectively** (n= 17). Co-expression of desmin and vimentin by the same cell result in overlapping of the fluors, and appears yellow. Images A), B), and C) were taken of the same tumour section at increasing magnification (A) 20x, B) 40 x, and C) 60 x magnification). In image A) co-staining pattern of desmin and vimentin appear to be in cross and vertical sections of blood vessels.

4.3.3 Desmin and Vimentin IF

Desmin and vimentin staining was performed on seventeen of the tumour samples to assess co-localisation. Desmin and vimentin co-localised in stromal areas close to the outer edges of the crypts (Fig. 7).

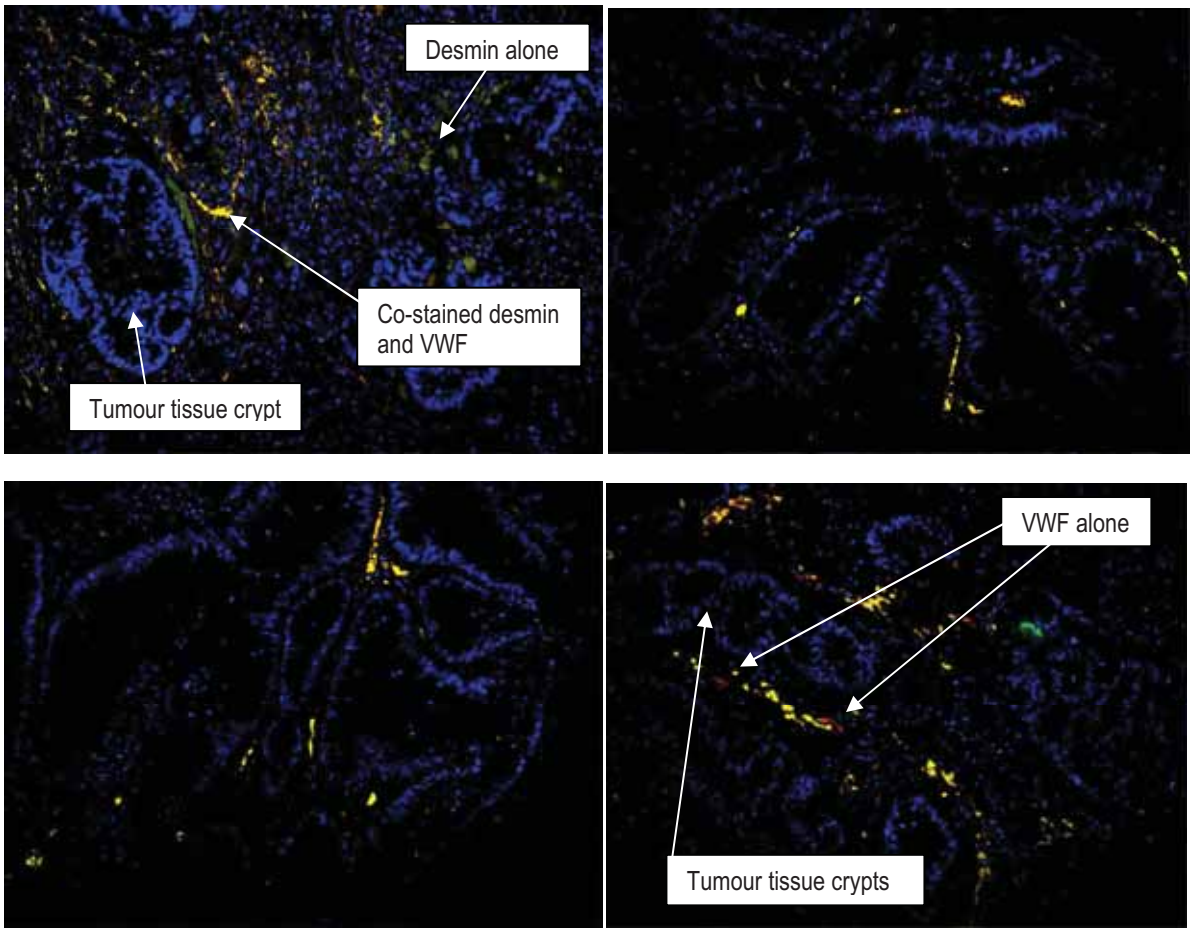

Fig 8. Immunofluorescence staining performed on stage III tumours with antibodies for desmin and von Willebrand factor. Desmin was visualised with an Alexa 488 (green) and von Willebrand factor (VWF) was visualised with an Alexa 568 (red). Co-localisation of the proteins appears yellow. Sections were also stained with the nuclei stain DAPI (blue). Images were taken at 20 x magnification.

4.3.4 Desmin and von Willebrand factor IF

Desmin and von Willebrand factor staining was performed on the stage III samples to assess co-localisation. The majority of desmin stained cells co-localised with von Willebrand factor, in a small percentage of cases co-localisation of the proteins was not observed (Fig. 8). In the normal tissue sections resected from late stage CRC patients high levels of desmin and von Willebrand factor co-localisation was also observed as displayed in Fig. 9.

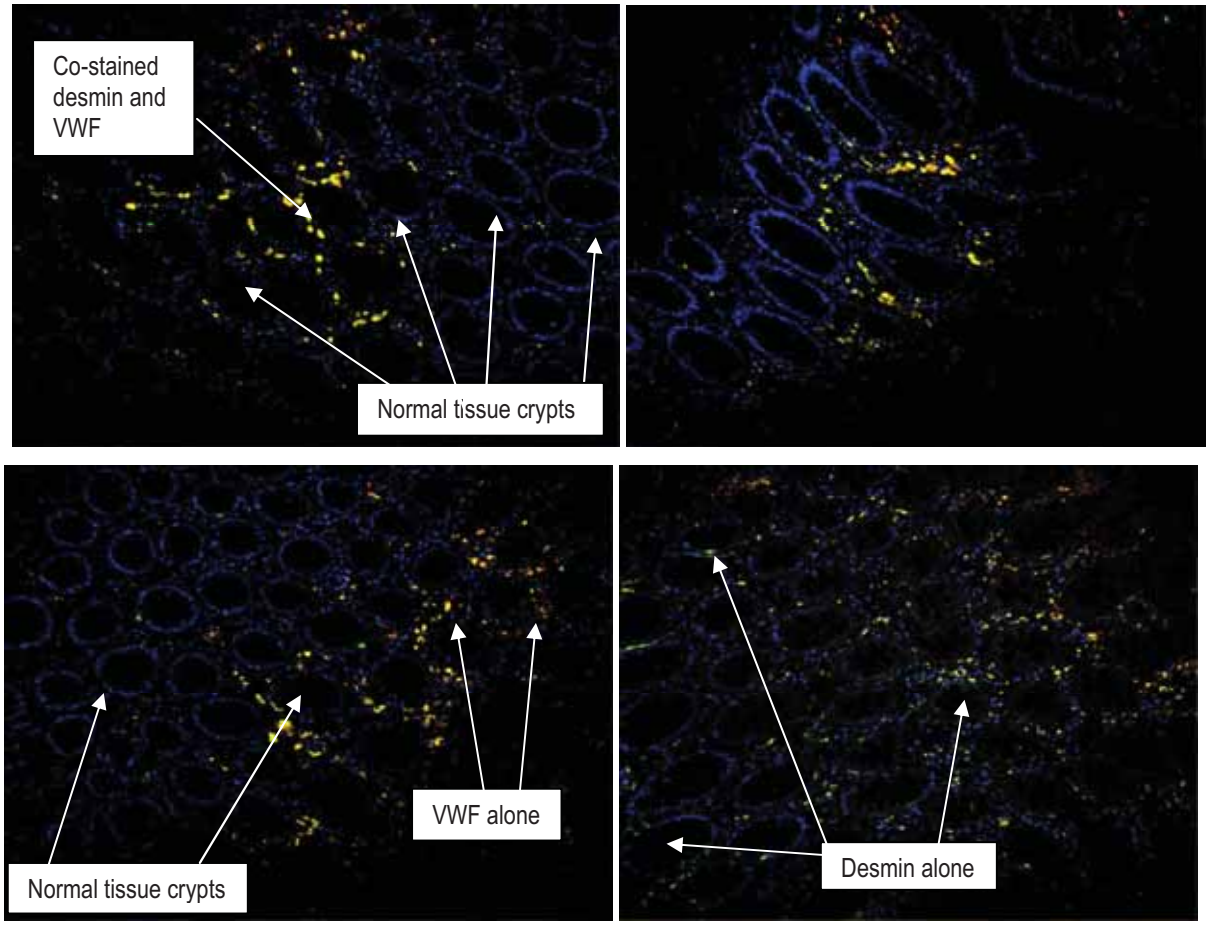

Fig 9. **Immunofluorescence staining performed on the matched normal tissues (of the stage III tumours) with antibodies for desmin and von Willebrand factor**. Desmin was visualised with an Alexa 488 (green) and von Willebrand factor was visualised with an Alexa 568 (red). Co-localisation of the proteins appears yellow. Sections were also stained with the nuclei stain DAPI, appearing blue. Images were taken at 20 x magnification.

4.4 Discussion

4.4.1 Desmin as a marker of pericytes in CRC

In the previous 2D DIGE study, the muscle cell protein desmin was found to be significantly increased in tissue from late stage colon tumours compared to matched normal mucosa. IF identified the desmin expressing cells to be situated amongst the stromal element, directly adjacent to the cancerous glands. Previously, such cells had been described as myofibroblasts [181] or pericytes[182] and it was hypothesised that the cells of interest could be myofibroblasts, mural cells (pericytes and vascular smooth-muscle cells) or muscularis mucosal cells. The stained desmin expressing cells co-localised with vimentin in close association with cells positive for the endothelial cell marker von Willebrand factor, indicating they are most likely pericytes. Pericytes are embedded in the vascular basement membrane of blood microvessels and make specific focal contacts with the endothelium. Vascular smooth-muscle cells are usually distinguished from pericytes by their location to the endothelium, their morphology, and to some extent their marker expression[203], although these criteria are not always absolute. Typically vascular smooth-muscle cells are separated form the vascular basement membrane by a layer of mesenchymal cells and extracellular matrix, with the vascular smooth-muscle cells forming a separate layer in the vascular wall. In contrast, pericytes are embedded in the endothelium with which they contribute and receive products such as growth factors.[203] In the majority of co-staining for desmin and von Willebrand factor, the two proteins appeared to be closely associated, with low levels of desmin alone visualised (Fig. 8, Fig. 9). This indicates the majority of the desmin expressing cells observed in the stromal area are likely to be pericytes, with lower levels of vascular smooth-muscle cells.

During the process of angiogenesis, endothelial cells sprout from pre-existing blood vessels to form microcapillaries. In the later stages of angiogenesis, pericytes coat the microcapillaries, stabilising them and defining them as mature vessels. This study revealed a significant increase in the level of desmin staining between stage III tumours compared to stage I and II tumours ($P<0.0001$), thus indicating the process of angiogenesis in the late stage patients was well established throughout the tumour tissue, and that developed microvessels had matured. These results suggest that the maturation of newly-formed microvessels may have important implications in the efficacy of anti-angiogenic cancer therapies.

4.4.2 Desmin expression in the late stage normal tissues

IF staining of desmin in normal tissues was visualised under the microscope, but was not quantified as the level of desmin staining was either negative, or extremely low and sparse (Fig. 4D). However, the level of desmin staining in the normal tissues of the late stage patients was substantial (Fig. 8), even in comparison to the level quantified in the early stage tumours. When tissue samples are collected following tumour

resection surgery, the area collected as 'normal' tissue is taken as far away from the tumour tissue as possible (at least 10 cm). The presence of desmin staining in the stromal areas of the normal tissues indicates the process of angiogenesis is occurring at significant distances from the tumour in the late stage patients.

4.4.3 Pericytes in cancer angiogenesis

Pericytes coat blood microvessels during angiogenesis and are required for the correct patterning, structural stability, development and maintenance of growing microvasculature networks.[206] [207] Uncoated vessels are considered to be unstable or immature, and responsive to angiogenic signals[208] [209] Mature vessels on the other hand are quiescent, are not dependent on angiogenic factors for survival[210], and remain once the maturation phase of angiogenesis has ended and vascular remodelling to meet metabolic demand has started.[211] They also provide resistance to angiogenic regression and hyperoxia.[207]

Pericytes have been shown to appear in the early stages of capillary sprouting[212], but traditionally it was thought that pericytes coated capillaries once the capillary plexus had formed, while other studies have suggested pericytes may direct vessel sprouting.[182] [213] Nehls *et al*. (1992)[214] found that developing pericytes in angiogenesis-induced rat tissues are strongly positive for desmin (negative for α SMA) and can be visualised at the advancing front of endothelial sprouts. It is thought they may bridge the gaps between endothelial sprouts preparing to merge, acting as guiding structures[214], while conversely, Gee *et al*. (2003)[208] found that pericytes only started to coat developing vessels in tumours after the sprouting stage, once the vessels had reached a larger size and had few proliferating endothelial cells. Interestingly Ponce *et al*. (2003)[206] found that during mast cell-mediated angiogenesis, 65% of capillary sprouts contained pericytes at their leading edge, whereas during normal maturation and wound healing angiogenesis only 35% of capillary sprouts contained pericytes at their leading edge. Similarly Brey *et al*. (2004)[204] did find not find pericytes at the tips of sprouting vessels during wound healing induced angiogenesis. These findings suggest the presence of pericytes at the leading edge of sprouts early in vessel development may be highly dependent on the type of angiogenic stimulus received.

4.4.4 Pericytes and anti-angiogenic cancer therapies

The success of anti-angiogenic strategies in the treatment of cancer has been linked to the maturity of the targeted blood vessels and the presence and level of pericytes. Anti-angiogenic strategies aim to inhibit endothelial cell growth, and hence the development of vasculature within solid tumours. By doing so the delivery of oxygen and nutrients to the tumour, as well as the removal of cellular waste products from the tumour is inhibited. Gee *et al*. (2003)[208] studied the effect of treating tumours at different stages of vessel

maturation with the anti-angiogenic therapy interleukin-12, with tumours defined as having immature, intermediate or mature vessels prior to treatment. Immature vessels were categorised as highly proliferative, non-perfused epithelial cell sprouts originating from pre-existing blood vessels, not covered by pericytes. Intermediate vessels were categorised as small, perfused vessels, not covered by pericytes while mature vessels were large and predominantly covered in pericytes. Recombinant interleukin-12 therapy successfully induced epithelial cell apoptosis in the tumours that contained pericyte negative vessels, reducing vessel density. This therapy had no reducing effect on the pericyte-covered vessels in the mature vasculature tumours with only the selective loss of non-pericyte covered vessels in these tumours observed.

Pericytes may help to protect vessels via the production of endothelial cell survival factors such as vascular endothelial growth factor (VEGF). VEGF stimulates the proliferation and chemo-attraction of endothelial cells, prevents endothelial cell apoptosis, maintains the viability of immature blood cells, and plays a role in the recruitment of pericytes to vessels.[207] Pericytes are attracted to vessels by platelet-derived growth factor (PDGF) produced by endothelial cells, and without PDGF expression, pericytes fail to develop around the capillaries formed during angiogenesis.[215] It is thought that the recruited pericytes then produce VEGF and this in turn stimulates the survival of endothelial cells, with the system working as an endocrine feedback loop.[212] Withdrawal of VEGF from tumours with immature vasculature has been shown to result in endothelial cell apoptosis and the loss of pericyte negative blood vessels.[207]

A study by Hasumi *et al*. (2007)[216] assessed the efficacy of VEGF and PDGF inhibitors in combination therapy to treat tumours with high levels of pericyte coverage, compared to tumours with low levels of pericyte coverage on the vasculature in a mouse melanoma model. The combination therapy decreased the growth rate of both tumour types, but growth was only significantly decreased in the tumours with low levels of pericytes. Vessel density and size was also decreased in these tumours. The study found the treatment only decreased the number of α SMA positive pericytes, loosely attached to the vessel walls, not the number of desmin positive pericytes with close attachment to the endothelial cells.

These studies[216] [207,208] [212] suggest colorectal tumours with mature vasculature, as defined by the presence of pericytes, would be less responsive to treatment with anti-angiogenic therapies compared to tumours with immature vasculature. The level of desmin expression surrounding neoplastic glands within the tumour stroma may have use as a marker for responsiveness to anti-angiogenic treatments. Interestingly, all of the late stage patients assessed in this work had relatively high levels of desmin staining, indicating the presence of pericytes and mature blood vessels. The treatment of late stage CRC patients with anti-angiogenic therapies has had poor response rates. Bevacizumab, a humanised monoclonal antibody against VEGF, has been shown to have had only a modest effect on survival rates when used with standard treatment (infusional regimes of 5 FU/LV with either irinotecan or oxaliplatin) (reviewed in [79]). The anti-

angiogenic tyrosine kinase inhibitors Sunitinib and Vatalanib have also failed to deliver significantly increased disease free survival rates (reviewed in [79]). Poor outcomes of these drug trials may have been due to the presence of mature vasculature within the targeted tumours.

4.4.5 Origin of pericytes

The process of angiogenesis occurs via the emanation of endothelial cells from pre-existing functional blood vessels. The precise origin of the pericytes that coat mature vessels in vivo in human tumours however is uncertain. Such pericytes may originate from pre-existing mural cells from blood vessels, or they may originate from the activated (myo)fibroblast population of the developing tumour stroma.

4.4.6 Pericytes can originate from mural cells and vascular progenitor cells

The growth factor PDGF stimulates the migration of pericytes to newly-formed vessels and it has been speculated that vascular smooth muscle cells and pericytes may be able to migrate from the blood vessels at the basement membrane to the interstitial collagenous stroma.[193-195 196,197] Lindahl *et al.* (1997)[215] studied the process of angiogenesis in embryonic mouse brain and found pericytes originate from smooth-muscle cell progenitors in the arterial walls and vascular plexa. The pericytes migrate along the capillary sprouts containing PDGF expressing endothelial cells, and settle on the vessels to form mature vasculature. Similarly it has been shown that smooth muscle cells from the intimal aspect of rat aorta cultured in collagen under serum-free conditions, migrate to forming microvessels during angiogenesis and differentiate into pericytes.[217]

4.4.6.1 Pericytes can originate from vascular progenitor cells

Hagedorn *et al*. (2004)[218] found VEGF treatment of mouse embryoid body cultures under normal culture conditions, lead to the conversion of normal vascular progenitor CD31+ cells into cells with endothelial and mural cell characteristics. The expression of desmin and α SMA in the CD31+ cells was dependent upon the age of the cultures and the length of the VEGF treatment, with the expression of mural cell markers occurring in the mid stage cultures six to nine days post-plating. Detailed morphological analysis by confocal microscopy showed the VEGF stimulated vascular progenitor cells assembled into vascular chords in embryoid body cultures, and appeared to show a coordinated expression pattern of endothelial and mural cell markers during embryoid body differentiation. Hagedorn *et al*. (2004)[218] hypothesised that vascular progenitor cells have the potential to become endothelial cells or pericytes in response to VEGF as part of a security mechanism to ensure the availability of all blood vessel components during certain phases of

vascular development. Other studies have also displayed the ability of VEGF treatment to induce vascular progenitor cells to differentiate into either endothelial or mural cells. Treatment of the mouse embryonic derived stem cell line Flk-1+ with VEGF lead to the differentiation of cells into vascular progenitor cells.[219] When injected into tumour-bearing mice, the cells were incorporated into developing vasculature mainly as endothelial cells, but also as mural cells and could be detected in the vascular walls.

4.4.7 Pericytes can originate from activated fibroblast cells

There is evidence describing the differentiation of fibroblasts to pericytes during the process of capillary sprouting.[220] In the mesentery of rats, Rhodin and Fujita[220] described mesenteric tissue fibroblasts settling on young capillary sprouts and differentiating into pericytes during the process of angiogenesis. The newly-formed pericytes reinforced the vessel walls and acted to trap leaking platelets, red blood cells, and plasma. Conversely, Lin *et al*. (2002)[221] found pericytes of the kidney migrate and differentiate into myofibroblasts in the fibrosis that occurs due to inflammatory injury.

4.4.8 Fibroblasts in cancer

Fibroblasts normally participate in the wound healing process by the expression of extra cellular matrix proteins, and the production of chemokines and cytokines, helping to mediate the inflammatory response.[200] Fibroblasts activate to become myofibroblasts which express myosin and α SMA, enabling them to exert contractile forces in order to reduce wound size in the healing process. However, uncontrolled proliferation and activation of fibroblasts to myofibroblasts leads to fibrosis. There are a number of types of myofibroblasts with tissue specific functions, such as contractile glomerular mesangial cells, kidney hepatic satellite cells, and pericytes that function as regulators of blood flow.[222] [223]

Fibroblastic stromal cells have altered expression profiles in the instance of wound healing, where they take on a more myofibroblast phenotype, and there is evidence suggesting this process can stimulate cancer invasion in rats.[199] There is also evidence suggesting smooth-muscle cells of the muscularis mucosa in early invasive adenocarcinomas take on a more myofibroblast phenotype.[198] Fibroblasts and myofibroblasts in cancerous tissue are known to aid in the growth and metastasis of tumours, and may differentiate into pericytes aiding the process of angiogenesis. In CRC, tumour-infiltrating myofibroblasts have been described as migratory cells that accumulate at the invasive front and help to degrade the basement membrane.[224] Similarly, stromal cells have been shown to produce matrix metalloproteinase (MMP-2) in CRC, aiding in invasion and metastasis by basement membrane degradation.[225] Radovic *et al.* (2001)[226] studied the distribution of fibroblasts in inflammatory-regenerative and dysplastic epithelial lesions of flat bowel mucosa in comparison to normal and adenocarcinoma tissues using IHC, and found an increase in the expression of the smooth-muscle markers α SMA, vimentin and desmin in the adenocarcinoma tissues. Such markers are expressed by pericytes.

It is known that stromal reaction to epithelial tumours can result in fibrosis, generating granulation tissue fibroblasts or myofibroblasts.[200] Granulation starts to disappear in the wound healing of normal tissue via apoptosis of the myofibroblasts[227], but the same apoptosis does not seem to occur in the case of epithelial tumour fibrosis. The phenotype of the myofibroblasts in fibrotic lesions can be varied, and during the differentiation of proto-myofibroblasts to myofibroblasts the expression of smooth-muscle cell markers, such as desmin and smooth muscle-cell myosin, heavy chains can occur.[200] It is thought that desmin is not a marker of typical myofibroblasts, but can be expressed by myofibroblasts associated with lesions[197], and that fully differentiated myofibroblasts, even in the cases of granulation tissue and tumour stroma, are generally desmin negative.[228] Fibroblasts that develop desmin expression as part of a wound healing response caused by cancer, may be differentiating to pericytes.

4.4.9 The origin of tumour associated fibroblasts

As tumours increase in size, they develop a stromal element containing activated fibroblasts or myofibroblasts and these cells have been referred to as tumour associated (myo)fibroblasts (TAF). TAF assist tumour development via the expression of proteins involved in matrix degradation (such as matrix metalloprotinase), angiogenesis (such as VEGF), cell proliferation (such as insulin growth factor 2 (IGF2) and hepatocyte growth factor (HGF)) (reviewed in [229]). TAF can be defined by four criteria; (1) the expression of fibroblast-specific protein (FSP) and fibroblast activating protein (FAP), (2) the expression of genes associated with increased tumour aggression, such as stromelysin 1 (SL-1), thrombospondin 1 (Tsp-1) and tenascin- C (Tn-c), (3) the cells have myofibroblast or pro-vascularising potential, assessed by the expression of proteins such as desmin and α SMA and (4) the expression of growth factors such as transforming growth factor β (TGF β), HGF, basic fibroblast growth factor (bFGF) and epidermal growth factor (EGF).[230 231]

It is thought that the stromal element of developing tumours may have four possible origins; 1) the recruitment and differentiation of resident tissue stem cells to myofibroblasts, 2) the transition of epithelial cells to mesenchymal cells in the tumour parenchyma, known as epithelial-mesenchymal transition (EMT), 3) fibroblast recruitment into the tumour tissue and 4) the recruitment of bone marrow fibroblasts from the circulation into the tumour.[232 233 234 235]

4.4.9.1 Origin of TAF; mesenchymal stem cells

Mesenchymal stem cells (MSC) have been shown to home to tumours and participate in tumour stroma formation. Human tumours admixed with human MSC in a murine xenograft model showed cells expressing

the activated fibroblast markers fibroblast activating protein (FAP), fibroblast-specific protein (FSP), α SMA, tenascin-C (Tn-C), thrombospondin-1 (Tsp-1), stromelysin-1 (SL-1) and desmin.[231] It is thought the MSC are recruited to the tumour-associated fibrovascular networks, forming pericyte cells that coat microvessels during angiogenesis.

Spaeth *et al*. (2009)[231] showed that activated fibroblasts and myofibroblasts contribute to the formation of microvascular structures in a murine xenograft ovarian cancer model as detected by the expression of fibroblast markers, α SMA and desmin. In their model they detected microvascular formation confined to the tumour growth, characterised by networks of straight, looping and branching arced septa. Spaeth *et al*. (2009)[231] proposed that mesenchymal stem cells (MSC) are the origin of the TAF. In their murine tumour xenograft model, human tumours admixed with human MSC-developed cells with the activated fibroblast markers FAP, FSP, α SMA, TnC, Tsp1, SL1 and desmin. The presence of the MSC in the tumours enhanced the expression of EGF and HGF. They suggest that during tumourigenesis, MSC form a component of the tumour stroma that can develop into pericyte cells which form the microvessels involved in neovascularisation, as well as a fibroblastic populations that contribute to matrix remodelling and tumour development.

4.4.9.2 Epithelial mesenchymal transition

Epithelial mesenchymal transition (EMT) is thought to be one of the first events in the metastasis of tumour cells (reviewed in [236]). During EMT, epithelial cells downregulate their adhesion systems, lose polarity and the expression of epithelial cell markers, while acquiring the expression of mesenchymal cells markers, taking on a more mesenchymal-like phenotype. This results in reduced cell-to-cell adhesion and interaction, with increased migratory capacity. Typically epithelial cells undergoing EMT lose the expression of proteins such as E-cadherin, occludin, claudins, catenins and cytokeratins, and gain the capacity to express proteins such as N-cadherin, vimentin, TnC, laminin β 1, collagen type VI α and certain proteinases.[237] [238]

During the initial stages of EMT, prior to metastasis, tumour cells are still reliant upon paracrine and juxtacrine signalling within the tissue microenvironment. Epithelial-stromal interactions play an important role in tumour development, and carcinoma cells interact with various cell types within the stromal environment (such as macrophages, endothelial cells, lymphocytes, fibroblasts and pericytes) via the production of hormones, cytokines, chemokines and proteases.[231]

A number of signalling pathways and molecules are involved in EMT, and are increased in expression during tumourigenesis, such as receptor tyrosine kinases for growth factors, the TGF β superfamily, NF kappa B, and the Wnt, NOTCH and hedgehog pathways.[239,240] Following EMT, at the beginning of metastasis,

migrating carcinoma cells must survive in the absence of cell-to-cell contacts and adhesion. VEGF is a candidate survival factor, as expression of the protein is increased in response to EMT, with concomitant increases in Flt1, a VEGF receptor tyrosine kinase.[241] Increased VEGF expression in the later stages of EMT and the initial stages of metastasis would also stimulate angiogenesis and promote the development of desmin-expressing pericyte cells.

Willis *et al*. (2005)[242] studied the occurrence of EMT in idiopathic pulmonary fibrosis (IPF). IPF involves the development of patchy areas of fibrosis in the lung, and initially was thought to be caused by inflammation, resulting in fibroblast activation. However, the use of anti-inflammatory drugs in IPF treatment has been shown to have little impact on the disease pathogenesis in patients. It is now thought that IPF may be caused by epithelial cell injury with a deregulation of repair and epithelial cell signalling, resulting in granulation and fibrosis. Similarly, stromal reaction to epithelial tumours can result in fibrosis, generating granulation tissue fibroblasts or myofibroblasts.[200] Granulation starts to disappear in the wound healing of normal tissue via apoptosis of the myofibroblasts[227], but the same apoptosis does not seem to occur in the case of epithelial tumour fibrosis or IPF. Willis *et al*. (2005)[242] found that exposing primary culture rat alveola epithelial cells to TGF β, known to induce fibrosis, resulted in the transition of the epithelial cells to a more myofibroblast-like phenotype. The alveolar epithelial cells started to express the mesenchymal markers α SMA, type 1 collagen, vimentin, and desmin, and had a decrease in the expression of the epithelial markers such as cytokeratins, ZO-1 and aquaporin 5. The study concluded alveolar epithelial cells may participate in the development of IPF through transdifferentiation to activated fibroblasts. Studies in renal fibrosis have also shown that sites of injury in the kidney can arise from epithelial cell differentiation to activated fibroblasts (reviewed in [243]). The deregulation and differentiation of epithelial cells to activated fibroblasts in cancer and IPF may help explain the progressiveness and relentlessness of the diseases.

Anterior subcapsular cataracts (ASC) develop from the aberrant growth and differentiation of lens epithelial cells to form fibrotic plaques. The development of ASC is associated with an impaired wound healing response, much like cancer, following ocular trauma, eye surgery or other eye diseases. Changes in ASC are also characteristic of EMT. The lens epithelial cells in the plaques become spindle-shaped like myofibroblast cells and accumulate in a collagenous matrix. Lens cells in ASC abnormally express proteins such as α SMA, type I and II collagen, fibronectin and tenascin. Exposure of rat epithelial lens cells to TGF β has been shown to induce the expression of these proteins, plus desmin.[244] It is thought ASC in humans may be due to increased levels of TGF β, which would help explain the development of lens plaques by EMT and the resulting fibrosis.

4.4.9.3 Bone marrow recruitment

The recruitment of bone marrow-derived progenitor cells, mesenchymal stem cells or hematopoietic stem cells, into the stroma of tumours has been described. A study by Brittan *et al*. (2002)[245] studied the ability of extraintestinal cells to incorporate into the colons and small intestines of female mice that had received male bone marrow transplants, and in intestinal biopsies of women who had developed graft versus host disease after receiving bone marrow transplants from male donors. The study showed bone marrow-derived cells with myofibroblast phenotype in the mice and human intestine biopsies using in situ hybridisation to detect Y-chromosomes and IHC. IHC for myofibroblast markers showed organised networks or pericytes that were derived from the donor bone marrow. A similar study analysing sex mis-matched transplants in humans found 30% of kidney myofibroblasts are of extrarenal origin.[246]

4.4.10 Desmin as a histopathology marker

For use as a histopathology marker for tumour staging and angiogenic development desmin appears to have good potential. The usefulness of desmin as a marker lies largely in the fact that it is not expressed by the tumour, but as a result of angiogenesis, a process that is consistent and occurs eventually in all CRC patients. The abundance of markers expressed by tumour cells needs to be quantified and a threshold needs to be set in order to determine if a patient is marker positive or negative. This can be very difficult due to huge genetic variation between patients and can result in high levels of false positive and negative results. Desmin would be a more consistent marker across patients as it is expressed by all pericyte cells that develop into the tumour tissue as a result of angiogenesis, which occurs in all colorectal cancers once they reach a certain size. The only situation where desmin could not be appropriately used as a histopathology marker is when a section of tumour tissue has penetrated through the muscularis mucosal area. Histopathology sections studied in a case such as this may generate false positive results as all muscle cells express desmin.

If desmin were to be used as a marker of tumour staging or angiogenic development it would be relatively easy and cost effective. Given histopathology is performed onall resected colorectal tissues, desmin could be incorporated into routine histopathology tests. Using desmin as a marker in thes manner would be cheap and would not require any extra equipment (other than antibodies) or training for those performing the tests.

4.4.11 Critique of techniques used

The work presented in this chapter was based on immunofluorescence studies. The great advantage of immunofluorescence is the visualization of tissue morphology, showing the cellular location of the cells expressing the protein of interest. Multiple proteins can also be visualized at the same time allowing co-

localisation studies. Both frozen and paraffin embedded tissues were used, both have advantages and disadvantages. Large numbers of frozen tissues were available for the study, however sectioning frozen tissue and maintaining good morphology can be difficult. Hence for the co-localisation work paraffin embedded sections were used. The disadvantage of paraffin sections is the possible loss of antigens during the antigen retrieval process or conversely the inability to access some antigens as they remain fixed in the tissue.

4.5 Conclusion

Initially desmin was identified as significantly increased in abundance in a pilot study that aimed to analyse alterations in cancerous epithelial cells and the surrounding microenvironment. Proteins differentially expressed between tumour-normal epithelial cells and in the stromal elements closely associated with the epithelial glands were collected using LMD, and analysed by saturation labelling 2D DIGE and MS. Using IF and three different markers, the desmin expressing cells were deemed to be pericytes, a result of angiogenesis. The level of desmin expression was significantly higher in the late stage samples compared to the early stage samples, P=0.0001. In the angiogenic process, the coating of newly-formed microvessels with pericytes marks their maturation, and there is evidence to suggest tumours with mature microvessels are immune to anti-angiogenic therapies. This study indicates the level of desmin expression by pericytes coating microvessels, closely associated with the neoplastic glands amongst the stromal element, has potential use as a histopathology marker for late stage patients, and may act as a biomarker for the identification of patients who would not benefit from the current anti-angiogenic therapies due to the presence of mature tumour microvasculature.

5 Cytokeratin 8 Phosphorylation in CRC

5.1 Introduction

5.1.1 Cytokeratin 8 and CRC

The cytokeratins (CK) 8, 18 and 19 were found to be significantly upregulated >2 fold in laser microdissected (LMD) tumour samples, compared to matched paired normal mucosa from eight stage II CRC patients in the 2D DIGE study (Fig. 1, Table 1). Three isoforms of CK8 were detected as being significantly upregulated in the tumour tissues by ≥4 fold, with the most acidic form having the highest level of upregulation. The three isoforms appear at approximately the same molecular weight with differing isoelectric points (pI), and so were predicted to be a result of post-translational modifications. Phosphorylation was predicted to be contributing to the CK8 isoforms detected, as CK8 has 23 confirmed phosphorylation sites. The expression level and phosphorylation of CK8 in CRC was chosen for further analysis.

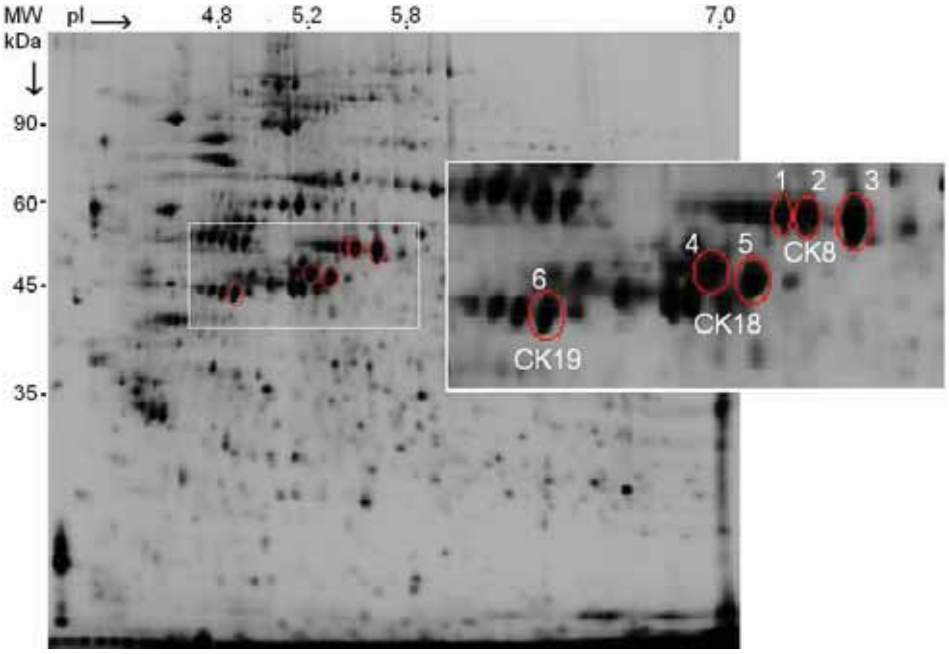

Fig 1. A scanned DeCyder 2D gel image with the identified cytokeratin proteins significantly increased in the tumour tissues compared to matched normal mucosa. The numbered protein spots in the boxed enlarged gel area correlate to the data given in Table 1. The gel image used in this figure is the same image used in Fig. 4 Chapter 3.

Table 1. Quantitative 2D DIGE data for the identified CK proteins.

				Individual Tumour-Normal Abundance Ratios							
Spot	ID	Ave. Ratio [a]	*P* [b]	1	2	3	4	5	6	7	8
1	CK8	4.56	0.0003	2.50	8.70	3.50	6.20	5.20	5.10	1.30	3.90
2	CK8	4.36	0.0052	1.30	7.50	4.30	7.50	3.40	7.70	0.80	2.00
3	CK8	3.98	0.0019	1.40	4.50	2.70	4.40	5.30	5.70	0.95	6.80
4	CK18	4.22	0.013	1.20	10.50	4.40	2.00	4.60	8.50	1.60	0.80
5	CK18	4.00	0.037	0.70	9.60	4.20	3.00	4.60	7.70	1.70	0.48
6	CK19	2.34	0.018	0.93	4.32	1.71	2.01	1.83	4.96	0.87	2.13

[a] Average tumour-normal abundance ratio
[b] Significance value, Student's paired T-test
Calculations performed using DeCyder software

5.1.2 Cytokeratins as intermediate filament proteins

Cytokeratins are intermediate filament (IF) proteins with the principle function of protecting cells from mechanical stress via association with the cell adhesion machinery desmosomes (cell to cell adhesion) and hemidesmosomes (cell to basement membrane adhesion), which anchor keratins to the cell membrane.[247] There are twelve acidic type I epithelial cytoskeletal keratins (CK9–CK20), with a pKi of 4–6, and eight basic type II epithelial cytokeratins with a pKi of 6–8 (CK1–CK8).[248] All epithelial cells express at least one type I and one type II keratin, which assemble into obligatory noncovalent heteropolymers in a 1:1 molar ratio.[248] CK8 and CK18 are the major intermediate filament components of simple or single-layered epithelia of the gastrointestinal tract, liver, exocrine pancreas and mammary glands.[249] Cellular CK8 interacts with CK18 to form insoluble 10 nm filaments that extend from nucleus to internal leaflet of plasma membrane, where they interact with desmosomes and hemidesmosomes to bridge transmembrane domain proteins via plakins.[116,117] CK19 is also highly abundant in epithelial cells and has been shown in CK18 knock out mice to act as a replacement for CK18, interacting with CK8 to form a normal cytoskeleton.[250]

5.1.3 Cytokeratins in cancer

CK8 and CK18 are good clinical histopathological markers as they are expressed specifically in epithelial cells normally and throughout cell transformation and cancer progression.[251] Increased expression of CK8/18 has been correlated with increases in metastasis and invasion in melanoma cell lines[252] and transfection of CK8/18 into mouse fibroblast L-cells has been shown to induce an enhanced migratory and invasive capacity.[253] Stratified epithelial cells, from a non-malignant buccal mucosa cell line, transfected to express CK8/18 intermediate filament pairs, developed a malignant phenotype and formed tumours with lung metastasis when injected into nude mice.[254] In a study analysing squamous cell carcinomas, the highest expression levels of CK8/18 were observed at the invasive front of the tumours[255] and other work has shown CK8/18 expression levels of primary squamous cell carcinomas could be used to define cancer subgroups, with increased expression associated with poorer prognosis after multivariate analysis.[256] In healthy individuals, cytokeratins have been detected in the circulation, although levels are normally low (reviewed in [257]). Serum levels of tissue polypeptide antigen (TPA), made up of the degradation products of CK8/18/19[258], are known to be significantly increased in carcinoma patients. The detection of TPA by antibodies in the sera of patients with epithelial cancers such as breast, lung, head and neck, bladder and colorectal cancer has been suggested for use in diagnostic testing (reviewed in [257]).

5.1.4 CK8 phosphorylation

The basic structure of all IF proteins is a central coiled-coil α-helix domain 'rod' flanked by a non-α-helical N-terminal 'head' and C-terminal 'tail' domain.[248] The head and tail domains of keratins contain the most structural heterogeneity, and are the most exposed domains, hence these are the areas that undergo phosphorylation.[259] The phosphorylation of IF proteins has been shown to regulate assembly, disassembly and organisation in vitro and in vivo.[152-154] Toivola *et al*. (1997)[154] demonstrated that phosphorylation of IF is essential for the correct function of cytokeratins, and when serine/threonine phosphatase activity is downregulated, cell junctions and the organisation of IF and microfilament assembly is disrupted. Increased phosphorylation of CK8/18 results in increased disassembly, solubilisation and the inhibition of subunit polymerisation.[154]

CK8 is normally homogeneously distributed in intracellular intermediate filaments that bridge to the plasma membrane.[260] During mitosis, cytokeratins become soluble, unravel, and reorganise into granules that form large aggregate bodies[261], or form part of intermediate filament bundles that remain closely associated with the mitotic spindle.[262] Chou *et al*. (1994)[263] compared the levels of phosphorylated and glycosylated CK8/18 in mitotically arrested cells to mitotically enriched cells (both in G2/M phase). Mitotic arrest resulted in an increase in the number of terminal N-acetylglucosamines of CK8/18. Phosphorylation was detected in both the mitotically arrested and enriched cells, but a distinct hyperphosphorylated form of CK8 was seen in the arrested cells. A small amount of hyperphosphorylated CK8 occurs during regular mitosis, with low steady state levels in resting cells. Hyperphosphorylation of CK8 is also seen in heat stressed cells.[119] When comparing basally phosphorylated CK8 and CK18 to hyperphosphorylated CK8 and CK18 by 2DE, a distinctly different gel pattern is observed[264], with a number of more acidic isoforms detected. The hyperphosphorylated form of CK8 appears at a slightly higher molecular weight on a 1D gel.[119]

5.1.5 Study Design

The phosphorylation of IF proteins has been shown to regulate assembly, disassembly and organisation in vitro and in vivo.[152,153] Toivola *et al*. (1997)[154] showed that phosphorylation of IF is essential for the correct function of cytokeratins, and when serine/threonine phosphatase activity is down regulated, cell junctions and the organisation of IF and microfilament assembly are disrupted. Increased phosphorylation of CK8/18 results in increased disassembly, solubilisation and the inhibition of subunit polymerisation.[154] This allows CK8 to act as a phosphate 'sink', inhibiting phospho-activation of pro-apoptotic substrates by stress-activated protein kinases, and thus inhibiting apoptosis.[265] The CK8 serine residues 73 and 431 are known to be phosphorylated by the MAP kinases JNK and p38 during stress, and by ERK1 in response to EGFR signalling.[155,157,158] Increased signalling via the EGFR

pathway has been well documented in CRC, and can be a result of upregulation of activating ligands such as EGF and TGF α or by activating mutations in EGFR itself. Constitutive activation of the EGFR Ras/Raf/MEK/ERK signalling pathway occurs in almost 50% of CRC patients due to mutations in the KRAS and BRAF genes.[159-161] Little is known of the frequency and type of CK8 phospho-isoform expression in CRC.

In order to determine which of the phosphorylation sites were most likely contributing to the CK8 isoforms detected by 2D DIGE, phosphopeptides from the CK8 isoforms were analysed by metal oxide affinity chromatography mass spectrometry. The phosphorylated residues serine 23 and serine 431 were detected. Levels of phosphoserine (PS) 23, PS431 and PS73 were analysed in 30 matched pairs of colorectal tumour-normal tissue by western blot. Analysis of PS73 levels was performed, as this residue is known to be phosphorylated as a result of EGFR signalling. Expression levels of CK8 were analysed at the RNA by real-time RT-PCR to assess the potential of CK8 as part of the immunobead RT-PCR marker panel. In order to determine if EGFR signalling was contributing to the levels of PS23, PS73 and PS431 in the tumours, the CRC cell line Caco2 was treated with an antibody that blocked the ligand-binding site of EGFR and the levels of PS23, PS431 and PS73 were analysed.

5.1.6 Aims

To determine the percentage of patients with a CK8 tumour-normal expression ratio of ≥2 fold at the RNA level, in order to analyse the potential of SET as an immunobead RT-PCR panel marker, and to determine if CK8 is increased in early stage compared to late stage patients.

To determine the CK8 serine residues commonly phosphorylated in CRC.

To determine if the level of phosphorylated CK8, using antibodies against specific phosphoryated residues, is significantly different between matched paired tumour-normal samples.

To determine the effect of decreasing EGFR/Ras/Raf/MEK/ERK signalling on the levels of chosen CK8 phosphorylated residues.

5.1.7 Hypotheses

- CK8 is significantly increased in expression at the RNA level between matched paired tumour-normal tissues and will be useful as an immunobead RT-PCR panel marker.
- CK8 phosphorylation is significantly increased in CRC.
- Decreased signalling of the EGFR/Ras/Raf/MEK/ERK pathway will result in decreased levels of some phosphorylated CK8 residues, such as serines 73 and 431.
- Levels of CK8 residues phosphorylated by ERK (such as PS73 and PS431) will be significantly increased in CRC patients with mutations in the KRAS or BRAF genes.

5.2 Materials and methods

5.2.1 Real-time RT-PCR

To determine if CK8 was upregulated at the RNA level, relative real-time RT-PCR was performed on 32 CRC tumour-normal matched paired tissues. For RNA extraction, cryo-sections (30 μ) were pulverised in a mortar and pestle under liquid nitrogen. RNA was extracted using Tri Reagent (Sigma, St Louis, MO) (Ref Chapter 2). RNA integrity was checked by denaturing gel electrophoresis. Samples that did not show distinct 28S and 18S bands were excluded from further analysis. RNA was quantified at 260 nm using the NanoDrop ND-1000 Spectrophotometer (NanoDrop Technologies, Wilmington, DE). Total RNA (1 μg per sample) was reverse transcribed in a 20 μl reaction volume as detailed in Chapter 2.

Relative real-time PCR for CK8, and the housekeeping genes, phosphomannomutase I (PMM1) and proteasome subunit Y (PSMB6), was performed separately using the MJ Research DNA Engine Opticon 2 (Biorad, Hercules, CA). Two microlitres of the reverse transcription mix was used in each PCR in a final reaction volume of 20 μl as detailed in Chapter 3. PMM1 and PSMB6 had previously been reported as good housekeeping genes for CRC.[266] CK8 primers were obtained from SA Biosciences. The PMM1 and PSMB6 primers were obtained from GeneWorks (Thebarton, SA, Australia) (sequences in Chapter 2). The RT negative control consisted of RNA and master mix without reverse transcriptase, while the PCR negative (no target) control consisted of PCR master mix alone. All samples were amplified in triplicate and the mean C(t) value was obtained.

CK8 tumour to normal expression ratios were calculated using the $\Delta C(t)$ method of relative quantification.[267] The $2^{-\Delta\Delta C(t)}$ method was then used to compare the expression of CK8 in the tumour samples compared to matched normal mucosa after normalisation to both PMM1 and PSMB6 separately (refer to chapter 2 for method in detail). A Kruskal-Wallis significance test was performed on the tumour-normal fold change ratios obtained by each method. All statistics were performed using GraphPad Prism 4 software.

5.2.2 Enrichment and identification of CK8 phosphorylated proteins

In order to identify phosphorylated CK8 residues, 750 μg of protein extracted from SW480 cells was separated by 2DE using 24 cm pH 3–7 NL IPG strips and 8%–15% polyacrylamide gels (chapter 2). Gels were stained with Coomassie blue and de-stained in 20% methanol/7.5 % acetic acid. The three CK8 isoforms of interest were individually excised from the gels and digested with trypsin (chapter 2).

Phosphorylated peptides were then enriched using Phos Trap Titanium Dioxide (TiO2) (Perkin Elmer) magnetic beads according to the manufacturer's recommendations.

The eluted peptide solution (1.5 μl) was spotted onto a 600 μm AnchorChip (Bruker Daltonics, Bremen, Germany) target plate with 1 μl of 2,5-DHB (10 mg/ml) matrix in 50% ACN/0.1% TFA/0.1% PA. MALDI TOF MS/MS was carried out as previously described.[95] Briefly, MALDI-TOF mass spectra were acquired using a Bruker ultraflex III MALDI TOF/TOF mass spectrometer (Bruker Daltonics) operating in reflection mode under the control of the flexControl software v3.0 (Bruker Daltonics). External calibration was performed using peptide standards (Bruker Daltonics) that were analysed under the same conditions. Spectra were obtained randomly over the surface of the matrix spot at laser intensity determined by the operator. A signal to noise ratio threshold of ten was used for peak selection. Peak masses and intensities of TOF and LIFT spectra were detected with flexAnalysis v3.0 (Bruker Daltonics). MS and MS/MS spectra were subjected to smoothing, background subtraction and peak detection using flexAnalysis and the SNAP algorithm. The spectra and mass lists were exported to BioTools v3.1 (Bruker Daltonics) where the MS and corresponding MS/MS spectra were combined and submitted to the in-house Mascot database-searching engine (Matrix Science: http://www.matrixscience.com). Data was matched against the SwissProt 57.1 database. Search parameters were; a mass tolerance of MS 100 ppm, MS/MS tolerance of 0.5 Da, mammalian taxonomy (64,438 sequences), the variable modifications of oxidisation of methionines and phosphorylation of S, T and Y, the fixed modification carbamidomethylation of cysteines, and two missed trypsin cleavages. Positive protein identifications were assigned on the basis of combined ion scores that exceeded the calculated deprecated protein identification threshold. In addition, an in silico digest of CK8 was performed using the sequence editor platform of BioTools to identify potential phosphopeptides.

Precursor ions, suspected to be phosphorylated peptides, were chosen for MS/MS analysis. Spectra ion annotation was performed using MOWSE and probability scores. For spectra that matched to precursor ions of potential phosphorylated peptides, annotation was performed using BioTools and the different phosphorylation positions were evaluated manually.

Preceding MALDI TOF/TOF analysis was performed by myself with the assistance of Mark Condina (Adelaide Proteomics, Adelaide Univeristy).

5.2.3 Western blotting

5.2.3.1 2DE conformation of CK8 phosphorylation sites

2D western blots of protein extracted from the CRC cell line Caco2 was performed with phospho-specific antibodies against PS23, PS431 and PS73 in order to verify the three CK8 isoforms of interest were in fact phosphorylated at these sites. The Caco2 cell line was purchased from the American Type Culture Collection (ATCC, Rockville, MD) and maintained in RPMI 1640 at 37°C, 5% CO_2. Cells were washed, pelleted and lysed in TUC buffer (2 M Thiourea, 7 M urea, 4% CHAPS, 1 x Halt Phosphatase Inhibitor Cocktail (Pierce)) and quantified using the EZQ kit (Invitrogen) according to manufacturer's recommendations. Three hundred micrograms of protein was separated by 2DE using 24 cm pH 3–7 NL IPG strips and 8%–15% polyacrylamide gels (chapter 2). Following electrophoresis, protein was transferred using a semi-dry apparatus for one hour at 70 mA per blot onto low fluorescent PVDF membrane. Membranes were blocked in 5% skim milk PBST, washed and incubated overnight with the primary antibody. The antibodies used were CK8 PS73 (ab32579, Abcam) at 1:1000, CK8 PS23 (EP1629Y, Novus Biologicals) at 1:5000 and CK8 PS431 (ab59434, Abcam) at 1:1000. Membranes were washed and incubated in the dark at room temperature for 1.5 hours with ECL Plex fluorescent detection Cy3 (anti-mouse) antibody (GE Healthcare) at a 1:1000 dilution. Membranes were washed, air-dried, and imaged using the Typhoon Imager (GE Healthcare).

5.2.3.2 1DE analysis of CK8 phosphorylation in CRC

To determine the levels of CK8 and the phosphorylated isoforms, western blotting was performed on 30 CRC tumour-normal matched samples. For protein extraction, 30 μ cryo-sections were pulverised in a mortar and pestle under liquid nitrogen and placed in 200 μl of buffer containing 0.2% SDS, 10% glycerol, 62.5 mM TrisHCl, 6 M urea, 1 x Halt Phosphatase Inhibitor Cocktail (Pierce), 65 mM DTT and 150 U Benzonase. Samples were purified using the 2D Clean Up Kit (GE Healthcare) and quantified using the EZQ assay (Invitrogen). Fifty μg of each sample was loaded onto 4%–20% polyacrylamide gels and electrophoresed at 200 V. Protein was transferred onto low fluorescent PVDF membrane, blocked and incubated with antibodies against PS23, PS431 and PS73 (Chapter 2). Blotting for unmodified CK8 was also performed using a CK8 antibody (ab9023, Abcam) at a 1:500 dilution. A β actin loading control antibody was included on all blots (mouse monoclonal β actin (sc47778, Santa Cruz) at 1:500, or a rabbit polyclonal β actin (ab8227, Abcam) at 1:1000). Membranes were washed and incubated in the dark at room temperature for 1.5 hours with ECL Plex fluorescent detection Cy3 (anti-mouse) and Cy5 (anti-rabbit) antibodies (GE Healthcare) at a 1:1000 dilution. Membranes were washed, air-dried, and imaged using the Typhoon Imager (GE healthcare).

The primary CK8 antibody and β actin levels were detected using fluorescent Cy3 and Cy5 labelled antibodies, and quantified using Image Quant v5 software. Levels of CK8 expression were normalised to β actin expression in each sample and the ratio of tumour to normal protein expression was calculated. For the western blotting performed with the CK8 phospho-specific antibodies, following normalisation to β actin, each sample was normalised to total CK8 expression in each sample. This was done to ensure that detected differences in phosphorylation levels between tumour-normal pairs was not due to increased CK8 levels overall. The ratio of tumour to normal protein expression was then calculated. All statistics were performed using GraphPad Prism 4 software (2 tailed Wilcoxon matched pairs test).

5.2.4 Blocking EGFR signalling in Caco2 cells

To determine if EGFR signalling was contributing to the levels of phosphorylated CK8, the CRC cell line Caco2 was treated with the sc-120 antibody (Santa Cruz) that blocks the ligand-binding site of EGFR. Caco2 cells were plated in duplicate at 1 x 10^5 cells per well in a 24-well plate in a total volume of 350 μl RPMI media with 10% foetal calf serum. Cells were treated with 1 μg of antibody per well. This amount was determined to be saturating by flow cytometry as described in Chapter 2 (Fig. 10). Treated and untreated control cells were harvested at four, six and eight hours post-antibody treatment by lysis in 50 μl of buffer containing 0.2% SDS, 10% glycerol, 62.5 mM TrisHCl, 6 M urea, 1 x Halt Phosphatase Inhibitor Cocktail (Pierce) and 150 U Benzonase. Lysates were quantified and western blotting was performed on 25 μg of each sample for CK8 PS23, PS73, PS431 and a β actin loading control as previously described. This experiment was repeated three times.

5.3 Results

5.3.1 Real-time RT-PCR

Real-time RT-PCR for CK8 was performed on RNA extracted from ten stage 1, sixteen stage II and six stage III CRC tumour-normal matched paired tissues to determine if CK8 was upregulated in tumour samples at the RNA level. The tumour-normal expression ratios of CK8 were calculated using the 2-ΔC(t) method of relative quantification to the same amount of total starting RNA, and again after normalisation to the housekeeping genes PMM1 and PSMB6 using the $2^{-\Delta\Delta C(t)}$ method (Fig. 2). Tumour-normal ratios calculated using the 2-ΔC(t) method compared to the 2-ΔΔC(t) method (after normalisation to the housekeeping genes) were not significantly different, P=0.052 (repeated measures ANOVA). When averaging the relative abundance ratios for each patient obtained from the different methods, 43% of patients had a tumour to normal CK8 expression ratio of >2 fold. There was no significant difference in the ratio of CK8 expression between stage I, II and III tumours.

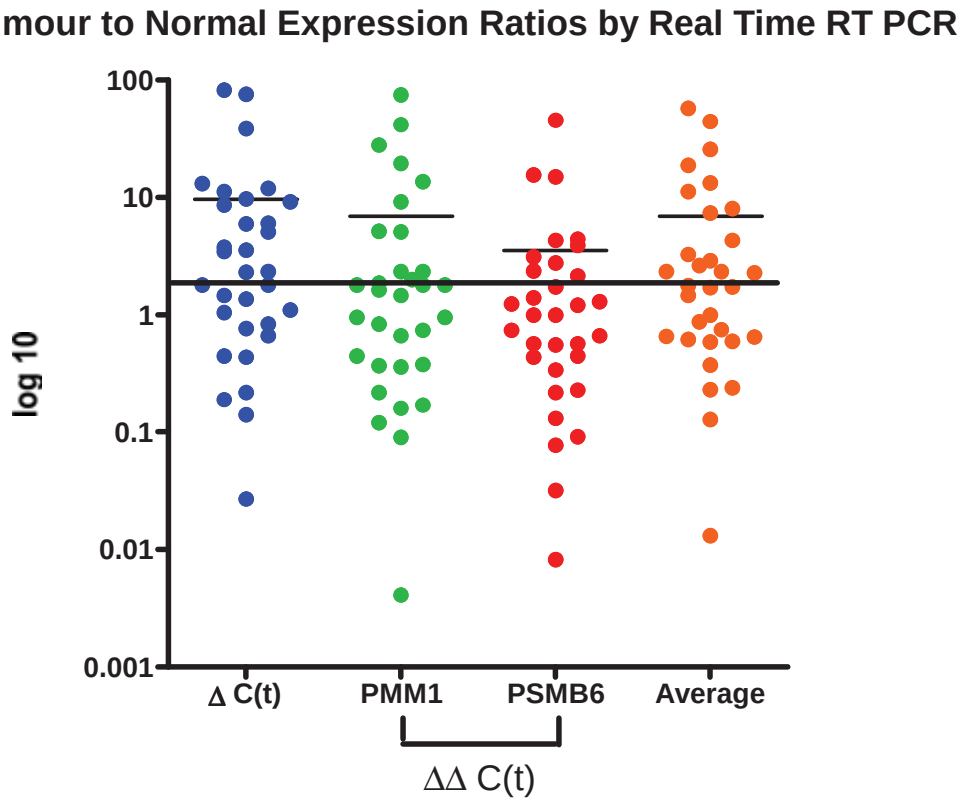

Fig 2. Real-time RT-PCR results for CK8 expression in 32 tumour-normal tissue pairs. Tumour to normal expression ratios calculated by normalisation to same amount total starting RNA using the 2-ΔC(t) method, or to the housekeeping genes PMM1 or PSMB6 using the 2-ΔΔC(t) method. Calculating the expression ratios using the different methods did not show significantly different results, P=0.052 (repeated measures ANOVA). Data points in the fourth column labelled average are the averaged tumour to normal expression ratios obtained using the different methods of normalisation. The black continuous line represents a 2 fold tumour-normal expression ratio.

5.3.2 Phosphorylation site identification

The CK8 isoforms detected as increased in tumour tissue were excised from a 2D gel and digested with trypsin. Phosphorylated peptides were enriched using Phos Trap TiO2 beads and subjected to MALDI-TOF/TOF MS analysis. Precursor ions with m/z ratios of potential phosphopeptides were chosen for MS/MS analysis. MALDI-TOF MS spectrum of stock CK8 trypsin digest prior to phosphopeptide enrichment, and after phosphopeptide enrichment, can be seen in Fig. 3.

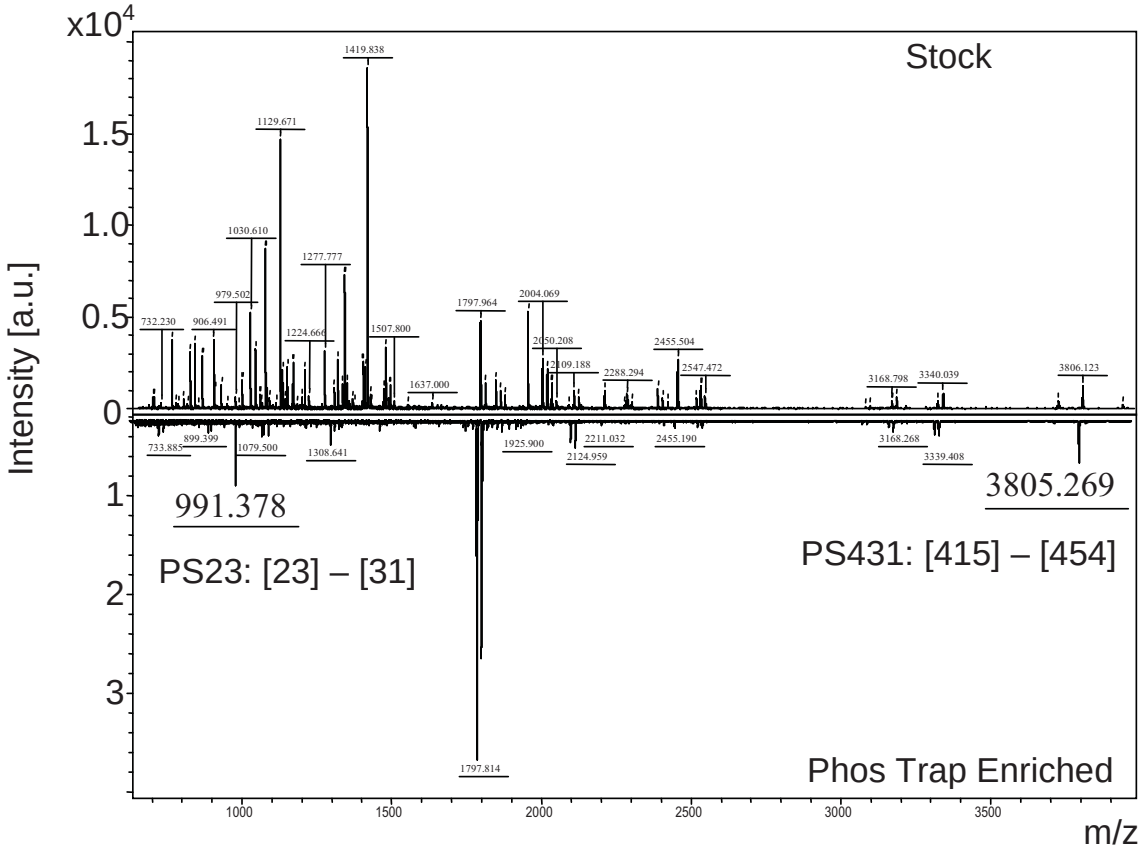

Fig 3. MALDI-TOF MS spectrum of stock CK8 trypsin digest prior to phosphopeptide enrichment (top), and after phosphopeptide enrichment (bottom) using Phos Trap beads. The precursor ions of the peptides containing the phosphorylated residues PS23 and PS431 can be seen in the enriched MALDI-TOF spectra at m/z 991.378 and 3805.269 respectively.

Two precursor ions at m/z 991.378 and 3805.269 were identified in the CK8 isoforms, and matched to previously annotated phosphopeptides by performing an in silico digest of CK8 using the sequence editor platform of BioTools. Complete y-ion sequence was successfully obtained for the [M+H]+-ion 991.378 ([23]–[37] SYTSGPGSR), with the loss of 80 and 98 being detected (Fig. 4). Partial sequence and the mass loss of a phosphate were obtained from the [M+H]+-ion 3805.269 ([415]–[454] TTSGYAGGLS(s)A(y)GGL(t)(s)PGLSYSLGSSFGSGAGSSSFSR) (Fig. 5). The exact residue that had lost the phosphate group could not be successfully assigned. Using BioTools, all possible phosphorylation sites within the peptide were analysed and ranked according to probability. The peptide contains four potential phosphorylation sites according to the Uniprot database (http://www.uniprot.org/uniprot/P05787) of which two have been assigned by similarity and two by annotation. The serine residue 431 was scored as having the highest probability of phosphorylation using BioTools. Phosphorylation of this residue was confirmed by 2D western blotting.

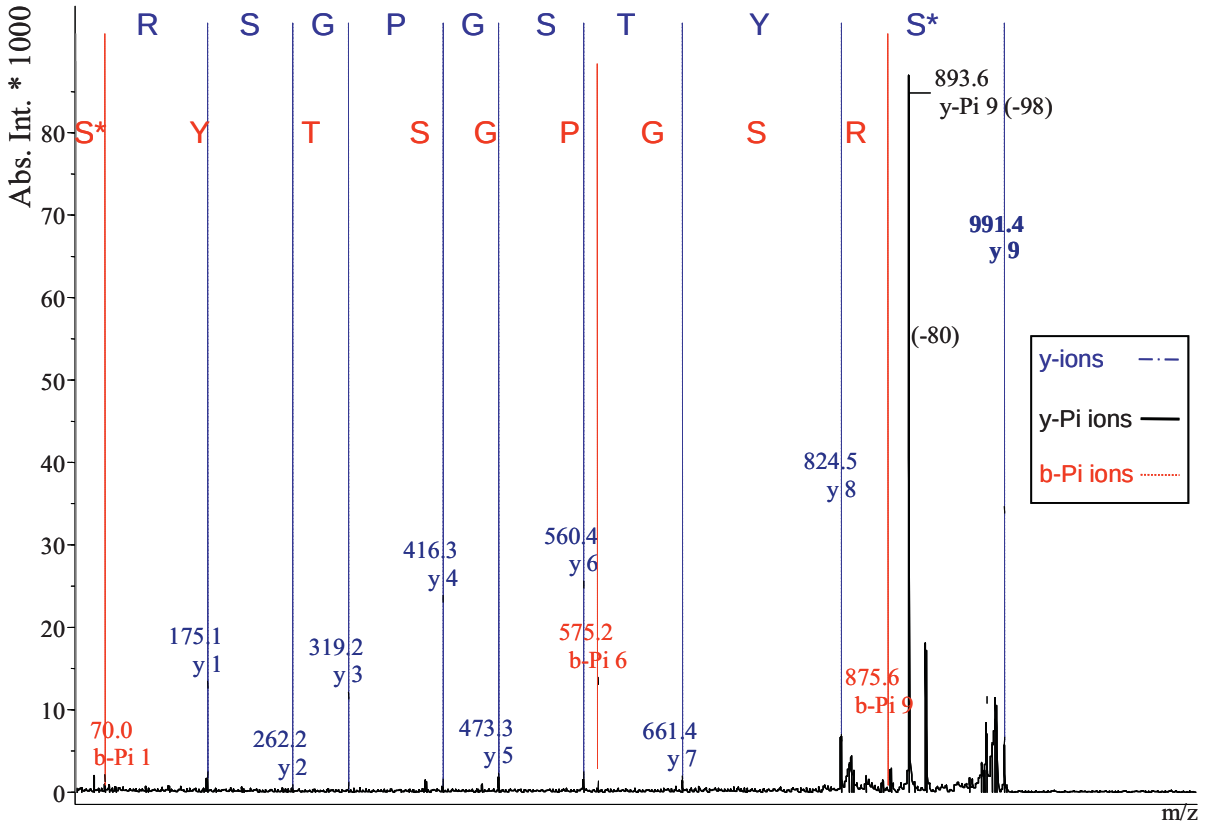

Fig 4. Tandem MS analysis of [M+H]+: 991.4 Da (pSYTSGPGSR). A mass loss of 98 from the terminal Y ion series serine residue was detected, indicating the loss of a phosphate group. This phosphorylated peptide, conferring to phosphoserine 23, was detected in the most acidic CK8 isoform by MALDI TOF/TOF.

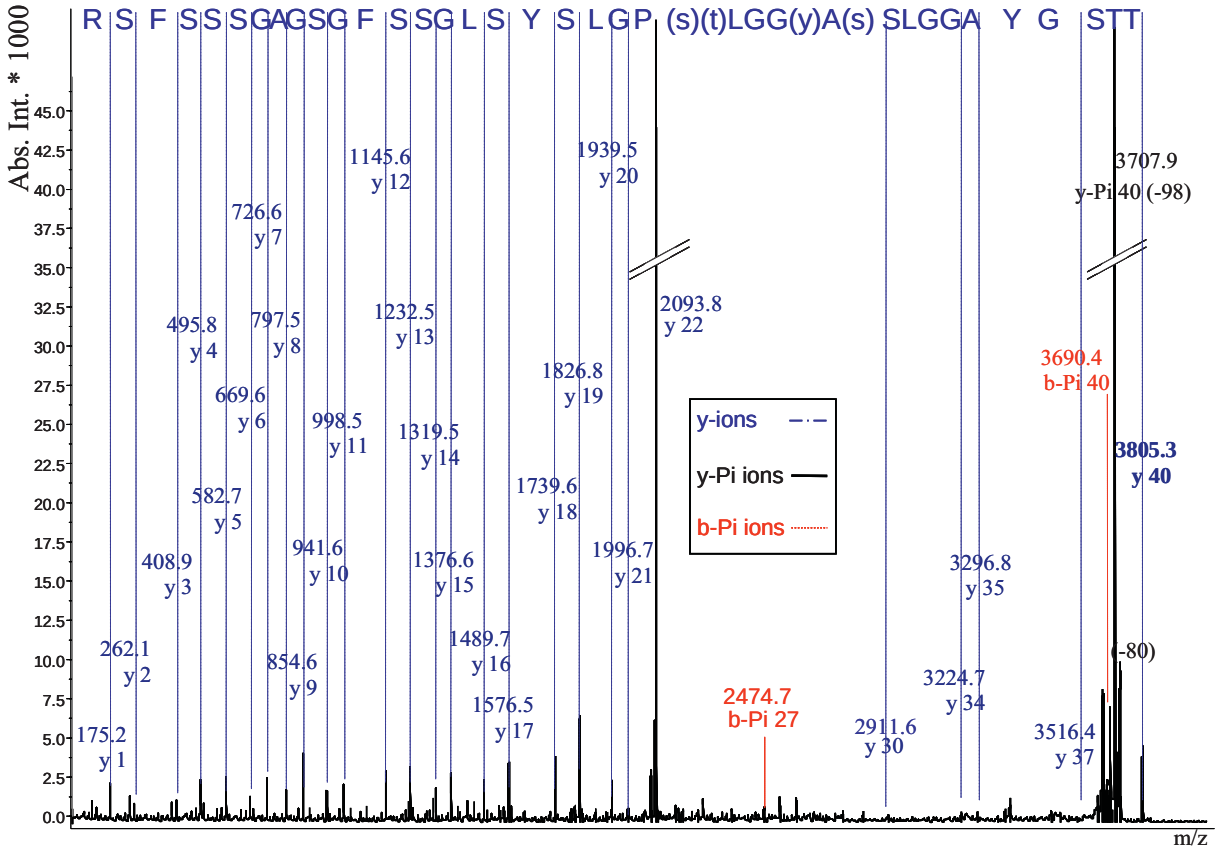

Fig 5. Representative spectra from the tandem MS analysis of [M+H]+: 3805.3 Da (TTSGYAGGLS(s)(y)GGL(t)(s)PGLSYSLGSSFGSGAGSSSFSR). Mass losses of 80 and 98 from the Y-ion series were detected indicating the loss of a phosphate group, but the exact residue of phosphorylation could not be determined. Using BioTools and manual annotation, the most probable phosphorylated residue was calculated as PS431. Phosphorylation of this residue was confirmed by 2D western blotting.

5.3.3 Confirmation of phosphorylation sites by 2D western blot

2D western blots were performed on protein extracted from the CRC cell line Caco2 in order to confirm the presence of the serine-phosphorylated residues 23, 431 and 73. Each of the three phospho-specific antibodies reacted with all three of the CK8 isoforms of interest (Fig. 6).

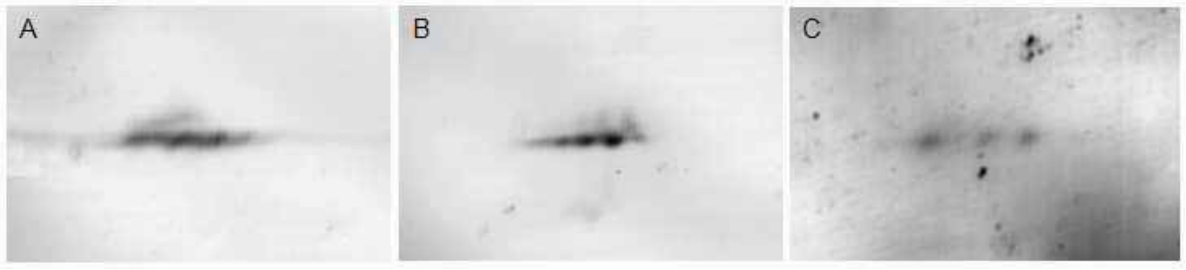

Fig 6. 2D Western blots confirming the phosphorylated serine residues 23, 431 and 73. 2D western blots confirming the presence of the CK8 phosphorylated residues A) 23, B) 431 and C) 73 in the three CK8 isoforms detected as upregulated in CRC by the 2D DIGE study. The most acidic isoform of CK8 is to the left of the blot and the most basic isoform is to the right of the blot.

5.3.4 Quantification of phospho-CK8 by western blotting

Western blotting was used to compare the expression levels of CK8, CK8 PS23, PS73 and PS431 in 30 matched pairs of tumour-normal tissue samples (Fig. 7). All samples were normalised to β actin, and phosphoserine-specific results were normalised a second time to total CK8. The median expression level (arbitrary units) of unmodified CK8 in the tumour samples was 2.75 compared to 1.8 in the matched normal samples. This was not significantly different, P=0.053 (Wilcoxon signed rank test). However, for the phospho-CK8 isoforms, the median expression in the tumour and normal samples was significantly different; CK8 PS23 0.667 and 0.29 respectively, P=0.004; CK8 PS431 1.02 and 0.30 respectively, P=0.03; CK8 PS73 0.18 and 0.06 respectively, P=0.0005 (Wilcoxon signed rank test). Among the 30 patients, 16/30 (53%) showed overexpression (tumour: normal ratio ≥2) for PS23, 17/30 (57%) for PS431 and 20/30 (67%) for PS73. On comparing the tumour-normal expression ratios of the individual isoforms between different tumour stages, only CK8 PS73 showed a significant increase in late stage tumours (stage III and IV) versus stage I (P=0.038, Mann Whitney test).

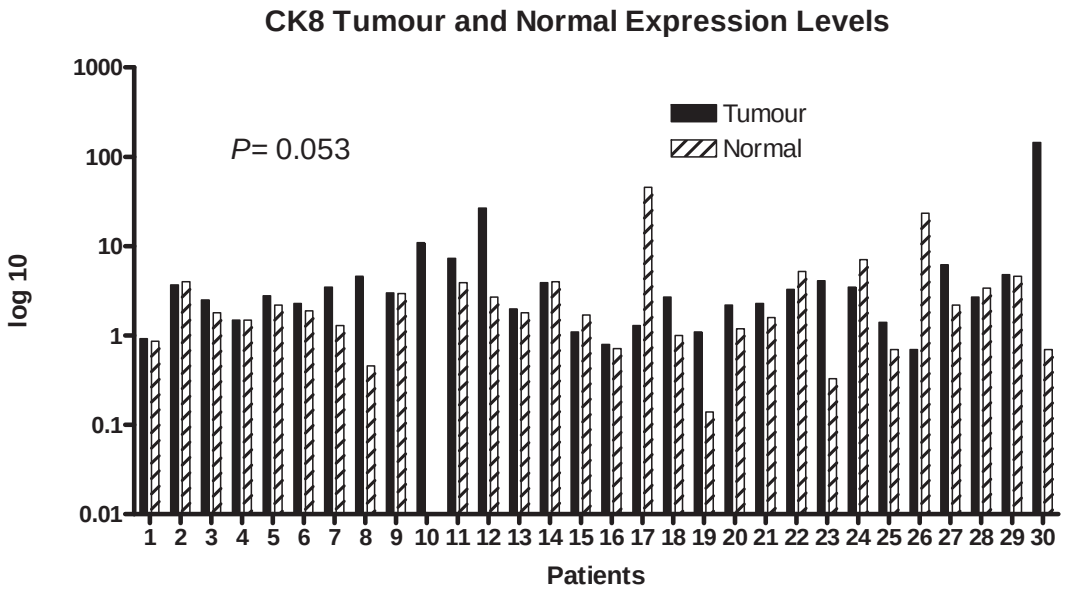
CK8 Tumour and Normal Expression Levels
1000
100
10
1
0.1
0.01
log 10
P= 0.053
Tumour
Normal
1 2 3 4 5 6 7 8 9 10 11 12 13 14 15 16 17 18 19 20 21 22 23 24 25 26 27 28 29 30
Patients

A)

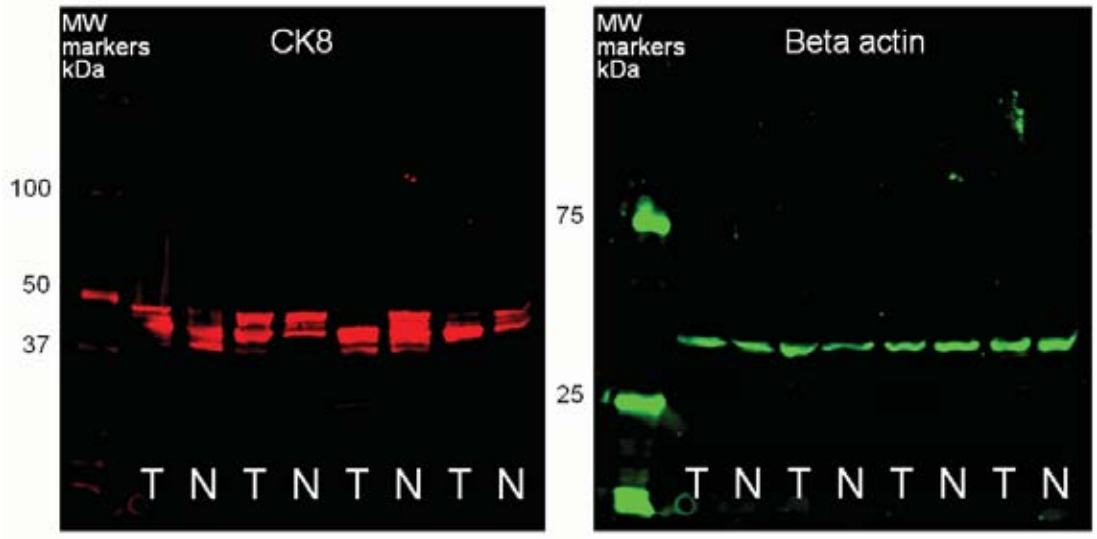
MW
markers
kDa
CK8
100
50
37
T N T N T N T N
MW
markers
kDa
Beta actin
75
25
T N T N T N T N

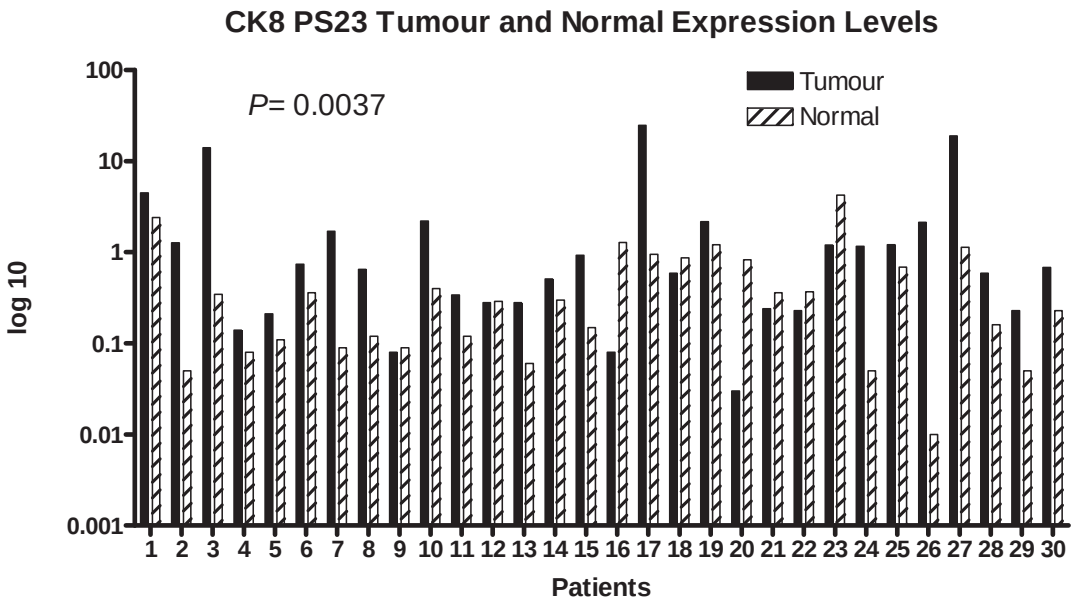
CK8 PS23 Tumour and Normal Expression Levels
P= 0.0037
Tumour
Normal
log 10
100
10
1
0.1
0.01
0.001
1 2 3 4 5 6 7 8 9 10 11 12 13 14 15 16 17 18 19 20 21 22 23 24 25 26 27 28 29 30
Patients

B)

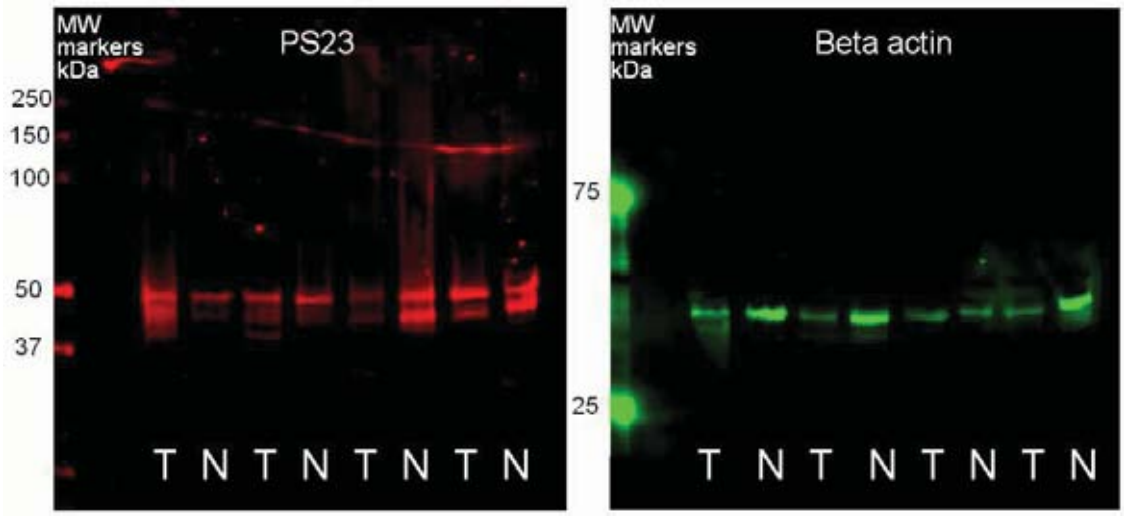
MW markers kDa
PS23
250
150
100
50
37
T N T N T N T N
MW markers kDa
Beta actin
75
25
T N T N T N T N

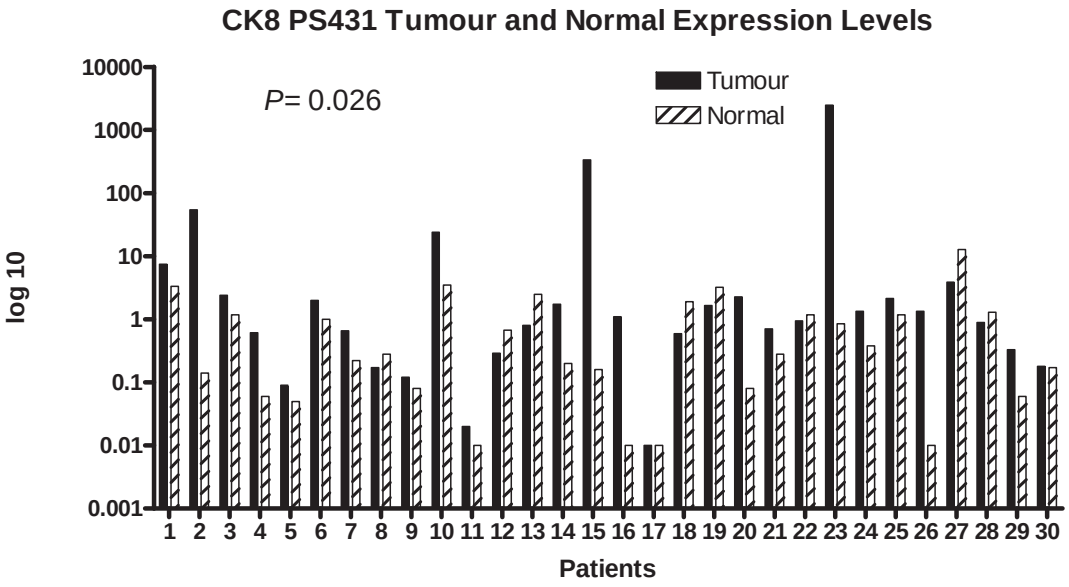
CK8 PS431 Tumour and Normal Expression Levels
P= 0.026
Tumour
Normal
log 10
10000
1000
100
10
1
0.1
0.01
0.001
1 2 3 4 5 6 7 8 9 10 11 12 13 14 15 16 17 18 19 20 21 22 23 24 25 26 27 28 29 30
Patients

C)

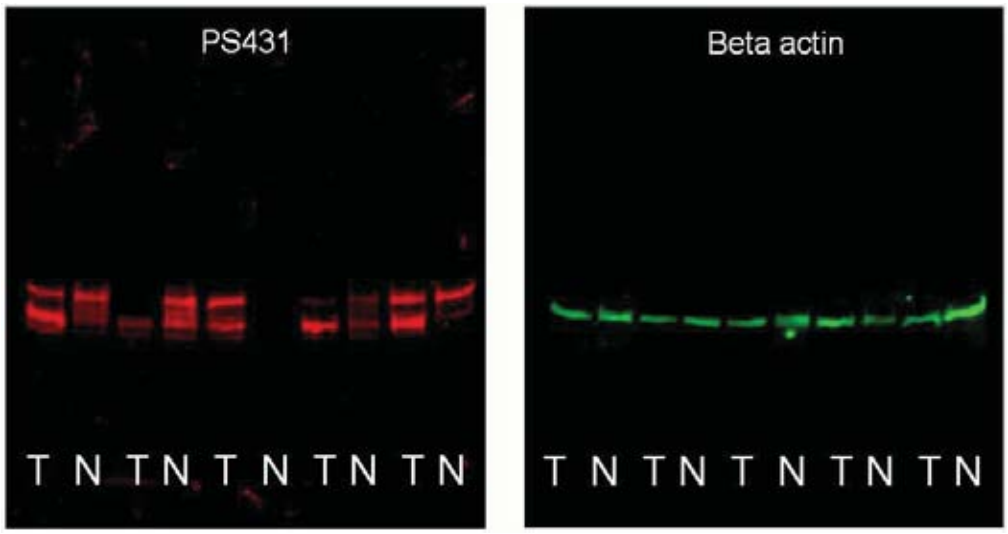
PS431
T N TN T N TN TN
Beta actin
T N TN T N TN TN

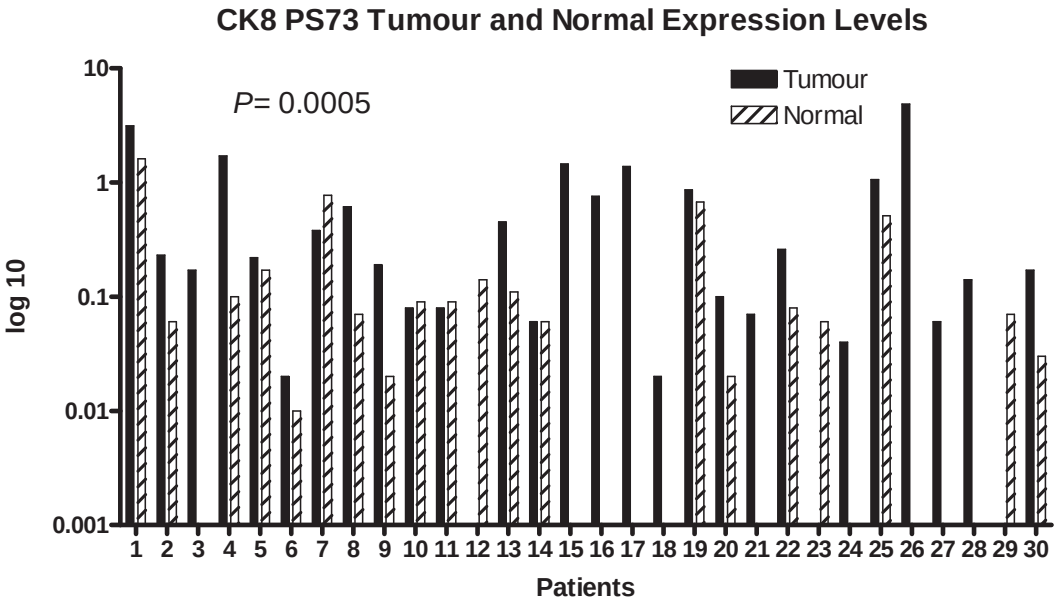

D)

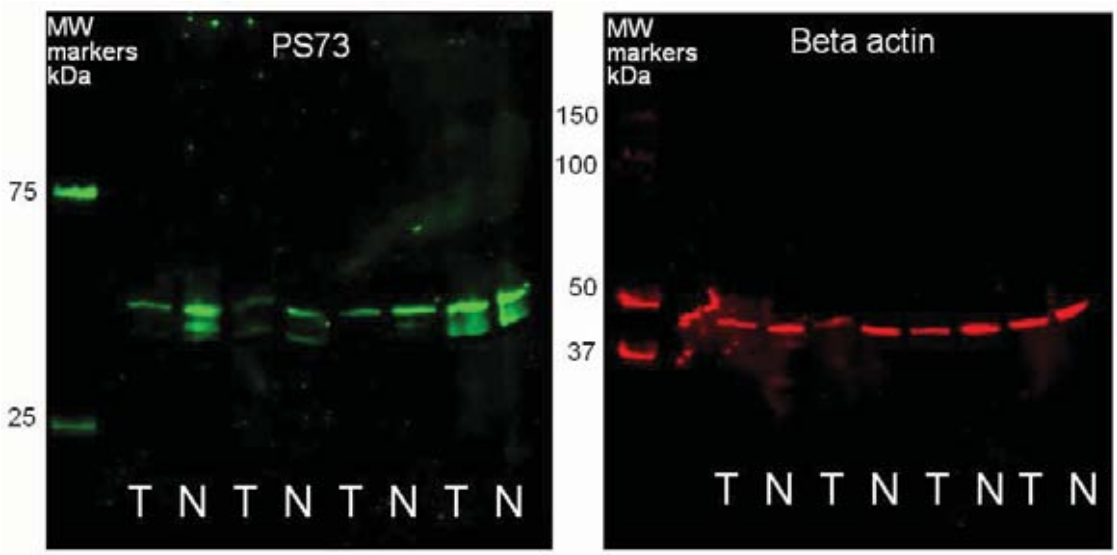

Fig 7. Expression levels of A) CK8, B) PS23, C) PS431 and D) PS73 in matched pairs of tumour-normal tissues determined by western blotting. Beneath each interleaved bar graph is a representative western blot. The median expression level (arbitrary units) of unmodified CK8 in the tumour samples was 2.75 compared to 1.8 in the matched normal samples (P=0.053). The median expression of the phospho-CK8 isoforms between the tumour-normal samples was significantly different: CK8 PS23 0.667 and 0.29 respectively, P=0.004; CK8 PS431 1.02 and 0.30 respectively, P=0.03; CK8 PS73 0.18 and 0.06 respectively, P=0.0005. Among the 30 patients, 16/30 (53%) showed overexpression (tumour-normal ratio ≥2) for PS23, 17/30 (57%) for PS431 and 20/30 (67%) for PS73. The primary antibodies for CK8, PS23 and PS431 were raised in a rabbit and were detected with an anti-rabbit Cy5, appearing red. The beta actin control on these blots was raised in a mouse and was detected with an anti-mouse Cy3, appearing green. The PS73 antibody was raised in a mouse, hence was detected with the anti-mouse Cy3, appearing green. For these blots a rabbit beta actin control was used and detected with an anti-rabbit Cy5, appearing red. The molecular weight markers used on these blots are 'Dual Color' prestained SES-PAGE standards (Biorad). The standards appearing at the MW of 250 kDa, 150 kDa, 100 kDa, 50 kDa, 37 kDa, 20 kDa, 15 kDa and 10 kDa are prestained with Cy5, appearing red. The standards ar the MW of 75 kDa and 25 kDa are prestained with Cy3, appearing green.

5.3.5 Blocking EGFR signalling in Caco2 cells decreases levels of PS73 and PS431

To determine if EGFR signalling was contributing to the levels of serine 23, 73 and 431 phosphorylation seen in the tumour samples, Caco2 cells, wild-type for BRAF and KRAS, were treated with the sc-120 antibody (Santa Cruz) that blocks ligand binding and activation of EGFR. Cells were treated with a saturating amount of sc-120 as determined by flow cytometry (Fig. 8). Treated and untreated cell lysates were analysed by western blotting for PS23, PS73 and PS431. Treatment of Caco2 cells with the sc-120 antibody led to a significant decrease in the levels of PS73 (P<0.0001) and PS431 (P<0.0001) six hours and eight hours post-treatment (Fig 9). At the four hour time point, levels of PS73 were 81.5% ±8.8 that of the untreated cells. At the six and eight hour time points, PS73 levels had decreased to 40.7% ±5.1 and 42.3% ±5.3 that of the untreated cells respectively. Levels of PS431 were 91.7% ±5.2 that of the untreated cells at four hours, and decreased to 36.7% ±7.5 and 34.0% ±2.1 of the untreated cells at the six and eight hour time points respectively. PS23 levels were not significantly different after treatment with the sc-120 antibody, P=0.73 (Fig. 9).

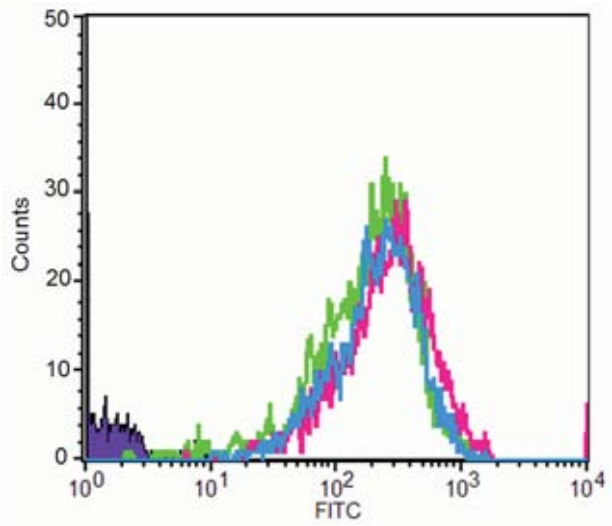

Key	Name	Parameter	Gat
	contrl cells primary ab 2.003	FL1-H	G1
	0.5 ug ab 2.004	FL1-H	G1
	1.0 ug ab 2.005	FL1-H	G1
	2.0 ug ab 2.006	FL1-H	G1

Fig 8. Flow cytometry to determine the amount of sc-120 antibody to saturate the surface of the Caco2 cells. One microgram of antibody per 1 x 10^5 cells appeared to be saturating.

A)

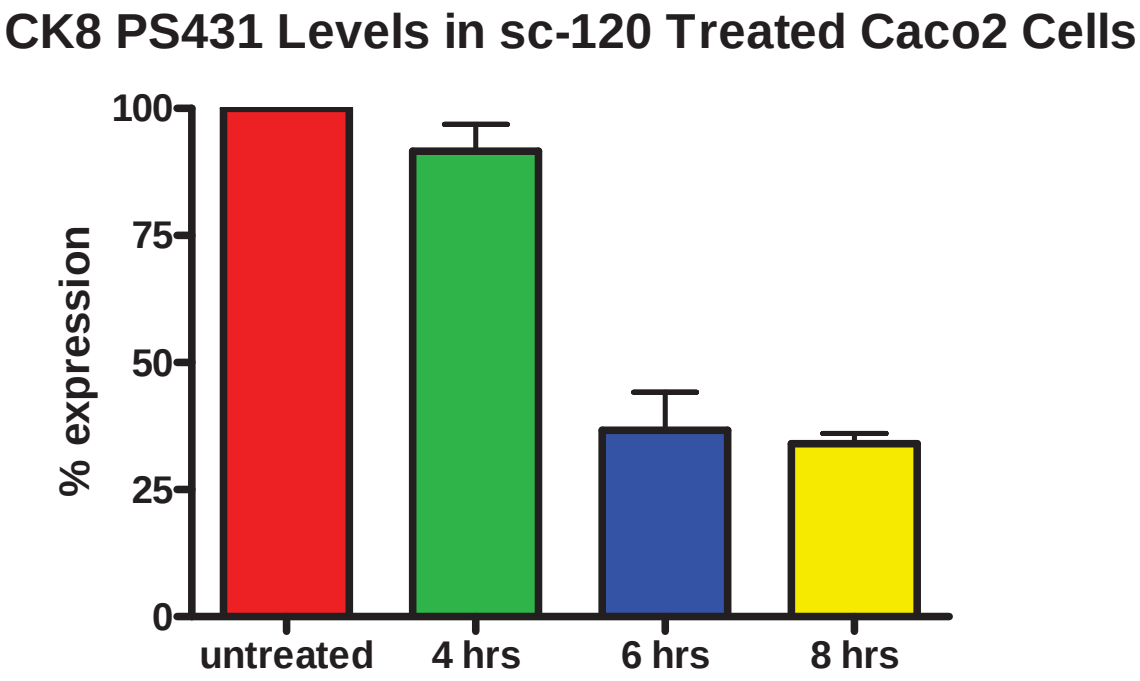
CK8 PS431 Levels in sc-120 Treated Caco2 Cells
% expression
100
75
50
25
0
untreated
4 hrs
6 hrs
8 hrs

B)

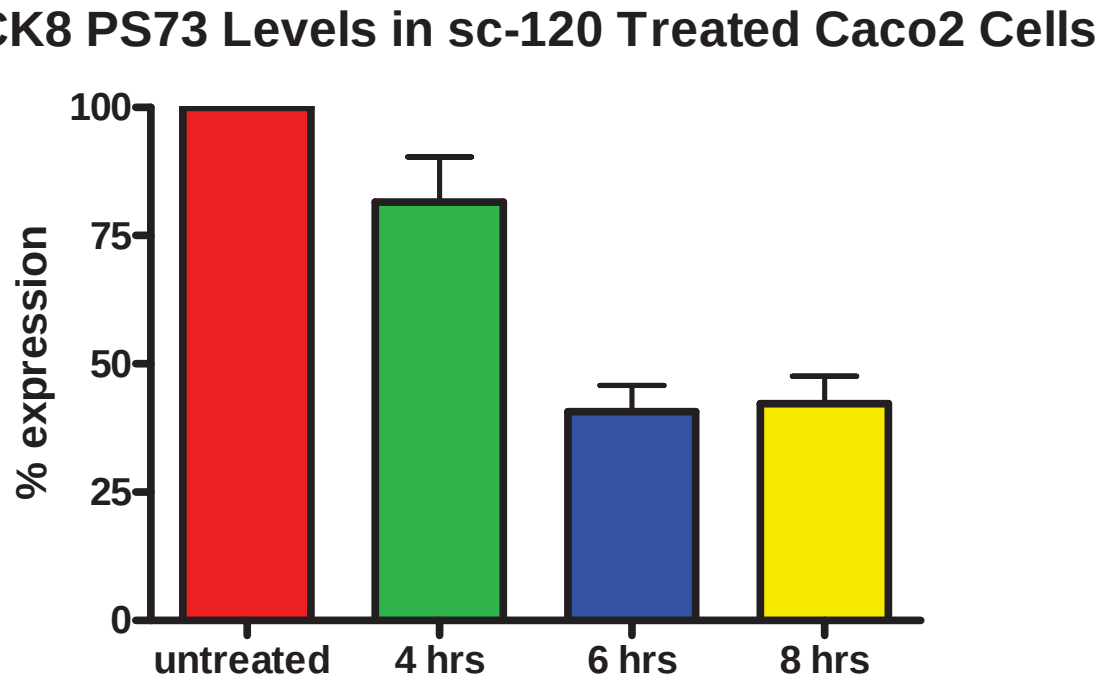
CK8 PS73 Levels in sc-120 Treated Caco2 Cells
% expression
100
75
50
25
0
untreated
4 hrs
6 hrs
8 hrs

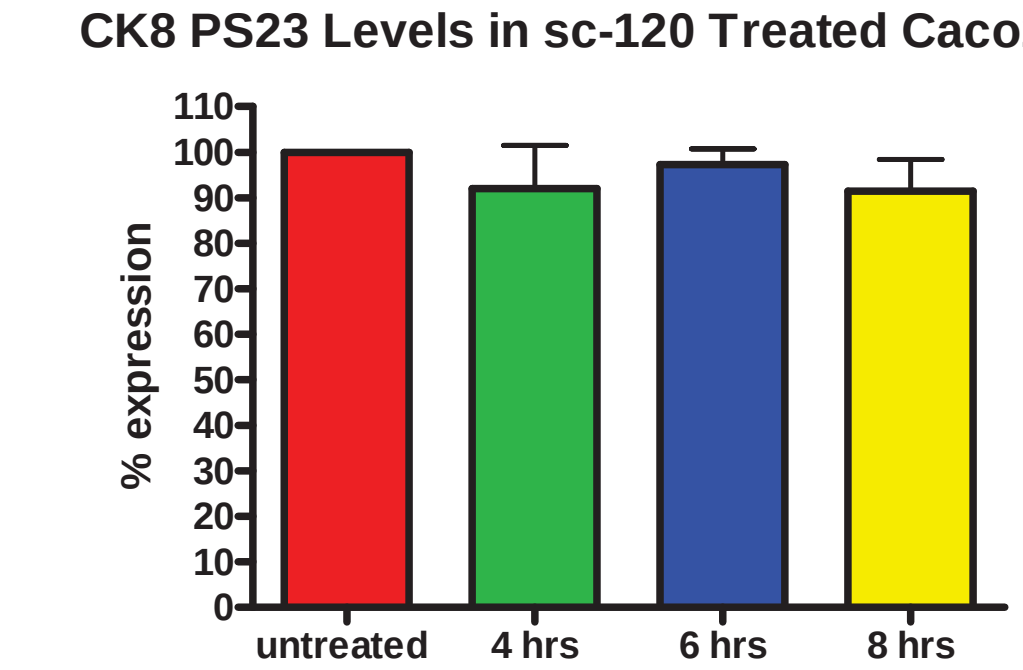

C)

D) **PS431** **PS73** **PS23**

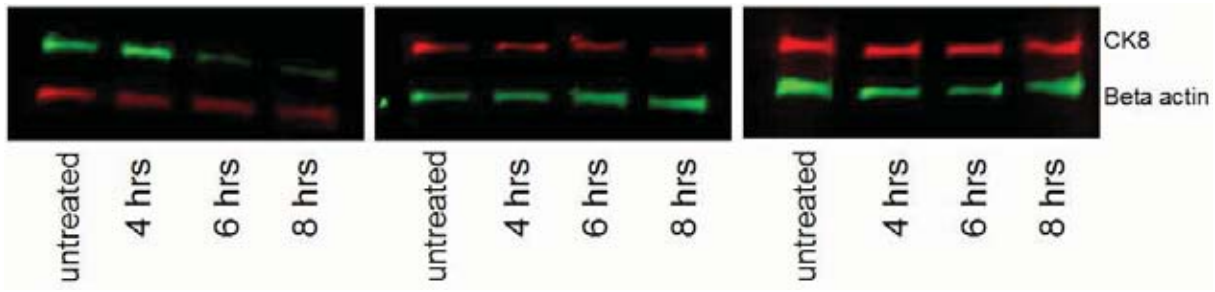

Fig 9. Blocking and inhibition of EGFR signalling in Caco2 cells leads to decreased PS73 and PS431 levels. Caco2 cells were treated with the EGFR ligand-binding blocking antibody sc-120 for four hours, six hours, and eight hours (n=6 per treatment group). Western blotting was performed on the cell lysates with antibodies against CK8 PS23, PS73 and PS431. Levels of A) PS73 and B) PS431 were significantly reduced six hours and eight hours post sc-120 treatment, *P*<0.0001 (ANOVA). C) Levels of PS23 remained unchanged by treatment with sc-120, P=0.73 (ANOVA). D) Representative western blot of Caco2 cells untreated and treated with the sc-120 antibody.

5.4 Discussion

Cytokeratins 8, 18 and 19 were found to be significantly upregulated in laser microdissected tissue from eight stage II tumour samples compared to matched normal by 2D DIGE. CK8 was chosen for further investigation as three isoforms of the protein were found to be significantly upregulated across the eight tumour samples ≥4 fold. It was hypothesised that the increase in abundance of the three CK8 isoforms in the tumour samples compared to matched normal was a result of increased phosphorylation. The level of CK8 expression in matched paired tumour-normal tissues was analysed at the mRNA level by relative real-time RT-PCR, and at the protein level by western blotting.

5.4.1 CK8 as a panel marker in the immunobead RT-PCR technique

Real-time RT-PCR for CK8 was performed on RNA extracted from ten stage I, sixteen stage II, and six stage III CRC tumour-normal matched paired tissues to determine if CK8 was upregulated in tumour samples at the RNA level. The tumour-normal expression ratios of CK8 were calculated using the $2^{-\Delta C(t)}$ method of relative quantification to the same amount of total starting RNA, and again after normalisation to the housekeeping genes PMM1 and PSMB6 using the $2^{-\Delta\Delta C(t)}$ method (Fig. 2). Calculating the tumour-normal abundance ratios using the $2^{-\Delta C(t)}$ or $2^{-\Delta\Delta C(t)}$ methods did not show significantly different results, $P=0.052$ (repeated measures ANOVA). When averaging the relative abundance ratios for each patient obtained from the different methods, 43% of patients had a tumour to normal CK8 expression ratio of >2 fold. There was no significant difference in the ratio of CK8 expression between stage I, II and III samples. The disparity in results generated by calculating the tumour-normal abundance ratios to the same amount of total starting RNA or to the different housekeeping genes could have been caused by difference in reverse transcription efficiencies between samples, or by expression levels of the housekeeping genes not being equal in matched tumour-normal tissue pairs.

CK8 may have potential use as a marker in the immunobead RT-PCR panel used to detect tumour cells extracted from patient's lavage and blood samples following surgery. The expression of CK8 at the mRNA level is relatively high, hence transcript from a single epithelial cell is likely to be detectable by real-time RT-PCR. CK8 expression is also specific to epithelial cells, and hence would not be expressed by any contaminating cell that may be unintentionally extracted by the immunobeads. If the differential expression of CK8 between normal and cancerous epithelial cells is not large enough to determine their disease state, CK8 could be used as a control marker to ensure cells extracted by the immunobeads were epithelial and not contaminating leucocytes.

5.4.2 The phosphorylation of CK8 is significantly increased in tumour tissue compared to matched normal mucosa

The phosphorylation of CK8 serine residues 23 and 431 were chosen for analysis in CRC patient tissues given their identification by MALDI-TOF/TOF MS. The phosphorylation of CK8 at serine 73 was also chosen for analysis as the residue is phosphorylated by the kinase p42/ERK1 , activated by EGFR signalling. The phosphorylation of these residues in the three CK8 isoforms detected as being increased in tumours by the DIGE study was confirmed by 2D western blotting (Fig. 5). The levels of PS23, PS431 and PS73 were analysed in a cohort of 30 matched paired tumour-normal samples. Phosphorylation levels of all residues were found to be significantly increased in tumour compared to matched normal tissues (PS23 P=0.004, PS431 P=0.03, and PS73 P=0.001). Multiple bands for CK8 were detected in some patient samples by western blotting within the molecular weight range of ~ 40 to 55 kDa (Fig. 8), indicating proteolytic cleaved forms of CK8.

5.4.3 CK8 phosphorylation results discussion

All 3 CK8 phospho-antibodies (PS23, PS431, PS73) detected the 3 CK8 isoforms of interest identified in the 2D DIGE study. It was predicted that a portion of the CK8 in each isofom had a level of serine 23 and 431 phosphorylation given epithelial cells have basal PS23 and PS431 levels. This is not the case for PS73 which is either 'on' or 'off', but is known to be 'on' during cell replication, so could be expected to be commonly seen in CK8 isoforms in tumour tissue. The 2D western blots aiming to detect the presence or absence of PS23, PS431 and PS73 in the 3 isoforms of CK8 were carried out using the colon cancer cell line SW480. As SW480 cells are epithelial, significant levels of PS23 and PS431 were expected, and as the cell line proliferates quickly, significant levels of PS73 were expected. Given phosphorylation of these residues is common, it was not unexpected to see an amount of PS23, PS431 and PS73 in each CK8 isoform. It was not expected that these phospho-residues were generating the individual isoforms (ie were present in the more acidic isoforms and not the basic), but that there was a differential level of PS23, PS431 and PS73 between the tumour-normal tissues for each individual CK8 isoform. Hence the main aim of this section was to determine if there were differential levels of CK8 serine 23, 431 and 73 phosphorylation between the tumour and normal samples overall. Amino acid modifications such as the phosphorylation of other CK8 residues, acetylation or glycosylation may be the cause of the individual CK8 isoforms seen on the 2D gels and western blots. CK8 has 36 confirmed amino acid modifications, 23 of which are phosphorylated serine residues excluding 23, 431 and 73. Differential phosphorylation of residues such as these in different populations of CK8 may result in the multiple isoforms detected by 2DE.

Interestingly, whilst all normal tissues showed detectible levels of CK8 phosphorylation on residues 23 and 431, 10 normal tissues out of the 30 tumour- normal pairs tested showed no detectable level of PS73 phosphorylation (the beta actin control levels in these samples appeared normal) (results displayed in the bar graph in Fig. 7D). For the individual tissue samples levels of CK8 PS23, PS431 and PS73 differed from the overall level of CK8 (and often to the level of the other PS residues studied) when normalised to the beta actin control. This shows that the antibodies did have a level of specificity. However, if the beta actin control had not been present for each sample on each blot, this conclusion could not have been made.

5.4.3.1 PS23

Serine 23 phosphorylation occurs in the head domain of CK8 and is highly conserved. The conserved motif SRSX (underlined serine is phosphorylated, X represents an aliphatic/aromatic residue) is found in all type II keratins, and is conserved across species except for Xenopus.[157] CK8 has a basal level of serine 23 phosphorylation, and the domain containing the site has been implicated in desmoplakin binding[268], which is involved in cell adhesion.

5.4.3.2 PS73

The phosphorylation of CK8 at serine 73 is modulated in an on/off manner.[269] Serine 73 is phosphorylated by the MAPK family kinases p38, p42/ERK1, and JNK, and by a PKCε-related kinase[155,156,158], causing increased solubility.[154,260,269] CK8 is phosphorylated at serine 73 during mitosis[155 260], causing intracellular redistribution.[154,260,270] A small portion of CK8 is hyperphosphorylated during mitosis, with large amounts of CK8 hyperphosphorylation occurring during mitotic arrest, in times of stress and during apoptosis.[155] During cellular stress, CK8 becomes hyperphosphorylated, acting as a phosphate 'sink' for stress-activated protein kinases and thereby inhibiting pro-apoptotic molecules and protecting the cell from apoptosis.[265]

Out of the MAP kinases p38, p42 and JNK, Ku *et al*. (2002)[156] found p38 phosphorylated serine 73 exclusively, generating hyperphosphorylated CK8, whereas p42/ERK1 and JNK phosphorylated both serine 431 and 73, generating normal and hyperphosphorylated CK8 forms. The formation of Mallory bodies in liver epithelial cells has been shown to be a result of CK8 hyperphosphorylation at serine 73 and 431 by p38.[271] The hyperphosphorylation increased the solubility of CK8, inhibiting degradation of the protein. Ridge *et al*. (2005)[272] showed shear stress, occurring in fluid-filled and collapsed lungs, activates protein kinase C (PKC) δ in alveolar epithelial cells. PKC δ then phosphorylates CK8 serine 73, modulating keratin IF disassembly and reorganisation.

CK8 phosphorylation has shown to be mediated by the stress-activated kinase JNK in response to Fas receptor activation. JNK is known to be involved in cellular responses to physical stresses, inflammatory cytokines and apoptosis, and is activated by the death receptors Fas receptor and tumour necrosis factor receptor. Fas receptor stimulation in HT-29 cells leads to CK8 serine 73 hyperphosphorylation, likely by JNK.[158] Hyperphosphorylated CK8 then disassembles from intermediate filaments, solubilises, and is not degraded, despite caspase activation, unlike CK18 and other caspase targeted proteins. CK8 hyperphosphorylation and JNK activation caused by Fas receptor stimulation appear to be apoptosis and caspase independent, hence hyperphosphorylated CK8 serine 73 may help protect the IF network from caspase degradation in the Fas receptor resistant cell line HT-29.[158] Ku and Omary (2006)[265] found the human disease associated CK8 mutation of Glycine 61 to cystine inhibits the phosphorylation of serine 73 by stress-activated MAP kinases. This leads to the targeting of CK8 for caspase degradation, and cells with the mutation are predisposed to apoptosis.

5.4.3.3 PS431

MAP kinases p42/ERK1 and JNK, plus cdc2 kinases, have been shown to phosphorylate CK8 at serine 431.[156,157] Serine 431 has basal low levels of phosphorylation on CK8, which is increased upon EGF stimulation and mitotic arrest.[157] Along with phosphorylation of serine 73, phosphorylation of serine 431 has been associated with intermediate filament reorganisation.[157] As discussed, Mallory body formation in the liver has been attributed to the hyperphosphorylation of CK8 at serine 73 and 431.[271]

5.4.4 CK8 phosphosphorylation and the EGFR/Ras/Raf/ERK pathway

It has been shown that the residues 431 and 73 are phosphorylated by the MAP kinase p42/ERK1, which is activated in response to EGFR signalling. It was hypothesised that increased levels of PS431 and PS73 in the tumour tissues was in part due to increased p42/ERK1 activation as a result of increased EGFR signalling. Blocking of EGFR in Caco2 cells showed a significant decrease (P<0.0001) in PS73 and PS431 levels by 59% and 66% respectively, indicating EGFR/Ras/Raf/ERK signalling may play a significant role in the increased PS73 and PS431 levels in CRC.

5.4.4.1 EGFR signalling and ERK activation

EGFR is activated by the extracellular ligand-binding of certain growth factors such as epidermal growth factor (EGF) and transforming growth factor α (TGF α), which selectively bind EGFR. Upon ligand-binding, EGFR dimerises and receptor tryrosine kinase activity of the cytoplasmic domain is activated, resulting in auto tyrosine phosphorylation of the intracellular portion of EGFR. Docking proteins that

contain SH2 domains such as GRB2 then bind to the phosphorylated tyrosine residues of the activated receptor. The SH3 domain of GRB2 binds to the nucleotide exchange factor SOS. Docking of the GRB2-SOS complex to phosphorylated EGFR activates SOS, which promotes the removal of GDP from Ras, allowing Ras to bind GTP and become active. There are three p21Ras small GTPases; H-Ras, N-Ras and K-Ras. Once active, Ras phosphorylates and activates Raf1 (reviewed in [273]). Raf1 phosphorylates MEK1 and MEK2 (known as ERK kinases) on serine residues 217 and 221, phosphorylate and activate p42/ERK1 and p44/ERK2. Active p42/ERK1 and p44/ERK2 can phosphorylate a number of cytoplasmic proteins or translocate to the nucleus and activate several transcription factors and genes to promote cell proliferation and protection from apoptosis.[273,274]

The upregulation or mutation of proteins in the EGFR signalling pathway has been found to be advantageous to CRC growth and survival. Hyper-proliferative aberrant crypt foci have been shown to have significantly increased transcript levels of EGFR, and significantly increased protein levels of the EGFR signalling components phosphoactive ErbB2, phosphoactive extracellular signal regulated kinase, cyclin D1, phosphoactive Ras and EGFR.[275] KRAS mutations are detected in approximately 36% of CRC.[159] Wild-type Ras normally becomes inactive shortly after activation, but mutant Ras remains constitutively active. KRAS mutations are known to be an early event in CRC[276], and are commonly present in aberrant crypt foci which are thought to be early precursors of CRC (reviewed in [277]). Mutations in BRAF, a serine/threonine kinase of the Raf family, are present in 9%–12% of CRC[160,161], and are present in a high proportion of sporadic CRC with microsatellite instability.[278] Mutations in KRAS and BRAF appear to be mutually exclusive[161], hence up to 50% of colorectal tumours contain EGFR pathway mutations. Mutations in Ras and Raf proteins result in constitutive activation and MAPK signalling.[279]

5.4.4.2 Phosphorylation of CK8 by the other MAP kinase; JNK and p38

JNK and p38, which have also been shown to phosphorylate CK8 residues 431 and 73, are activated in response to stress and a number of cytokines. Activation of these MAP kinases occurs through a protein kinase G/MEKK1/SEK1 signalling cascade. JNK activation results in the activation of the transcription factor c-Jun and the synthesis of activating protein 1 (AP1), known to be involved in cell proliferation and apoptosis.[280] Activation of p38 is known to be involved in the regulation of cell proliferation and differentiation, and it has been suggested that p38 plays a significant role in the protection of cells from apoptosis.[281]

5.5 Conclusion

The levels of PS23, PS431 and PS73 were all found to be significantly increased in colorectal tumours compared to matched normal mucosa (Fig. 8). The kinase p42/ERK has been shown to phosphorylate serine residues 431 and 73[156,157], and is known to be constitutively activated in up to 50% of CRC due to mutations in the EGFR/Ras/Raf/ERK signalling pathway. Blocking of EGFR with the ligand-binding site antibody sc-120 in Caco2 cells resulted in a significant decrease (P<0.0001) by 59% and 65% in PS73 and PS431 levels respectively (Fig. 9).

The MAP kinase p38 and JNK are also known to phosphorylate serines 431 and 73[155-158], and blocking of EGFR would have had no direct effect on the activity of these kinases. Currently the kinase or kinases that phosphorylate CK8 serine 23 are unknown. Treatment of Caco2 cells with the sc-120 antibody did not significantly affect PS23 levels, indicating kinases involved in the EGFR signalling pathway are not involved in the phosphorylation of this residue. This supports previously published work.[157]

Phosphorylation is essential for the correct function of cytokeratins, regulating cell junctions and the organisation of intermediate filament and microfilament assembly. Increased phosphorylation of CK8 as a result of increased Ras/Raf/ERK signalling would lead to increased disassembly and solubilisation (Fig. 12). This would be advantageous in cancer as it acts as a protective mechanism from degradation by increasing intermediate filament solubility and disassembly, protecting the cells from apoptosis[265 271 158] by acting as a phosphate 'sink', inhibiting phospho-activation of pro-apoptotic substrates by stress activated protein kinases.[265]

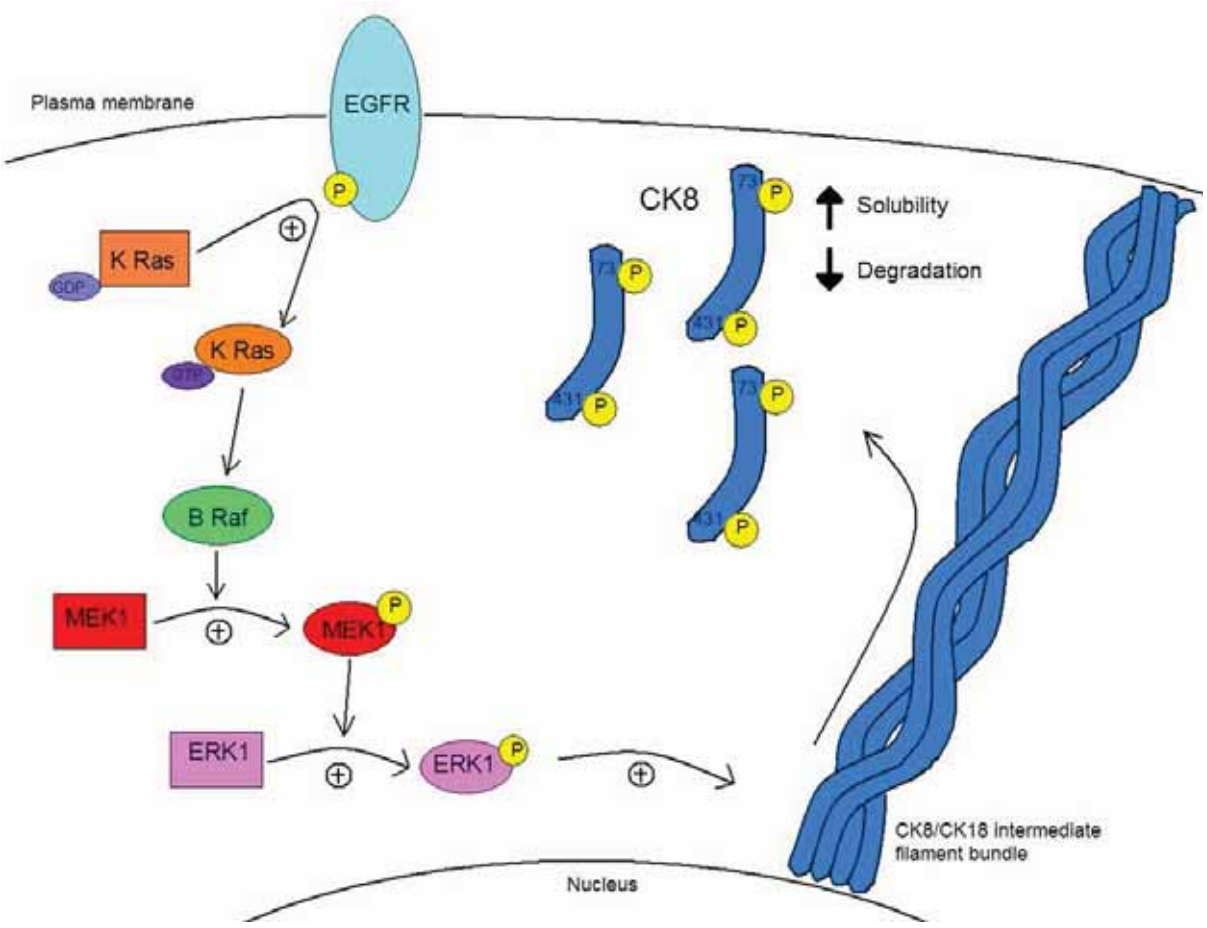

Fig 12. Phosphoserine levels of CK8 residues 23, 73 and 431 were found to be significantly increased in human colorectal cancer. Inhibition of EGFR activation and Ras/Raf/MEK/ERK signalling decreased CK8, PS73 and PS431 levels in Caco2 cells, likely due to decreased ERK1 activation, a known kinase of PS73 and PS431. Constitutive activation of Ras/Raf/MEK/ERK is common in CRC due to mutations in KRAS or BRAF, which would result in increased PS73 and PS431 levels, which may help inhibit CK8 degradation and cancer cell apoptosis.

6 The Protein SET

6.1 Introduction

6.1.1 The Protein SET

In the 2D DIGE study, the protein SET (named after Suvar3–9 Enhancer of zeste Trithorax) was found to have an average increase in tumour to normal abundance of 2.32 fold, P=0.021. Of the eight samples analysed in the DIGE study, four showed a matched paired tumour to normal expression ratio of around 1 (1.18, 1.1, 0.9 and 1.25) indicating a normal distribution. However, the remaining four samples showed significantly higher expression ratios of 2.7, 3.3, 3.73 and 4.55. Despite the fact that only 50% of the patients in the DIGE study showed a tumour-normal increase of >2 fold, SET was chosen for further analysis given the magnitude of the fold change in the patients who had increased tumour expression and given there was no published literature on the role of SET in CRC at the commencement of this work. Importantly SET was also chosen for further analysis as the protein was hypothesised to play a role in the regulation of Wnt signalling, an important pathway involved in the adenoma-carcinoma sequence of tumourigenesis.[30]

The protein SET is a multifunctional protein, conserved between species[282], with increased expression levels during development[283], wide tissue distribution with nuclear and cytoplasmic localisation and endoplasmic reticulum association. SET has a calculated isoelectric point of 4.07 with a molecular weight of approximately 34 kDa. Other names for SET include phosphatase 2A inhibitor (I2PP2A), template-activating factor I (TAF-I), HLA-DR-associated protein II (PHAPII) and inhibitor of granzyme A-activated DNase (IGAAD). SET has been shown to be involved in wide range of pathways and cellular processes as discussed below.

SET was first identified as a potential CAN fusion protein in an acute undifferentiated leukaemia patient using genomic and cDNA cloning experiments.[162] von Lindern *et al*. (1992)[162] found the SET-CAN fusion gene to encode a 5 kb transcript, with a sequence predicting a 155 kDa SET-CAN fusion protein. SET was identified as having a highly acidic C-terminal amino acid sequence that shared a high level of homology to the NAP1 C-terminal sequence. Overall NAP1 and SET share 25% homology[162] and both belong to the nucleosome assembly protein family. A later study found SET to be predominantly localised in the nucleus[284] and hypothesised that SET may induce the nuclear translocation of the SET-CAN fusion protein in acute undifferentiated leukaemia, as CAN is present normally in the cytoplasm. Adachi *et al*. (1994)[284] also found SET to have wide distribution in various human cell lines and as being phosphorylated in vivo, predominantly on phosphoserine residues.

SET and NAP1 have both been shown to interact directly with B-type cyclins using affinity chromatography.[282] NAP1 is phosphorylated by cyclin/p34^{cdc2} kinase complexes in vitro[282], a process that may help induce mitosis. Due to NAP1 and SET homology, it was suggested that fusion of SET to the CAN protein in leukaemia may inappropriately target CAN for phosphorylation by cyclin B/p34^{cdc2} kinase complexes. SET was also found to bind to the cyclin-dependent kinase (CDK) inhibitor p21^{Cip1} using affinity chromatography, and was able to reverse the inhibition of cyclin E-CDK2 induced by p21^{Cip1}, suggesting SET may play a role in G1/S transition via the regulation of cyclin E-CDK2 activity.[163] Canela *et al.* (2003)[164] found the overexpression of SET in COS and HCT116 cells blocks cell cycle progression at G2/M transition and inhibits cyclin B-CDK1 activity, suggesting SET may also play a role in G2/M transition via the regulation of cyclin B-CDK1 activity.

Li *et al*. (1995, 1996)[167,168] identified SET as an inhibitor of the tumour suppressor serine/threonine protein phosphatase 2A (PP2A) from purified extracts of bovine kidney. SET has been shown to inhibit PP2A by inducing phosphorylation of PP2Ac on tyrosine 307, inactivating the catalytic activity of PP2A.[285] Neviani *et al*. (2005)[285] correlated an inactivation of PP2A in BRC/ABL chronic myelogenous leukaemia blast crisis (CML-BC^{CD34+}) cells with increased expression levels of SET, and showed SET expression is induced in a BRC/ABL dose and kinase-dependent manner. They also showed that knocking down SET expression restored PP2A activity, which induced apoptosis, decreased proliferation, impaired colony formation, inhibited tumourigenesis and restored differentiation in BCR/ABL transformed cells. Knocking down S*Et al*lowed PP2A to induce the dephosphorylation and proteosome degradation of the BCR/ABL protein mediated by SHP-1. PP2A also has tumour suppressor activity via its ability to dephosphorylate and deactivate other factors involved in cell cycle progression, proliferation, survival and differentiation[286], such as Myc, STAT5, MAPK, Akt, BAD and Rb.[287-292]

Al-Murrani *et al*. (1999)[165] showed levels of the proto-oncogene c-Jun and its DNA binding increased in HEK 293 cells transfected with SET. Conversely, when SET expression was knocked down or expression of the catalytic subunit of PP2A (PP2Ac) was driven by transfection, levels of c-Jun and the binding of its DNA, decreased in the cells. Similarly phosphorylation of c-Jun at serine 63 increased in the cells expressing SET and decreased in those expressing PP2Ac. The transcriptional activity of activator protein-1 (AP-1) was also increased with SET and decreased with PP2Ac expression. c-Jun forms part of the AP-1 transcription factor complex, enhancing the DNA binding activity of c-Jun.[293]

Seo *et al*. (2001)[294] identified SET as part of a histone acetylation inhibitor complex. It is known that histone acetylation alters gene expression and that P300/CPB and PCAF are transcriptional co-activators with acetyltransferase activity. SET was found to be part of a complex with pp32 that inhibits

the histone acetyltransferase activity of P300/CPB and PCAF by binding to their substrate histones, occluding them and creating 'histone masking'.

6.1.2 SET, PP2A and Wnt signalling

Of particular interest was the potential role of SET in the Wnt signalling pathway via the inhibition of PP2A. It is known that 90%[295] of all patients with CRC acquire Wnt signalling pathway mutations, an early event and an initiating factor of the adenoma-carcinoma sequence.[296] PP2A is a component of the GSK3 β complex that tags β catenin for ubiquitin proteasome degradation. Wnt signalling mutations in APC or β catenin proteins result in the inability of the GSK3 β complex to successfully target β catenin for destruction. This leads to constitutive activation of β catenin, a transcriptional co-activator of the TCF/LEF transcription factors.

6.1.3 The PP2A holoenzyme

PP2A is a holoenzyme complex that is normally comprised of three functional components; a catalytic subunit, a scaffolding/structural subunit, and a regulatory subunit, depicted in Fig. 1. Different combinations of subunits give PP2A a diverse range of activities and substrate specificities.[297] The catalytic subunit (PP2Ac) interacts with a scaffolding subunit (PR65) to form the core of the enzyme. The core enzyme then has the potential to associate with a variety of B regulatory subunits, which give the holoenzyme functional specificity. The B subunit is made up of four families—B, B', B'' and B'''—each with multiple isoforms.[298]

6.1.3.1 PP2Ac/C

The catalytic subunit has a large conserved domain that forms a bimetallic active site for phospho-ester hydrolysis. PP2Ac targets phosphate groups on serine and threonine residues and under some conditions, can also target phosphorylated tyrosine residues.[299] The catalytic subunit is encoded by two different genes, C α and C β. C α expression levels are around 10 fold that of C β, and loss of C α in mice and yeast is fatal.[300]

6.1.3.2 PR65/A

There are two forms of the scaffolding protein encoded by two different genes. The PR65 α subunit is dominant, being present in 90% of holoenzymes, with only 10% of holoenzymes containing PR65 αβ [301] due to the low level of PR65 αβ expression in adult tissues. However, in oocyte and early vertebrate development, PR65 mRNA expression is dominant over PR65 α.[302] [303] The PR65 subunits interact with

a catalytic subunit via four C-terminal Huntington/elongation/A-subunit/TOR (HEAT) repeats.[301] Upon formation of the core PP2A enzyme, PR65 folds in on itself[304 305], giving PP2Ac access to any substrate that has been recruited by a B regulatory subunit.

6.1.3.3 Regulatory B subunits

To date, fifteen different genes have been identified that encode at least 26 different alternative transcripts and splice forms of the B subunits. The B subunits are divided into five families that only share sequence similarity in a small number of amino acids that allow interaction with the N-terminal HEAT domains of the PR65 scaffold subunit.[306] It is the B subunits that are thought to mediate substrate specificity of the holoenzyme complex[297 307 308], and can be expressed in a tissue specific manner. It is predicted around 30 PP2A holoenzyme combinations are likely to exist.[298] Below is a table detailing the identified B isoforms and the families to which they belong (Table 1).

Table 1. The B regulatory subunit family members

Regulatory B subunits	Family members
B/PR55	α, β, γ, δ. Transcribed from four different genes.[309]
B'/PR61	α, β, γ, δ, ε. Transcribed by five different genes.[310]
B''/PR72	PR72, PR130, PR59, PR70, G5PR. Transcribed by three different genes.[298]
B'''/PR53/PTPA	PR53, also known as PTPase activator (PTPA). Appears to act more like a chaperone effecting the activity of PP2Ac by transiently inducing phosphotyrosyl phosphatase (PTP) activity of PP2Ac/PR65 complexes.[311 312]

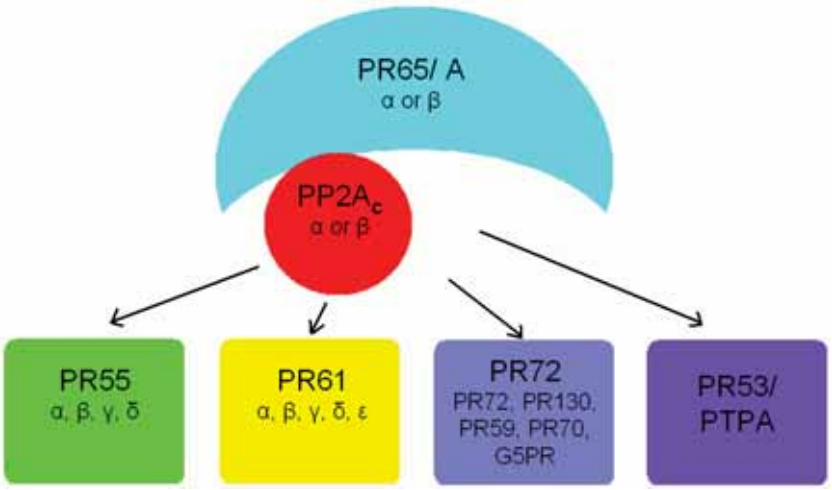

Fig 1. The PP2A holoenzyme. The complex is normally comprised of three functional components; a catalytic subunit 'C', a scaffolding/structural subunit 'A', and a regulatory subunit 'B'. The catalytic subunit (PP2Ac) interacts with a scaffolding subunit (PR65) to form the core of the enzyme that has the potential to associate with a variety of B regulatory subunits, which give the holoenzyme functional specificity. The B subunit is made up of four families—PR55/B, PR61/B', PR72/B'' and PR53/B'''—each with multiple isoforms.

6.1.4 PP2A in Wnt signalling at the plasma membrane

PP2A is involved in the Wnt signalling pathway via two mechanisms, one at the plasma membrane and the other within the GSK3 β complex. PP2Ac α is found mainly at the plasma membrane of a cell in the absence of Wnt signalling. Here it forms a complex with E cadherin and β catenin that mediates interactions with the actin cytoskeleton. This complex is stabilised by PP2Ac α. In PP2Ac $\alpha^{-/-}$ knockout mice embryos, β catenin is redistributed to the cytoplasm and is degraded, regardless of whether Wnt signalling is present or not.[313]

6.1.5 PP2A in Wnt signalling in the GSK3 β complex

PP2Ac β localises mainly to the cytoplasm and nucleus. In the cytoplasm, the PP2A holoenzyme is comprised of an A subunit, a β C subunit and a B'/PR61 family subunit which associates with axin in the GSK3 β complex. The GSK3 β complex itself is comprised of axin, APC, PP2A and GSK3 β. In the absence of Wnt signal, GSK3 β is constitutively active, phosphorylating and activating APC and axin and also phosphorylating β catenin, targeting it for degradation. GSK3 β activity is regulated by Dsh and in the presence of Wnt signal, Dsh is recruited to the plasma membrane, is phosphorylated and activated, resulting in the dissociation of GSK3 β complex and the accumulation of β catenin. PP2A plays an important role in the GSK3 β complex; when PP2A is associated with the complex, β catenin degradation is enhanced, when PP2A is dissociated from the complex β catenin accumulation occurs.[314]

In normal cells, PP2A may also be able to inhibit Wnt pathway activity upstream of the GSK3 β complex via Dsh. Activation of Wnt signalling results in the hyperphosphorylation of Dsh and the inhibition of the GSK3 β complex. Once Wnt stimulation stops, it is thought PP2A may dephosphorylate Dsh, causing inactivation, allowing for the resumption of GSK3 β complex activity[314] and subsequent β catenin degradation. Interestingly, it has also been suggested that PP2Ac may be able to directly dephosphorylate β catenin, salvaging it from degradation.[297] Of particular interest to this work was the interaction of SET with PP2A in Wnt signalling. Given that SET is known to inhibit the activity of PP2Ac, one aim was to analyse the effect of knocking down SET on β catenin levels in epithelial cells with normal Wnt signalling, and in epithelial cells with constitutively activated Wnt signalling.

6.1.6 PP2A is a negative regulator of Wnt signalling during embryogenesis

In Xenopus embryos, PP2A has been shown to enhance β catenin degradation and inhibit Wnt signalling[315 46], while CK1 (as discussed in Chapter 1) has been shown to act as a positive regulator, inducing secondary axis formation via activation of the Wnt pathway.[316 317] Gao[314] suggests CK1 may activate the Wnt pathway by phosphorylating members of the GSK3 β complex, causing the dissociation of PP2A. CK1 is known to phosphorylate Dsh, APC, axin and β catenin in vitro, with inhibition of CK1 in vitro or in vivo, resulting in increased association of PP2A, GSK3 β and β catenin within the GSK3 β complex. This is thought to result in increased targeting of β catenin for degradation and reduced Wnt signalling. Gao[314] observed CK1 decreases the interaction of PP2Ac and the scaffolding subunit PR65 with the GSK3 β complex by phosphorylating members of the GSK3 β complex, causing the complex to dissociate. Because of this interaction, the presence of both CK1 and PP2A within the same complex is likely to be transient. Gao[314] suggests that in the presence of active CK1, β catenin levels are increased due to the de-stabilisation of the GSK3 β complex and Wnt signalling is able to propagate. In the absence of CK1, PP2A is present in the GSK3 β complex, resulting in decreased β catenin levels due to inhibited Wnt signalling (Fig. 2). As SET was found to be significantly increased in CRC, and given PP2A appears to be a negative regulator of the Wnt pathway, it can be hypothesised that knocking down SET would lead to increased PP2A activity and decreased Wnt signalling.

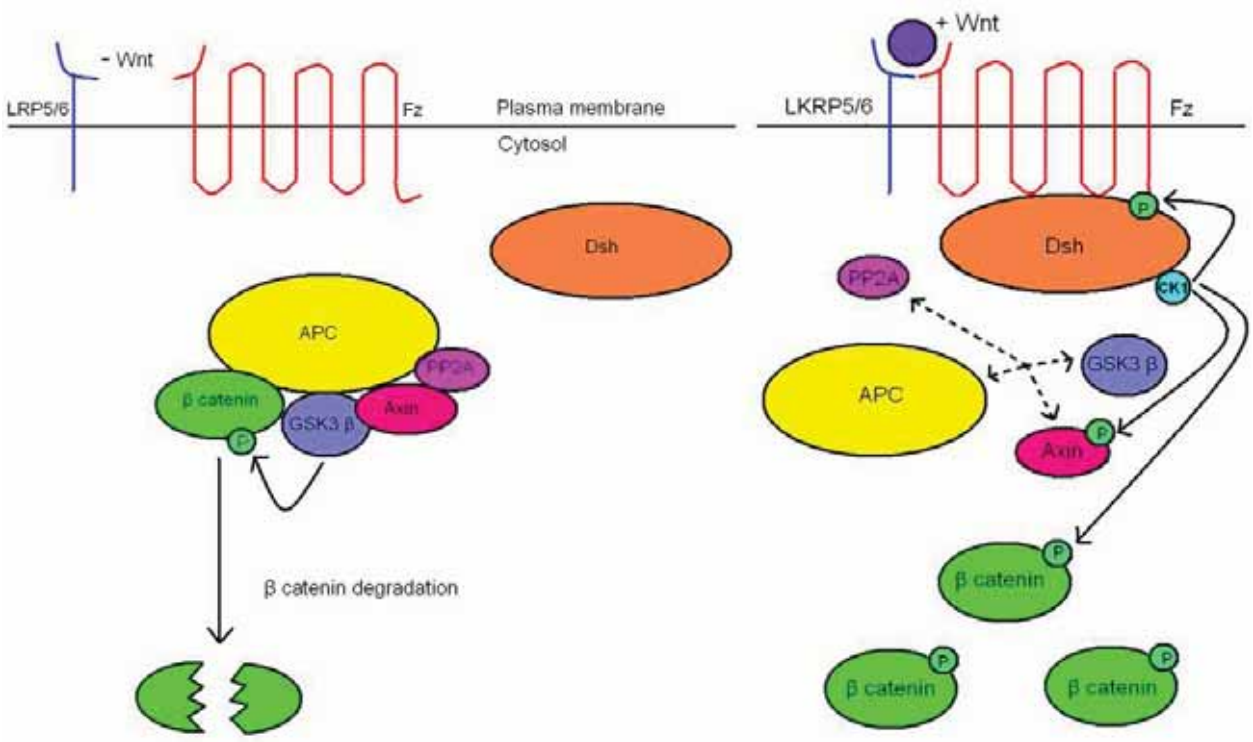

Fig 2. The negative and positive regulation of Wnt signalling by PP2A and CK1 respectively. In the absence of Wnt signal (LHS), PP2A acts as a counter regulatory phosphatase to CK1, keeping the GSK3 β complex intact. In the presence of Wnt signal (RHS), CK1 phosphorylates APC, axin and β catenin, reducing their affinity for other members of the GSK3 β complex such as PP2A, GSK3 β and β catenin, causing the complex to dissociate allowing β catenin to accumulate.

6.1.7 The effect of knocking down SET on PP2A and Wnt signalling

As SET is an inhibitor of the catalytic subunit of PP2A, it was of interest to assess the effect of knocking down SET on β catenin expression levels in the SW480 and HEK293 cell lines. SW480 cells are a colon cancer cell line with a known mutation in the APC protein leading to constitutive Wnt pathway activation and β catenin expression. HEK293 cells are epithelial cell lines that do not have any known mutations in the Wnt signalling pathway (http://www.atcc.org/, product number CRL-1573). These cell lines were chosen for analysis as they are both epithelial, with one line, SW480, being active for Wnt signalling and representative of the majority of CRC, and the other line, HEK293, having low to no active Wnt signalling. In the SW480 cells, if SET acts only on PP2A as part of the GSK3 β complex, then no change in β catenin levels may be observed due to constitutive pathway activation. If there is a low level of Wnt signalling in the HEK293 cells, then reducing SET levels would likely enhance PP2A tumour suppressive activity, causing inhibition of Wnt signalling and reduced β catenin levels.

6.1.8 The role of SET in other cancer signalling pathways

Up to 90%[295] of CRC patients have mutations in either APC or β catenin that result in constitutive Wnt signalling similar to the truncating APC mutation in the SW480 cells. One aim of this work was to determine if SET inhibited PP2A as part of the GSK3 β complex. If SET were to inhibit PP2A as part of the GSK3 β complex, then no change in β catenin levels would be seen by knocking down SET using siRNA in the SW480 cells, as Wnt signalling in these cells is already constitutively active. This result could then be applied to the 90% of CRC patients who have APC or β catenin mutations, meaning the upregulation of SET in CRC is not relevant to Wnt signalling. Because of this potential outcome, preliminary data on the role of SET in other CRC signalling pathways was collected by analysing cell lysates from SW480 SET siRNA knocked down cells with RT^2 Profiler PCR Array 'Human Cancer Pathway Finder' plates (SA Biosciences, PAHS-033). The RT^2 Profiler PCR Arrays are 96 well plates designed to allow the expression analysis of multiple genes for a single sample simultaneously by real-time RT-PCR. The Human Cancer Pathway Finder array contains primer sets against 80 genes representative of the six biological processes involved in transformation and tumourigenesis; 1) cell cycle control and DNA damage repair, 2) apoptosis and cell senescence, 3) signal transduction molecules and transcription factors, 4) adhesion, 5) angiogenesis and 5) invasion and metastasis. Each plate also contains five reference genes, genomic DNA controls, RT controls and PCR controls. SW480 cell lysates form SET siRNA treated and negative siRNA treated control cells were analysed using the RT^2 Profiler PCR Array plates, giving a number of genes that may be directly or indirectly regulated by SET.

6.1.9 The study design

The expression of SET in 32 tumour-normal tissue pairs at the RNA level was analysed by real-time RT-PCR. This was done in order to assess the percentage of patients with increased tumour expression at the RNA level, to determine if SET is increased in early stage patients, and to assess the possible use of SET expression as a biomarker in the immunobead RT-PCR marker panel. The role of SET in the Wnt signalling pathway was chosen for further investigation as SET inhibits PP2A, a known tumour suppressor and part of the complex that targets β catenin for degradation. The regulation of β catenin is of great importance in CRC, and mutations in β catenin or APC are known to be an early initiating event of the adenoma-carcinoma sequence. SET is known to inhibit PP2Ac by inducing phosphorylation of tyrosine residue 307, inactivating the catalytic activity of PP2A.[285] Given that 90%[295] of CRC patients have Wnt signalling pathway mutations in APC or β catenin, it is also important to know if SET is interacting with a PP2A holoenzyme upstream of the GSK3 β complex (i.e. inhibiting the interaction between PP2A and Dsh), downstream (i.e. inhibiting the dephosphorylation of β catenin by PP2A), or as part of the GSK3 β complex. If PP2A is playing a regulatory role in Wnt signalling downstream of the GSK3 β complex, via the dephosphorylation of β catenin and SET acts to inhibit PP2A, then SET may have potential as a therapeutic target for CRC, as this treatment would aid patients with mutations in β catenin or APC.

Small interfering RNA (siRNA) was used to knock down the expression of the SET gene in SW480 and HEK cell line cells, and subsequent β catenin levels were measured by western blot. SW480 cells are a primary colon cancer cell line with a truncating mutation in APC. Due to this mutation, the GSK3 βcomplex is unable to successfully target β catenin for degradation, resulting in accumulation of β catenin and constitutive activation of Wnt signalling. Because of this, it was expected that there may be no change in β catenin expression levels in the SET siRNA treated SW480 cells. HEK 293 (human embryonal kidney) cells were also treated with SET siRNA, as they are a transformed normal cell line with no Wnt signalling pathway mutations. Initially this experiment had intended to be performed on cultured normal embryonic colon cells, but difficulties were encountered with culturing enough cells for treatment. Preliminary data was also collected on the other cancer pathways. SET may be involved in using siRNA treated SW480 cells and the RT^2 Profiler PCR Arrays (SA Biosciences).

6.1.10 Aims

To determine the percentage of patients with a SET tumour-normal expression ratio of ≥2 fold at the RNA level, to analyse the potential of SET as an immunobead RT-PCR panel marker and to determine the relative levels of SET expression among early stage compared to late stage patients.

To determine if SET knock down by transient RNA interference affects β catenin levels by inhibiting PP2A as part of the GSK3 β complex, downstream of the complex, or upstream of the complex when Wnt signalling is constitutively active in SW480 cells and when Wnt signalling is low in the HEK293 cells.

To determine the effect of knocking down SET levels in SW480 cells on other genes and pathways involved in CRC using siRNA interference and RT^2 Profiler PCR Arrays (SA Biosciences).

6.1.11 Hypotheses

- That SET is significantly increased in expression at the RNA level between matched paired tumour-normal tissues and will be useful as an immunobead RT-PCR panel marker to detect circulating tumour cells.
- In normal epithelial cells with low levels of Wnt signalling, PP2A has an overall negative effect on the Wnt pathway and β catenin activation. Hence, knocking down SET in HEK293 cells will result in a decrease in β catenin levels due to increased PP2A activity.
- In the SW480 cells, if PP2A acts to inhibit Wnt signalling as part of the GSK3 β complex, then knocking down SET will have no observable effect on β catenin accumulation as the GSK3 β complex is inactive in these cells due to an APC mutation.
- In the SW480 cells, if PP2A regulates Wnt signalling down-stream of the GSK3 β complex by dephosphorylating β catenin, knocking down SET levels will produce an observable change in β catenin accumulation.

6.2 Materials and methods

6.2.1 Real-time RT-PCR

To determine if SET was upregulated at the RNA level, relative real-time RT-PCR was performed on 32 CRC tumour-normal matched paired tissues. For RNA extraction, cryo-sections (30 μ) were pulverised in a mortar and pestle under liquid nitrogen. RNA was extracted using Tri Reagent (Sigma, St Louis, MO) (Ref Chapter 3). RNA integrity was checked by denaturing gel electrophoresis. Samples that did not show distinct 28S and 18S bands were excluded from further analysis. RNA was quantified at 260 nm using the NanoDrop ND-1000 Spectrophotometer (NanoDrop Technologies, Wilmington, DE). Total RNA (1 μg per sample) was reverse transcribed in a 20 μl reaction volume as detailed in Chapter 3.

Relative real-time RT-PCR for SET, and the reference genes phosphomannomutase I (PMM1) and proteasome subunit Y (PSMB6) was performed separately using the MJ Research DNA Engine Opticon 2 (Biorad, Hercules, CA). Two microlitres of the reverse transcription mix was used in each PCR in a final reaction volume of 20 μl as detailed in Chapter 3. PMM1 and PSMB6 had previously been reported as good reference genes for CRC.[266] SET primers were obtained from SA Biosciences (Frederick, MD, USA) and PMM1 and PSMB6 primers were obtained from GeneWorks (Thebarton, SA, Australia) (sequences in Chapter 3). The RT negative control consisted of RNA and master mix without reverse transcriptase, while the PCR negative (no target) control consisted of PCR master mix alone. All samples were amplified in triplicate and the mean C(t) value was obtained.

SET tumour to normal expression ratios were calculated using the $\Delta^{C(t)}$ method of relative quantification.[267] The $2^{-\Delta\Delta C(t)}$ method was then used to compare the expression of SET in the tumour samples compared to matched normal mucosa after normalisation to both PMM1 and PSMB6 separately (refer to chapter 3 for details). A Kruskal-Wallis test was performed on the tumour-normal fold change ratios obtained by each method. All statistics were performed using GraphPad Prism 4 software.

6.2.2 SET knock down using siRNA

SW480 and Hek 293 cells were cultured to approximately 50% confluence for siRNA treatment. The SET siRNA sequences (SET Validated Stealth RNAi, refer Chapter 2) were tested at concentrations of 25 μM, 50 μM, 75 μM and 100 μM. Treatment at 100 μM gave the largest knockdown determined by real-time RT-PCR. Cells were treated in 24 well plates, at 1 x 10^5 cells per well. In addition to cells treated with the SET siRNA, Cy3 labelled negative siRNA (Invitrogen) treated cells were used as a

positive transfection control, Stealth RNAi negative control duplexes (Stealth RNAi negative control LO GC) with a GC content similar to that of the SET siRNA duplexes were used as a negative control, and untreated cells were also used as negative controls. All treatment conditions were plated in quadruplicate. Twenty-four hours post-plating the Cy3 labelled transfection control cells were removed from the bottom of each well, washed thoroughly in PBS, and placed on glass slides. Transfection efficiency was calculated by counting the number of Cy3 fluorescing cells under a fluorescence microscope in comparison to the total number of cells viewed under white light. A minimum of 90% transfection efficiency had to be obtained. Seventy-two hours (day 3) post-plating, two wells from the SET siRNA treated, negative control siRNA, and untreated control wells were harvested for RNA. One hundred and twenty hours (day 5) after plating, the remaining duplicate wells were harvested for protein. This experiment was performed with SW480 and HEK cells and was repeated.

6.2.3 RNA isolation and real-time RT-PCR

RNA was isolated using the SV Total RNA Isolation System (Promega). Media was removed from treated, untreated and negative siRNA wells, and cells were washed three times with PBS. 175 μl of SV RNA lysis buffer was added to each well. RNA was purified using the spin column method as detailed in Chapter 3, and re-suspended in 100 μl of UPW. RNA was quantified at 260 nm using the NanoDrop ND-1000 Spectrophotometer (NanoDrop Technologies, Wilmington, DE). In order to assess SET knock down at the mRNA level 250 ng of total, RNA from each sample was reverse transcribed, and real-time RT-PCR was carried out using SET primers (SA Biosciences) and PMM1 primers as previously described. The $2^{-\Delta\Delta C(t)}$ method was used to compare the expression of SET in the siRNA treated and negative siRNA control samples compared to untreated control cells after normalisation to PMM1.

6.2.4 Protein extraction and western blotting

For protein extraction, 100 μl of sample buffer (2% SDS, 10% glycerol, 62.5 mM TrisHCl, 6 M urea, 1 x phosphatase inhibitors, 150 U Benzonase) was added to each of the appropriate wells. Protein was quantified using the EZQ assay (Invitrogen). DTT was added to each sample at 65 mM and incubated at room temperature for fifteen minutes. Twenty-five μg of each sample was loaded onto 4%–20% polyacrylamide mini gels and 1D electrophoresis was carried out at 200 V. Protein was transferred using a semi-dry apparatus for one hour at 70 mA per blot onto low fluorescent PVDF membrane. Membranes were blocked in blocking buffer (5% skim milk PBST), washed in PBST and incubated overnight with the primary antibodies for SET (sc25564, Santa Cruz) at a 1:200 dilution, and a β actin loading control (sc47778, Santa Cruz) at a at 1:500 dilution. Western blots were repeated for overnight incubation with primary antibodies for β catenin (ab32572, Abcam) at a 1:5000 dilution, and a β actin loading control (sc47778, Santa Cruz) at a 1:500 dilution.

Following primary antibody incubation, membranes were washed in PBST and incubated in the dark at room temperature for 1.5 hours with ECL Plex fluorescent detection Cy3 (anti-mouse) and Cy5 (anti-rabbit) antibodies (GE Healthcare) at a 1:1000 dilution. Membranes were washed, air-dried and imaged using the Typhoon Imager (GE healthcare). The levels of SET, β catenin and β actin abundance were quantified, based on the levels of Cy3 and Cy5 fluorescent intensity using Image Quant v5 software. A background correction was performed during this process. Levels of SET and β catenin expression were normalised to the level of β actin expression in each sample. The expression ratios of SET and β catenin in the siRNA treated and negative siRNA control cells, in comparison to the untreated control cells, were calculated.

6.2.5 RT^2 Profiler PCR Arrays

Reverse transcription was performed on 1 μg of both the SET siRNA treated and negative siRNA control SW480 RNA samples using the RT^2 First Strand Kit (SA Biosciences) according to manufacturer's recommendations. Samples were analysed on individual RT^2 Profiler PCR Array plates (Cancer Pathway Finder PCR Arrays, PAHS-033) (SA Biosciences) according to the manufacturer's protocol. PCR was carried out using the Opticon 3 (MJ research). The RT and PCR array was repeated for each of the samples. For data analysis, the C(t) threshold was set at the same level for all PCRs and results were uploaded into the RT^2 Profiler PCR Array Data Analysis Website (http://www.sabiosciences.com/pcr/arrayanalysis.php). The website calculated the relative expression of the SET siRNA treated and negative siRNA control samples using the $2^{-\Delta\Delta C(t)}$ method, after normalisation to the reference genes on the array plate, giving fold change expression values.

6.3 Results

6.3.1 Real-time RT-PCR

Prior to RT-PCR, the integrity of all RNA tumour and normal samples was analysed by denaturing gel electrophoresis. An example of a RNA denaturing gel is shown in Fig. 3. RNA was extracted from 40 tumour-normal pairs, of which eight tumour-normal pairs had to be excluded from analysis due to RNA degradation. Real-time RT-PCR was performed on the remaining 32 matched paired tumour-normal tissues from nine stage I, seventeen stage II and six stage III CRC patients. The relative tumour to normal expression ratios for each sample was calculated to the same amount of total starting RNA using the $\Delta C(t)$ method, and then again against the reference genes PMM1 and PSMB6 using the $2^{-\Delta\Delta C(t)}$ method. Data is displayed in a scatter plot in Fig. 4. When using the $\Delta C(t)$ method 27/32 (83.4%) of patients had a tumour-normal expression ratio of ≥2 fold. When using the $2^{-\Delta\Delta C(t)}$ method, normalising to PMM1 or to PSMB6, 21/31 (67.8%) and 20/31 (62.5%) of patients had a tumour-normal expression ratio of ≥2 fold respectively. Calculating the tumour-normal abundance ratio for each patient using the different methods and reference genes did not yield significantly different results, P=0.39 (repeated measures ANOVA). When averaging the relative abundance ratios for each patient obtained from the different methods, 75% (24/32) of patients had a tumour to normal SET expression ratio of >2 fold. Twelve and a half percent (4/32) of patients had a tumour-normal expression ratio of 1 to 2 fold and 12.5% had reduced abundance relative to the tumour. The tumour-normal expression ratios between stage I, II and III patients was not significantly different when averaging the relative abundance ratios for each patient obtained from the different calculation methods, P=0.63 (ANOVA) (Fig. 5).

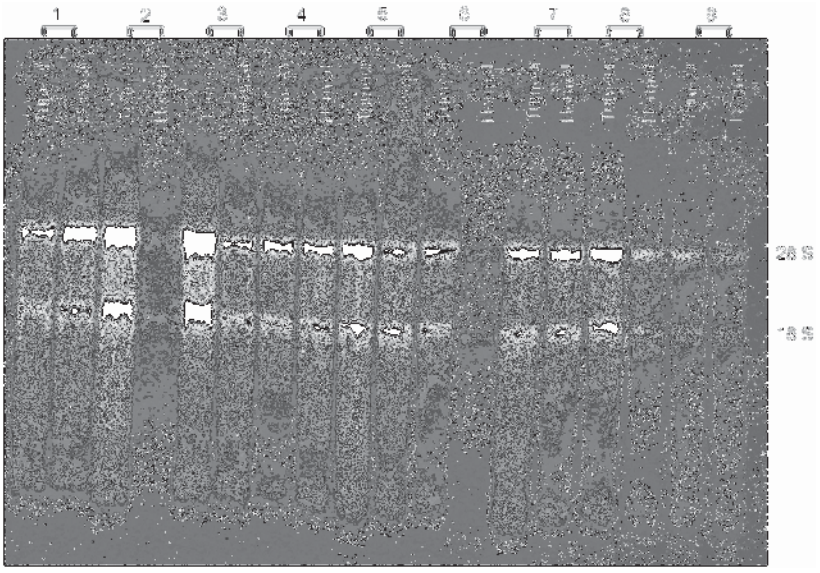

Fig 3. Example of a RNA check gel. RNA was extracted from whole tissue using Tri Reagent and the integrity of each sample was then checked by denaturing gel electrophoresis. Samples that did not show distinct 28S and 18S bands were excluded from further analysis. In the above gel nine matched paired tumour-normal tissue samples were analysed, the samples 2 normal and 6 normal did not show distinct 28S and 18S bands, hence these tissue pairs were used in RT-PCR analysis.

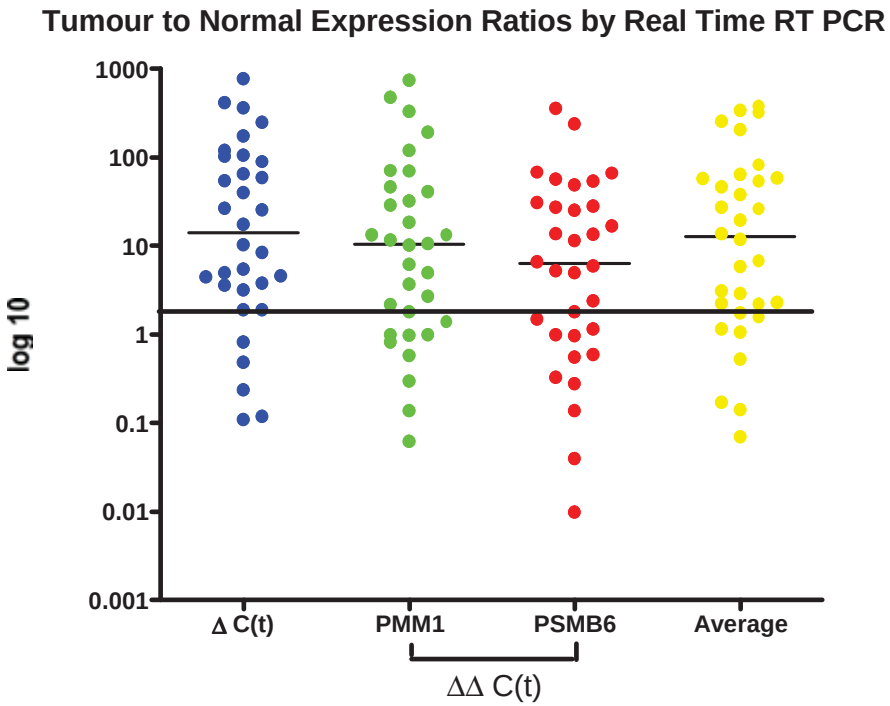

Fig 4. Relative real-time RT-PCR on matched paired tumour normal tissues (n=32) for the genes SET, PMM1 and PSMB6. Tumour to normal SET expression ratios were calculated using ΔC(t) method (by normalising to the same amount of total starting RNA), and by normalising to the reference genes PMM1 and PSMB6 using the $2^{-\Delta\Delta C(t)}$ method. The different methods of normalisation did not give significantly different results, P=0.39 (repeated measures ANOVA). Data points in the fourth column labelled average are the averaged tumour to normal expression ratios obtained using the different methods of normalisation. The black continuous line represents a 2 fold expression ratio.

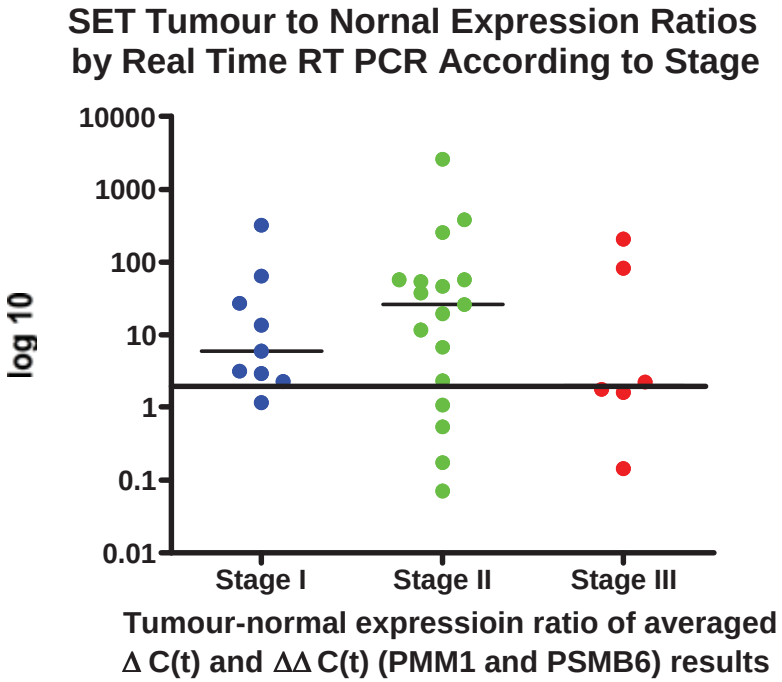

Fig 5. The averaged ΔC(t), PMM1 and PSMB6 tumour to normal expression ratios for each sample according to tumour stage. The level of SET expression between the stage I (n= 9), II (n= 17), and III (6) tumours is not significantly different, P=0.63 (ANOVA). The black line represents a 2 fold expression ratio.

6.3.2 SET siRNA knock down-SET expression at the transcript level

SET expression was transiently knocked down in SW480 and HEK cells using siRNA. Seventy-two hours post transfection, RNA was extracted from the SET siRNA treated, negative siRNA control, and untreated cells (n=4 per group). Levels of SET expression in each sample were assessed by real-time RT-PCR and normalised to PMM1 expression. For analysis purposes, the untreated cells were considered to have 100% SET expression. In the HEK cells, the mean level of SET expression in the negative siRNA control and SET siRNA treated cells was 92.44% ± 25.15 and 20.07 ± 3.89 respectively (Fig. 6A). In the SW480 cells, the mean level of SET expression in the negative siRNA control and SET siRNA treated cells was 106.6% ± 38.55 and 17.20 ± 2.09 respectively (Fig. 6B).

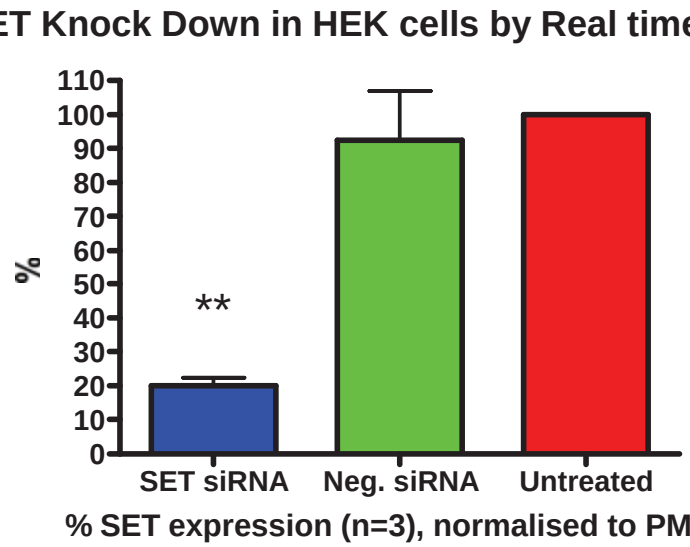

A)

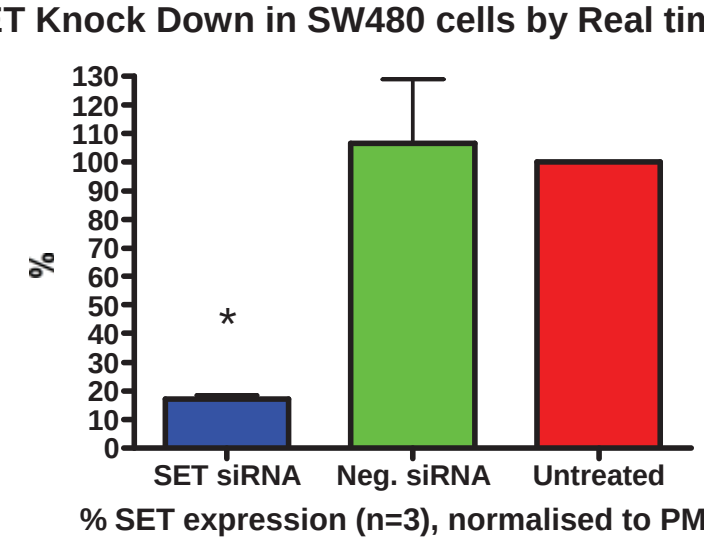

B)

Fig 6. Real-time RT-PCR on A) HEK and B) SW480 lysates from SET siRNA treated, negative siRNA treated, and untreated cells (n=4 per group) for the SET gene and the reference gene PMM1. Levels of SET expression in each sample were normalised to the levels of PMM1 expression. The ratio of SET expression in the SET siRNA treated and negative siRNA treated cells were then calculated against the untreated control samples. The level of SET expression in the SET siRNA treated HEK and SW480 cells was significantly reduced compared to the negative siRNA treated cells, P=0.008 and P=0.016 respectively.

6.3.3 SET siRNA knock down—SET and β catenin expression at the protein level

Five days post transfection, SET and β catenin protein expression levels were analysed by western blotting in the SET siRNA treated, negative siRNA control and untreated cells (n=4 per group). The expression of SET and β catenin was normalised to the level of β actin expression in each sample.

6.3.3.1 SW480 cells

SET abundance in the SW480 cells was significantly reduced in the siRNA treated cells compared to the negative siRNA and untreated controls, P=0.0002 (ANOVA). The mean level of SET expression was 11.98% ±5.34, in comparison to the negative siRNA and untreated controls at 106.9% ±32.71 and 101.00 % ±16.45 respectively (Fig. 7). The level of β catenin expression in the SET siRNA treated samples was not significantly different, P=0.55 (ANOVA). The mean level of β catenin expression in SET siRNA treated cells was 106.5% ±39.31, in comparison to the negative siRNA and untreated controls at 122.5% ±17.56 and 100.0% ±20.63 respectively (Fig. 7).

6.3.3.2 HEK cells

SET abundance in the HEK cells was significantly reduced in the siRNA treated cells compared to the negative siRNA and untreated controls, P=0.0001 (ANOVA). The mean level of SET expression was 11.61% ±4.28, in comparison to the negative siRNA and untreated controls at 71.84% ±3.31 and 100.00% ±0.49 respectively (Fig. 8). The mean level of β catenin expression in SET siRNA treated cells was 75.5% ±6.93, in comparison to the negative siRNA and untreated controls at 102.4% ±10.37 and 100% ±0.31 respectively (Fig. 8). The reduction in β catenin abundance levels by 24.5% in the SET siRNA treated samples was significantly different in comparison to the negative siRNA and untreated cells, P=0.0009 (ANOVA).

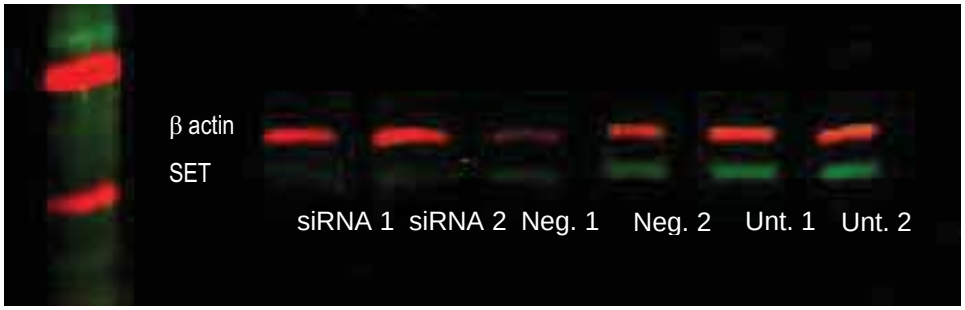

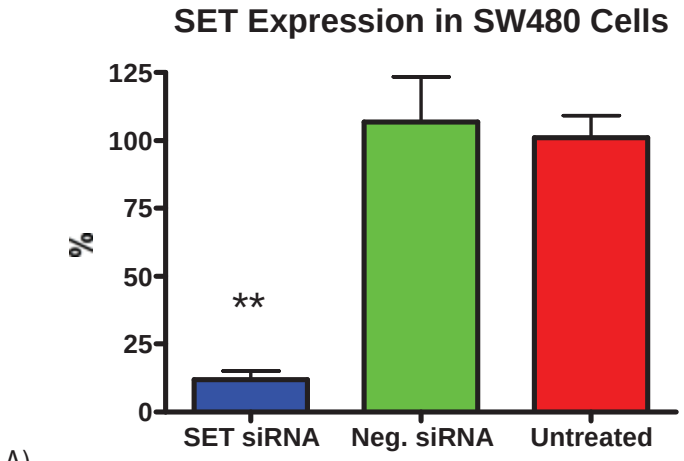

A)

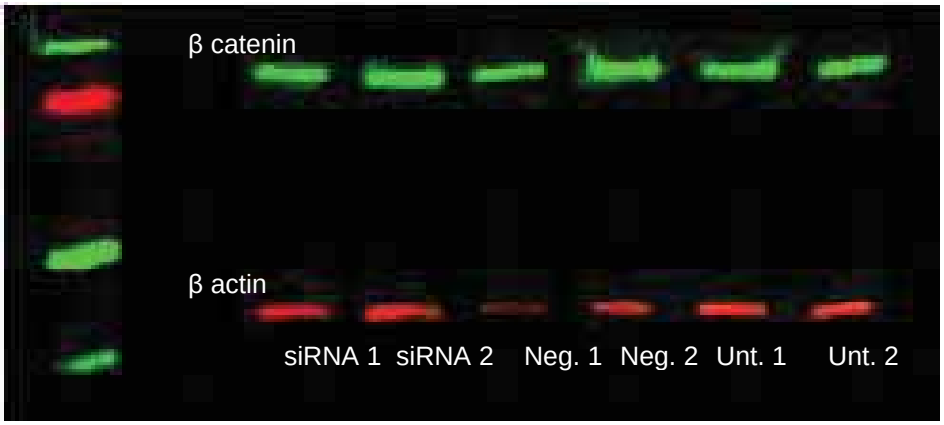

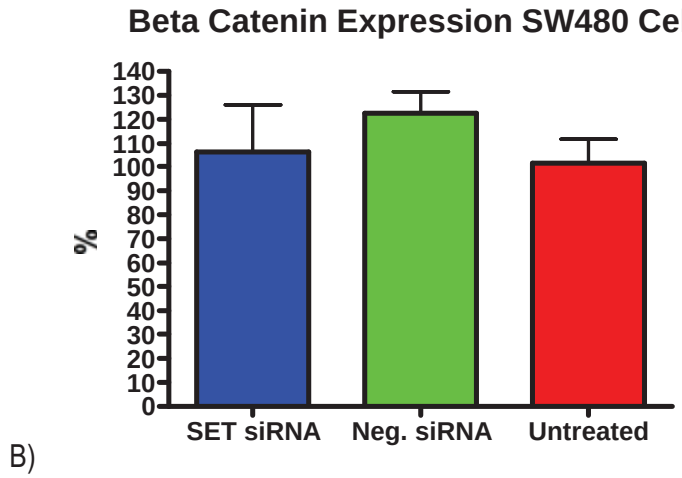

B)

Fig 7. SET and β catenin expression in the SW480 SET siRNA treated, negative siRNA control and untreated cells (n=4 per group). Cells were lysed five days post treatment, and SET and β catenin protein levels were quantified by western blotting. All samples were normalised to a β actin loading control. Representative western blots are displayed for SET (A), and β catenin (B). The level of SET expression in the SET siRNA treated SW480 cells was significantly reduced compared to the negative siRNA and untreated control cells, P=0.0002. Levels of β catenin expression were unchanged, P=0.55.

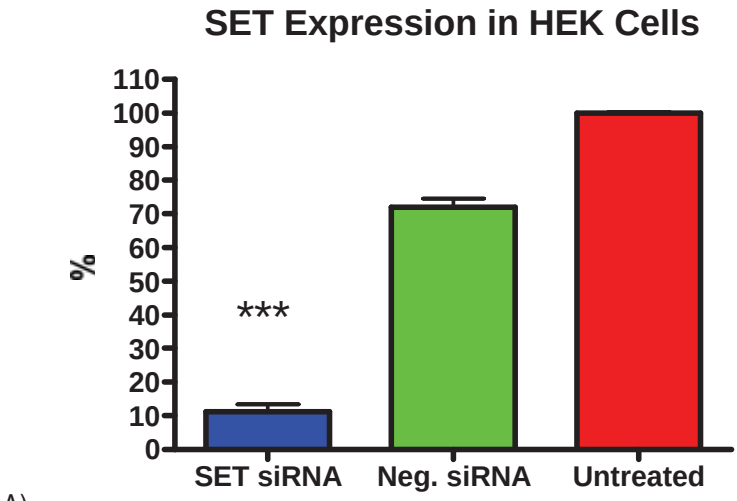

A)

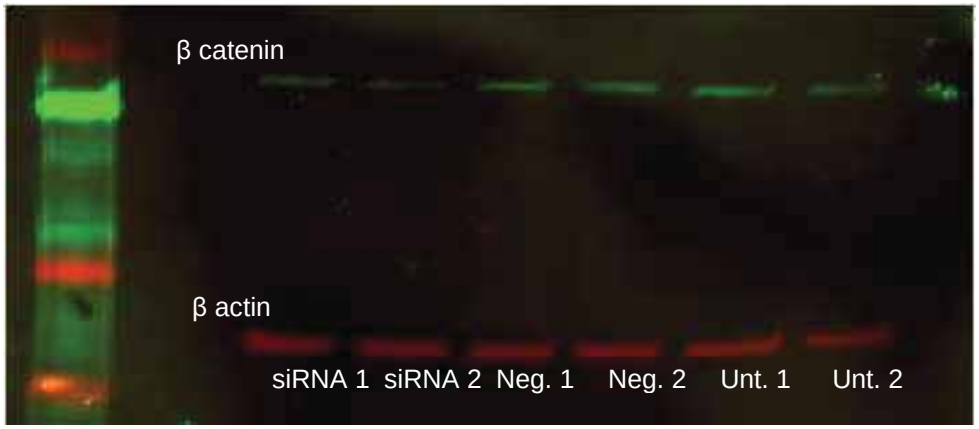

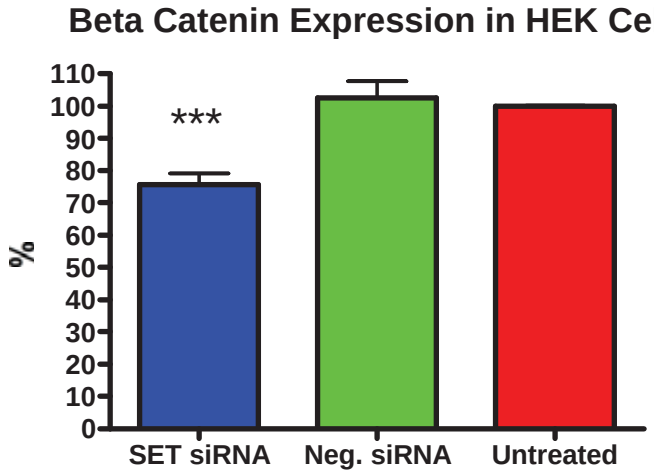

B)

Fig 8. SET and β catenin expression in the HEK SET siRNA treated, negative siRNA control and untreated cells. (n=4 per group). Cells were lysed five days post treatment, and SET and β catenin protein levels were quantified by western blotting. All samples were normalised to a β actin loading control. Representative western blots are displayed for SET (A), and β catenin (B). The level of SET and β catenin expression in the SET siRNA treated HEK cells was significantly reduced compared to the negative siRNA and untreated control cells, P=0.0001 and P=0.0009 respectively.

6.3.4 SET siRNA treated SW480 lysates analysed using the RT^2 Profiler PCR 'Human Cancer Pathway Finder' Array

As the SW480 cells contain a Wnt signalling pathway mutation, it was predicted knocking down SET in these cells would have no effect on β catenin levels. In order to assess the cancer associated signalling pathways SET may be involved in, RNA lysates from the SW480 negative siRNA control and SET siRNA treated cells were analysed using RT^2 Profiler PCR 'Human Cancer Pathway Finder' Arrays in duplicate. For each gene the ΔC(t) values of the treated and control samples were normalised to the reference genes hypoxanthine phosphoribosyltransferase 1 (HPRT1) and ribosomal protein L13A (RPL13A). The normalised ΔC(t) values for each of the genes on the original and repeat Profiler Array plates were then averaged. The fold change ratio between the SET siRNA treated and control lysates for each gene was calculated using the ΔΔC(t) method. The normalised and averaged ΔC(t) value of each gene, the standard deviation for each of the averaged ΔC(t) values, the Refseq number for each gene (NCBI reference sequence number), and the fold change ratio between the SET siRNA treated and control lysates is displayed in Table 2. Good reproducibility between the PCR array plates was achieved. The calculated fold change of the reference genes HPRT1 and RPL13A between the SET siRNA treated and negative siRNA control was negligible at 1.007 and -1.007 respectively. A heat map of all 80 genes and their change in expression is shown in Fig. 9, with Fig. 10 displaying the genes organised in lists representative of the six biological processes involved in transformation and tumourigenesis.

Table 2. RT Profiler array results of the SET siRNA treated and negative siRNA treated control SW480 cells

Gene [a]	Refseq [b]	Ave. Δ(Ct) SET siRNA [c]	SDV [d]	Ave. Δ(Ct) control [e]	SDV [f]	Fold change [g]
AKT1	NM_005163	2.51	0.08	2.15	0.02	-1.29
ANGPT1	NM_001146	7.97	0.57	7.21	0.56	-1.70
ANGPT2	NM_001147	8.39	0.23	7.83	0.02	-1.47
APAF1	NM_001160	4.21	0.46	4.02	0.37	-1.14
ATM	NM_000051	5.33	0.41	5.13	0.46	-1.15
BAD	NM_004322	5.22	0.01	4.72	0.1	-1.42
BAX	NM_004324	1.76	0.05	1.72	0.09	-1.03
BCL2	NM_000633	8.11	0.17	7.28	1.01	-1.78
BCL2L1	NM_138578	3.62	0.09	3.28	0.14	-1.27
BRCA1	NM_007294	3.36	0.36	3.01	0.39	-1.28
CASP8	NM_001228	5.91	0.06	5.56	0.05	-1.27
CCNE1	NM_001238	9.57	0.51	9.59	0.51	1.01
CDC25A	NM_001789	3.81	0.22	3.64	0.37	-1.12
CDK2	NM_001798	2.18	0.16	1.95	0.43	-1.17
CDK4	NM_000075	-0.09	0.16	-0.32	0.21	-1.17
CDKN1A	NM_000389	0.78	0.02	0.59	0.17	-1.14
CDKN2A	NM_000077	2.64	0.05	2.35	0.07	-1.22
CFLAR	NM_003879	4.1	0.19	3.79	0.07	-1.24
CHEK2	NM_007194	4.79	0.29	4.44	0.2	-1.27
COL18A1	NM_030582	4.09	0.36	3.73	0.01	-1.28
E2F1	NM_005225	5.58	0.01	5.02	0.02	-1.48
ERBB2	NM_004448	6.7	0.26	6.2	0.34	-1.42
ETS2	NM_005239	2.11	0.19	2.81	0.01	1.63
FAS	NM_000043	8.41	0.67	8.79	0.63	1.3
FGFR2	NM_000141	4.94	0.26	4.41	0.2	-1.44
FOS	NM_005252	4.33	0.43	4.18	0.7	-1.11
GZMA	NM_006144	6.98	0.51	6.15	0.25	-1.78
HTATIP2	NM_006410	1.46	0.4	1.17	0.46	-1.23
IFNA1	NM_024013	7.48	0.41	6.98	0.31	-1.41
IFNB1	NM_002176	8.57	0.12	8.15	0.12	-1.34
IGF1	NM_000618	7.56	0.39	7.33	0.62	-1.17
IL8	NM_000584	5.99	0.38	5.67	0.61	-1.25
ITGA1	NM_181501	4.06	0.69	3.71	0.51	-1.27
ITGA2	NM_002203	4.25	0.2	4.38	0.12	1.09
ITGA3	NM_002204	2.72	0.22	2.36	0.27	-1.28
ITGA4	NM_000885	7.54	0.18	7.19	0.58	-1.27
ITGAV	NM_002210	1.91	0.14	1.95	0.19	1.03
ITGB1	NM_002211	1.54	0.46	0.72	0.48	-1.77
ITGB3	NM_000212	7.78	0.63	7.08	0.38	-1.62
ITGB5	NM_002213	1.26	0.12	0.68	0.05	-1.49
JUN	NM_002228	5.49	0.28	5.67	0.43	1.13
MAP2K1	NM_002755	1.82	0.15	1.7	0.06	-1.08
MCAM	NM_006500	2.92	0.43	2.6	0.49	-1.25

[a] Gene symbol

[b] NCBI reference sequence number

[c] The averaged ΔC(t) values of the replica array plates for the SET siRNA treated SW480 cells

[d] The standard deviation for each of the averaged SET siRNA treated ΔC(t) values

[e] The averaged ΔC(t) values of the replica array plates for the negative siRNA control SW480 cells

[f] The standard deviation for each of the averaged negative siRNA control ΔC(t) values

[g] The fold change expression ratio between the SET siRNA treated and negative siRNA treated control, calculated using the ΔΔC(t) method

Table 2. RT Profiler array results of the SET siRNA treated and negative siRNA treated control SW480 cells

Gene [a]	Refseq [b]	Ave. ∆(Ct) SET siRNA [c]	SDV [d]	Ave. ∆(Ct) control [e]	SDV [f]	Fold change [g]
MDM2	NM_002392	3.29	0.8	3.09	0.67	-1.14
MET	NM_000245	4.4	0.48	4.81	0.25	1.33
MMP1	NM_002421	6.55	0.37	6.3	0.68	-1.19
MMP2	NM_004530	6.7	0.02	6.11	0.19	-1.51
MMP9	NM_004994	6.54	0.27	6.32	0.11	-1.16
MTA1	NM_004689	1.46	0.28	1.34	0.36	-1.09
MTA2	NM_004739	4.18	0.03	3.8	0.34	-1.31
MTSS1	NM_014751	5.33	0.34	5.37	0.27	1.03
MYC	NM_002467	3.69	0.47	3.78	0.41	1.06
NFKB1	NM_003998	2.41	0.06	2.51	0.1	1.07
NFKBIA	NM_020529	2.95	0.15	2.97	0.03	1.02
NME1	NM_000269	-0.01	0.07	0.01	0.02	1.01
NME4	NM_005009	1.97	0.02	1.82	0.51	-1.11
PDGFA	NM_002607	3.31	0.5	3.2	0.6	-1.08
PDGFB	NM_002608	2.52	0.05	2.51	0.08	-1
PIK3R1	NM_181504	3.87	0.61	3.77	0.34	-1.07
PLAU	NM_002658	5.09	0.08	5.12	0.08	1.02
PLAUR	NM_002659	2.52	0.19	2.28	0.17	-1.19
PNN	NM_002687	0.99	0.06	0.95	0.1	-1.03
RAF1	NM_002880	4.43	0.05	4.15	0.15	-1.21
RB1	NM_000321	1.13	0.56	0.88	0.49	-1.19
S100A4	NM_002961	-2.02	0.17	-2.13	0.11	-1.08
SERPINB5	NM_002639	5.67	0.11	5.2	0.14	-1.39
SERPINE1	NM_000602	2.69	0.64	2.16	0.6	-1.45
SNCG	NM_003087	4.97	0.18	4.73	0.04	-1.18
SYK	NM_003177	7.05	0.81	6.37	1.21	-1.61
TEK	NM_000459	7.72	0.23	7.31	0.82	-1.32
TERT	NM_198253	12.46	0.07	12.47	1.05	1
TGFB1	NM_000660	7.63	0.78	7.71	0.78	1.06
TGFBR1	NM_004612	5.83	0.12	5.42	0.07	-1.33
THBS1	NM_003246	5.43	0.05	4.6	0.1	-1.78
TIMP1	NM_003254	0.23	0.07	0.11	0.22	-1.09
TIMP3	NM_000362	8.32	0.6	7.71	0.41	-1.53
TNF	NM_000594	7.56	0.25	7.05	0.17	-1.43
TNFRSF10B	NM_003842	2.78	0.32	2.62	0.39	-1.11
TNFRSF1A	NM_001065	8.34	0	7.9	0.51	-1.36
TNFRSF25	NM_003790	7.95	0.47	7.85	0.25	-1.07
TP53	NM_000546	0.67	0.62	0.36	0.38	-1.24
TWIST1	NM_000474	9.51	0.41	8.94	0.01	-1.49
EPDR1	NM_017549	2.08	0.12	2.13	0.19	1.04
VEGFA	NM_003376	8.64	0.64	8.77	0.63	1.09

[a] Gene symbol
[b] NCBI reference sequence number
[c] The averaged ∆C(t) values of the replica array plates for the SET siRNA treated SW480 cells
[d] The standard deviation for each of the averaged SET siRNA treated ∆C(t) values
[e] The averaged ∆C(t) values of the replica array plates for the negative siRNA treated control SW480 cells
[f] The standard deviation for each of the averaged negative siRNA treated control ∆C(t) values
[g] The fold change expression ratio between the SET siRNA treated and negative siRNA treated control, calculated using the ∆∆C(t) method

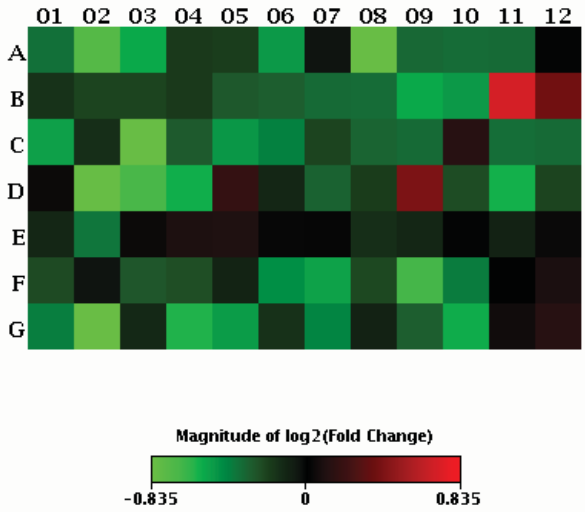

Layout	01	02	03	04	05	06	07	08	09	10	11	12
A	AKT1 **-1.29**	ANGPT1 **-1.69**	ANGPT2 **-1.47**	APAF1 **-1.14**	ATM **-1.15**	BAD **-1.42**	BAX **-1.03**	BCL2 **-1.78**	BCL2L1 **-1.27**	BRCA1 **-1.28**	CASP8 **-1.27**	CCNE1 **1.01**
B	CDC25A **-1.12**	CDK2 **-1.17**	CDK4 **-1.17**	CDKN1A **-1.14**	CDKN2A **-1.22**	CFLAR **-1.24**	CHEK2 **-1.27**	COL18A1 **-1.28**	E2F1 **-1.48**	ERBB2 **-1.42**	ETS2 **1.63**	FAS **1.30**
C	FGFR2 **-1.44**	FOS **-1.11**	GZMA **-1.78**	HTATIP2 **-1.23**	IFNA1 **-1.41**	IFNB1 **-1.34**	IGF1 **-1.17**	IL8 **-1.25**	ITGA1 **-1.27**	ITGA2 **1.09**	ITGA3 **-1.28**	ITGA4 **-1.27**
D	ITGAV **1.03**	ITGB1 **-1.77**	ITGB3 **-1.62**	ITGB5 **-1.49**	JUN **1.13**	MAP2K1 **-1.08**	MCAM **-1.25**	MDM2 **-1.14**	MET **1.33**	MMP1 **-1.19**	MMP2 **-1.51**	MMP9 **-1.16**
E	MTA1 **-1.09**	MTA2 **-1.31**	MTSS1 **1.03**	MYC **1.06**	NFKB1 **1.07**	NFKBIA **1.02**	NME1 **1.01**	NME4 **-1.11**	PDGFA **-1.08**	PDGFB **-1.00**	PIK3R1 **-1.07**	PLAU **1.02**
F	PLAUR **-1.19**	PNN **-1.03**	RAF1 **-1.21**	RB1 **-1.19**	S100A4 **-1.08**	SERPINB5 **-1.39**	SERPINE1 **-1.45**	SNCG **-1.18**	SYK **-1.61**	TEK **-1.32**	TERT **1.00**	TGFB1 **1.06**
G	TGFBR1 **-1.33**	THBS1 **-1.78**	TIMP1 **-1.09**	TIMP3 **-1.53**	TNF **-1.43**	TNFRSF10B **-1.11**	TNFRSF1A **-1.36**	TNFRSF25 **-1.07**	TP53 **-1.24**	TWIST1 **-1.49**	EPDR1 **1.04**	VEGFA **1.09**

Fig 9. Heat map of the genes analysed in the RT² Profiler PCR 'Human Cancer Pathway Finder' Array of the SET siRNA treated SW480 cells. The fold increase or decrease of the genes and their expression ratios (SET siRNA treated cells compared to negative siRNA treated control) are presented in a table below.

Cell Cycle Control and DNA Damage Repair

E2F1	-1.48
BRCA1	-1.28
CHEK2	-1.27
TP53	-1.24
CDKN2A	-1.22
RB1	-1.19
CDK4	-1.17
CDK2	-1.17
ATM	-1.15
MDM2	-1.14
CDKN1A	-1.14
CDC25A	-1.12
S100A4	-1.08
CCNE1	1.01

Apoptosis and Cell Senescence

BCL2	-1.78
GZMA	-1.78
BAD	-1.42
TNFRSF1A	-1.36
CASP8	-1.27
BCL2L1	-1.27
CFLAR	-1.24
HTATIP2	-1.23
APAF1	-1.14
TNFRSF10B	-1.11
TNFRSF25	-1.07
BAX	-1.03
TERT	1.00
FAS	1.30

Invasion and Metastasis

TIMP3	-1.53
MMP2	-1.51
TWIST1	-1.49
SERPINE1	-1.45
SERPINB5	-1.39
MTA2	-1.31
MMP1	-1.19
PLAUR	-1.19
MMP9	-1.16
NME4	-1.11
TIMP1	-1.09
MTA1	-1.09
NME1	1.01
PLAU	1.02
MET	1.33

Angiogenesis

THBS1	-1.78
ANGPT1	-1.70
ANGPT2	-1.47
FGFR2	-1.44
TNF	-1.43
IFNA1	-1.41
IFNB1	-1.34
TGFBR1	-1.33
TEK	-1.32
COL18A1	-1.28
IL8	-1.25
IGF1	-1.17
PDGFA	-1.08
PDGFB	-1.00
VEGFA	1.09

Signal Transduction and Transcription Factors

ERBB2	-1.42
AKT1	-1.29
RAF1	-1.21
SNCG	-1.18
FOS	-1.11
MAP2K1	-1.08
PIK3R1	-1.07
NFKBIA	1.02
MYC	1.06
NFKB1	1.07
JUN	1.13
ETS2	1.63

Adhesion

ITGB1	-1.77
ITGB3	-1.62
SYK	-1.61
ITGB3	-1.49
ITGB5	-1.49
ITGA3	-1.28
ITGA1	-1.27
ITGA4	-1.27
MCAM	-1.25
PNN	-1.03
ITGAV	1.03
MTSS1	1.03
ITGA2	1.09

Fig 10. The fold increase or decrease of the genes analysed in the RT² Profiler PCR 'Human Cancer Pathway Finder' Array of the SET siRNA treated SW480 cells. The genes are organised in lists representative of the six biological processes involved in transformation and tumourigenesis. The fold ratio of each gene in the SET siRNA treated SW480 cells compared to the negative siRNA treated control cells is given.

6.4 Discussion

6.4.1 SET as a RT-PCR CRC marker

Real-time RT-PCR was performed on 32 matched paired tumour-normal tissues from nine stage I, seventeen stage II and six stage III CRC patients. Expression of SET at the RNA level was chosen for analysis in order to determine if the gene had any potential as an immunobead RT-PCR panel marker. The relative tumour to normal expression ratios for each of the samples was calculated to the same amount of total starting RNA using the $\Delta C(t)$ method, and then again against the reference genes PMM1 and PSMB6 using $2^{-\Delta\Delta C(t)}$ method. Calculating the tumour-normal abundance ratios using the $\Delta C(t)$ or $2^{-\Delta\Delta C(t)}$ method did not yield significantly different results, P=0.39 (repeated measures ANOVA) (Fig. 4). The tumour-normal expression level of SET between stage I, stage II and stage III patients was not significantly different (Fig.5), P=0.63 (ANOVA). This suggests SET has the potential to be a marker of early and late stage patients.

Calculating the tumour-normal abundance ratios to the same amount of total starting RNA and to one or more reference genes is important. Difference in reverse transcription efficiencies between samples means calculating ratios against the same amount of total starting RNA alone may give misleading results, however reference genes may also give misleading results. The expression level of a reference gene within an individual's tumour and normal tissue cannot be guaranteed to be exactly equal, as tumour and normal cells may be replicating at different rates.

These results suggest SET may have potential as a marker in the immunobead RT-PCR technique used to detect tumour cells extracted from patient's lavage and blood samples following surgery. SET would need to be used as part of a panel of markers, not as a single marker, given 25% of patients screened did not have a tumour-normal increase in expression of >2 fold. For SET to make a good immunobead panel marker, the expression of the transcript from a single tumour cell would need to be detectable by real-time RT-PCR. Preferably the expression of the transcript from a single normal epithelial cell would be undetectable, or significantly lower than the tumour expression level by at least 2 fold. Ideally SET would also not be expressed by monocytes or lymphocytes, as a small number may be non-specifically captured by the immunobeads along with any epithelial cells. As SET has a wide tissue distribution, the gene is likely to be expressed in monocytes and lymphocytes, however this is not an issue as the lab has since shown that SET expression was not detectable in normal blood samples processed using the immunobeads.

6.4.2 SET in the Wnt signalling pathway

The interaction of SET with PP2A in the Wnt signalling pathway was of interest due to the high proportion of CRC patients with Wnt signalling pathway mutations resulting in constitutive β catenin activity. The relationship between the PP2A holoenzyme and β catenin degradation is complicated. As part of the GSK3 β complex, PP2A appears to help target β catenin for destruction in the absence of Wnt signalling via the regulatory subunit PR61, but in the presence of Wnt signalling i.e. in cancer, PP2A is inhibited and β catenin accumulates in the cytosol[297] and translocates to the nucleus. SET is a known inhibitor of PP2Ac. It has also been suggested PP2Ac may directly dephosphorylate β catenin downstream of Wnt signalling, salvaging the molecule from degradation[297], however it has also been shown that PP2Ac is responsible for dephosphorylating Dsh thereby helping to maintain the GSK3 β complex in an active form, enabling β catenin phosphorylation and degradation.[314] These conflicting activities are probably dependent on the relative amount of the various β regulatory subunits of the PP2A holoenzyme at the time.

Knocking down SET in the HEK 293 cells showed a decrease in β catenin expression levels by 24.5% in comparison to untreated control cells, P=0.0009, where as no change in β catenin expression was observed in the SW480 SET siRNA treated cells. As the HEK 293 cells do not contain any known Wnt signalling pathway mutations and the SW480 cells contain an APC mutation resulting in constitutive activation of β catenin. The constitutive activation of the Wnt pathway in the SW480 cells results in consistently high levels of β catenin, hence any change in β catenin levels that may have occurred due to the SET knock down would most likely have been masked by the overexpression of β catenin in the SW480 cells.

6.4.3 Hypotheses for reduced β catenin levels in the SET knock down HEK 293 cells

SET is known to inhibit the activity of the catalytic PP2A subunit, PP2Ac[285], stopping the holoenzyme from dephosphorylating and inactivating substrate molecules. In the SET siRNA knock down HEK 293 cells, a significant decrease of 24.5% in β catenin levels was observed indicating SET does have an effect on Wnt signalling in normal epithelial cells. It is possible that reduced SET levels led to increased PP2A activity as part of the GSK3 β complex, which in turn resulted in inhibited β catenin accumulation, as suggested by Gao *et al*. (2002)[314] that PP2A activity was increased upstream of the GSK β complex at the level of Dsh, or that reduced SET levels led to reduced β catenin levels via an indirect mechanism.

6.4.3.1 Indirect influence of SET on Wnt signalling

SET may not directly regulate PP2A when it is part of the GSK3 β complex. A large proportion of total cellular SET (up to half) has been found to be associated with nuclear matrix or chromatin where it may enhance the phosphorylation status of transcriptional regulators via the inhibition of PP2A, leading to an increase in transcription and expression of certain genes.[318] β catenin is known to induce the transcription of TCF/Lef transcription factors and reduced levels of SET may have led to increased nuclear PP2A activity with dephosphorylation and inactivation of other transcriptional regulators. As discussed in the introduction, SET has a large range of substrates and plays a role in a variety of different signalling cascades, hence knocking down SET expression may have led to reduced β catenin levels via other indirect mechanisms involving a number of other proteins or pathways.

6.4.3.2 Influence of SET on Wnt signalling via PP2A as part of the GSK3 β complex

PP2A has been shown to enhance β catenin degradation and inhibit the Wnt pathway[315 46], in the absence of Wnt signal and CK1 activity. Gao *et al*.[314] suggest that in the presence of Wnt signal, CK1 promotes the pathway activity via the phosphorylation of GSK3 β complex components such as APC, axin and β catenin, reducing their affinity for other complex components such as PP2A, GSK3 β and β catenin, releasing them from the complex so that β catenin is not degraded. In this system, PP2A appears to act as a counter regulatory phosphatase to CK1, hence its inhibition by SET would amplify the phosphorylation of complex components by CK1, resulting in increased Wnt signalling. PP2A may also be able to inhibit Wnt pathway activity upstream of the GSK3 β complex via Dsh. Activation of Wnt signalling results in the hyperphosphorylation of Dsh and the inhibition of the GSK3 β complex. Once Wnt stimulation stops, it is thought PP2A may dephosphorylate Dsh, causing inactivation, allowing for the resumption of GSK3 β complex activity[314] and subsequent β catenin degradation. In the HEK293 cells, Wnt pathway activation and β catenin levels would have been low, as compared to the SW480 cells. Hence, following this model, reduced SET levels would have allowed for increased PP2A activity resulting in increased inhibition of Wnt signalling and decreased levels of β catenin (Fig. 9), which was masked in the SW480 cells due to the huge excess of β catenin already present.

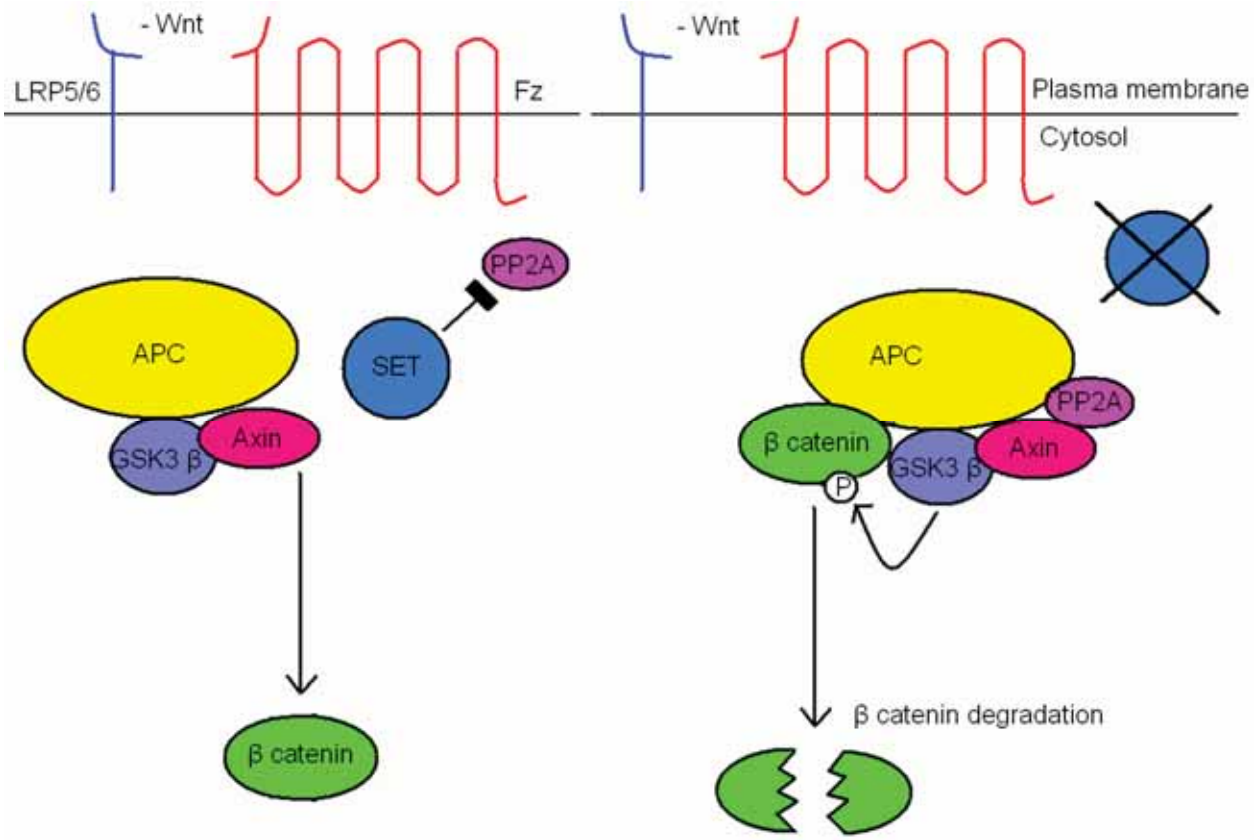

Fig 9. Inhibition of S*Et al*ows for increased PP2A activity resulting in a decrease in β catenin levels.

6.4.4 SET as a therapeutic target of Wnt signalling in CRC

A significant reduction in β catenin levels was observed when SET was knocked down in the HEK 293 cells, which have no known Wnt signalling mutation. However, as 90%[295] of CRC patients contain a mutation in either APC or β catenin itself, (which allows the protein to evade phosphorylation by the GSK3 β complex) reducing levels of SET in these cancers would have no effect on β catenin levels as seen in the SW480 SET siRNA knock down cells. Given the results of the SET siRNA experiments in the SW480 cells, SET does not appear to be a good CRC therapeutic target in relation to Wnt signalling.

6.4.5 SET siRNA knock down and RT^2 Profiler PCR Array analysis

In order to assess the effect of knocking down SET in SW480 cells on other cancer pathways involved in CRC, preliminary data was collected by analysing the siRNA knock down of SET in SW480 cells using RT^2 Profiler PCR Array 'Human Cancer Pathway Finder' plates (SA Biosciences). SET siRNA transfected, negative control siRNA transfected and mock-transfected lysates were analysed using RT^2 Profiler PCR Arrays. The relative level of expression of 84 genes involved in the cancer process was analysed in SW480 cells transfected with SET siRNA compared to negative siRNA control cells using the 'Human Cancer Pathway Finder' arrays. The array plates contained genes representative of the six main processes involved in transformation and tumourigenesis; cell cycle control and DNA damage

repair, apoptosis and cell senescence, invasion and metastasis, angiogenesis, signal transduction molecules and transcription factors and adhesion. The majority of genes appeared to be decreased in expression, with only three genes showing an increase in expression by >1.30 fold in the SET knock down cells. Twenty-one of the genes had a fold change in the range of ±1.10, indicating the knock down of SET expression had little effect on these genes. The majority of the genes, 53, had a reduced fold change expression in the SET siRNA treated cells of between -1.10 and -1.65. Five genes, Bcl2, Gzma, Thbs1, Angpt1 and Itg β 1, had a reduced fold change expression of more than -1.70, with one gene, Ets2, having a fold change expression of +1.60.

Below is a discussion of the possible ways SET may be interacting with the six most differentially expressed genes and the signalling pathways they are involved in, according to the current literature. It is important to note that this data is preliminary, as the arrays have only been performed in duplicate. Future work would include repeating the knock down experiments with profiler arrays and confirmation of differential expression at the protein level by western blotting.

6.4.5.1 BCL2, B cell CLL/lymphoma 2

The Bcl-2 family is made up of 25 known genes that regulate mitochondrial outer membrane permeabilisation. These genes can be pro-apoptotic, such as Bax, BAD, Bak and Bok, or anti-apoptotic, such as Bcl-2 itself, Bcl-xL and Bcl-w. The gene Bcl-2 was found to be altered in expression by -1.78 fold in the SW480 SET siRNA knock down cells, compared to the negative control cells. Bcl-2 is a known target of PP2A.[319] During signalling of the survival agonist IL-3, Bcl-2 is phosphorylated at the serine residue 70. The phosphorylation of this residue is vital for the Bcl-2 suppression of apoptosis following IL-3 withdrawal or during toxic chemotherapy. PP2A dephosphorylates Bcl-2 at the serine 70 residue, inducing apoptosis.[319] When cells are treated with the PP2A inhibitor, okadaic acid, the dephosphorylation of Bcl-2 is blocked and apoptosis is inhibited.[320] Deng *et al*. (1998)[319] suggest that the catalytic subunit of PP2A dephosphorylates Bcl-2, and Ruvolo *et al*. (2002)[320] suggest that the B56 α subunit regulates the phosphatase activity of PP2A in regard to Bcl-2. Ruvolo *et al*. (2002)[320] found the B56 α subunit to associate and co-localise at the mitochondrial membrane with Bcl-2, and that over expression of B56 α promotes PP2A activity resulting in Bcl-2 dephosphorylation and the induction of apoptosis.

Interestingly, the pro-apoptotic molecule BAD mRNA, also of the Bcl-2 family, was decreased by 30% in the SET siRNA treated cells. Phosphorylated BAD is sequestered by 14–3–3 proteins, rendering the protein inactive. Dephosphorylation of BAD at the serine residue 112 initiates the activation of BAD.[291] Activated BAD is targeted to the mitochondrial membrane where it promotes cell death by binding and

inactivating Bcl-2 and Bcl-xL. The main phosphatase that dephosphorylates BAD at serine 112 is PP2A, and it has been shown that inhibition of PP2A rescues cells from BAD induced apoptosis.

Hence, via the dephosphorylation of both the pro-apoptotic BAD and the anti-apoptotic Bcl-2 proteins, PP2A induces cell death. As SET is an inhibitor of PP2A, knocking down SET in SW480 cells may lead to an increase in PP2A activity, the dephosphorylation of BAD and Bcl-2 and an increase in apoptosis. PP2A is also a known phosphatase of the pro-apoptotic Bcl-2 family member Bax, with dephosphorylation of Bax resulting in the induction of apoptosis. Bax was included in the array plate, but was unchanged in expression in the SET siRNA treated cells.

6.4.5.2 GZMA, Granzyme A

Granzyme A (GzmA) is a serine protease released in cytotoxic granules by natural killer cells and cytotoxic T lymphocytes, used to target the death of virus-infected and tumour cells.[321] In the SET siRNA knock down SW480 cells GzmA expression was altered by -1.78 fold, compared to the negative control cells. GzmA induces single-strand DNA damage allowing DNA degradation by histones, loss of cell membrane integrity and loss of mitochondrial transmembrane potential. A target of GzmA is the SET complex containing SET, the DNA ending protein HMG-2, the base excision repair pathway apurinic endonuclease Ape1, PP2A inhibitor protein pp32 and the transcriptional regulator and nucleoside diphosphate kinase NM23-H1.[166] The SET complex also contains other proteins yet to be identified. SET, HMG-2 and Ape1 are substrates of GzmA and their cleavage destroys all function.[166] The SET complex is normally associated with the endoplasmic reticulum and can shuttle to the nucleus, but the actual function of the complex is unknown. It has been suggested to be involved in the response to oxidative stress, as cleavage of Ape1 by GzmA prevents cellular repair and recovery from oxidative stress damage.[166]

The SET complex is known to be involved in DNA damage caused by GzmA induced apoptosis.[322] The protein SET is a known inhibitor of NM23-H1, which is a known tumour metastasis suppressor.[166] NM23-H1 is a GzmA activated DNase that is inactive when bound to SET in the SET complex. When GzmA is introduced into target cells, SET is cleaved, allowing NM23-H1 to translocate to the nucleus. NM23-H1 nicks chromosomal DNA and apoptosis is induced in a caspase-independent manner. This effect was seen after GzmA loading or after cytotoxic T lymphocyte attack, a mechanism used to kill tumour cells. When SET was silenced using siRNA, K526 cells were more sensitive to GzmA-induced DNA nicks. Conversely when SET expression was driven via transfection, a decrease in GzmA-induced DNA nicks was seen.[166]

6.4.5.3 THSB1, Thrombospondin

Thrombospondin 1 (TSP-1) was found to be altered in expression by -1.78 fold in the SET siRNA treated cells compared to the negative control cells. TSP-1 is an inhibitor of angiogenesis, is able to sequester and clear VEGF[323] and is an activator of TGF β 1.[324-327] TGF β 1 is an endogenous regulator of angiogenesis and is a tumour suppressor in normal epithelial cells. TGF β is secreted in a latent form that needs to be converted into a biologically active molecule in order to regulate cell proliferation. TSP-1 is one of only a few proteins able to activate TGF β[328]and active TGF β has been shown to induce TSP-1 expression {Okamoto, 2002 #34 The oncogenes jun[329,330], src[331] and myc[332] are known regulators of TSP-1. Active myc increases the turnover and decreased stability of TSP-1 transcripts.[329,330] Ras promotes the phosphorylation and activation of myc, in doing so decreases TSP-1 levels.[333]

TGF β 1 was also shown to be down-regulated in the SET siRNA treated cells by 25%. The most well-known and documented pathway induced by TGF β signalling is the Smad pathway.[334] A number of Smad independent pathways may also be induced by TGF β signalling[335] through which Ras[336], PI3K[337] and Rho small GTP binding proteins[338,339] can be activated. Subsequently, proteins such as JNK[340] and the MAPK p38[341,342] are activated. It appears PP2A may play a role in a number of these pathways. TAK-1 is a kinase activated in response to TGB β 1 signalling and is important for TGF β 1 signal transduction.[343] Upon stimulation, TAK-1 is autophosphorylated on the threonine residue 187 in the TAK-1 activation loop. PP2A has been shown to dephosphorylate TAK-1 at this residue and inactivate the protein[344], inhibiting the signalling of various downstream cascades such as JNK, p38 and NF kappa β (this inhibition however is dependent on the cell type and signalling context).[345] TGF β has been shown to activate PP2A in response to mitogenic signalling, which in turn dephosphorylates and inactivates retinoblastoma protein to inhibit fibroblast proliferation.[346] TGF β 1 has also been found to activate PP2A in normal chondrocytes.[347] PP2A is also thought to play a role in TGF β inhibition of EGF stimulated cell proliferation in Smad4 deficient cells. Upon EGF stimulation, TGF-β activated a serine/threonine phosphatase thought to be PP2A, via a Smad4 independent pathway, which resulted in ERK2 deactivation. PP2A has been found to interact with the TGF β receptor complex and JNK, and is known to dephosphorylate activated MEK and ERK. Interestingly a study by Batut *et al*. (2008) found that depending on the β regulatory subunit within the PP2A holoenzyme, TGF β/Activin/Nodal signalling during Xenopus embryo development may be positively or negatively regulated.

6.4.5.4 Angiopoietin 1, ANGP1

Angiopoietin 1 (Ang1) is an important survival factor for endothelial cells forming immature vasculature during angiogenesis and was altered -1.70 fold in the SET siRNA treated cells compared to negative control cells. Ang1 is an activating ligand of Tie-2, an endothelium specific receptor tyrosine kinase.

Binding of Ang1 to the Tie2 extracellular domain induces phosphorylation of the Tie2 intracellular tyrosine kinase domain [348]. Activated Tie2 then binds to the Src homology domain containing adaptor protein Grb7 that phosphorylates the p85 subunit of PI3K. Activated PI3K can induce Akt, FAK, Rho1/Rac1, ERK1/2 or eNOS signalling.[349] Activation of Tie-2 by Ang1 has not been shown to induce endothelial cell proliferation, but has been shown to induce endothelial cell migration, vessel tube formation, sprouting and cell survival.[349] Ang1 has also been shown to have anti-permeability and anti-inflammatory functions. Neither Ang1 nor Tie-2 have been shown to interact with SET or PP2A. However, PI3K signalling is essential for Ang1 function[349] and PP2A has been shown to regulate PI3K. The α isoform of the PP2A regulatory subunit A has been shown to act as a tumour suppressor via the negative regulation of PI3K. Mutations in the A α PP2A subunit have been shown to lead to PI3K/Akt pathway activation.[350] [351] Ang1 was decreased by 41% in the SET siRNA knock down cells. PP2A activity would have been increased in these cells and may have resulted in increased suppression of PI3K. This would have led to a reduction in Ang1/Tie2/PI3K signalling in the SET siRNA treated cells.

6.4.5.5 ITG1, Integrin β 1

Integrins are a family of heterodynamic transmembrane receptors comprised of an α and β subunit. There are eighteen β subunits and eight α subunits that can bind to form 24 different receptors. β 1 subunits containing integrins form the largest sub-group of integrins, forming twelve receptors with different ligand-binding properties (reviewed in [352]). Integrins mediate cell matrix interactions and cellular adhesion, and can activate and mediate cell signalling pathways in conjunction with growth factor induced signals.

Integrin β 1 (ITGB1) was altered in expression by -1.77 fold in the SET isRNA treated SW480 cells compared to negative control cells. The interaction of integrins and PP2A has been previously described. Mulrooney *et al*. (2000) showed PP2A co-localises with ITGB1 at focal adhesion sites, and the dephosphorylation of ITGB1 at serine 785 is required for movement in focal adhesion sites. Treatment of parietal endoderm cells with the PP2A inhibitor, okadiac acid, increased the level of ITGB1 phosphorylation and resulted in the selective removal of ITGB1 from focal adhesion sites, indicating PP2A is required for ITGB1 adhesion. PP2A is also important in ITGB2 cell adhesion (Brockdorff 2007). Ivaska *et al*. (2002)[353] found that α 2 β 1 integrin binding to collagen activates PP2A. Activated PP2A then dephosphorylates and inactivates Akt.

ITGB3 was also found to be decreased in the SET siRNA knock down cells by 38%. ITGB3 is the main platelet integrin, and PP2Ac associates constitutively with ITGB3 in resting platelets and HEK cells.[354] During platelet adhesion when ITGB3 binds to fibrogen, PP2A activity and association with ITGB3 is

decreased. Overexpression of PP2Ac decreases ITGB3 mediated fibrogen binding. Knocking down PP2Ac expression increases ERK1/2 activity, and increases the adhesion of ITGB3 to fibrogen and von Willebrand factor. Via this mechanism PP2Ac can negatively regulate ITGB3 signalling and adhesion via ERK1/2 suppression.[354]

6.4.5.6 V-Ets erythroblastosis virus E26 oncogene homolog 2, EST2

The Ets (E26 transformation specific) proteins form a family of transcription factors with over 30 evolutionarily conserved members. They are the target of a number of major signalling pathways induced by the activation of the closely related EGFR and HER2/Neu pathways.[355] The Ets2 protein has been shown to play a role in cell proliferation and tumour progression, and contains a MAP kinase phosphorylation domain (reviewed in [356]). Inhibition of Ets2 has shown to reduce tumourigenicity[357] [358] and overexpression has shown to increase proliferation and tumourigenicity.[359] In the SET siRNA treated SW480 cells, Ets2 was increased in expression by 1.63 fold compared to negative control cells.

Telomerase activity is regulated positively by the phosphorylation of hTERT by PKC and negatively by dephosphorylation by PP2A.[167,168] The hTERT promoter has a number of transcription factor and repressor binding sites. The oncogene c-myc is a primary transcription factor of hTERT. EGF may also stimulate hTERT via MAPK activity, and TGF β has been shown to inhibit hTERT transcription.[168] Overexpression of Ets2 induces hTERT gene promoter activity.[360] Ets2 acts as a transcription factor for c-myc, which drives hTERT expression. Ets2 has also been shown to bind to the hTERT gene promoter[361] and may directly stimulate hTERT transcription. Hence SET knock down could encourage hTERT activity, which is required to maintain telomere length in carcinoma cells, via Ets2 overexpression.

6.4.6 SET as a therapeutic target of CRC

The data obtained form the RT^2 Profiler PCR Array 'Human Cancer Pathway Finder' plates suggest that SET may have potential as a therapeutic target in some signalling pathways. However, this work needs to be repeated as the data displayed and discussed here is only preliminary. The expression of genes at the protein level in the SET siRNA knock down cells needs to be analysed as RNA and protein levels within a cell do not always correlate. Reducing SET levels in the SW80 cells led to a decrease in the anti-apoptotic Bcl-2, a decrease in Gzma which targets tumour cells for apoptosis and activates the tumour metastasis suppressor NM23-H1, a decrease in the inhibitor of angiogenesis Tsp-1, a decrease in the Ang-1, a promoter of angiogenesis, plus a decrease in ITGB 1 which leads to reduced cell adhesion and may promote cell metastasis. However, reducing SET levels also led to an increase in

Est-2, a gene known to promote cell proliferation, tumourigenicity and hTERT expression, which results in the positive regulation of telomerase and hence promotes tumour growth.

The use of SET as a therapeutic target could be problematic given SET interacts with and influences several proteins and pathways, with some that positively regulate cancer progression and some that negatively regulate cancer progression. Compounding to this problem is that fact that SET influences a large number of signalling pathways based on interaction with PP2A. This could be problematic as the regulatory B subunits of PP2A have many and varied roles and in some cases the same B subunit may even have the potential to act as a positive or negative regulator of the same pathway.

6.5 Conclusion

SET appears to be a good RT-PCR marker of CRC, with early stage tumours having the same level of increased SET expression as late stage tumours. Given SET is upregulated in 75% of patients by ≥2 fold, SET could have use as part of a panel of markers in the immunobead RT-PCR technique. In cells containing a Wnt signalling pathway mutation, reducing SET levels has no effect on β catenin, but reducing SET levels in epithelial cells with no Wnt pathway mutations leads to a significant reduction (25%) in β catenin levels. Preliminary data from the RT Profiler arrays suggested SET may have use as a therapeutic target for CRC, however the full potential of SET in this area remains to be elucidated. Proteomic profiling of SET knock down cells to analyse the effect of reduced SET expression on oncogenic and tumour suppressor proteins would help determine the use of SET as a therapeutic target.

7 Final Discussion

7.1 The interactions of the proteins of interest

This thesis has established desmin, SET and CK8 to be upregulated in CRC. The signalling pathways in which these proteins are involved can be linked and related to tumour progression. The interaction of SET and PP2A is not only relevant to the Wnt signalling pathway, but also relevant to CK8 phosphorylation by ERK, and to angiogenesis resulting in the recruitment of desmin expressing pericyte cells. Fig. 1 details the interacting pathways.

7.1.1 SET/ PP2A and ERK/ CK8

The effect of PP2A on the Ras/Raf/MEK/ERK signalling pathway has direct relevance to CK8 phosphorylation levels. PP2A has been shown to dephosphorylate the serine residue 431 in response to hypo-osmotic stress in HT29 cells, however under these conditions of hypo-osmotic stress the dephosphorylation of the serine residue 73 by PP2A was not observed.[362] Hence, increased expression of SET in CRC may promote increased CK8 PS431 levels.

PP2A is also known to dephosphorylate and inactivate MEK1/2 and ERK1/2[363 364], which would result in reduced CK8 PS73 and PS431 levels. Treatment of cells with the PP2A inhibitors, okadaic acid and SV40 small T antigen, have been shown to induce MEK and ERK phosphorylation and activity.[363 364] The interaction of a number of the PP2A B subunits with ERK has been studied. PP2A holoenzymes containing PR56 have the ability to inhibit ERK1/2 phosphorylation in drosophila S2 cells.[365] Interestingly, growth factor induction of the early response gene IEX-1, a known substrate of ERK, results in the phosphorylation of PR56 by ERK and causes the dissociation of PP2A subunits from the holoenzyme, resulting in the protection of ERK from dephosphorylation.[366] In the human neuronal PC6–3 cells, overexpression of the B55 gamma subunit induces ERK activity, whereas overexpression of B55 α and δ subunits result in ERK dephosphorylation and inhibition[367 368], displaying how PP2A can be a positive or negative regulator of the same protein, based on the regulatory B subunit present in the holoenzyme.

PP2A also regulates the Ras/Raf/MEK/ERK signalling pathway upstream of MEK and ERK. PP2A is able to bind to the adapter protein, Shc, which binds to Grb2 and the intracellular domain of the signalling receptor resulting in the activation of Ras, preventing the tyrosine phosphorylation of Shc and inhibiting the signal progression.[369] It has also been suggested that PP2A can positively regulate Raf-1 signalling[370], as PP2A can dephosphorylate critical sites on Raf-1 and KSR, a Raf-1 binding partner and scaffold protein, allowing their recruitment to the membrane and participation in the signalling cascade.[371 372] PP2A also works in conjunction with prolylisomerase to dephosphorylate critical inhibitory sites on Raf-1 that prevent activation.[373]

Fukukawa *et al*. (2005)[318] studied the effect of SET on MEK and ERK activation. As SET is a potent inhibitor of PP2A, as is okadaic acid, it was predicted that increased expression of SET would also lead to increased activation of the Ras/Raf/MEK/ERK pathway. However, overexpression of SET suppressed MEK and ERK activation following EGF stimulation, while the knock down of SET promoted MEK and ERK activation. Fukukawa *et al*. (2005)[318] had several possible explanations for this. They found SET to be localised to the nucleus, in contrast to okadaic acid, which is active in the cytoplasm. Okadaic acid is able to inhibit cytoplasmic PP2A, stopping the dephosphorylation of activated ERK, unlike nuclear localised SET. It has also been reported that the inhibitory activity of SET on PP2A depends on the binding substrate of PP2A[167] and SET may be unable to inhibit PP2A when bound to phosphorylated ERK. Fukukawa *et al.* (2005)[318] found that half of all cellular SET was associated with nuclear matrix or chromatin, where it may enhance the phosphorylation status of transcriptional regulators via the inhibition of PP2A, leading to an increase transcription and expression of certain genes. Via this indirect mechanism, the expression of certain genes may result in decreased activated MEK. Taken in context, this would suggest increased levels of SET in CRC would inhibit ERK activity, resulting in decreased levels of CK8 phosphorylation. However, this is an over simplified statement given the Ras/Raf/MEK/ERK is regulated at multiple stages throughout the pathway by a number of different proteins. CK8 is also phosphorylated by kinases other then ERK, plus a large percentage of CRC patients develop Ras and Raf mutations which result in constitutive pathway activation regardless of other factors.

7.1.2 SET/ PP2A and desmin

In the SET siRNA knock down cells compared to mock transfection control cells angiopoietin 1 (Ang1) was found to have a fold change reduction of -1.70, using the RT Profiler Array plates. Interestingly, Ang1 is involved in angiogenesis and the recruitment of desmin expressing pericytes and PP2A is involved in the regulation of Ang1 signalling. PDGF has been shown to regulate Ang1 expression in mural cells, with increased expression of PDGF, resulting in increased expression of Ang1[374] and decreased expression of PDGF, resulting in decreased expression of Ang1.[375] The regulation of Ang1 by PDGF is thought to be via the PI3K pathway[374] with increased levels of PDGF stimulating the production of Ang1. Ang1 then binds to its receptor, Tie2, activating Grb7, and resulting in the phosphorylation and activation of PI3K. PI3K activation then leads to the activation of ERK1/2 or the Akt/mTor pathway, which results in the expression of VEGF. During the process of angiogenesis VEGF production by pericytes stimulates the proliferation and chemo-attraction of endothelial cells, prevents endothelial cell apoptosis and maintains the viability of immature blood cells.[207] In return, endothelial cells express PDGF, which attracts migrating pericytes to newly-formed blood vessels. PP2A negatively regulates PI3K, resulting in the inhibition of VEGF and ultimately PDGF production, hence increased levels of SET would inhibit PP2A, thus aiding in the process of angiogenesis and pericyte recruitment.

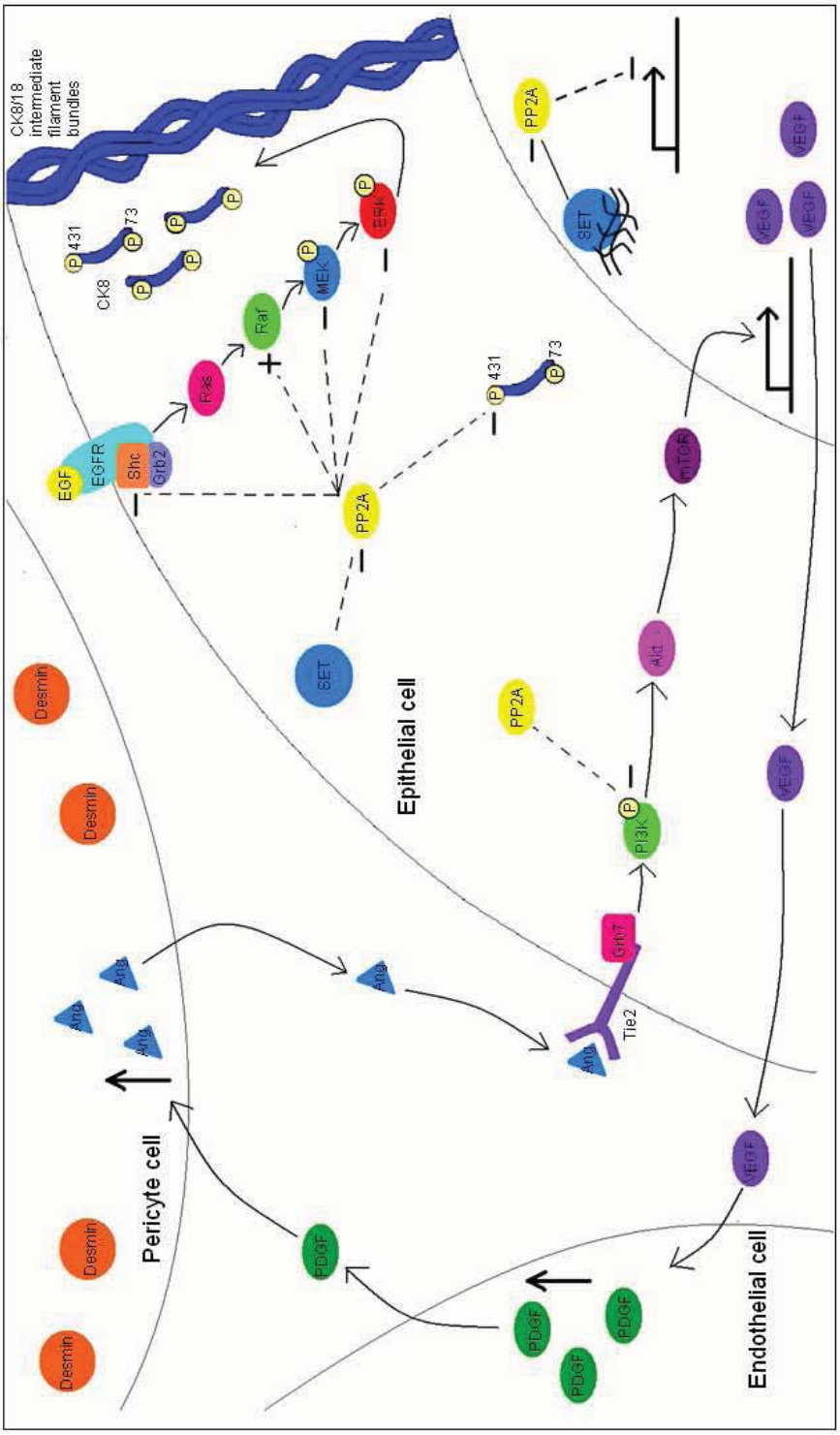

Fig 1. The interactions of the proteins of interest. Increased EGFR/Ras Raf/MEK/ERK signalling results in increased CK8 phosphorylation at serine residues 73 and 431. PP2A has the ability to regulate this signalling pathway at multiple points via the inhibition of Shc, MEK, and ERK, or the positive regulation of Raf. PP2A is also able to dephosphorylate CK8 at PS431, hence increased SET levels may promote increased PS431 levels via the inhibition of PP2A. There is evidence to suggest that chromatin associated nuclear SET enhances the phosphorylation of transcriptional regulators via the inhibition of PP2A, leading to an increase transcription and expression of certain genes that may indirectly result in decreased activation of MEK. PP2A is also involved in the regulation of PI3K/Akt/mTOR signalling. During angiogenesis endothelial cells increase their expression and secretion of PDGF in order to attract desmin expressing pericyte cells to coat newly-formed blood vessels. PDGF stimulates the expression of Ang1 by pericytes, which is secreted and binds to the Tie2 receptor. Tie2 signalling results in the activation of Grb7, leading to PI3K phosphorylation, Akt and mTOR activation, and VEGF expression. VEGF may then bind to its receptors on endothelial cells stimulating the expression of PDGF, creating a feedback loop. PP2A can dephosphorylate and inactivate PI3K, inhibiting this signalling loop. Overexpression of SET would result in continuing activation of the signalling loop.

7.2 Critical review of the biomarker discovery process

The aim of the biomarker discovery phase of this project was to identify proteins significantly increased in abundance in cancerous colon tissue compared to matched normal epithelial cells. This was achieved by the collection of samples using LMD and the separation and identification of proteins by 2D DIGE and LC MS/MS. One great advantage of using IEF with SDS PAGE is the high level of resolution obtainable. This is due to the total physicochemical independence of the two parameters used to separate the proteins; pI and MW. Other advantages include the fast resolution of samples and the relatively low cost of the technique. The pI and MW of protein spots on a 2D gel can also be calculated, which aid in protein identification or following protein identification may give clues as to whether the protein was modified or truncated.

However, 2DE also has some significant disadvantages in the resolution of proteins with more extreme characteristics. For examples proteins with extreme pH and proteins of high (>250 kDa) and low (<15 kDa) MW are difficult to resolve. Another significant problem with 2DE is the loss of very hydrophobic proteins from buffer solutions as they tend to precipitate. These criticisms are reflected in the set of 8 DIGE gels presented in Chapter 3. All of the proteins identified have 'average' parameters in terms of pI and MW, and all were relatively hydrophilic. For instance, the apparent pI of the identified proteins ranged from 3.9 to 6.2, with apparent MW ranging from 29 kDa to 85 kDa. Hence there may have been a number of proteins of interest that were too large or small, too hydrophobic to be resolved and detected by 2D DIGE.

The issues involving the resolution of proteins with a more extreme pI or MW could have been resolved, to an extent, by running more than 1 2D DIGE gel per sample. Running the same samples over gels with differing polyacrylamide percentages or gradients would allow for better resolution of high and low MW proteins. For example, 8% polyacrylamide gels could be used to resolve higher MW proteins and 8-15% polyacrylamide gels could be used to separate and resolve MW proteins with a mid-range MW. Tris-tricine PAGE, as opposed to tris-glycine PAGE (used throughout this study), could be used to capture and resolve lower MW proteins. The resolution and identification of proteins with a more extreme pI could have been achieved using multiple IPG strips with differing pH gradients. For example, acidic proteins could be separated using pH 3-5.6 IPG strips, more neutral proteins using pH 5.3-6.5 IPG strips and basic proteins using pH 7-11 strips. The use of such IPG strips would have also given greater sample separation, resulting in the visualization and analysis of more proteins. Unfortunately in this instance samples could not be run over several gels for 2 main reasons; time and low sample yields. The first stage of the biomarker discovery process involved sample collection via LMD. The biggest limitation of LMD is the small sample yield obtainable in a given time period. For this reason only enough protein was collected to run a single 2D DIGE

experiment per sample. Despite the low protein yields obtainable, the limitations of LMD were out-weighed by the importance of working with enriched tumour and normal epithelial cell populations.

7.3 Future Directions

7.3.1 DIGE study

From the minimal labelling DIGE study, seventeen individual proteins were identified as being significantly upregulated by ≥2 fold, a number of protein spots were also detected as significantly decreased in the tumour compared to matched normal tissues. Proteins downregulated in the tumour samples were not chosen for further analysis in this work as upregulated proteins are easier to detect, hence more suitable as biomarkers. However, the identification of proteins downregulated in CRC would potentially advance the detailing of the molecular pathways involved in the development of the disease and elucidate potential therapeutic targets. Identifying the significantly downregulated proteins, verifying their downregulation in a larger cohort of patients and analysing the effect of driving protein expression on tumour cell proliferation, apoptosis, invasion and adhesion could form the basis of another project. The mining of the minimal labelling DIGE gels for more information is of value given the analysis was performed on laser microdissected tissue, making the experiment more sensitive and specific. The collection of samples was unique, and to my knowledge, this is the only study that had been performed with LMD tissue and minimal labelling DIGE on CRC.

7.3.2 Desmin as a marker of staging and anti-angiogenic therapies

Currently the staging of colorectal cancer relies heavily on the analysis of sampled lymph nodes, with the presence of lymph node metastasis being the most important prognostic factor in determining the 5-year survival of patients. Correlations between the number of lymph nodes sampled and survival rates for stage II patients have been reported[376 377], with inadequate lymph node sampling resulting in a failure to find metastasis positive nodes and ultimately under staging. This means stage III patients, misdiagnosed as stage II patients, may not be offered potentially beneficial adjuvant therapy. The College of American Pathologists recommends a minimum of twelve lymph nodes be sampled and analysed.[378] A study by Chen *et al*. (2006)[378] analysed the compliance of American surgeons with the suggested guidelines and the overall survival associated with the compliance. They found that the resection of too few lymph nodes was a poor prognostic indicator and that the sampling of at least fifteen nodes increased the median overall survival by 11 months in stage I patients, 54 months in stage II patients, and 21 months in stage III patients. This was due to the upstaging of patients to the correct category and subsequently the provision of the correct

treatment and application of adjuvant therapy. This work shows that lymph node sampling to determine stage in CRC can be inadequate.

The histopathological staining for the level of desmin expression by immunofluorescence appeared to differentiate early from late stage patients well. Histopathology is routinely performed on resected tumour tissues following surgery and desmin could be included in this staining to be used in conjunction with lymph node analysis to aid in the staging of patients. Future directions for this work include a study analysing the survival benefits for staging patients using lymph node sampling plus desmin histopathology.

7.3.3 CK8

There is evidence to suggest that high levels of CK8 phosphorylation lead to reduced CK8 degradation[265 271 158] caused by increased intermediate filament disassembly and solubilisation.[265 271 158] Increasing CK8 resistance to degradation may increase cellular resistance to apoptosis, therefore increased levels of phosphorylated CK8 may aid in cancer cell survival. The mechanism by which CK8 phosphorylation and solubilisation makes the protein resistant to degradation is of interest. CK8 is thought to aid in the inhibition of apoptosis by acting act as a phosphate 'sink', inhibiting phospho-activation of pro-apoptotic substrates by stress activated protein kinases.[265] Further elucidation of this mechanism may give further insight as to how carcinoma cells evade apoptosis.

7.3.4 SET

Seventy-five percent of patients had a tumour to normal SET expression ratio of >2 fold as determined by relative real-time RT-PCR. These results suggest SET has potential use as a marker in the RT-PCR panel used to detect tumour cells extracted from patient's lavage and blood samples, following surgery, by the immunobead technique. The tumour-normal expression level of SET between stage I, stage II and stage III patients was not significantly different, hence SET has the potential to be a marker of early through to late stage patients. To properly determine the usefulness of SET as a RT-PCR marker in the immunobead technique, future work may include assessing the level of SET expression in single normal epithelial cell compared to a tumour cell, plus looking at SET expression in monocytes and lymphocytes, as a small number may be non-specifically captured by the immunobeads hence low/no SET expression in these cells would be ideal.

The preliminary data collected analysing the RNA profile of the SET siRNA knock down SW480 cells using the RT Profiler arrays suggests SET may have potential as a therapeutic target. At the RNA level, a number of genes that promote cancer were downregulated, however a small number of genes that promote cancer

were upregulated. It is also important to note that the RNA and protein levels within a cell do not necessarily correlate and a way to more accurately assess the potential of SET as a therapeutic target would be to perform proteomic profiling experiments on SET siRNA knock down cells compared to control cells. In-depth sensitive analysis of samples could be achieved following SET siRNA treatment by DIGE labelling cell lysates, fractionating the lysates prior to 2DE by in-solution IEF (allowing proteins to be separated into small pI ranges, eg pH 3–4, 4–5, 5–6 etc.) and performing 2DE on each fraction with IPG strips selected according to the pI of the proteins within the fraction. This allows for more in-depth mining of proteins as opposed to the analysis of whole cell lysates on a single gel. Following separation by 2DE gels, this could be analysed using the DeCyder software, determining protein spots that were increased or decreased in expression as a result of SET knock down, with the proteins of interest being identified using LC-MS/MS. Other forms of sensitive analysis include quantitative label free mass spectrometry. Such experiments would elucidate important regulatory roles and pathways of SET that may not be uncovered using arrays with designated targets. If SET were to be seriously considered as a therapeutic target, these experiments would be imperative as every effect of reducing SET levels would need to be uncovered to assess not only its therapeutic potential, but also its safety.

7.4 Concluding remarks

To my knowledge this is the first study to analyse laser microdissect CRC tissue using minimal labelling 2D DIGE with LC-MS/MS. From this work, seventeen individual proteins were found to be significantly increased in expression ≥2 fold in the tumour compared to matched normal tissues. From this profiling study, the phosphorylation levels of the protein CK8 were chosen for further analysis and were found to be significantly increased in tumours in a larger cohort of patients, at least in part due to increased Ras/Raf/MEK/ERK signalling. Increased phosphorylation of CK8 is known to inhibit protein degradation and may aid in evading tumour cell apoptosis. The protein SET was also chosen from the profiling study and was found to be upregulated in a larger cohort of patients, giving it potential as an immunobead RT-PCR panel marker. SET may also have potential as a therapeutic target for CRC, however this needs further elucidation. Finally the protein desmin was analysed and was found to have potential as an immunohistochemistry marker for the staging of patients, which may aid in determining the treatment course patients are given following tumour resection surgery. Desmin may also have potential as a marker for determining the potential efficacy of anti-angiogenic therapies in patients.

8 References

1. Grothey, A. & Sargent, D. Overall survival of patients with advanced colorectal cancer correlates with availability of fluorouracil, irinotecan, and oxaliplatin regardless of whether doublet or single-agent therapy is used first line. *J Clin Oncol* **23**, 9441-2 (2005).

2. Lichtenstein, P. et al. Environmental and heritable factors in the causation of cancer--analyses of cohorts of twins from Sweden, Denmark, and Finland. *N Engl J Med* **343**, 78-85 (2000).

3. Rustgi, A. K. The genetics of hereditary colon cancer. *Genes Dev* **21**, 2525-38 (2007).

4. Cheah, P. Y. Recent advances in colorectal cancer genetics and diagnostics. *Crit Rev Oncol Hematol* **69**, 45-55 (2009).

5. Kinzler, K. W. et al. Identification of FAP locus genes from chromosome 5q21. *Science* **253**, 661-5 (1991).

6. Nishisho, I. et al. Mutations of chromosome 5q21 genes in FAP and colorectal cancer patients. *Science* **253**, 665-9 (1991).

7. Groden, J. et al. Identification and characterization of the familial adenomatous polyposis coli gene. *Cell* **66**, 589-600 (1991).

8. Saito, T. et al. Possible Association Between Higher [bgr]-Catenin mRNA Expression and Mutated [bgr]-Catenin in Sporadic Desmoid Tumors: Real-Time Semiquantitative Assay by TaqMan Polymerase Chain Reaction. **82**, 97-103 (0000).

9. Fishel, R. et al. The human mutator gene homolog MSH2 and its association with hereditary nonpolyposis colon cancer. *Cell* **75**, 1027-38 (1993).

10. Parsons, R. et al. Hypermutability and mismatch repair deficiency in RER+ tumor cells. *Cell* **75**, 1227-36 (1993).

11. Vasen, H. F. & Boland, C. R. Progress in genetic testing, classification, and identification of Lynch syndrome. *Jama* **293**, 2028-30 (2005).

12. Aaltonen, L. A. et al. Clues to the pathogenesis of familial colorectal cancer. *Science* **260**, 812-6 (1993).

13. Ionov, Y., Peinado, M. A., Malkhosyan, S., Shibata, D. & Perucho, M. Ubiquitous somatic mutations in simple repeated sequences reveal a new mechanism for colonic carcinogenesis. *Nature* **363**, 558-61 (1993).

14. Sieber, O. M. et al. Myh deficiency enhances intestinal tumorigenesis in multiple intestinal neoplasia (ApcMin/+) mice. *Cancer Res* **64**, 8876-81 (2004).

15. Al-Tassan, N. et al. Inherited variants of MYH associated with somatic G:C-->T:A mutations in colorectal tumors. *Nat Genet* **30**, 227-32 (2002).

16. Farrington, S. M. et al. Germline susceptibility to colorectal cancer due to base-excision repair gene defects. *Am J Hum Genet* **77**, 112-9 (2005).

17. Hemminki, A. et al. A serine/threonine kinase gene defective in Peutz-Jeghers syndrome. *Nature* **391**, 184-7 (1998).

18. Tiainen, M., Ylikorkala, A. & Makela, T. P. Growth suppression by Lkb1 is mediated by a G(1) cell cycle arrest. *Proc Natl Acad Sci U S A* **96**, 9248-51 (1999).

19. Collins, S. P., Reoma, J. L., Gamm, D. M. & Uhler, M. D. LKB1, a novel serine/threonine protein kinase and potential tumour suppressor, is phosphorylated by cAMP-dependent protein kinase (PKA) and prenylated in vivo. *Biochem J* **345 Pt 3**, 673-80 (2000).

20. Sapkota, G. P. et al. Phosphorylation of the protein kinase mutated in Peutz-Jeghers cancer syndrome, LKB1/STK11, at Ser431 by p90(RSK) and cAMP-dependent protein kinase, but not its farnesylation at Cys(433), is essential for LKB1 to suppress cell vrowth. *J Biol Chem* **276**, 19469-82 (2001).

21. Marignani, P. A., Kanai, F. & Carpenter, C. L. LKB1 associates with Brg1 and is necessary for Brg1-induced growth arrest. *J Biol Chem* **276**, 32415-8 (2001).

22. Karuman, P. et al. The Peutz-Jegher gene product LKB1 is a mediator of p53-dependent cell death. *Mol Cell* **7**, 1307-19 (2001).

23. Martin, S. G. & St Johnston, D. A role for Drosophila LKB1 in anterior-posterior axis formation and epithelial polarity. *Nature* **421**, 379-84 (2003).

24. Shaw, R. J. et al. The tumor suppressor LKB1 kinase directly activates AMP-activated kinase and regulates apoptosis in response to energy stress. *Proc Natl Acad Sci U S A* **101**, 3329-35 (2004).

25. Woods, A. et al. LKB1 is the upstream kinase in the AMP-activated protein kinase cascade. *Curr Biol* **13**, 2004-8 (2003).

26. Giardiello, F. M., Brensinger, J. D. & Petersen, G. M. AGA technical review on hereditary colorectal cancer and genetic testing. *Gastroenterology* **121**, 198-213 (2001).

27. Howe, J. R. et al. Germline mutations of the gene encoding bone morphogenetic protein receptor 1A in juvenile polyposis. *Nat Genet* **28**, 184-7 (2001).

28. Howe, J. R. et al. Mutations in the SMAD4/DPC4 gene in juvenile polyposis. *Science* **280**, 1086-8 (1998).

29. Young, J. & Jass, J. R. The case for a genetic predisposition to serrated neoplasia in the colorectum: hypothesis and review of the literature. *Cancer Epidemiol Biomarkers Prev* **15**, 1778-84 (2006).

30. Miyoshi, Y. et al. Somatic mutations of the APC gene in colorectal tumors: mutation cluster region in the APC gene. *Hum Mol Genet* **1**, 229-33 (1992).

31. Thibodeau, S. N. et al. Microsatellite instability in colorectal cancer: different mutator phenotypes and the principal involvement of hMLH1. *Cancer Res* **58**, 1713-8 (1998).

32. Bettstetter, M. et al. Distinction of hereditary nonpolyposis colorectal cancer and sporadic microsatellite-unstable colorectal cancer through quantification of MLH1 methylation by real-time PCR. *Clin Cancer Res* **13**, 3221-8 (2007).

33. Dionigi, G. et al. Differences between familial and sporadic forms of colorectal cancer with DNA microsatellite instability. *Surg Oncol* **16 Suppl 1**, S37-42 (2007).

34. Domingo, E. et al. BRAF screening as a low-cost effective strategy for simplifying HNPCC genetic testing. *J Med Genet* **41**, 664-8 (2004).

35. Kambara, T. et al. Role of inherited defects of MYH in the development of sporadic colorectal cancer. *Genes Chromosomes Cancer* **40**, 1-9 (2004).

36. Colebatch, A. et al. The role of MYH and microsatellite instability in the development of sporadic colorectal cancer. *Br J Cancer* **95**, 1239-43 (2006).

37. Potter, J. D. Colorectal cancer: molecules and populations. *J Natl Cancer Inst* **91**, 916-32 (1999).

38. Papapolychroniadis, C. Environmental and other risk factors for colorectal carcinogenesis. *Tech Coloproctol* **8 Suppl 1**, s7-9 (2004).

39. Satia, J. A. et al. Diet, lifestyle, and genomic instability in the North Carolina Colon Cancer Study. *Cancer Epidemiol Biomarkers Prev* **14**, 429-36 (2005).

40. Gunter, M. J. & Leitzmann, M. F. Obesity and colorectal cancer: epidemiology, mechanisms and candidate genes. *J Nutr Biochem* **17**, 145-56 (2006).

41. Reya, T. & Clevers, H. Wnt signalling in stem cells and cancer. **434**, 843-850 (2005).

42. He, X., Semenov, M., Tamai, K. & Zeng, X. LDL receptor-related proteins 5 and 6 in Wnt/beta-catenin signaling: arrows point the way. *Development* **131**, 1663-77 (2004).

43. Komiya, Y. & Habas, R. Wnt signal transduction pathways. *Organogenesis* **4**, 68-75 (2008).

44. Giles, R. H., van Es, J. H. & Clevers, H. Caught up in a Wnt storm: Wnt signaling in cancer. *Biochimica et Biophysica Acta (BBA) - Reviews on Cancer* **1653**, 1-24 (2003).

45. Ikeda, S., Kishida, M., Matsuura, Y., Usui, H. & Kikuchi, A. GSK-3beta-dependent phosphorylation of adenomatous polyposis coli gene product can be modulated by beta-catenin and protein phosphatase 2A complexed with Axin. *Oncogene* **19**, 537-45 (2000).

46. Seeling, J. M. et al. Regulation of beta-catenin signaling by the B56 subunit of protein phosphatase 2A. *Science* **283**, 2089-91 (1999).

47. Mao, J. et al. Low-density lipoprotein receptor-related protein-5 binds to Axin and regulates the canonical Wnt signaling pathway. *Mol Cell* **7**, 801-9 (2001).

48. Zeng, X. et al. Initiation of Wnt signaling: control of Wnt coreceptor Lrp6 phosphorylation/activation via frizzled, dishevelled and axin functions 10.1242/dev.013540. *Development* **135**, 367-375 (2008).

49. Yamamoto, H. et al. Phosphorylation of Axin, a Wnt Signal Negative Regulator, by Glycogen Synthase Kinase-3beta Regulates Its Stability 10.1074/jbc.274.16.10681. *J. Biol. Chem.* **274**, 10681-10684 (1999).

50. van de Wetering, M. et al. Armadillo Coactivates Transcription Driven by the Product of the Drosophila Segment Polarity Gene dTCF. *Cell* **88**, 789-799 (1997).

51. Giese, K., Cox, J. & Grosschedl, R. The HMG domain of lymphoid enhancer factor 1 bends DNA and facilitates assembly of functional nucleoprotein structures. *Cell* **69**, 185-195 (1992).

52. Roose, J. et al. The Xenopus Wnt effector XTcf-3 interacts with Groucho-related transcriptional repressors. **395**, 608-612 (1998).

53. Brantjes, H., Roose, J., van de Wetering, M. & Clevers, H. All Tcf HMG box transcription factors interact with Groucho-related co-repressors 10.1093/nar/29.7.1410. *Nucl. Acids Res.* **29**, 1410-1419 (2001).

54. Laurent-Puig, P., Beroud, C. & Soussi, T. APC gene: database of germline and somatic mutations in human tumors and cell lines 10.1093/nar/26.1.269. *Nucl. Acids Res.* **26**, 269-270 (1998).

55. Bienz, M. & Clevers, H. Linking colorectal cancer to Wnt signaling. *Cell* **103**, 311-20 (2000).

56. Samowitz, W. S. et al. {beta}-Catenin Mutations Are More Frequent in Small Colorectal Adenomas Than in Larger Adenomas and Invasive Carcinomas. *Cancer Res* **59**, 1442-1444 (1999).

57. Morin, P. J. et al. Activation of beta -Catenin-Tcf Signaling in Colon Cancer by Mutations in beta -Catenin or APC
10.1126/science.275.5307.1787. *Science* **275**, 1787-1790 (1997).

58. AIHW. in *Cancer* (ed. 2004, A. I. o. H. a. W. A. a. t. A. A. o. C. R. A.) (Canberra, 2004).

59. AIHW. in *Cancer* (ed. (AACR), A. I. o. H. a. W. A. a. t. A. A. o. C. R.) (Canberra, 2003).

60. Registry, S. A. C. *Epidemiology of Cancer in South Australia. Incidence, Mortality and Survival 1977 to 1996.* (Open book, Adelaide, 1997).

61. Cascinu, S. et al. Colorectal cancer in the adjuvant setting: perspectives on treatment and the role of prognostic factors 10.1093/annonc/mdg725. *Ann Oncol* **14**, ii25-29 (2003).

62. Locker, G. Y. et al. ASCO 2006 update of recommendations for the use of tumor markers in gastrointestinal cancer. *J Clin Oncol* **24**, 5313-27 (2006).

63. Liefers, G. J. et al. Micrometastases and survival in stage II colorectal cancer. *N Engl J Med* **339**, 223-8 (1998).

64. McArdle, C. ABC of colorectal cancer: effectiveness of follow up. *Bmj* **321**, 1332-5 (2000).

65. Lloyd, J. M. et al. Identification of Early-Stage Colorectal Cancer Patients at Risk of Relapse Post-Resection by Immunobead Reverse Transcription-PCR Analysis of Peritoneal Lavage Fluid for Malignant Cells 10.1158/1078-0432.CCR-05-1473. *Clin Cancer Res* **12**, 417-423 (2006).

66. Schott, A. et al. Isolated tumor cells are frequently detectable in the peritoneal cavity of gastric and colorectal cancer patients and serve as a new prognostic marker. *Ann Surg* **227**, 372-9 (1998).

67. Hardingham, J. E. et al. Immunobead-PCR: a technique for the detection of circulating tumor cells using immunomagnetic beads and the polymerase chain reaction. *Cancer Res* **53**, 3455-8 (1993).

68. Guller, U. et al. Disseminated single tumor cells as detected by real-time quantitative polymerase chain reaction represent a prognostic factor in patients undergoing surgery for colorectal cancer. *Ann Surg* **236**, 768-75; discussion 775-6 (2002).

69. Litvinov, S. V. et al. Expression of Ep-CAM in cervical squamous epithelia correlates with an increased proliferation and the disappearance of markers for terminal differentiation. *Am J Pathol* **148**, 865-75 (1996).

70. Pokorny, R. M., Hunt, L. & Galandiuk, S. What's new with tumor markers for colorectal cancer? *Dig Surg* **17**, 209-15 (2000).

71. Crawford, N. P., Colliver, D. W. & Galandiuk, S. Tumor markers and colorectal cancer: utility in management. *J Surg Oncol* **84**, 239-48 (2003).

72. Fletcher, R. H. Carcinoembryonic antigen. *Ann Intern Med* **104**, 66-73 (1986).

73. McIver, C. M., Lloyd, J. M., Hewett, P. J. & Hardingham, J. E. Dipeptidase 1: a candidate tumor-specific molecular marker in colorectal carcinoma. *Cancer Lett* **209**, 67-74 (2004).

74. Chen, G. et al. Detection of occult metastasis in lymph nodes from colorectal cancer patients: a multiple-marker reverse transcriptase-polymerase chain reaction study. *Dis Colon Rectum* **47**, 679-86 (2004).

75. Petrelli, N. et al. The modulation of fluorouracil with leucovorin in metastatic colorectal carcinoma: a prospective randomized phase III trial. Gastrointestinal Tumor Study Group. *J Clin Oncol* **7**, 1419-26 (1989).

76. Fakih, M. The role of targeted therapy in the treatment of advanced colorectal cancer. *Curr Treat Options Oncol* **9**, 357-74 (2008).

77. Piedbois, P. & Buyse, M. What can we learn from a meta-analysis of trials testing the modulation of 5-FU by leucovorin? Advanced Colorectal Meta-analysis Project. *Ann Oncol* **4 Suppl 2**, 15-9 (1993).

78. Folkman, J. Tumor angiogenesis: therapeutic implications. *N Engl J Med* **285**, 1182-6 (1971).

79. Pohl, A. et al. Targeting metastatic colorectal cancer in 2008: a long way from 5-FU. *Oncology (Williston Park)* **22**, 456-62; discussion 462-3, 467-8, 474 passim (2008).

80. Salomon, D. S., Brandt, R., Ciardiello, F. & Normanno, N. Epidermal growth factor-related peptides and their receptors in human malignancies. *Critical Reviews in Oncology/Hematology* **19**, 183-232 (1995).

81. Messa, C., Russo, F., Caruso, M. G. & Di Leo, A. EGF, TGF-alpha, and EGF-R in human colorectal adenocarcinoma. *Acta Oncol* **37**, 285-9 (1998).

82. Porebska, I., Harlozinska, A. & Bojarowski, T. Expression of the tyrosine kinase activity growth factor receptors (EGFR, ERB B2, ERB B3) in colorectal adenocarcinomas and adenomas. *Tumour Biol* **21**, 105-15 (2000).

83. Ng, K. & Zhu, A. X. Targeting the epidermal growth factor receptor in metastatic colorectal cancer. *Critical Reviews in Oncology/Hematology* **65**, 8-20 (2008).

84. Cunningham, D. et al. Cetuximab monotherapy and cetuximab plus irinotecan in irinotecan-refractory metastatic colorectal cancer. *N Engl J Med* **351**, 337-45 (2004).

85. Gorg, A., Weiss, W. & Dunn, M. J. Current two-dimensional electrophoresis technology for proteomics. *Proteomics* **4**, 3665-85 (2004).

86. Stead, D. A. et al. Information quality in proteomics. *Brief Bioinform* **9**, 174-88 (2008).

87. Unlu, M., Morgan, M. E. & Minden, J. S. Difference gel electrophoresis: a single gel method for detecting changes in protein extracts. *Electrophoresis* **18**, 2071-7 (1997).

88. Friedman, D. B. et al. Proteome analysis of human colon cancer by two-dimensional difference gel electrophoresis and mass spectrometry. *Proteomics* **4**, 793-811 (2004).

89. Alfonso, P. et al. Proteomic expression analysis of colorectal cancer by two-dimensional differential gel electrophoresis. *Proteomics* **5**, 2602-11 (2005).

90. Bi, X. et al. Proteomic Analysis of Colorectal Cancer Reveals Alterations in Metabolic Pathways: Mechanism of Tumorigenesis 10.1074/mcp.M500432-MCP200. *Mol Cell Proteomics* **5**, 1119-1130 (2006).

91. Kim, H. J. et al. Identification of S100A8 and S100A9 as serological markers for colorectal cancer. *J Proteome Res* **8**, 1368-79 (2009).

92. Ott, V. et al. Accuracy of two-dimensional electrophoresis for target discovery in human colorectal cancer. *Pharmacogenomics J* **1**, 142-51 (2001).

93. Lawrie, L. C., Curran, S., McLeod, H. L., Fothergill, J. E. & Murray, G. I. Application of laser capture microdissection and proteomics in colon cancer. *Mol Pathol* **54**, 253-8 (2001).

94. Sugiyama, Y. et al. Analysis of differential gene expression patterns in colon cancer and cancer stroma using microdissected tissues. *Gastroenterology* **128**, 480-6 (2005).

95. Condina, M. R., Guthridge, M. A., McColl, S. R. & Hoffmann, P. A sensitive magnetic bead method for the detection and identification of tyrosine phosphorylation in proteins by MALDI-TOF/TOF MS. *Proteomics* **9**, 3047-57 (2009).

96. Laidlaw, A. M., Copeland, B., Ross, C. M. & Hardingham, J. E. Extent of over-expression of hepatocyte growth factor receptor in colorectal tumours is dependent on the choice of normaliser. *Biochem Biophys Res Commun* **341**, 1017-21 (2006).

97. Rathsam, C. et al. Two-dimensional fluorescence difference gel electrophoretic analysis of Streptococcus mutans biofilms. *J Proteome Res* **4**, 2161-73 (2005).

98. Zhou, G. et al. 2D differential in-gel electrophoresis for the identification of esophageal scans cell cancer-specific protein markers. *Mol Cell Proteomics* **1**, 117-24 (2002).

99. Sitek, B. et al. Novel approaches to analyse glomerular proteins from smallest scale murine and human samples using DIGE saturation labelling. *Proteomics* **6**, 4337-45 (2006).

100. Tzivion, G., Gupta, V. S., Kaplun, L. & Balan, V. 14-3-3 proteins as potential oncogenes. *Semin Cancer Biol* **16**, 203-13 (2006).

101. Lu, B., Xu, J., Zhu, Y., Zhang, H. & Lai, M. Systemic analysis of the differential gene expression profile in a colonic adenoma-normal SSH library. *Clin Chim Acta* **378**, 42-7 (2007).

102. Lakshmikuttyamma, A., Selvakumar, P., Kanthan, R., Kanthan, S. C. & Sharma, R. K. Overexpression of m-calpain in human colorectal adenocarcinomas. *Cancer Epidemiol Biomarkers Prev* **13**, 1604-9 (2004).

103. Zou, Z. et al. Maspin, a serpin with tumor-suppressing activity in human mammary epithelial cells. *Science* **263**, 526-9 (1994).

104. Sager, R., Sheng, S., Pemberton, P. & Hendrix, M. J. Maspin: a tumor suppressing serpin. *Curr Top Microbiol Immunol* **213 (Pt 1)**, 51-64 (1996).

105. Lacroix, M. Significance, detection and markers of disseminated breast cancer cells. *Endocr Relat Cancer* **13**, 1033-67 (2006).

106. Toillon, R. A. et al. Proteomics demonstration that normal breast epithelial cells can induce apoptosis of breast cancer cells through insulin-like growth factor-binding protein-3 and maspin. *Mol Cell Proteomics* **6**, 1239-47 (2007).

107. Law, R. H. et al. The high resolution crystal structure of the human tumor suppressor maspin reveals a novel conformational switch in the G-helix. *J Biol Chem* **280**, 22356-64 (2005).

108. Song, S. Y. et al. Expression of maspin in colon cancers: its relationship with p53 expression and microvessel density. *Dig Dis Sci* **47**, 1831-5 (2002).

109. Umekita, Y., Souda, M. & Yoshida, H. Expression of maspin in colorectal cancer. *In Vivo* **20**, 797-800 (2006).

110. Zheng, H. et al. Maspin expression was involved in colorectal adenoma-adenocarcinoma sequence and liver metastasis of tumors. *Anticancer Res* **27**, 259-65 (2007).

111. Findeisen, P. et al. Systematic identification and validation of candidate genes for detection of circulating tumor cells in peripheral blood specimens of colorectal cancer patients. *Int J Oncol* **33**, 1001-10 (2008).

112. Datta, P. K., Chytil, A., Gorska, A. E. & Moses, H. L. Identification of STRAP, a novel WD domain protein in transforming growth factor-beta signaling. *J Biol Chem* **273**, 34671-4 (1998).

113. Halder, S. K. et al. Oncogenic function of a novel WD-domain protein, STRAP, in human carcinogenesis. *Cancer Res* **66**, 6156-66 (2006).

114. Kim, C. J. et al. Overexpression of serine-threonine receptor kinase-associated protein in colorectal cancers. *Pathol Int* **57**, 178-82 (2007).

115. Gonias, S. L., Hembrough, T. A. & Sankovic, M. Cytokeratin 8 functions as a major plasminogen receptor in select epithelial and carcinoma cells. *Front Biosci* **6**, D1403-11 (2001).

116. Garrod, D. R. Desmosomes and hemidesmosomes. *Curr Opin Cell Biol* **5**, 30-40 (1993).

117. Owaribe, K., Nishizawa, Y. & Franke, W. W. Isolation and characterization of hemidesmosomes from bovine corneal epithelial cells. *Exp Cell Res* **192**, 622-30 (1991).

118. Ku, N. O. & Omary, M. B. Identification of the major physiologic phosphorylation site of human keratin 18: potential kinases and a role in filament reorganization. *J Cell Biol* **127**, 161-71 (1994).

119. Liao, J., Lowthert, L. A. & Omary, M. B. Heat stress or rotavirus infection of human epithelial cells generates a distinct hyperphosphorylated form of keratin 8. *Exp Cell Res* **219**, 348-57 (1995).

120. Hofmann, T. et al. Prognostic relevance of disseminated tumour cells in bone marrow of patients with transitional cell carcinoma. *Eur J Cancer* **43**, 2678-84 (2007).

121. Nosotti, M. et al. Immunocytochemical detection of occult tumor cells in the bone marrow: prognostic impact on early stages of lung cancer. *Eur Surg Res* **41**, 267-71 (2008).

122. Linder, S., Havelka, A. M., Ueno, T. & Shoshan, M. C. Determining tumor apoptosis and necrosis in patient serum using cytokeratin 18 as a biomarker. *Cancer Lett* **214**, 1-9 (2004).

123. Wang, X. et al. Mass spectrometric characterization of the affinity-purified human 26S proteasome complex. *Biochemistry* **46**, 3553-65 (2007).

124. Voges, D., Zwickl, P. & Baumeister, W. The 26S proteasome: a molecular machine designed for controlled proteolysis. *Annu Rev Biochem* **68**, 1015-68 (1999).

125. Verma, R., Oania, R., Graumann, J. & Deshaies, R. J. Multiubiquitin chain receptors define a layer of substrate selectivity in the ubiquitin-proteasome system. *Cell* **118**, 99-110 (2004).

126. Pickart, C. M. & Cohen, R. E. Proteasomes and their kin: proteases in the machine age. *Nat Rev Mol Cell Biol* **5**, 177-87 (2004).

127. Gaczynska, M., Rock, K. L. & Goldberg, A. L. Role of proteasomes in antigen presentation. *Enzyme Protein* **47**, 354-69 (1993).

128. Adams, J. The development of proteasome inhibitors as anticancer drugs. *Cancer Cell* **5**, 417-21 (2004).

129. Sun, W. et al. Proteome analysis of hepatocellular carcinoma by two-dimensional difference gel electrophoresis: novel protein markers in hepatocellular carcinoma tissues. *Mol Cell Proteomics* **6**, 1798-808 (2007).

130. Ford, L. P., Suh, J. M., Wright, W. E. & Shay, J. W. Heterogeneous nuclear ribonucleoproteins C1 and C2 associate with the RNA component of human telomerase. *Mol Cell Biol* **20**, 9084-91 (2000).

131. Bahassi el, M. et al. Critical regulation of genes for tumor cell migration by AP-1. *Clin Exp Metastasis* **21**, 293-304 (2004).

132. Van den Abbeele, A. et al. Downregulation of gelsolin family proteins counteracts cancer cell invasion in vitro. *Cancer Lett* **255**, 57-70 (2007).

133. Zimmermann, U. et al. Increased expression and altered location of annexin IV in renal clear cell carcinoma: a possible role in tumour dissemination. *Cancer Lett* **209**, 111-8 (2004).

134. Duncan, R., Carpenter, B., Main, L. C., Telfer, C. & Murray, G. I. Characterisation and protein expression profiling of annexins in colorectal cancer. *Br J Cancer* **98**, 426-33 (2008).

135. Hayes, M. J. & Moss, S. E. Annexins and disease. *Biochem Biophys Res Commun* **322**, 1166-70 (2004).

136. Chen, W., Syldath, U., Bellmann, K., Burkart, V. & Kolb, H. Human 60-kDa heat-shock protein: a danger signal to the innate immune system. *J Immunol* **162**, 3212-9 (1999).

137. Tang, D. et al. Expression of heat shock proteins and heat shock protein messenger ribonucleic acid in human prostate carcinoma in vitro and in tumors in vivo. *Cell Stress Chaperones* **10**, 46-58 (2005).

138. Isidoro, A. et al. Breast carcinomas fulfill the Warburg hypothesis and provide metabolic markers of cancer prognosis. *Carcinogenesis* (2005).

139. Soltys, B. J. & Gupta, R. S. Cell surface localization of the 60 kDa heat shock chaperonin protein (hsp60) in mammalian cells. *Cell Biol Int* **21**, 315-20 (1997).

140. Piselli, P. et al. Different expression of CD44, ICAM-1, and HSP60 on primary tumor and metastases of a human pancreatic carcinoma growing in scid mice. *Anticancer Res* **20**, 825-31 (2000).

141. Shin, B. K. et al. Global profiling of the cell surface proteome of cancer cells uncovers an abundance of proteins with chaperone function. *J Biol Chem* **278**, 7607-16 (2003).

142. Cappello, F. et al. The expression of HSP60 and HSP10 in large bowel carcinomas with lymph node metastase. *BMC Cancer* **5**, 139 (2005).

143. Lin, K. M. et al. Combined and individual mitochondrial HSP60 and HSP10 expression in cardiac myocytes protects mitochondrial function and prevents apoptotic cell deaths induced by simulated ischemia-reoxygenation. *Circulation* **103**, 1787-92 (2001).

144. Xanthoudakis, S. et al. Hsp60 accelerates the maturation of pro-caspase-3 by upstream activator proteases during apoptosis. *EMBO J* **18**, 2049-56 (1999).

145. Samali, A., Cai, J., Zhivotovsky, B., Jones, D. P. & Orrenius, S. Presence of a pre-apoptotic complex of pro-caspase-3, Hsp60 and Hsp10 in the mitochondrial fraction of jurkat cells. *EMBO J* **18**, 2040-8 (1999).

146. Tomonaga, T. et al. Identification of altered protein expression and post-translational modifications in primary colorectal cancer by using agarose two-dimensional gel electrophoresis. *Clin Cancer Res* **10**, 2007-14 (2004).

147. Chen, G. et al. Proteomic analysis of lung adenocarcinoma: identification of a highly expressed set of proteins in tumors. *Clin Cancer Res* **8**, 2298-305 (2002).

148. Lachaise, F. et al. Relationship between posttranslational modification of transaldolase and catalase deficiency in UV-sensitive repair-deficient xeroderma pigmentosum fibroblasts and SV40-transformed human cells. *Free Radic Biol Med* **30**, 1365-73 (2001).

149. Grisendi, S. & Pandolfi, P. P. Two decades of cancer genetics: from specificity to pleiotropic networks. *Cold Spring Harb Symp Quant Biol* **70**, 83-91 (2005).

150. Taldone, T., Sun, W. & Chiosis, G. Discovery and development of heat shock protein 90 inhibitors. *Bioorg Med Chem* **17**, 2225-35 (2009).

151. Mimnaugh, E. G., Chavany, C. & Neckers, L. Polyubiquitination and proteasomal degradation of the p185c-erbB-2 receptor protein-tyrosine kinase induced by geldanamycin. *J Biol Chem* **271**, 22796-801 (1996).

152. Inagaki, M., Nakamura, Y., Takeda, M., Nishimura, T. & Inagaki, N. Glial fibrillary acidic protein: dynamic property and regulation by phosphorylation. *Brain Pathol* **4**, 239-43 (1994).

153. Ku, N. O., Liao, J., Chou, C. F. & Omary, M. B. Implications of intermediate filament protein phosphorylation. *Cancer Metastasis Rev* **15**, 429-44 (1996).

154. Toivola, D. M., Goldman, R. D., Garrod, D. R. & Eriksson, J. E. Protein phosphatases maintain the organization and structural interactions of hepatic keratin intermediate filaments. *J Cell Sci* **110 (Pt 1)**, 23-33 (1997).

155. Liao, J., Ku, N. O. & Omary, M. B. Stress, apoptosis, and mitosis induce phosphorylation of human keratin 8 at Ser-73 in tissues and cultured cells. *J Biol Chem* **272**, 17565-73 (1997).

156. Ku, N. O., Azhar, S. & Omary, M. B. Keratin 8 phosphorylation by p38 kinase regulates cellular keratin filament reorganization: modulation by a keratin 1-like disease causing mutation. *J Biol Chem* **277**, 10775-82 (2002).

157. Ku, N. O. & Omary, M. B. Phosphorylation of human keratin 8 in vivo at conserved head domain serine 23 and at epidermal growth factor-stimulated tail domain serine 431. *J Biol Chem* **272**, 7556-64 (1997).

158. He, T., Stepulak, A., Holmstrom, T. H., Omary, M. B. & Eriksson, J. E. The intermediate filament protein keratin 8 is a novel cytoplasmic substrate for c-Jun N-terminal kinase. *J Biol Chem* **277**, 10767-74 (2002).

159. Andreyev, H. J., Norman, A. R., Cunningham, D., Oates, J. R. & Clarke, P. A. Kirsten ras mutations in patients with colorectal cancer: the multicenter "RASCAL" study. *J Natl Cancer Inst* **90**, 675-84 (1998).

160. Davies, H. et al. Mutations of the BRAF gene in human cancer. *Nature* **417**, 949-54 (2002).

161. Rajagopalan, H. et al. Tumorigenesis: RAF/RAS oncogenes and mismatch-repair status. *Nature* **418**, 934 (2002).

162. von Lindern, M. et al. Can, a putative oncogene associated with myeloid leukemogenesis, may be activated by fusion of its 3' half to different genes: characterization of the set gene. *Mol Cell Biol* **12**, 3346-55 (1992).

163. Estanyol, J. M. et al. The protein SET regulates the inhibitory effect of p21(Cip1) on cyclin E-cyclin-dependent kinase 2 activity. *J Biol Chem* **274**, 33161-5 (1999).

164. Canela, N. et al. The SET protein regulates G2/M transition by modulating cyclin B-cyclin-dependent kinase 1 activity. *J Biol Chem* **278**, 1158-64 (2003).

165. Al-Murrani, S. W., Woodgett, J. R. & Damuni, Z. Expression of I2PP2A, an inhibitor of protein phosphatase 2A, induces c-Jun and AP-1 activity. *Biochem J* **341 (Pt 2)**, 293-8 (1999).

166. Fan, Z., Beresford, P. J., Oh, D. Y., Zhang, D. & Lieberman, J. Tumor suppressor NM23-H1 is a granzyme A-activated DNase during CTL-mediated apoptosis, and the nucleosome assembly protein SET is its inhibitor. *Cell* **112**, 659-72 (2003).

167. Li, M., Guo, H. & Damuni, Z. Purification and characterization of two potent heat-stable protein inhibitors of protein phosphatase 2A from bovine kidney. *Biochemistry* **34**, 1988-96 (1995).

168. Li, M., Makkinje, A. & Damuni, Z. The myeloid leukemia-associated protein SET is a potent inhibitor of protein phosphatase 2A. *J Biol Chem* **271**, 11059-62 (1996).

169. Wang, P., Bouwman, F. G. & Mariman, E. C. Generally detected proteins in comparative proteomics--a matter of cellular stress response? *Proteomics* **9**, 2955-66 (2009).

170. Petrak, J. et al. Deja vu in proteomics. A hit parade of repeatedly identified differentially expressed proteins. *Proteomics* **8**, 1744-9 (2008).

171. Aboseif, S., El-Sakka, A., Young, P. & Cunha, G. Mesenchymal reprogramming of adult human epithelial differentiation. *Differentiation* **65**, 113-8 (1999).

172. Vaccariello, M., Javaherian, A., Wang, Y., Fusenig, N. E. & Garlick, J. A. Cell interactions control the fate of malignant keratinocytes in an organotypic model of early neoplasia. *J Invest Dermatol* **113**, 384-91 (1999).

173. De Wever, O. & Mareel, M. Role of tissue stroma in cancer cell invasion. *J Pathol* **200**, 429-47 (2003).

174. Brown, L. F. et al. Vascular stroma formation in carcinoma in situ, invasive carcinoma, and metastatic carcinoma of the breast. *Clin Cancer Res* **5**, 1041-56 (1999).

175. Olumi, A. F. et al. Carcinoma-associated fibroblasts direct tumor progression of initiated human prostatic epithelium. *Cancer Res* **59**, 5002-11 (1999).

176. Cunha, G. R. et al. Normal and abnormal development of the male urogenital tract. Role of androgens, mesenchymal-epithelial interactions, and growth factors. *J Androl* **13**, 465-75 (1992).

177. Haffen, K., Kedinger, M., Simon-Assmann, P. M. & Lacroix, B. Mesenchyme-dependent differentiation of intestinal brush-border enzymes in the gizzard endoderm of the chick embryo. *Prog Clin Biol Res* **85 Pt B**, 261-70 (1982).

178. Kratochwil, K. Tissue combination and organ culture studies in the development of the embryonic mammary gland. *Dev Biol (N Y 1985)* **4**, 315-33 (1986).

179. Glasser, S. R. & Julian, J. Intermediate filament protein as a marker of uterine stromal cell decidualization. *Biol Reprod* **35**, 463-74 (1986).

180. Adegboyega, P. A., Mifflin, R. C., DiMari, J. F., Saada, J. I. & Powell, D. W. Immunohistochemical study of myofibroblasts in normal colonic mucosa, hyperplastic polyps, and adenomatous colorectal polyps. *Arch Pathol Lab Med* **126**, 829-36 (2002).

181. Richman, P. I., Tilly, R., Jass, J. R. & Bodmer, W. F. Colonic pericrypt sheath cells: characterisation of cell type with new monoclonal antibody. *J Clin Pathol* **40**, 593-600 (1987).

182. Verhoeven, D. & Buyssens, N. Desmin-positive stellate cells associated with angiogenesis in a tumour and non-tumour system. *Virchows Arch B Cell Pathol Incl Mol Pathol* **54**, 263-72 (1988).

183. Ogawa, M., LaRue, A. C. & Drake, C. J. Hematopoietic origin of fibroblasts/myofibroblasts: Its pathophysiologic implications. *Blood* **108**, 2893-6 (2006).

184. Viegas-Pequignot, E., Li, Z. L., Dutrillaux, B., Apiou, F. & Paulin, D. Assignment of human desmin gene to band 2q35 by nonradioactive in situ hybridization. *Hum Genet* **83**, 33-6 (1989).

185. Li, Z. et al. Cardiovascular lesions and skeletal myopathy in mice lacking desmin. *Dev Biol* **175**, 362-6 (1996).

186. Li, Z. et al. Desmin is essential for the tensile strength and integrity of myofibrils but not for myogenic commitment, differentiation, and fusion of skeletal muscle. *J Cell Biol* **139**, 129-44 (1997).

187. Ishikawa, H., Bischoff, R. & Holtzer, H. Mitosis and intermediate-sized filaments in developing skeletal muscle. *J Cell Biol* **38**, 538-55 (1968).

188. Stromer, M. H. The cytoskeleton in skeletal, cardiac and smooth muscle cells. *Histol Histopathol* **13**, 283-91 (1998).

189. Tidball, J. G. Desmin at myotendinous junctions. *Exp Cell Res* **199**, 206-12 (1992).

190. Thornell, L. E. & Eriksson, A. Filament systems in the Purkinje fibers of the heart. *Am J Physiol* **241**, H291-305 (1981).

191. Milner, D. J., Weitzer, G., Tran, D., Bradley, A. & Capetanaki, Y. Disruption of muscle architecture and myocardial degeneration in mice lacking desmin. *J Cell Biol* **134**, 1255-70 (1996).

192. Paulin, D., Huet, A., Khanamyrian, L. & Xue, Z. Desminopathies in muscle disease. *J Pathol* **204**, 418-27 (2004).

193. Gabbiani, G. Control of smooth muscle cell activation. *Arterioscler Thromb Vasc Biol* **24**, 804-5 (2004).

194. Mitchell, J. et al. Alpha-smooth muscle actin in parenchymal cells of bleomycin-injured rat lung. *Lab Invest* **60**, 643-50 (1989).

195. Tsukada, T., McNutt, M. A., Ross, R. & Gown, A. M. HHF35, a muscle actin-specific monoclonal antibody. II. Reactivity in normal, reactive, and neoplastic human tissues. *Am J Pathol* **127**, 389-402 (1987).

196. Rockey, D. C. & Friedman, S. L. Cytoskeleton of liver perisinusoidal cells (lipocytes) in normal and pathological conditions. *Cell Motil Cytoskeleton* **22**, 227-34 (1992).

197. Skalli, O. et al. Myofibroblasts from diverse pathologic settings are heterogeneous in their content of actin isoforms and intermediate filament proteins. *Lab Invest* **60**, 275-85 (1989).

198. Ban, S. et al. Phenotypic change of muscularis mucosae in early invasive colorectal adenocarcinoma. *J Clin Pathol* **53**, 878-81 (2000).

199. Dingemans, K. P., Zeeman-Boeschoten, I. M., Keep, R. F. & Das, P. K. Transplantation of colon carcinoma into granulation tissue induces an invasive morphotype. *Int J Cancer* **54**, 1010-6 (1993).

200. Gabbiani, G. The myofibroblast in wound healing and fibrocontractive diseases. *J Pathol* **200**, 500-3 (2003).

201. Quinlan, R. A. & Franke, W. W. Heteropolymer filaments of vimentin and desmin in vascular smooth muscle tissue and cultured baby hamster kidney cells demonstrated by chemical crosslinking. *Proc Natl Acad Sci U S A* **79**, 3452-6 (1982).

202. Quinlan, R. A. & Franke, W. W. Molecular interactions in intermediate-sized filaments revealed by chemical cross-linking. Heteropolymers of vimentin and glial filament protein in cultured human glioma cells. *Eur J Biochem* **132**, 477-84 (1983).

203. Armulik, A., Abramsson, A. & Betsholtz, C. Endothelial/pericyte interactions. *Circ Res* **97**, 512-23 (2005).

204. Brey, E. M., McIntire, L. V., Johnston, C. M., Reece, G. P. & Patrick, C. W., Jr. Three-dimensional, quantitative analysis of desmin and smooth muscle alpha actin expression during angiogenesis. *Ann Biomed Eng* **32**, 1100-7 (2004).

205. Middleton, J. et al. A comparative study of endothelial cell markers expressed in chronically inflamed human tissues: MECA-79, Duffy antigen receptor for chemokines, von Willebrand factor, CD31, CD34, CD105 and CD146. *J Pathol* **206**, 260-8 (2005).

206. Ponce, A. M. & Price, R. J. Angiogenic stimulus determines the positioning of pericytes within capillary sprouts in vivo. *Microvasc Res* **65**, 45-8 (2003).

207. Benjamin, L. E., Golijanin, D., Itin, A., Pode, D. & Keshet, E. Selective ablation of immature blood vessels in established human tumors follows vascular endothelial growth factor withdrawal. *J Clin Invest* **103**, 159-65 (1999).

208. Gee, M. S. et al. Tumor vessel development and maturation impose limits on the effectiveness of anti-vascular therapy. *Am J Pathol* **162**, 183-93 (2003).

209. Jain, R. K. Normalizing tumor vasculature with anti-angiogenic therapy: a new paradigm for combination therapy. *Nat Med* **7**, 987-9 (2001).

210. Abramsson, A. et al. Analysis of mural cell recruitment to tumor vessels. *Circulation* **105**, 112-7 (2002).

211. Darland, D. C. & D'Amore, P. A. Cell-cell interactions in vascular development. *Curr Top Dev Biol* **52**, 107-49 (2001).

212. Reinmuth, N. et al. Induction of VEGF in perivascular cells defines a potential paracrine mechanism for endothelial cell survival. *Faseb J* **15**, 1239-41 (2001).

213. Morikawa, S. et al. Abnormalities in pericytes on blood vessels and endothelial sprouts in tumors. *Am J Pathol* **160**, 985-1000 (2002).

214. Nehls, V., Denzer, K. & Drenckhahn, D. Pericyte involvement in capillary sprouting during angiogenesis in situ. *Cell Tissue Res* **270**, 469-74 (1992).

215. Lindahl, P., Johansson, B. R., Leveen, P. & Betsholtz, C. Pericyte loss and microaneurysm formation in PDGF-B-deficient mice. *Science* **277**, 242-5 (1997).

216. Hasumi, Y. et al. Identification of a subset of pericytes that respond to combination therapy targeting PDGF and VEGF signaling. *Int J Cancer* **121**, 2606-14 (2007).

217. Nicosia, R. F. & Villaschi, S. Rat aortic smooth muscle cells become pericytes during angiogenesis in vitro. *Lab Invest* **73**, 658-66 (1995).

218. Hagedorn, M. et al. VEGF coordinates interaction of pericytes and endothelial cells during vasculogenesis and experimental angiogenesis. *Dev Dyn* **230**, 23-33 (2004).

219. Yurugi-Kobayashi, T. et al. Effective contribution of transplanted vascular progenitor cells derived from embryonic stem cells to adult neovascularization in proper differentiation stage. *Blood* **101**, 2675-8 (2003).

220. Rhodin, J. A. & Fujita, H. Capillary growth in the mesentery of normal young rats. Intravital video and electron microscope analyses. *J Submicrosc Cytol Pathol* **21**, 1-34 (1989).

221. Lin, J. L. et al. Isolation and sequencing of a novel tropomyosin isoform preferentially associated with colon cancer. *Gastroenterology* **123**, 152-62 (2002).

222. Powell, D. W. et al. Myofibroblasts. I. Paracrine cells important in health and disease. *Am J Physiol* **277**, C1-9 (1999).

223. Tomasek, J. J., Gabbiani, G., Hinz, B., Chaponnier, C. & Brown, R. A. Myofibroblasts and mechano-regulation of connective tissue remodelling. *Nat Rev Mol Cell Biol* **3**, 349-63 (2002).

224. Martin, M., Pujuguet, P. & Martin, F. Role of stromal myofibroblasts infiltrating colon cancer in tumor invasion. *Pathol Res Pract* **192**, 712-7 (1996).

225. Poulsom, R. et al. Stromal expression of 72 kda type IV collagenase (MMP-2) and TIMP-2 mRNAs in colorectal neoplasia. *Am J Pathol* **141**, 389-96 (1992).

226. Radovic, S., Selak, I., Babic, M. & Bratovic, I. Demonstration of perycriptal fibroblasts in inflammatory-regenerative and dysplastic epithelial lesions of the flat colonic mucosa. *Adv Clin Path* **5**, 139-45 (2001).

227. Desmouliere, A., Redard, M., Darby, I. & Gabbiani, G. Apoptosis mediates the decrease in cellularity during the transition between granulation tissue and scar. *Am J Pathol* **146**, 56-66 (1995).

228. Truong, L. D. et al. The diagnostic utility of desmin. A study of 584 cases and review of the literature. *Am J Clin Pathol* **93**, 305-14 (1990).

229. Silzle, T., Randolph, G. J., Kreutz, M. & Kunz-Schughart, L. A. The fibroblast: sentinel cell and local immune modulator in tumor tissue. *Int J Cancer* **108**, 173-80 (2004).

230. Kunz-Schughart, L. A. & Knuechel, R. Tumor-associated fibroblasts (part I): Active stromal participants in tumor development and progression? *Histol Histopathol* **17**, 599-621 (2002).

231. Spaeth, E. L. et al. Mesenchymal stem cell transition to tumor-associated fibroblasts contributes to fibrovascular network expansion and tumor progression. *PLoS One* **4**, e4992 (2009).

232. Dong, J. et al. VEGF-null cells require PDGFR alpha signaling-mediated stromal fibroblast recruitment for tumorigenesis. *EMBO J* **23**, 2800-10 (2004).

233. Jodele, S. et al. The contribution of bone marrow-derived cells to the tumor vasculature in neuroblastoma is matrix metalloproteinase-9 dependent. *Cancer Res* **65**, 3200-8 (2005).

234. Udagawa, T., Puder, M., Wood, M., Schaefer, B. C. & D'Amato, R. J. Analysis of tumor-associated stromal cells using SCID GFP transgenic mice: contribution of local and bone marrow-derived host cells. *Faseb J* **20**, 95-102 (2006).

235. Koyama, H. et al. Significance of tumor-associated stroma in promotion of intratumoral lymphangiogenesis: pivotal role of a hyaluronan-rich tumor microenvironment. *Am J Pathol* **172**, 179-93 (2008).

236. Geiger, T. R. & Peeper, D. S. Metastasis mechanisms. *Biochimica et Biophysica Acta (BBA) - Reviews on Cancer* **In Press, Uncorrected Proof**.

237. Christofori, G. New signals from the invasive front. *Nature* **441**, 444-50 (2006).

238. Jechlinger, M. et al. Expression profiling of epithelial plasticity in tumor progression. *Oncogene* **22**, 7155-69 (2003).

239. Huber, M. A., Beug, H. & Wirth, T. Epithelial-mesenchymal transition: NF-kappaB takes center stage. *Cell Cycle* **3**, 1477-80 (2004).

240. Huber, M. A., Kraut, N. & Beug, H. Molecular requirements for epithelial-mesenchymal transition during tumor progression. *Curr Opin Cell Biol* **17**, 548-58 (2005).

241. Oft, M. et al. TGF-beta1 and Ha-Ras collaborate in modulating the phenotypic plasticity and invasiveness of epithelial tumor cells. *Genes Dev* **10**, 2462-77 (1996).

242. Willis, B. C. et al. Induction of epithelial-mesenchymal transition in alveolar epithelial cells by transforming growth factor-beta1: potential role in idiopathic pulmonary fibrosis. *Am J Pathol* **166**, 1321-32 (2005).

243. Kalluri, R. & Neilson, E. G. Epithelial-mesenchymal transition and its implications for fibrosis. *J Clin Invest* **112**, 1776-84 (2003).

244. Lovicu, F. J. et al. TGFbeta induces morphological and molecular changes similar to human anterior subcapsular cataract. *Br J Ophthalmol* **86**, 220-6 (2002).

245. Brittan, M. et al. Bone marrow derivation of pericryptal myofibroblasts in the mouse and human small intestine and colon. *Gut* **50**, 752-7 (2002).

246. Grimm, P. C. et al. Neointimal and tubulointerstitial infiltration by recipient mesenchymal cells in chronic renal-allograft rejection. *N Engl J Med* **345**, 93-7 (2001).

247. Green, K. J. & Gaudry, C. A. Are desmosomes more than tethers for intermediate filaments? *Nat Rev Mol Cell Biol* **1**, 208-16 (2000).

248. Fuchs, E. & Weber, K. Intermediate filaments: structure, dynamics, function, and disease. *Annu Rev Biochem* **63**, 345-82 (1994).

249. Oshima, R. G., Baribault, H. & Caulin, C. Oncogenic regulation and function of keratins 8 and 18. *Cancer Metastasis Rev* **15**, 445-71 (1996).

250. Magin, T. M. et al. Lessons from keratin 18 knockout mice: formation of novel keratin filaments, secondary loss of keratin 7 and accumulation of liver-specific keratin 8-positive aggregates. *J Cell Biol* **140**, 1441-51 (1998).

251. Moll, R., Franke, W. W., Schiller, D. L., Geiger, B. & Krepler, R. The catalog of human cytokeratins: patterns of expression in normal epithelia, tumors and cultured cells. *Cell* **31**, 11-24 (1982).

252. Hendrix, M. J. et al. Coexpression of vimentin and keratins by human melanoma tumor cells: correlation with invasive and metastatic potential. *J Natl Cancer Inst* **84**, 165-74 (1992).

253. Chu, Y. W., Runyan, R. B., Oshima, R. G. & Hendrix, M. J. Expression of complete keratin filaments in mouse L cells augments cell migration and invasion. *Proc Natl Acad Sci U S A* **90**, 4261-5 (1993).

254. Raul, U. et al. Implications of cytokeratin 8/18 filament formation in stratified epithelial cells: induction of transformed phenotype. *Int J Cancer* **111**, 662-8 (2004).

255. Schaafsma, H. E. et al. Distribution of cytokeratin polypeptides in human transitional cell carcinomas, with special emphasis on changing expression patterns during tumor progression. *Am J Pathol* **136**, 329-43 (1990).

256. Fillies, T. et al. Cytokeratin 8/18 expression indicates a poor prognosis in squamous cell carcinomas of the oral cavity. *BMC Cancer* **6**, 10 (2006).

257. Barak, V., Goike, H., Panaretakis, K. W. & Einarsson, R. Clinical utility of cytokeratins as tumor markers. *Clin Biochem* **37**, 529-40 (2004).

258. Mellerick, D. M., Osborn, M. & Weber, K. On the nature of serological tissue polypeptide antigen (TPA); monoclonal keratin 8, 18, and 19 antibodies react differently with TPA prepared from human cultured carcinoma cells and TPA in human serum. *Oncogene* **5**, 1007-17 (1990).

259. Omary, M. B., Ku, N. O., Tao, G. Z., Toivola, D. M. & Liao, J. "Heads and tails" of intermediate filament phosphorylation: multiple sites and functional insights. *Trends Biochem Sci* **31**, 383-94 (2006).

260. Gires, O., Andratschke, M., Schmitt, B., Mack, B. & Schaffrik, M. Cytokeratin 8 associates with the external leaflet of plasma membranes in tumour cells. *Biochem Biophys Res Commun* **328**, 1154-62 (2005).

261. Franke, W. W., Schmid, E., Grund, C. & Geiger, B. Intermediate filament proteins in nonfilamentous structures: transient disintegration and inclusion of subunit proteins in granular aggregates. *Cell* **30**, 103-13 (1982).

262. Jones, J. C., Goldman, A. E., Yang, H. Y. & Goldman, R. D. The organizational fate of intermediate filament networks in two epithelial cell types during mitosis. *J Cell Biol* **100**, 93-102 (1985).

263. Chou, C. F. & Omary, M. B. Mitotic arrest with anti-microtubule agents or okadaic acid is associated with increased glycoprotein terminal GlcNAc's. *J Cell Sci* **107 (Pt 7)**, 1833-43 (1994).

264. Liao, J., Ku, N. O. & Omary, M. B. Two-dimensional gel analysis of glandular keratin intermediate filament phosphorylation. *Electrophoresis* **17**, 1671-6 (1996).

265. Ku, N. O. & Omary, M. B. A disease- and phosphorylation-related nonmechanical function for keratin 8. *J Cell Biol* **174**, 115-25 (2006).

266. Rubie, C. et al. Housekeeping gene variability in normal and cancerous colorectal, pancreatic, esophageal, gastric and hepatic tissues. *Mol Cell Probes* **19**, 101-9 (2005).

267. Livak, K. J. & Schmittgen, T. D. Analysis of relative gene expression data using real-time quantitative PCR and the 2(-Delta Delta C(T)) Method. *Methods* **25**, 402-8 (2001).

268. Kouklis, P. D., Hutton, E. & Fuchs, E. Making a connection: direct binding between keratin intermediate filaments and desmosomal proteins. *J Cell Biol* **127**, 1049-60 (1994).

269. Omary, M. B., Ku, N. O., Liao, J. & Price, D. Keratin modifications and solubility properties in epithelial cells and in vitro. *Subcell Biochem* **31**, 105-40 (1998).

270. Strnad, P., Windoffer, R. & Leube, R. E. Induction of rapid and reversible cytokeratin filament network remodeling by inhibition of tyrosine phosphatases. *J Cell Sci* **115**, 4133-48 (2002).

271. Nan, L. et al. Mallory body (cytokeratin aggresomes) formation is prevented in vitro by p38 inhibitor. *Exp Mol Pathol* **80**, 228-40 (2006).

272. Ridge, K. M. et al. Keratin 8 phosphorylation by protein kinase C delta regulates shear stress-mediated disassembly of keratin intermediate filaments in alveolar epithelial cells. *J Biol Chem* **280**, 30400-5 (2005).

273. Fang, J. Y. & Richardson, B. C. The MAPK signalling pathways and colorectal cancer. *Lancet Oncol* **6**, 322-7 (2005).

274. Lewis, T. S., Shapiro, P. S. & Ahn, N. G. Signal transduction through MAP kinase cascades. *Adv Cancer Res* **74**, 49-139 (1998).

275. Cohen, G. et al. Epidermal Growth Factor Receptor Signaling Is Up-regulated in Human Colonic Aberrant Crypt Foci
10.1158/0008-5472.CAN-05-0308. *Cancer Res* **66**, 5656-5664 (2006).

276. Bos, J. L. et al. Prevalence of ras gene mutations in human colorectal cancers. *Nature* **327**, 293-7 (1987).

277. Pretlow, T. P. & Pretlow, T. G. Mutant KRAS in aberrant crypt foci (ACF): initiation of colorectal cancer? *Biochim Biophys Acta* **1756**, 83-96 (2005).

278. Weisenberger, D. J. et al. CpG island methylator phenotype underlies sporadic microsatellite instability and is tightly associated with BRAF mutation in colorectal cancer. *Nat Genet* **38**, 787-93 (2006).

279. Hoshino, R. et al. Constitutive activation of the 41-/43-kDa mitogen-activated protein kinase signaling pathway in human tumors. *Oncogene* **18**, 813-22 (1999).

280. Soh, J. W. et al. Protein kinase G activates the JNK1 pathway via phosphorylation of MEKK1. *J Biol Chem* **276**, 16406-10 (2001).

281. Liao, Y. & Hung, M. C. Regulation of the activity of p38 mitogen-activated protein kinase by Akt in cancer and adenoviral protein E1A-mediated sensitization to apoptosis. *Mol Cell Biol* **23**, 6836-48 (2003).

282. Kellogg, D. R., Kikuchi, A., Fujii-Nakata, T., Turck, C. W. & Murray, A. W. Members of the NAP/SET family of proteins interact specifically with B-type cyclins. *J Cell Biol* **130**, 661-73 (1995).

283. Carlson, S. G. et al. Expression of SET, an inhibitor of protein phosphatase 2A, in renal development and Wilms' tumor. *J Am Soc Nephrol* **9**, 1873-80 (1998).

284. Adachi, Y., Pavlakis, G. N. & Copeland, T. D. Identification and characterization of SET, a nuclear phosphoprotein encoded by the translocation break point in acute undifferentiated leukemia. *J Biol Chem* **269**, 2258-62 (1994).

285. Neviani, P. et al. The tumor suppressor PP2A is functionally inactivated in blast crisis CML through the inhibitory activity of the BCR/ABL-regulated SET protein. *Cancer Cell* **8**, 355-68 (2005).

286. Sontag, E. Protein phosphatase 2A: the Trojan Horse of cellular signaling. *Cell Signal* **13**, 7-16 (2001).

287. Gomez, N. & Cohen, P. Dissection of the protein kinase cascade by which nerve growth factor activates MAP kinases. *Nature* **353**, 170-3 (1991).

288. Sato, S., Fujita, N. & Tsuruo, T. Modulation of Akt kinase activity by binding to Hsp90. *Proc Natl Acad Sci U S A* **97**, 10832-7 (2000).

289. Yokoyama, N., Reich, N. C. & Miller, W. T. Involvement of protein phosphatase 2A in the interleukin-3-stimulated Jak2-Stat5 signaling pathway. *J Interferon Cytokine Res* **21**, 369-78 (2001).

290. Avni, D. et al. Active localization of the retinoblastoma protein in chromatin and its response to S phase DNA damage. *Mol Cell* **12**, 735-46 (2003).

291. Chiang, C. W. et al. Protein phosphatase 2A dephosphorylation of phosphoserine 112 plays the gatekeeper role for BAD-mediated apoptosis. *Mol Cell Biol* **23**, 6350-62 (2003).

292. Yeh, E. et al. A signalling pathway controlling c-Myc degradation that impacts oncogenic transformation of human cells. *Nat Cell Biol* **6**, 308-18 (2004).

293. Lee, J. S., Favre, B., Hemmings, B. A., Kiefer, B. & Nagamine, Y. Okadaic acid-dependent induction of the urokinase-type plasminogen activator gene associated with stabilization and autoregulation of c-Jun. *J Biol Chem* **269**, 2887-94 (1994).

294. Seo, S. B. et al. Regulation of histone acetylation and transcription by INHAT, a human cellular complex containing the set oncoprotein. *Cell* **104**, 119-30 (2001).

295. Thorstensen, L. et al. Genetic and epigenetic changes of components affecting the WNT pathway in colorectal carcinomas stratified by microsatellite instability. *Neoplasia* **7**, 99-108 (2005).

296. Cho, K. R. & Vogelstein, B. Genetic alterations in the adenoma--carcinoma sequence. *Cancer* **70**, 1727-31 (1992).

297. Janssens, V. & Goris, J. Protein phosphatase 2A: a highly regulated family of serine/threonine phosphatases implicated in cell growth and signalling. *Biochem J* **353**, 417-39 (2001).

298. Eichhorn, P. J., Creyghton, M. P. & Bernards, R. Protein phosphatase 2A regulatory subunits and cancer. *Biochim Biophys Acta* **1795**, 1-15 (2009).

299. Fellner, T. et al. A novel and essential mechanism determining specificity and activity of protein phosphatase 2A (PP2A) in vivo. *Genes Dev* **17**, 2138-50 (2003).

300. J. Gotz, A. P., E. Ehler, B. Hemmings, W. Kues. Delayed embryonic lethality in mice lacking protein phosphatase 2A catalytic subunit C alpha *Proc. Natl. Acad. Sci.* , 12370 - 12375 (1998).

301. Groves, M. R., Hanlon, N., Turowski, P., Hemmings, B. A. & Barford, D. The structure of the protein phosphatase 2A PR65/A subunit reveals the conformation of its 15 tandemly repeated HEAT motifs. *Cell* **96**, 99-110 (1999).

302. Hendrix, P. et al. Analysis of subunit isoforms in protein phosphatase 2A holoenzymes from rabbit and Xenopus. *J Biol Chem* **268**, 7330-7 (1993).

303. Bosch, M. et al. The PR55 and PR65 subunits of protein phosphatase 2A from Xenopus laevis. molecular cloning and developmental regulation of expression. *Eur J Biochem* **230**, 1037-45 (1995).

304. Cho, U. S. & Xu, W. Crystal structure of a protein phosphatase 2A heterotrimeric holoenzyme. *Nature* **445**, 53-7 (2007).

305. Xu, Y. et al. Structure of the protein phosphatase 2A holoenzyme. *Cell* **127**, 1239-51 (2006).

306. Li, X. & Virshup, D. M. Two conserved domains in regulatory B subunits mediate binding to the A subunit of protein phosphatase 2A. *Eur J Biochem* **269**, 546-52 (2002).

307. Van Hoof, C. & Goris, J. Phosphatases in apoptosis: to be or not to be, PP2A is in the heart of the question. *Biochim Biophys Acta* **1640**, 97-104 (2003).

308. Schonthal, A. H. Role of serine/threonine protein phosphatase 2A in cancer. *Cancer Lett* **170**, 1-13 (2001).

309. Mayer, R. E. et al. Structure of the 55-kDa regulatory subunit of protein phosphatase 2A: evidence for a neuronal-specific isoform. *Biochemistry* **30**, 3589-97 (1991).

310. McCright, B., Rivers, A. M., Audlin, S. & Virshup, D. M. The B56 family of protein phosphatase 2A (PP2A) regulatory subunits encodes differentiation-induced phosphoproteins that target PP2A to both nucleus and cytoplasm. *J Biol Chem* **271**, 22081-9 (1996).

311. Cayla, X. et al. Isolation and characterization of a tyrosyl phosphatase activator from rabbit skeletal muscle and Xenopus laevis oocytes. *Biochemistry* **29**, 658-67 (1990).

312. Goris, J. et al. Conversion of a phosphoseryl/threonyl phosphatase into a phosphotyrosyl phosphatase. *Biochem J* **256**, 1029-34 (1988).

313. Gotz, J., Probst, A., Mistl, C., Nitsch, R. M. & Ehler, E. Distinct role of protein phosphatase 2A subunit Calpha in the regulation of E-cadherin and beta-catenin during development. *Mech Dev* **93**, 83-93 (2000).

314. Gao, Z. H., Seeling, J. M., Hill, V., Yochum, A. & Virshup, D. M. Casein kinase I phosphorylates and destabilizes the beta-catenin degradation complex. *Proc Natl Acad Sci U S A* **99**, 1182-7 (2002).

315. Li, X., Yost, H. J., Virshup, D. M. & Seeling, J. M. Protein phosphatase 2A and its B56 regulatory subunit inhibit Wnt signaling in Xenopus. *EMBO J* **20**, 4122-31 (2001).

316. Peters, J. M., McKay, R. M., McKay, J. P. & Graff, J. M. Casein kinase I transduces Wnt signals. *Nature* **401**, 345-50 (1999).

317. Sakanaka, C., Leong, P., Xu, L., Harrison, S. D. & Williams, L. T. Casein kinase iepsilon in the wnt pathway: regulation of beta-catenin function. *Proc Natl Acad Sci U S A* **96**, 12548-52 (1999).

318. Fukukawa, C. et al. The oncoprotein I-2PP2A/SET negatively regulates the MEK/ERK pathway and cell proliferation. *Int J Oncol* **26**, 751-6 (2005).

319. Deng, X., Ito, T., Carr, B., Mumby, M. & May, W. S., Jr. Reversible phosphorylation of Bcl2 following interleukin 3 or bryostatin 1 is mediated by direct interaction with protein phosphatase 2A. *J Biol Chem* **273**, 34157-63 (1998).

320. Ruvolo, P. P., Clark, W., Mumby, M., Gao, F. & May, W. S. A functional role for the B56 alpha-subunit of protein phosphatase 2A in ceramide-mediated regulation of Bcl2 phosphorylation status and function. *J Biol Chem* **277**, 22847-52 (2002).

321. Lieberman, J. & Fan, Z. Nuclear war: the granzyme A-bomb. *Curr Opin Immunol* **15**, 553-9 (2003).

322. Beresford, P. J. et al. Granzyme A activates an endoplasmic reticulum-associated caspase-independent nuclease to induce single-stranded DNA nicks. *J Biol Chem* **276**, 43285-93 (2001).

323. Greenaway, J. et al. Thrombospondin-1 inhibits VEGF levels in the ovary directly by binding and internalization via the low density lipoprotein receptor-related protein-1 (LRP-1). *J Cell Physiol* **210**, 807-18 (2007).

324. Schultz-Cherry, S., Lawler, J. & Murphy-Ullrich, J. E. The type 1 repeats of thrombospondin 1 activate latent transforming growth factor-beta. *J Biol Chem* **269**, 26783-8 (1994).

325. Schultz-Cherry, S., Ribeiro, S., Gentry, L. & Murphy-Ullrich, J. E. Thrombospondin binds and activates the small and large forms of latent transforming growth factor-beta in a chemically defined system. *J Biol Chem* **269**, 26775-82 (1994).

326. Schultz-Cherry, S. et al. Regulation of transforming growth factor-beta activation by discrete sequences of thrombospondin 1. *J Biol Chem* **270**, 7304-10 (1995).

327. Murphy-Ullrich, J. E. & Poczatek, M. Activation of latent TGF-beta by thrombospondin-1: mechanisms and physiology. *Cytokine Growth Factor Rev* **11**, 59-69 (2000).

328. Crawford, S. E. et al. Thrombospondin-1 is a major activator of TGF-beta1 in vivo. *Cell* **93**, 1159-70 (1998).

329. Mettouchi, A. et al. SPARC and thrombospondin genes are repressed by the c-jun oncogene in rat embryo fibroblasts. *EMBO J* **13**, 5668-78 (1994).

330. Dejong, V. et al. The Wilms' tumor gene product represses the transcription of thrombospondin 1 in response to overexpression of c-Jun. *Oncogene* **18**, 3143-51 (1999).

331. Slack, J. L. & Bornstein, P. Transformation by v-src causes transient induction followed by repression of mouse thrombospondin-1. *Cell Growth Differ* **5**, 1373-80 (1994).

332. Tikhonenko, A. T., Black, D. J. & Linial, M. L. Viral Myc oncoproteins in infected fibroblasts down-modulate thrombospondin-1, a possible tumor suppressor gene. *J Biol Chem* **271**, 30741-7 (1996).

333. Rak, J. et al. Oncogenes and tumor angiogenesis: differential modes of vascular endothelial growth factor up-regulation in ras-transformed epithelial cells and fibroblasts. *Cancer Res* **60**, 490-8 (2000).

334. Massague, J., Blain, S. W. & Lo, R. S. TGFbeta signaling in growth control, cancer, and heritable disorders. *Cell* **103**, 295-309 (2000).

335. Derynck, R. & Zhang, Y. E. Smad-dependent and Smad-independent pathways in TGF-beta family signalling. *Nature* **425**, 577-84 (2003).

336. Mulder, K. M. & Morris, S. L. Activation of p21ras by transforming growth factor beta in epithelial cells. *J Biol Chem* **267**, 5029-31 (1992).

337. Yi, J. Y., Shin, I. & Arteaga, C. L. Type I transforming growth factor beta receptor binds to and activates phosphatidylinositol 3-kinase. *J Biol Chem* **280**, 10870-6 (2005).

338. Edlund, S., Landstrom, M., Heldin, C. H. & Aspenstrom, P. Transforming growth factor-beta-induced mobilization of actin cytoskeleton requires signaling by small GTPases Cdc42 and RhoA. *Mol Biol Cell* **13**, 902-14 (2002).

339. Bhowmick, N. A. et al. Transforming Growth Factor-{beta}1 Mediates Epithelial to Mesenchymal Transdifferentiation through a RhoA-dependent Mechanism. *Mol. Biol. Cell* **12**, 27-36 (2001).

340. Atfi, A., Djelloul, S., Chastre, E., Davis, R. & Gespach, C. Evidence for a Role of Rho-like GTPases and Stress-activated Protein Kinase/c-Jun N-terminal Kinase (SAPK/JNK) in Transforming Growth Factor beta -mediated Signaling. *J. Biol. Chem.* **272**, 1429-1432 (1997).

341. Wang, L., Ma, R., Flavell, R. A. & Choi, M. E. Requirement of Mitogen-activated Protein Kinase Kinase 3 (MKK3) for Activation of p38alpha and p38delta MAPK Isoforms by TGF-beta 1 in Murine Mesangial Cells. *J. Biol. Chem.* **277**, 47257-47262 (2002).

342. Hanafusa, H. et al. Involvement of the p38 Mitogen-activated Protein Kinase Pathway in Transforming Growth Factor-beta -induced Gene Expression. *J. Biol. Chem.* **274**, 27161-27167 (1999).

343. Yamaguchi, K. et al. Identification of a member of the MAPKKK family as a potential mediator of TGF-beta signal transduction. *Science* **270**, 2008-11 (1995).

344. Kim, S. I., Kwak, J. H., Wang, L. & Choi, M. E. Protein phosphatase 2A is a negative regulator of transforming growth factor-beta1-induced TAK1 activation in mesangial cells. *J Biol Chem* **283**, 10753-63 (2008).

345. Ninomiya-Tsuji, J. et al. The kinase TAK1 can activate the NIK-I[kappa]B as well as the MAP kinase cascade in the IL-1 signalling pathway. *Nature* **398**, 252-256 (1999).

346. Van Berlo, J. H. et al. A-type lamins are essential for TGF-beta1 induced PP2A to dephosphorylate transcription factors. *Hum Mol Genet* **14**, 2839-49 (2005).

347. Lires-Dean, M. et al. Anti-apoptotic effect of transforming growth factor-beta1 on human articular chondrocytes: role of protein phosphatase 2A. *Osteoarthritis Cartilage* **16**, 1370-8 (2008).

348. Batut, J. et al. Two highly related regulatory subunits of PP2A exert opposite effects on TGF-beta/Activin/Nodal signalling. *Development* **135**, 2927-37 (2008).

349. Eklund, L. & Olsen, B. R. Tie receptors and their angiopoietin ligands are context-dependent regulators of vascular remodeling. *Exp Cell Res* **312**, 630-41 (2006).

350. Chen, W., Arroyo, J. D., Timmons, J. C., Possemato, R. & Hahn, W. C. Cancer-associated PP2A Aalpha subunits induce functional haploinsufficiency and tumorigenicity. *Cancer Res* **65**, 8183-92 (2005).

351. Sablina, A. A. & Hahn, W. C. The role of PP2A A subunits in tumor suppression. *Cell Adh Migr* **1**, 140-1 (2007).

352. Brakebusch, C. & Fassler, R. beta 1 integrin function in vivo: adhesion, migration and more. *Cancer Metastasis Rev* **24**, 403-11 (2005).

353. Ivaska, J. et al. Integrin alpha 2 beta 1 promotes activation of protein phosphatase 2A and dephosphorylation of Akt and glycogen synthase kinase 3 beta. *Mol Cell Biol* **22**, 1352-9 (2002).

354. Gushiken, F. C. et al. Protein phosphatase 2A negatively regulates integrin alpha(IIb)beta(3) signaling. *J Biol Chem* **283**, 12862-9 (2008).

355. Svensson, S. et al. ERK phosphorylation is linked to VEGFR2 expression and Ets-2 phosphorylation in breast cancer and is associated with tamoxifen treatment resistance and small tumours with good prognosis. *Oncogene* **24**, 4370-9 (2005).

356. Sharrocks, A. D. The ETS-domain transcription factor family. *Nat Rev Mol Cell Biol* **2**, 827-37 (2001).

357. Foos, G. & Hauser, C. A. Altered Ets transcription factor activity in prostate tumor cells inhibits anchorage-independent growth, survival, and invasiveness. *Oncogene* **19**, 5507-16 (2000).

358. Carbone, G. M. et al. Triplex DNA-mediated downregulation of Ets2 expression results in growth inhibition and apoptosis in human prostate cancer cells. *Nucleic Acids Res* **32**, 4358-67 (2004).

359. Hahne, J. C. et al. Ets-1 expression promotes epithelial cell transformation by inducing migration, invasion and anchorage-independent growth. *Oncogene* **24**, 5384-8 (2005).

360. Sarkar, P., Shiizaki, K., Yonemoto, J. & Sone, H. Activation of telomerase in BeWo cells by estrogen and 2,3,7,8-tetrachlorodibenzo-p-dioxin in co-operation with c-Myc. *Int J Oncol* **28**, 43-51 (2006).

361. Xiao, X. et al. Identification and characterization of rapidly dividing U937 clones with differential telomerase activity and gene expression profiles: role of c-Myc/Mad1 and Id/Ets proteins. *Leukemia* **16**, 1877-80 (2002).

362. Tao, G. Z. et al. Protein phosphatase-2A associates with and dephosphorylates keratin 8 after hyposmotic stress in a site- and cell-specific manner. *J Cell Sci* **119**, 1425-32 (2006).

363. Sontag, E. et al. The interaction of SV40 small tumor antigen with protein phosphatase 2A stimulates the map kinase pathway and induces cell proliferation. *Cell* **75**, 887-97 (1993).

364. Westermarck, J., Holmstrom, T., Ahonen, M., Eriksson, J. E. & Kahari, V. M. Enhancement of fibroblast collagenase-1 (MMP-1) gene expression by tumor promoter okadaic acid is mediated by stress-activated protein kinases Jun N-terminal kinase and p38. *Matrix Biol* **17**, 547-57 (1998).

365. Silverstein, A. M., Barrow, C. A., Davis, A. J. & Mumby, M. C. Actions of PP2A on the MAP kinase pathway and apoptosis are mediated by distinct regulatory subunits. *Proc Natl Acad Sci U S A* **99**, 4221-6 (2002).

366. Letourneux, C., Rocher, G. & Porteu, F. B56-containing PP2A dephosphorylate ERK and their activity is controlled by the early gene IEX-1 and ERK. *EMBO J* **25**, 727-38 (2006).

367. Strack, S. Overexpression of the protein phosphatase 2A regulatory subunit Bgamma promotes neuronal differentiation by activating the MAP kinase (MAPK) cascade. *J Biol Chem* **277**, 41525-32 (2002).

368. Van Kanegan, M. J., Adams, D. G., Wadzinski, B. E. & Strack, S. Distinct protein phosphatase 2A heterotrimers modulate growth factor signaling to extracellular signal-regulated kinases and Akt. *J Biol Chem* **280**, 36029-36 (2005).

369. Ugi, S., Imamura, T., Ricketts, W. & Olefsky, J. M. Protein phosphatase 2A forms a molecular complex with Shc and regulates Shc tyrosine phosphorylation and downstream mitogenic signaling. *Mol Cell Biol* **22**, 2375-87 (2002).

370. Abraham, D. et al. Raf-1-associated protein phosphatase 2A as a positive regulator of kinase activation. *J Biol Chem* **275**, 22300-4 (2000).

371. Ory, S., Zhou, M., Conrads, T. P., Veenstra, T. D. & Morrison, D. K. Protein phosphatase 2A positively regulates Ras signaling by dephosphorylating KSR1 and Raf-1 on critical 14-3-3 binding sites. *Curr Biol* **13**, 1356-64 (2003).

372. Kolch, W. Coordinating ERK/MAPK signalling through scaffolds and inhibitors. *Nat Rev Mol Cell Biol* **6**, 827-37 (2005).

373. Dougherty, M. K. et al. Regulation of Raf-1 by direct feedback phosphorylation. *Mol Cell* **17**, 215-24 (2005).

374. Nishishita, T. & Lin, P. C. Angiopoietin 1, PDGF-B, and TGF-beta gene regulation in endothelial cell and smooth muscle cell interaction. *J Cell Biochem* **91**, 584-93 (2004).

375. Dell, S., Peters, S., Muther, P., Kociok, N. & Joussen, A. M. The role of PDGF receptor inhibitors and PI3-kinase signaling in the pathogenesis of corneal neovascularization. *Invest Ophthalmol Vis Sci* **47**, 1928-37 (2006).

376. Swanson, R. S., Compton, C. C., Stewart, A. K. & Bland, K. I. The prognosis of T3N0 colon cancer is dependent on the number of lymph nodes examined. *Ann Surg Oncol* **10**, 65-71 (2003).

377. Prandi, M. et al. Prognostic evaluation of stage B colon cancer patients is improved by an adequate lymphadenectomy: results of a secondary analysis of a large scale adjuvant trial. *Ann Surg* **235**, 458-63 (2002).

378. Chen, S. L. & Bilchik, A. J. More extensive nodal dissection improves survival for stages I to III of colon cancer: a population-based study. *Ann Surg* **244**, 602-10 (2006).